UNIVERSITY OF SOUTHERN CALIFORNIA

DEPARTMENT OF CIVIL ENGINEERING

INFLUENCE OF LOCAL SOIL AND GEOLOGIC SITE CONDITIONS ON FOURIER SPECTRUM AMPLITUDES OF RECORDED STRONG MOTION ACCELERATIONS

by

M. D. Trifunac

Report No. CE 87-04

July, 1987

TABLE OF CONTENTS

INTRODUCTION

The idea that the local soil and geological site conditions may influence the amplitudes of recorded seismic waves has been around for many years and has been investigated by many researchers. This has been studied theoretically (e.g. Haskell, 1960; Tsai, 1969; Trifunac, 1971) and experimentally (e.g. Kanai, 1949,1957; Gutenberg, 1957; Duke, 1958; Medvedev, 1955) by considering various overall measures of strong shaking or its effects on different types of structures. Beginning in the 1960's and 1970's these studies took on more detailed and more complete nature because of the increased availability of recorded strong motion accelerograms. Through comparison of the shapes of the Fourier and response spectrum amplitudes, it became possible to describe the effects the local soil conditions have on the local site response (Seed et al., 1974) and to extend the results of Gutenberg (1957) about the effects of the local geologic conditions to the high frequency spectral amplitudes (Trifunac, 1976). Through the 1970's and early 1980's these studies were further refined by detailed regression analyses which were made possible by still larger numbers of well documented records of strong ground motion (Trifunac, 1976,1979; Trifunac and Lee, 1987a,b,c).

However, to this date these studies considered either the local soil or the local geologic site conditions and never combined the simultaneous effects of both media in the development of one and more general scaling relation. Since the typical dimensions of the local soil versus the local geologic site conditions are so different one might expect that their effects would be reflected in the recorded spectral amplitudes

in high and in low frequencies respectively. If both of these effects can be shown to contribute significantly to the variation of spectral amplitudes between 0.05 and 25 Hz, the frequency range of interest to earthquake engineering, then both soil and geologic site condition should be considered simultaneously. The purpose of this report is to investigate this and to find how these effects should be used in the empirical scaling of Fourier amplitude spectra.

PART I: SCALING OF FOURIER SPECTRA IN TERMS OF M, R, H, S, h, s_L and v

I.1 The Current Model

Trifunac and Lee (1987b) have recently completed a study which dealt with scaling of Fourier amplitude spectra, FS(T), in terms of magnitude, M, source-to-station distance R, focal depth, H, "size" of fault, S, component orientation, v and local geology, characterized by the representative depth of sediments, h (or by the local geological site parameter, s). Their scaling relation takes the form

$$\log_{10}FS(T) = M + \mathscr{A}tt(\Delta,M,T) + b_1(T)M + b_2(T)h + b_3(T)v + b_5(T) + b_6(T)M^2 \quad . \tag{I.1.1}$$

They deleted the term $b_4(T)\Delta$ because it was found to be insignificant. Here $\mathscr{A}tt(\Delta,M,T)$ is the new frequency dependent attenuation function. It is of the form (Trifunac and Lee, 1987a):

$$\mathscr{A}tt(\Delta,M,T) = \begin{cases} \mathscr{A}_0(T)\log_{10}\Delta & R \le R_0 \\ \mathscr{A}_0(T)\log_{10}\Delta_0 - (R-R_0)/200 & R > R_0 \end{cases} \tag{I.1.2}$$

with Δ, the representative source-to-station distance, given by

$$\Delta = S\ \ell n\left[\frac{R^2+H^2+S^2}{R^2+H^2+S_0^2}\right]^{-\frac{1}{2}} \tag{I.1.3}$$

and

$$\Delta_0 = S\ \ell n\left[\frac{R_0^2+H^2+S^2}{R_0^2+H^2+S_0^2}\right]^{-\frac{1}{2}} \quad . \tag{I.1.4}$$

S_0 is the coherence radius of the source (Gusev, 1983). The term $\mathcal{A}_0(T)\log_{10}\Delta$ is used to calculate the attenuation function at distances R less than some transition distance R_0, where $\Delta = \Delta_0$. For distances $R > R_0$, the attenuation becomes a linear function of distance R with slope equal to -1/200. R_0 is given by (Model III of Trifunac and Lee, 1987a):

$$R_0 = \frac{1}{2}\left(\frac{-200\mathcal{A}_0(T)(1-S_0^2/S^2)}{\ell n 10} + \sqrt{\frac{200\mathcal{A}_0(T)(1-S_0^2/S^2)}{\ell n 10} - 4H^2}\right), \quad (I.1.5)$$

and is a function of H, S, S_0 and $\mathcal{A}_0(T)$. More detailed discussion of this attenuation function can be found in Trifunac and Lee (1987a).

Regression analysis using the above model, equation I.1.1, has been performed on the Fourier amplitude data FS(T) at 91 discrete periods T ranging from 0.04 to 15.0 sec. The data has been selected from 1314 components of data from 104 earthquakes in the western United States. A screening procedure was used to minimize the biases in the model that could result from uneven distribution of data among the different magnitudes (Trifunac and Lee, 1987b).

Replacing the Richter's empirical attenuation function (Richter, 1958) with the frequency dependent attenuation function mentioned above, has not only contributed the additional flexibility to estimating the Fourier Spectral amplitudes, but also has decreased the residuals of actual data relative to the model predictions relative to our earlier regression models (Trifunac, 1976, 1979).

I.2 Updating the Database

The database of Trifunac and Lee (1987b) consists of 438 free-field records with 3 components each, or a total of 1314 components from 104 earthquakes for the years from 1933 to 1983. Table I.2.1 presents the list of all earthquakes in this database. It contains information on the name, date and time of each earthquake, the latitude and longitude of its epicenter, its focal depth, local magnitude and maximum intensity, if available. Each of the 438 free-field records are accompanied by the information on the address of the recording station, the latitude and longitude of the station, the local M.M.I. intensity that has been reported for the station site or estimated by Lee and Trifunac (1985), and the local geology classification characterized by the site parameter s or the depth of alluvium h. This list of earthquakes has been updated now to a total of 106, with addition of two recent earthquakes, the Coalinga Earthquake of 1983 and the Morgan Hill Earthquake of 1984, both in California. With the addition of 56 free-field records from these two earthquakes, the total number of free-field records is now 494, corresponding to 988 horizontal components and 494 vertical components, or a total of 1482 components.

To proceed with the present analysis, information on the soil site properties has been collected from various available sources, including different reports of the United States Geological Survey (U.S.G.S.), California Division of Mines and Geology (C.D.M.G.), Nuclear Regulatory Commission, University Reports and various consulting reports. At first this data has been characterized by a soil parameter, s_L, which was

TABLE I.2.1

1	3	10	1933	1754PST	33	37	00	-117	58	00	16.0	6.3	9	LONG BEACH, CALIF
2	10	2	1933	0110PST	33	47	00	-118	08	00	16.0	5.4	6	SOUTHERN CALIF
3	7	6	1934	1449PST	41	42	00	-124	36	00			5	EUREKA, CALIF
4	12	30	1934	0552PST	32	15	00	-115	30	00	16.0	6.5	9	LOWER CALIF
5	10	31	1935	1138MST	46	37	00	-111	58	00		6.0	8	HELENA, MT
6	10	31	1935	1218MST	46	37	00	-111	58	00			3	HELENA, MT
7	11	21	1935	2058MST	46	36	00	-112	00	00			6	HELENA, MT
8	11	28	1935	0742MST	46	37	00	-111	58	00			6	HELENA, MT
9	2	6	1937	2042PST	40	30	00	-125	15	00			5	HUMBOLDT BAY, CAL
10	4	12	1938	0825PST	32	53	00	-115	35	00	16.0	3.0		IMPERIAL VALLEY, CA
11	6	5	1938	1842PST	32	54	00	-115	13	00	16.0	5.0		IMPERIAL VALLEY, CA
12	6	6	1938	0435PST	32	15	00	-115	10	00	16.0	4.0		IMPERIAL VALLEY, CA
13	9	11	1938	2210PST	40	18	00	-124	48	00		5.5	6	NW CALIF
14	5	18	1940	2037PST	32	44	00	-115	30	00	16.0	6.7	10	IMPERIAL VALLEY, CA
15	2	9	1941	0145PST	40	42	00	-125	24	00		6.4		NW CALIF
16	6	30	1941	2351PST	34	22	00	-119	35	00	16.0	5.9	8	SANTA BARBARA, CAL
17	10	3	1941	0813PST	40	36	00	-124	36	00		6.4	7	NORTHERN CALIF
18	11	14	1941	0042PST	33	47	00	-118	15	00	16.0	5.4	8	TORRANCE-GARDENA CA
19	10	21	1942	0822PST	32	58	00	-116	00	00	16.0	6.5	7	BORREGO VALLEY, CAL
20	3	9	1949	0429PST	37	06	00	-121	18	00		5.3	7	NORTHERN CALIF
21	4	13	1949	1156PST	47	06	00	-122	42	00		7.1	8	WESTERN WASH
22	1	23	1951	2317PST	32	59	00	-115	44	00	16.0	5.6	7	IMPERIAL VALLEY, CA
23	10	7	1951	2011PST	40	17	00	-124	48	00		5.8	7	NW CALIF
24	7	21	1952	0453PDT	35	00	00	-119	01	00	16.0	7.7	11	KERN COUNTY, CALIF
25	7	23	1952		35	17	00	-118	39	00				KERN CNTY, CAL
26	9	22	1952	0441PDT	40	12	00	-124	25	00		5.5	7	NORTHERN CALIF
27	11	21	1952	2346PST	35	50	00	-121	10	00		6.0	7	SOUTHERN CALIF
28	6	13	1953	2017PST	32	57	00	-115	43	00	16.0	5.5	7	IMPERIAL VALLEY, CA
29	1	12	1954	1534PST	35	00	00	-119	01	00	16.0	5.9	8	WHEELER RIDGE, CALI
30	4	25	1954	1233PST	36	48	00	-121	48	00		5.3	7	CENTRAL CALIF
31	11	12	1954	0427PST	31	30	00	-116	00	00	16.0	6.3	5	LOWER CALIF
32	12	21	1954	1156PST	40	47	00	-123	52	00		6.5	7	EUREKA, CALIF
33	9	4	1955	1801PST	37	22	00	-121	47	00		5.8	7	SAN JOSE, CALIF
34	12	16	1955	2117PST	33	00	00	-115	30	00	16.0	4.3		IMPERIAL COUNTY, CA
35	12	16	1955	2142PST	33	00	00	-115	30	00	16.0	3.9		IMPERIAL COUNTY, CA
36	12	16	1955	2207PST	33	00	00	-115	30	00	16.0	5.4	7	IMPERIAL COUNTY
37	2	9	1956	0633PST	31	42	00	-115	54	00	16.0	6.8		EL ALAMO, BAJA CAL
38	2	9	1956	0725PST	31	42	00	-115	54	00		6.4		EL ALAMO, BAJA CAL
39	3	18	1957	1056PST	34	07	06	-119	13	12	13.8	4.7	6	SOUTHERN CALIF
40	3	22	1957	1048PST	37	40	00	-122	28	00		3.8	5	SAN FRANCISCO CA
41	3	22	1957	1144PST	37	40	00	-122	29	00		5.3	7	SAN FRANCISCO, CAL
42	3	22	1957	1515PST	37	39	00	-122	27	00		4.4	5	SAN FRANCISCO CA
43	3	22	1957	1627PST	37	39	00	-122	29	00		4.0	5	SAN FRANCISCO CA
44	1	19	1960	1926PST	36	47	00	-121	26	00		5.0	6	CENTRAL CALIF
45	6	5	1960	1718PST	40	49	00	-124	53	00		5.7	6	NORTHERN CALIF
46	4	8	1961	2323PST	36	30	00	-121	18	00	11.0	5.7	7	HOLLISTER, CALIF
47	9	4	1962	0917PST	40	58	00	-124	12	00		5.0	6	NORTHERN CALIF
48	4	29	1965	0729PST	47	24	00	-122	18	00		6.5	8	PUGET SOUND, WASH
49	7	15	1965	2346PST	34	29	06	-118	31	18	15.1	4.0	6	SOUTHERN CALIF
50	6	27	1966	2026PST	35	57	18	-120	29	54	6.0	5.6	7	PARKFIELD, CALIF
51	8	7	1966	0936PST	31	48	00	-114	30	00	16.0	6.3	6	GULF OF CALIF
52	9	12	1966	0841PST	39	24	00	-120	06	00		6.3	7	NORTHERN CALIF
53	12	10	1967	0407PST	40	30	00	-124	36	00		5.8	6	NORTHERN CALIF
54	12	18	1967	0925PST	37	00	36	-121	47	18		5.2	6	NORTHERN CALIF

TABLE I.2.1 (CONT.)

55	4	8	1968	1830PST	33	11	24	-116	07	42	11.1	6.4	7	BORREGO MTN, CALIF
56	9	12	1970	0630PST	34	16	12	-117	32	24	8.0	5.4	7	LYTLE CREEK, CALIF
57	2	9	1971	0600PST	34	24	42	-118	24	00	13.0	6.4	11	SAN FERNANDO, CALIF
58	10	15	1979	1417PST	32	37	59	-115	19	59	12.0	6.6		IMPERIAL VALLEY, CA
59	8	6	1979	0805PST	37	06	43	-121	31	59	9.6	5.9		COYOTE LAKE, CALIF
60	8	13	1978	2254GMT	34	21	04	-119	42	00	12.5	5.5		SANTA BARBARA, CAL
61	1	24	1980	1100PST	37	49	37	-121	47	13	5.9	5.9		MT. DIABLO, LIVERMO
62	1	26	1980	1833PST	37	45	00	-121	42	47	7.3	5.2		MT. DIABLO, LIVERMO
63	08	02	1975	2022GMT	39	26	58	-121	28	25	4.1	5.2		OROVILLE AFTERSHOCK
64	08	02	1975	2059GMT	39	26	00	-121	28	31	5.1	5.2		OROVILLE AFTERSHOCK
65	08	03	1975	0103GMT	39	29	19	-121	30	59	8.8	4.6		OROVILLE AFTERSHOCK
66	08	03	1975	0247GMT	39	28	52	-121	30	21	7.4	4.1		OROVILLE AFTERSHOCK
67	08	05	1975	0228GMT	39	24	18	-121	29	43	6.2	3.2		OROVILLE AFTERSHOCK
68	08	06	1975	0350GMT	39	29	46	-121	31	49	9.2	4.7		OROVILLE AFTERSHOCK
69	08	06	1975	1641GMT	39	29	31	-121	31	45	9.7	3.9		OROVILLE AFTERSHOCK
70	08	08	1975	0700GMT	39	29	50	-121	30	41	7.7	4.8		OROVILLE AFTERSHOCK
71	08	11	1975	0611GMT	39	27	29	-121	28	59	3.1	4.4		OROVILLE AFTERSHOCK
72	08	11	1975	1559GMT	39	30	20	-121	31	35	9.8	3.8		OROVILLE AFTERSHOCK
73	08	16	1975	0548GMT	39	28	12	-121	31	42	8.5	4.1		OROVILLE AFTERSHOCK
74	08	16	1975	1223GMT	39	29	52	-121	30	16	7.1	3.1		OROVILLE AFTERSHOCK
75	09	27	1975	2234GMT	39	31	12	-121	31	56	10.4	4.6		OROVILLE AFTERSHOCK
76	11	28	1974	2301GMT	36	54	0	-121	30	0	9.0	0.	6	HOLLISTER, CAL
77	1	11	1975	1737PST	40	13	12	-124	15	36	2.0	4.7	6	NORTHERN CAL
78	5	6	1975	1835PST	40	16	48	-124	40	12	0.	4.0		NORTHERN CAL
79	6	7	1975	0846GMT	40	34	12	-124	08	24	21.0	5.7	7	NORTHERN CAL
80	3	8	1971	1508PST	35	40	0	-118	24	12	6.0	4.7	5	CENTRAL CAL
81	5	2	1971	0608GMT	51	24	0	-177	12	0	43.0	7.1	6	ANDREANOF, ALASKA
82	9	12	1971	1132PST	41	17	54	-123	40	24	20.0	4.6	5	NORTHERN CAL
83	7	30	1972	2145GMT	56	49	12	-135	40	48	25.0	7.1	7	SOUTHEAST ALASKA
84	9	4	1972	1804GMT	36	38	13	-121	17	13	2.0	4.8	6	CENTRAL CAL
85	5	26	1980	1857GMT	37	32	37	-118	51	41	2.8	4.9		MAMMOTH AFTERSHOCK
86	5	27	1980	1450GMT	37	27	49	-118	49	24	2.4	6.3		MAMMOTH AFTERSHOCK
87	5	27	1980	1901GMT	37	36	15	-118	46	11	3.8	5.0		MAMMOTH AFTERSHOCK
88	5	28	1980	0516GMT	37	34	49	-118	53	09	3.3	4.8		MAMMOTH AFTERSHOCK
89	5	31	1980	1516GMT	37	32	22	-118	54	22	8.2	5.1		MAMMOTH AFTERSHOCK
90	6	11	1980	0441GMT	37	30	24	-119	02	34	14.1	5.0		MAMMOTH AFTERSHOCK
91	6	28	1980	0058GMT	37	33	23	-118	51	45	5.1	4.1		MAMMOTH AFTERSHOCK
92	10	16	1979	1616PDT	33	4	29	-115	33	16	5.0	4.9		IMPERIAL VALLEY AFT
93	10	16	1979	1445PDT	33	2	44	-115	29	24	3.9	4.6		IMPERIAL VALLEY AFT
94	10	16	1979	1114PDT	32	58	19	-115	36	22	4.7	4.2		IMPERIAL VALLEY AFT
95	10	15	1979	2319GMT	32	46	0	-115	26	29	9.5	5.0		IMPERIAL VALLEY AFT
96	4	26	1981	1209GMT	33	7	48	-115	39	0	8.0	5.6		WESTMORELAND, CAL
97	1	24	1980	1900GMT	37	50	24	-121	48	0	5.9	5.9		LIVERMORE, CAL
98	1	26	1980	0233GMT	37	45	36	-121	42	0	7.3	5.2		LIVERMORE, CAL
99	5	25	1980	0934PDT	37	36	32	-118	50	49	9.0	6.1		MAMMOTH AFTERSHOCK
100	5	25	1980	0949PDT	37	37	41	-118	55	37	14.	6.0		MAMMOTH AFTERSHOCK
101	5	25	1980	1245PDT	37	33	40	-118	49	52	16.	6.1		MAMMOTH AFTERSHOCK
102	5	25	1980	1336PDT	37	37	30	-118	51	32	2.	5.7		MAMMOTH AFTERSHOCK
103	5	26	1980	1158PDT	37	32	35	-118	53	17	5.	5.7		MAMMOTH AFTERSHOCK
104	5	27	1980	0751PDT	37	30	22	-118	49	34	14.	6.2		MAMMOTH AFTERSHOCK
105	5	2	1983	1642PDT	36	15	00	-120	16	48	9.	6.5		COALINGA EARTHQUAKE
106	4	24	1984	1315PST	37	19	01	-121	40	48	9.	6.2		MORGAN HILL EARTHQUAKE

assigned values 1 for deep soil sites, 2 for stiff soil sites and 3 for rock sites (Seed, et al., 1976). Subsequently, this characterization was changed to 0 for rock sites, 1 for stiff soil sites and 2 for deep soil sites for convenience in regression analysis.

I.3 The New Regression Analysis

To include the soil classification in the regression analysis, the regression equation of the Fourier amplitudes will now take the form:

$$\log_{10}FS(T) = M + \mathcal{A}tt(\Delta,M,T) + b_1(T)M + b_2(T)h + b_3(T)v + b_4(T)hv + b_5(T) + b_6(T)M^2 + b_7^{(1)}(T)S_L^{(1)} + b_7^{(2)}(T)S_L^{(2)} \quad . \tag{I.3.1}$$

Equation (I.3.1) is of the same form as equation (I.1.1), but with the addition of the new terms $b_4(T)hv$, $b_7^{(1)}(T)S_L^{(1)}$ and $b_7^{(2)}(T)S_L^{(T)}$. The terms $b_4(T)hv$ and $b_2(T)h$ will result in the factor multiplying the depth of alluvium, h, to be component dependent, so that for horizontal components with v = 0, and vertical components with v = 1, it takes the form:

$$b_2(T)h + b_4(T)hv = (b_2(T)+b_4(T)v)h = \begin{cases} b_2(T)h & ; \ v = 0 \ , \\ (b_2(T)+b_4(T))h & ; \ v = 1 \ . \end{cases} \tag{I.3.2}$$

The addition of the other two terms, $b_7^{(1)}(T)S_L^{(1)}$ and $b_7^{(2)}(T)S_L^{(2)}$, is to characterize the soil at the site, where

$$S_L^{(1)} = \begin{cases} 1 & \text{if } s_L = 1 \ , \\ 0 & \text{otherwise,} \end{cases}$$

and

$$S_L^{(2)} = \begin{cases} 1 & \text{if } s_L = 2 \ , \\ 0 & \text{otherwise} \ . \end{cases} \tag{I.3.3}$$

The use of the two variables $S_L^{(1)}$ and $S_L^{(2)}$ instead of one for s_L here is due to the fact that s_L is a qualitative or categorical variable which takes on the discrete values of 0, 1 and 2 for three distinct types of soil classification. It is thus different from all the other variables used, like magnitude or depth, h, which are quantitative variables, that is, variables with a well defined scale of measurement. In contrast, the qualitative variable for soil is not one with a natural scale of measurement. To account for the effect that the different classification of soil may have on the Fourier amplitudes, it is thus necessary to use indicator variables to account for the different levels of the classification (Montgomery and Peck, 1982). The variables $S_L^{(1)}$ and $S_L^{(2)}$ defined above thus serve as indicator variables for the soil parameter s_L.

To interpret the use of indicator variables, here in equation (I.3.1), consider the case $s_L = 0$ (rock site), for which both $S_L^{(1)} = S_L^{(2)} = 0$. The regression model becomes

$$\log_{10}FS(T) = M + \mathcal{A}tt(\Delta,M,T) + b_1(T)m + b_2(T)h + b_3(T)v + b_4(T)hv + b_5(T) + b_6(T)M^2 \quad , \tag{I.3.4}$$

which is except for $b_4(T)hv$ identical to that in equation (I.1.1). For the case $s_L = 1$ (stiff soil site), for which $S_L^{(1)} = 1$ and $S_L^{(2)} = 0$,

$$\log_{10}FS(T) = M + \mathcal{A}tt(\Delta,M,T) + b_1(T)M + b_2(T)h + b_3(T)v + b_4(T)hv + b_5(T) + b_6(T)M^2 + b_7^{(1)}(T) \quad , \tag{I.3.5}$$

similar to equation (I.3.4) with the addition of the term $b_7^{(1)}(T)$. Similarly, for the case $s_L = 2$ (deep soil site), for which $S_L^{(1)} = 0$ and $S_L^{(2)} = 1$,

$$\log_{10}FS(T) = M + \mathcal{A}tt(\Delta,M,T) + b_1(T)M + b_2(T)h + b_3(T)v + b_4(T)hv + b_5(T) + b_6(T)M^2 + b_7^{(2)}(T) , \quad (I.3.6)$$

with now the addition of a different term $b_7^{(2)}(T)$.

The use of indicator variables is thus equivalent to using different regression equations, one for each soil classification, to model the relationship between Fourier Spectral Amplitudes, FS(T) and soil parameter, s_L. These different regression equations will have the same dependence on all the other variables, but a different intercept (constant term) for each soil classification. We could have initially fit a separate regression model for each soil type instead of a single model with indicator variables. However, the single model approach here is preferred because there is only one final equation to work with instead of three, a simpler representation for all practical purposes! Furthermore, since all three soil classifications are assumed to have the same dependence on all the other variables, like magnitude and depth, it makes sense to combine the data from all soil types to produce a single regression model. This approach also gives one estimate, of the common error variance, and of the residual degrees of freedom.

An approach to the treatment of a qualitative variable in our earlier regression analyses is worth commenting on here. One can "measure" the soil site classification by an allocated code. Instead of using two

indicator variables to represent the three levels of the qualitative soil type, we could simply use the variable s_L in the regression analysis and fit the regression model as follows:

$$\log_{10}FS(T) = M + \mathcal{A}tt(\Delta,M,T) + b_1(T)M + b_2(T)h + b_3(T)v + b_4(T)hv + b_5(T) + b_6(T)M^2 + b_7(T)s_L \ . \tag{I.3.7}$$

This model implies that

$$E(\log_{10}FS(T)|s_L = 0 \text{ , rock site}) = M + \mathcal{A}tt(\Delta,M,T) + b_1(T)M + b_2(T)h + b_3(T)v + b_4(T)hv + b_5(T) + b_6(T)M^2 \ , \tag{I.3.8}$$

as in equation (I.3.3), but then

$$E(\log_{10}FS(T)|s_L = 1 \text{ , stiff soil site}) = E(\log_{10}FS(T)|s_L = 0) + b_7(T) \ ,$$

and

$$\begin{aligned} E(\log_{10}FS(T)|s_L = 2 \text{ , deep soil site}) &= E(\log_{10}FS(T)|s_L = 0) + 2b_7(T) \\ &= E(\log_{10}FS(T)|s_L = 1) + b_7(T) \ , \end{aligned} \tag{I.3.9}$$

which may be unrealistic. The allocated codes impose a particular metric on the levels of the qualitative soil classification. However, there is no quarantee that any such particular allocated code will lead to a

spacing that is appropriate. Indicator variables, on the other hand, are more appropriate for this type of a problem because they do not force any particular metric on the levels of the qualitative factor.

I.4 Database Selection for Regression Analysis

The database selection procedure for the Fourier amplitude data, FS(T), is essentially the same as that in the previous analysis of Trifunac and Lee (1987b). As before, the data are screened to minimize a possible bias in the model that could result from an uneven distribution of data among different magnitudes and from an excessive contribution from earthquakes that have been recorded abundantly. The only new feature is that an additional category, namely, soil classification, is included in the selection process. To carry out this screening the data is partitioned into six groups corresponding to magnitude ranges 2.0-2.9, 3.0-3.9, 4.0-4.9, 5.0-5.9, 6.0-6.9 and 7.0-7.9. The data in each of these magnitude ranges are next subdivided first according to the site classifications of s = 0, 1 and 2 (Trifunac and Lee, 1987b). The data within one magnitude range and one site classification are then further subdivided according to the soil classifications, s_L = 0, 1 and 2. Finally, the data within each of these subgroups are separated into two sets according to component orientation: one set for horizontal (v = 0) and one set for vertical (v = 1). The resulting data in each of the subsets correspond now to the Fourier spectral amplitudes from a specified magnitude range at a specified site classification, of a specified soil type and with specified component orientation. To properly balance the effects of attenuation at small and large distances, the data in each of the subsets are further subdivided into 2 groups: one for epicentral distances $\leq$ 100 km and the other for distances > 100 km. The data in each of these two final subsets are then arranged, as in our previous regression analyses, in increasing order in terms of their amplitudes. If the number of data in the first group (R $\leq$ 100 km) is

less than 19, all the data points are kept. Otherwise at most 19 points are selected from among the ordered set of data so that they correspond uniformly, as close as possible, to the 5th, 10th,..., up to the 95th percentiles. Similarly, at most 5 points are selected from the second group (R > 100 km) of data so that they correspond uniformly to around the 1/6, 1/3, 1/2, 2/3 and 5/6 x 100th percentiles. This selection procedure has the effect of reducing the biases described above.

The above selection process is repeated for each of the 91 periods in the range .04 sec. to 15 sec. In addition, at the long period end, data points with amplitudes that are smaller than the average digitization noise, i.e. those with signal-to-noise ratio less than one, are automatically eliminated from the selection process. This is the case for many of the data recorded from earthqaukes of smaller mangitudes and/or recorded at sites with larger epicentral distances. The number of selected data points used in the regression analysis at the long period end is thus less than for the intermediate and short period range.

The fitted coefficients at each period T resulting from linear regression will be denoted by $\hat{b}_1(T)$, $\hat{b}_2(T)$, $\hat{b}_3(T)$, $\hat{b}_4(T)$, $\hat{b}_5(T)$, $\hat{b}_6(T)$ $\hat{b}_7^{(1)}(T)$ and $\hat{b}_7^{(2)}(T)$ (see equation I.3.1) respectively.

For given values of T, h, v, Δ and s_L, $\log_{10}FS(T)$ represents a parabola when plotted versus M. Following our preceding analyses (e.g. Trifunac and Lee, 1987b), it is again assumed here that equation (I.3.1) applies only in the range $M_{min} \leq M \leq M_{max}$, where, for each period T:

$$M_{min}(T) = -\hat{b}_1(T)/(2\hat{b}_6(T)) \text{ , and}$$

$$M_{max}(T) = -(1+\hat{b}_1(T))/(2\hat{b}_6(T)) \quad . \qquad \text{(I.4.1)}$$

For $M \leq M_{min}$, M is used only in the first term of (I.3.1) and M_{min} is used with $b_1(T)$ and $b_6(T)$. For $M \geq M_{max}$, M_{max} is used in all the terms for M. In other words, equation (I.3.1) is modified to:

$$\log_{10}FS(T) = M_{<} + \mathcal{A}tt(\Delta,M,T)$$
$$+ \hat{b}_1(T)M_{<>} + \hat{b}_2(T)h + \hat{b}_3(T)v + \hat{b}_4(T)hv + \hat{b}_5(T) + \hat{b}_6(T)M_{<>}^2$$
$$+ b_7^{(1)}(T)S_L^{(1)} + b_7^{(2)}(T)S_L^{(2)} \quad ,$$

where

$$M_{<} = \min(M,M_{max}) \quad , \text{ and} \tag{I.4.2}$$

$$M_{<>} = \max(M_{min},M_{<}) = \begin{cases} M_{min} & M \leq M_{min} \\ M & M_{min} \leq M \leq M_{max} \\ M_{max} & M > M_{max} \quad . \end{cases} \tag{I.4.3}$$

I.5 Results of the Regression Analysis

Figure I.5.1 shows $\hat{b}_1(T)$ through $\hat{b}_6(T)$, $\hat{b}_7^{(1)}(T)$ and $\hat{b}_7^{(2)}(T)$, as full lines, and the corresponding estimates of the 80%, 90% and 95% confidence intervals represented by the dashed lines.

As can be seen from the figure, the coefficients for M, $\hat{b}_1(T)$, and M^2, $\hat{b}_6(T)$, as in the previous analysis (Trifunac and Lee, 1987b), are both significant in practically the whole period range considered (0.04 sec. to 14 sec.), except possibly at the short and long period ends. Note that this is in good agreement with the conclusions of previous analyses, where it was shown that the Fourier amplitudes do not just grow linearly with magnitude. It is noted here that the coefficient multiplying the depth of alluvium h, $\hat{b}_2(T)$, remains positive all through the period range and is essentially significant for all periods T, including the high frequency (low period) end. This is again in agreement with our previous analyses for both Fourier amplitudes (Trifunac and Lee, 1987b) and pseudo relative velocity amplitudes, PSV(T), at all five damping values (Trifunac and Lee, 1987c). The coefficient for the component direction v, $\hat{b}_3(T)$, is also in agreement with previous analyses. The new coefficient for hv, $\hat{b}_4(T)$, which was not considered in our previous work is negative in the whole period range and is significant in the mid period range. It is significant, with 90% confidence, in the period from 0.25 sec. to 2.5 sec. This term should thus be included in all subsequent analyses of Fourier and Response amplitudes. The coefficient for the constant term, $\hat{b}_6(T)$, is also in agreement with our previous work and is significant essentially in the whole period range. Finally, the new coefficients, $b_7^{(1)}(T)$ and $b_7^{(2)}(T)$, corresponding to the indicator

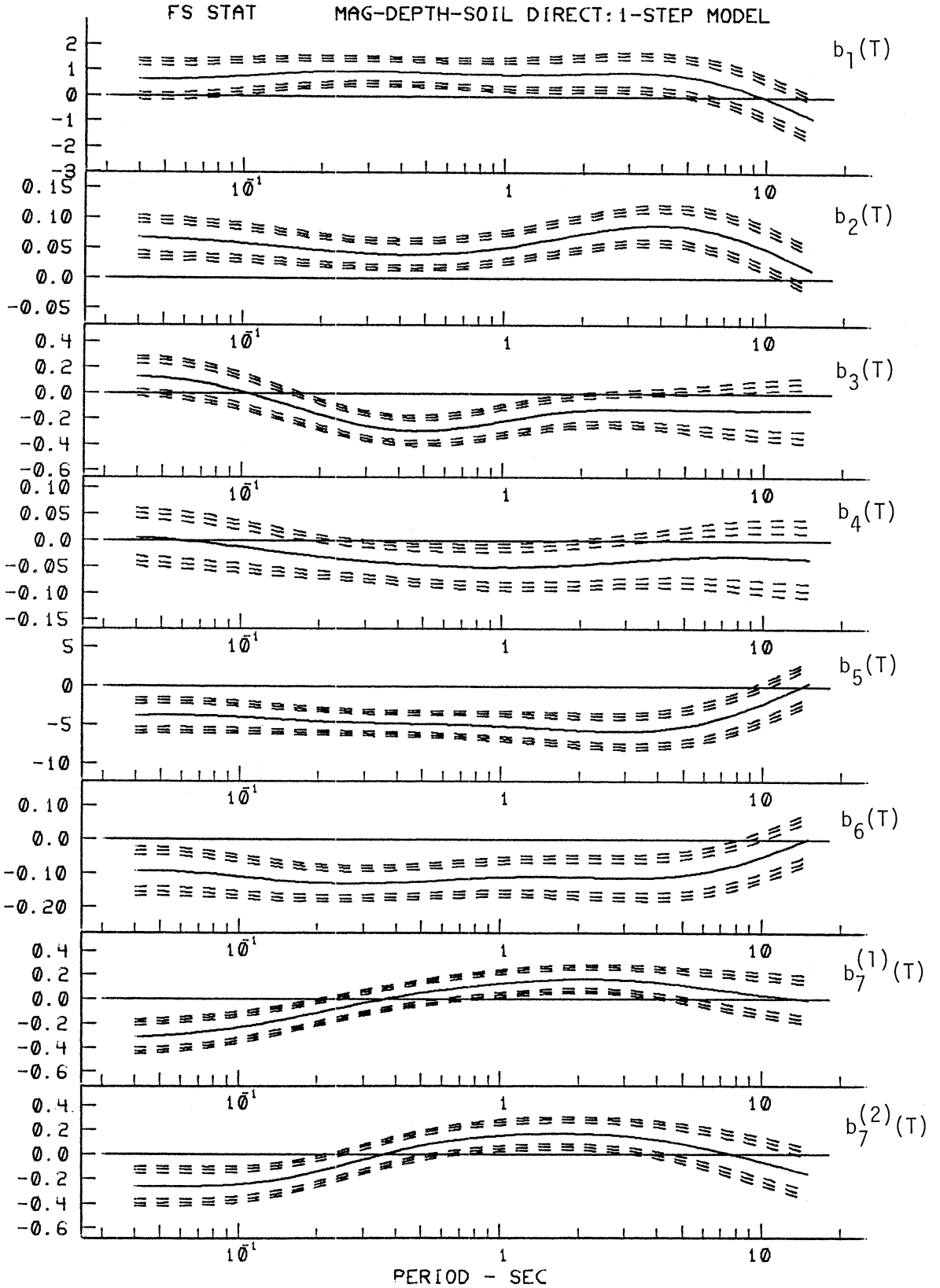
FS STAT MAG-DEPTH-SOIL DIRECT: 1-STEP MODEL
b1(T)
b2(T)
b3(T)
b4(T)
b5(T)
b6(T)
b7(1)(T)
b7(2)(T)
PERIOD - SEC

Figure I.5.1

variables $S_L^{(1)}$ ($s_L = 1$) and $S_L^{(2)}$ ($s_L = 2$) show an interesting trend. For periods up to 0.35 sec., both are negative and then become positive up to about 10 sec. periods. This means that in the period range below ~ .35 sec. the Fourier amplitudes are attenuated and between 0.35 and 10 sec., the Fourier amplitudes are amplified.

With FS(T) representing the Fourier amplitude spectra computed from recorded accelerograms, the residues are calculated as in our previous analyses (Trifunac and Lee, 1987b), from

$$\varepsilon(T) = \log_{10}[FS(T)] - \log_{10}[\hat{FS}(T)] \quad . \qquad (I.5.1)$$

Again, it is assumed that $\varepsilon(T)$ can be described by a normal distribution function with mean $\mu(T)$ and standard deviation $\sigma(T)$ as follows:

$$p(\varepsilon,T) = \frac{1}{\sigma(T)\sqrt{2\pi}} \int_{-\infty}^{\varepsilon(T)} \exp\left[-\frac{1}{2}\left(\frac{x-\mu(T)}{\sigma(T)}\right)^2\right]dx \ , \qquad (I.5.2)$$

where $p(\varepsilon,T)$ represents the probability that $\log_{10}[FS(T)] - \log_{10}[\hat{FS}(T)] \leq \varepsilon(T)$. For a given residual value $\varepsilon(T)$ at a particular period, T, the actual probability $p^*(\varepsilon,T)$ that $\varepsilon(T)$ will not be exceeded can be evaluated by finding the fraction of residuals $\varepsilon(T)$ (computed from the data-base at that particular period) which are smaller than the given value.

Using (I.5.2), the estimated probability $\hat{p}(\varepsilon,T)$ that $\varepsilon(T)$ will not be exceeded can also be evaluated and compared with the above fractions. For $p^*(\varepsilon,T)$ calculated at 91 periods, the residuals $\varepsilon(T)$ corresponding to $p^* = 0.1, 0.2, \ldots, 0.8$ and 0.9 are plotted in Figure I.5.2. The nine sets of curves, plotted versus period, T, from bottom to top correspond to the residual values at each of the probability levels, 0.1 through 0.9.

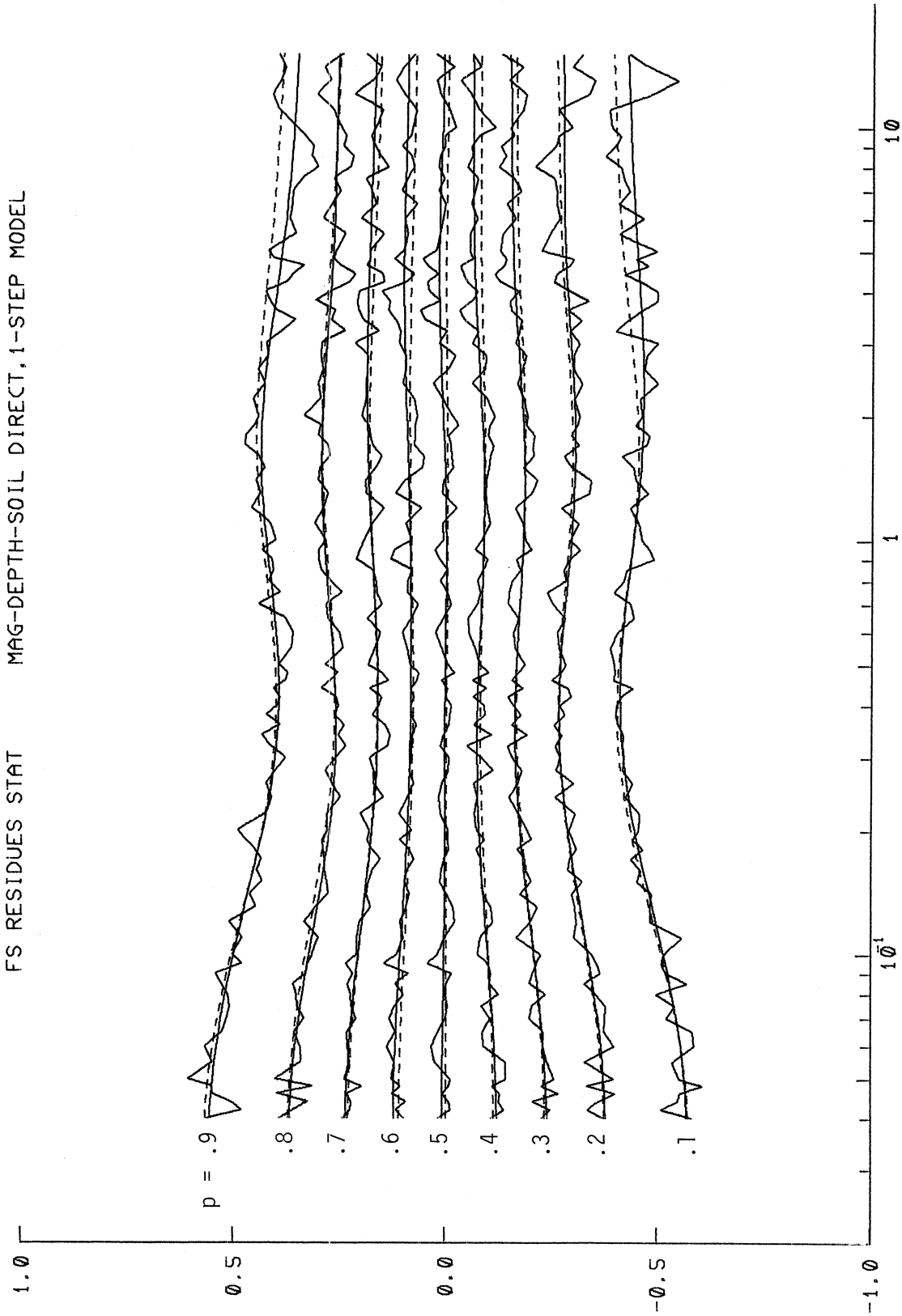
FS RESIDUES STAT
MAG-DEPTH-SOIL DIRECT, 1-STEP MODEL
1.0
0.5
0.0
-0.5
-1.0
p = .9
.8
.7
.6
.5
.4
.3
.2
.1
10⁻¹
1
10

Figure I.5.2

At each such level, the rough solid line represents the actual calculated residue values. The smooth solid curves are obtained by smoothing the rough solid curves along the period (T) axis. The smooth surface, $p^*(\varepsilon,T)$, from the nine solid curves thus represents the distribution of the computed Fourier amplitudes FS(T) about the estimated amplitudes $\hat{FS}(T)$ given in (I.4.2). By fitting $p(\varepsilon,T)$ in equation (I.5.2) to $p^*(\varepsilon,T)$ at 91 periods, the mean and standard deviation of the normal distribution function, $\hat{\mu}(T)$ and $\hat{\sigma}(T)$, are evaluated. Substituting these values into equation (I.5.2), with $p(\varepsilon,T)$ taking values 0.1 through 0.9, will result in $\hat{\varepsilon}(T)$ for the 9 probability levels. These are the nine dashed lines in Figure I.5.2. The surface $p^*(\varepsilon,T)$ that resulted from the new regression model in the present analysis is narrower in the ε range when compared with that of our previous analysis (Figure I.5.2 of Trifunac and Lee, 1985a).

Figure I.5.3 shows a plot of the statistical parameters. The smooth amplitudes of $\hat{\mu}(T)$ and $\hat{\sigma}(T)$ and their 95% confidence intervals are respectively given in the top two plots of the figure. The two full curves in the bottom of the figure are respectively the smoothed amplitudes of the computed χ^2, $\chi^2(T)$ and Komolgorov-Smirnov, KS(T), statistics. The dashed lines are their corresponding 95% cutoff levels. It is seen that in the whole period range considered, 0.04 sec. to 14 sec., both the χ^2 and K-S tests fail to reject the hypothesis that the distribution is normal. The density function in equation (I.5.2) thus represents an acceptable approximation to $p^*(\varepsilon,T)$.

Table I.5.1 presents, for 12 periods, between T = 0.04 sec. and T = 14 sec., the values of the smoothed regression coefficients $\hat{b}_1(T)$,

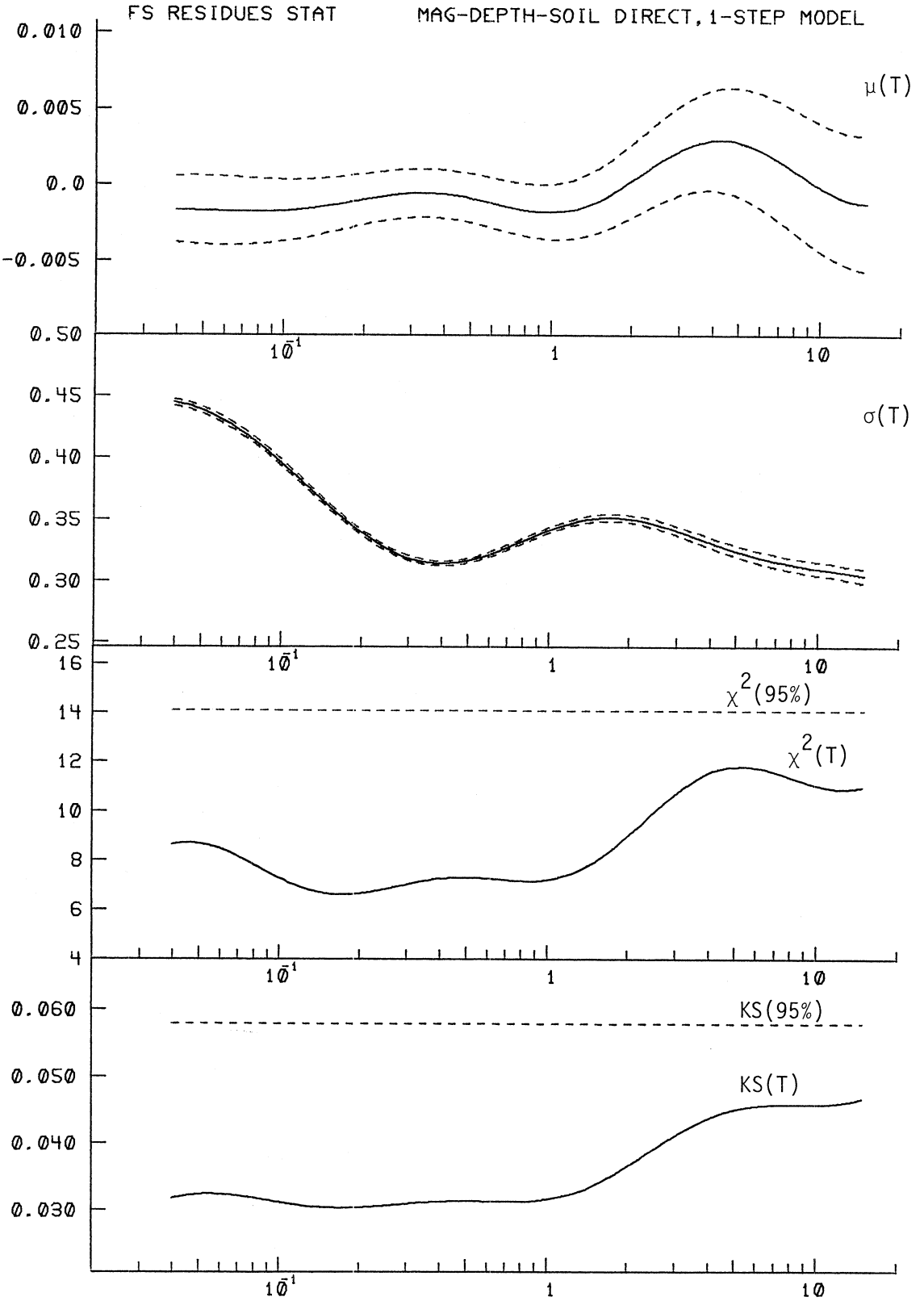
FS RESIDUES STAT
MAG-DEPTH-SOIL DIRECT, 1-STEP MODEL
μ(T)
σ(T)
χ²(95%)
χ²(T)
KS(95%)
KS(T)
0.010
0.005
0.0
-0.005
0.50
0.45
0.40
0.35
0.30
0.25
16
14
12
10
8
6
4
0.060
0.050
0.040
0.030
10⁻¹
1
10

Figure I.5.3

TABLE I.5.1

$$\log_{10} FS(T) = M_{<} + \mathcal{A}tt(\Delta,M,T) +$$

$$b_1(T)M_{<>} + b_2(T)h + b_3(T)v + b_4(T)hv + b_5(T) + b_6(T)M_{<>}^2 +$$

$$b_7^{(1)}(T)S_L^{(1)} + b_7^{(2)}(T)S_L^{(2)}$$

MAG-DEPTH-SOIL DIRECT:1-STEP MODEL

PERIOD, T(SEC)	.040	.065	.11	.19	.34	.50	.90	1.60	2.80	4.40	7.50	14.0
COEFFICIENTS:												
$b_1(T)$	.652	.667	.819	.962	.977	.927	.854	.876	.940	.856	.382	-.707
$b_2(T)$	.067	.063	.056	.047	.040	.039	.049	.067	.084	.087	.069	.020
$b_3(T)$	.127	.091	-.012	-.155	-.272	-.292	-.233	-.152	-.122	-.126	-.132	-.131
$b_4(T)$	.006	-.002	-.015	-.030	-.041	-.047	-.051	-.048	-.040	-.033	-.030	-.034
$b_5(T)$	-3.921	-3.876	-4.151	-4.532	-4.809	-4.924	-5.151	-5.568	-5.881	-5.529	-3.791	-.019
$b_6(T)$	-.095	-.098	-.114	-.127	-.128	-.123	-.112	-.110	-.113	-.110	-.080	-.006
$b_7^{(1)}(T)$	-.314	-.282	-.219	-.120	-.008	.052	.120	.161	.161	.127	.065	-.002
$b_7^{(2)}(T)$	-.264	-.260	-.238	-.151	-.012	.069	.144	.169	.152	.103	.004	-.144
M_{min}	3.429	3.389	3.604	3.780	3.810	3.773	3.814	3.991	4.155	3.897	2.376	.000
M_{max}	8.691	8.472	8.006	7.711	7.711	7.845	8.282	8.549	8.576	8.450	8.600	14.500
RESIDUES:												
p =.1	-.568	-.549	-.504	-.450	-.413	-.411	-.435	-.459	-.461	-.451	-.436	-.425
p =.2	-.378	-.363	-.330	-.291	-.267	-.269	-.290	-.303	-.293	-.281	-.274	-.272
p =.3	-.240	-.227	-.203	-.176	-.162	-.165	-.178	-.182	-.169	-.156	-.150	-.147
p =.4	-.121	-.112	-.096	-.080	-.073	-.077	-.086	-.086	-.074	-.064	-.061	-.059
p =.5	.007	.006	.003	.002	.003	.002	.001	.005	.015	.020	.016	.009
p =.6	.123	.117	.104	.092	.084	.083	.086	.093	.100	.103	.100	.094
p =.7	.236	.225	.201	.176	.162	.163	.175	.187	.189	.185	.178	.170
p =.8	.367	.349	.314	.277	.259	.265	.286	.296	.285	.272	.264	.257
p =.9	.557	.535	.491	.436	.398	.396	.421	.439	.423	.397	.372	.354
RESIDUE STATISTICS:												
$\mu(T)$	-.002	-.002	-.002	-.001	-.001	-.001	-.002	-.001	.002	.003	.001	-.001
$\sigma(T)$	.445	.426	.388	.343	.316	.317	.338	.352	.343	.328	.315	.305
$X^2(T)$	8.634	8.319	7.075	6.625	7.147	7.322	7.173	8.148	10.442	11.722	11.514	10.936
KS(T)	.032	.032	.031	.030	.031	.031	.031	.034	.040	.044	.046	.046

$\hat{b}_2(T)$, $\hat{b}_3(T)$, $\hat{b}_4(T)$, $\hat{b}_5(T)$, $\hat{b}_6(T)$, $\hat{b}_7^{(1)}(T)$, $\hat{b}_7^{(2)}(T)$, $M_{min}(T)$, $M_{max}(T)$, the nine smoothed calculated residue levels corresponding to $p^*(\varepsilon,T)$ = 0.1 through 0.9, the smoothed coefficients $\hat{\mu}(T)$, $\hat{\sigma}(T)$ in equation (I.5.2), the χ^2 and the Kolmogorov-Smirnov statistics. As in our previous analyses, the 12 periods presented will be sufficient for most practical computations, especially since the smoothness of the coefficients is such that any interpolation scheme will yield adequate estimates of FS(T) in the entire period range from 0.04 sec. to 14 sec.

I.6 Examples of Estimated Fourier Spectra

Figure I.6.1 presents four plots of estimated FS(T) spectra using equation (I.4.2). The top two plots are examples of FS(T) computed for magnitudes M = 4.5, 5.5, 6.5 and 7.5 at epicentral distance R = 0, focal depth H = 5 km, soil parameter s_L = 1 (stiff soil), for $p(\varepsilon,T)$ = 0.5 (equation (I.5.2)), and for horizontal and vertival motions. The solid lines in both plots correspond to the depth of sediments h = 0 km, while the dashed lines correspond to that of h = 4 km. The lower left figure illustrates the effect of epicentral distance R on the changes of spectral amplitudes for magnitude M = 6.5, focal depth H = 5 km, sedimentary depth h = 2 km, soil parameter s_L = 1, $p(\varepsilon,T)$ = 0.5 and for horizontal (solid lines) and vertical (dashed lines) components. Four sets of curves corresponding to R = 0, 25, 50 and 100 km are presented. The lower right plot in this figure illustrates the effect of focal depth H on the changes of spectral amplitudes for $p(\varepsilon,T)$ = 0.5, M = 6.5, R = 0 km, h = 2 km and s_L = 1 for both horizontal (solid) and vertical (dashed) components.

The diagonal dashed lines at the bottom of each plot in this and in all subsequent similar figures represent the average FS amplitude of the digitization and processing noise. The plot of each FS spectrum is presented only for those periods where the signal to noise ratios are not much less than unity, or where the slope of a curve in the log-log scale is not significantly greater than -1.

The trends of the computed FS(T) amplitudes in the figures presented here (I.6.1) are in many ways similar to those discussed in our previous analyses (Trifunac and Lee, 1985a). The top two sets of

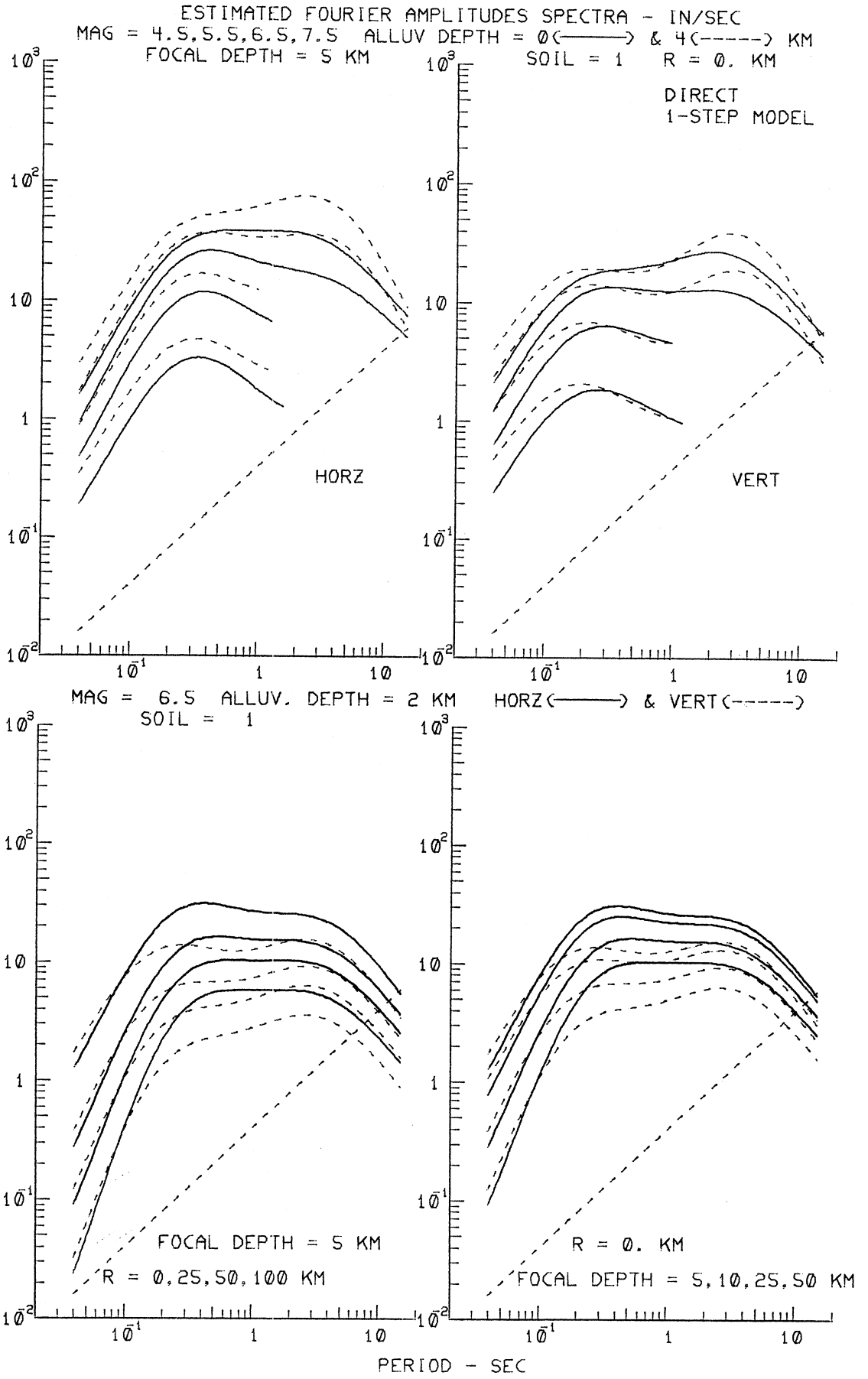
ESTIMATED FOURIER AMPLITUDES SPECTRA - IN/SEC
MAG = 4.5,5.5,6.5,7.5 ALLUV DEPTH = 0(———) & 4(-----) KM
FOCAL DEPTH = 5 KM
SOIL = 1 R = 0. KM
DIRECT
1-STEP MODEL
HORZ
VERT
MAG = 6.5 ALLUV. DEPTH = 2 KM
SOIL = 1
HORZ(———) & VERT(-----)
FOCAL DEPTH = 5 KM
R = 0,25,50,100 KM
R = 0. KM
FOCAL DEPTH = 5,10,25,50 KM
PERIOD - SEC

Figure I.6.1

graphs show that, as before, the rate of growth of amplitudes with magnitudes M decreases as M approached 7.5. The effect of local geologic conditions (alluvial depth), is significant for the whole range of periods from 0.04 sec. to 14 sec. for both horizontal and for vertical motions. This is now different from what we found in our previous analyses, where the geologic site characteristics were found to play an important role only at intermediate and long periods and no significant role at high frequencies. This difference can be attributed to the new form of the dependence of the site characteristics in the present analyses (equation (I.3.2)) on h and v simultaneously:

$$b_2(T)h + b_4(T)hv = (b_2(T) + b_4(T)v)h \quad , \qquad (I.6.1)$$

which results in the coefficient for the site characteristics to be component dependent. These new trends are also dependent on the simultaneous consideration of soil and geologic site conditions. The two plots at the bottom (of Figure I.6.1) exhibit similar characteristics and trends as found in our previous analyses.

Figure I.6.2 presents another four plots of estimated FS(T) amplitudes, to illustrate the effect of local soil conditions on FS(T). The top two plots are examples of FS(T) computed for magnitudes M = 4.5, 5.5, 6.5 and 7.5 at epicentral distance R = 0, focal depth H = 5 km, alluvial depth h = 2 km, for $p(\varepsilon,T) = 0.5$, and for the horizontal (v = 0) and vertical (v = 1) motions. The solid lines in both plots correspond to the local soil condition $s_L = 0$ (rock) while the dashed lines correspond to $s_L = 2$ (deep soil). The bottom two plots show examples of FS(T) for magnitude M = 6.5, epicentral distances R = 0, 25, 50 and 100 km, focal depth H = 5 km, alluvial depth h = 2 km, for $p(\varepsilon,T) = 0.5$, and for

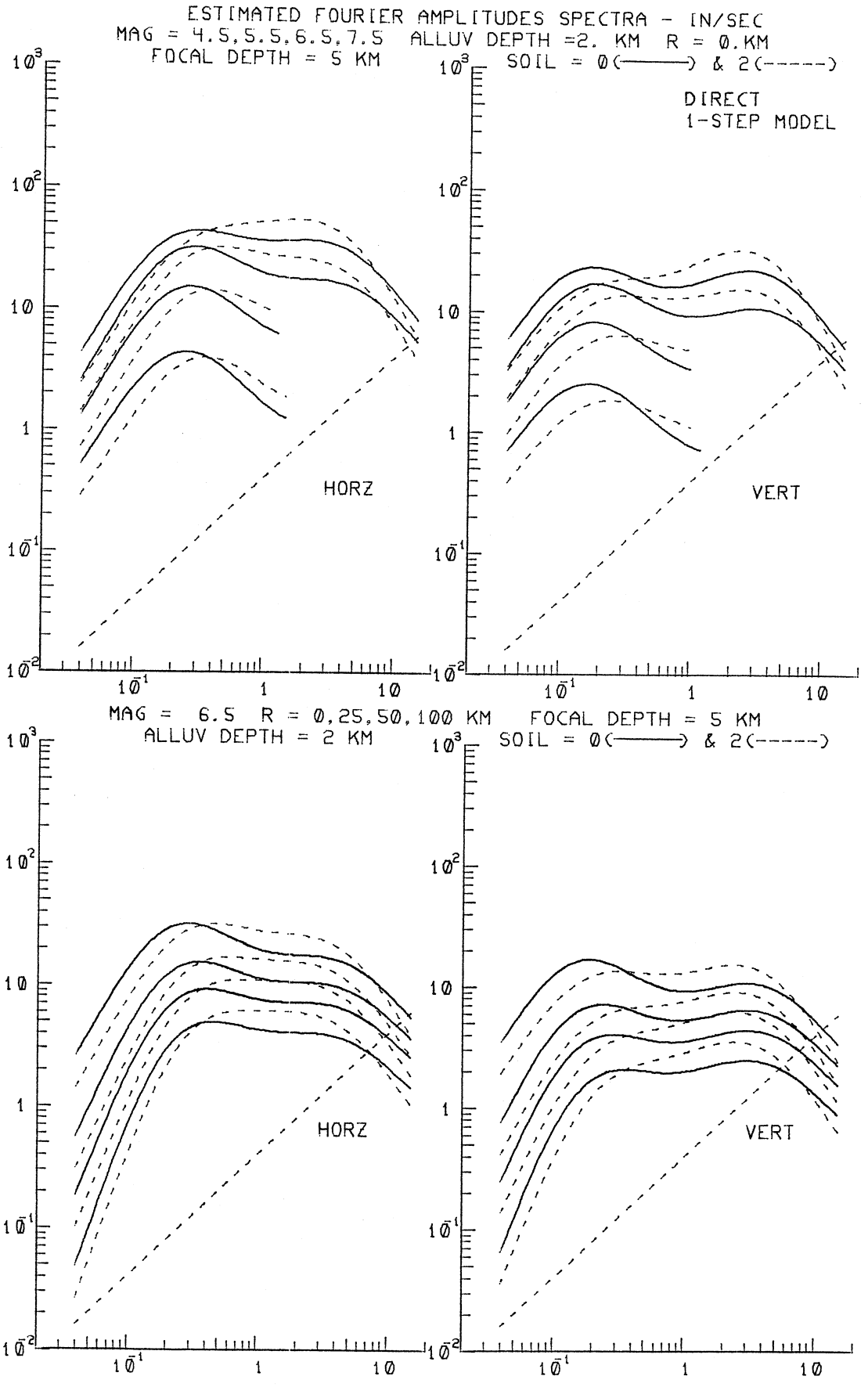
ESTIMATED FOURIER AMPLITUDES SPECTRA - IN/SEC
MAG = 4.5,5.5,6.5,7.5 ALLUV DEPTH =2. KM R = 0.KM
FOCAL DEPTH = 5 KM
SOIL = 0(——) & 2(-----)
DIRECT
1-STEP MODEL
HORZ
VERT
MAG = 6.5 R = 0,25,50,100 KM FOCAL DEPTH = 5 KM
ALLUV DEPTH = 2 KM
SOIL = 0(——) & 2(-----)
HORZ
VERT
PERIOD - SEC

Figure I.6.2

horizontal (v = 0) and vertical (v = 1) motions. The solid lines again correspond to s_L = 0 and the dashed lines to s_L = 2. In each set of the graphs, it is observed that for periods up to ~ 0.35 sec., the Fourier amplitudes FS(T) at rock sites (s_L = 0) are higher than those at deep soil sites (s_L = 2). Beyond 0.35 sec., this trend is reversed up to the periods of about 10 sec. so that for these intermediate periods, the Fourier amplitudes at deep soil sites are higher than those at the rock sites.

Figures I.6.3 and I.6.4 compare the differences of the effects the local geologic and local soil site characteristics have on FS(T). Figure I.6.3 consists of three plots, one for each local soil classification (s_L = 0, 1 and 2). For each plot, the FS(T) has been computed for the depth of alluvium equal to 0, 2 and 4 km. This figure shows that for all local soil site classifications, in the whole period range considered, the higher the alluvial depth, the higher will be the Fourier amplitudes. Figure I.6.4 also shows three plots, one for each alluvial depth equal to 0, 2 and 4 km. For each alluvium depth, the soil classification ranges from s_L = 0 (rock) to 1 (stiff soil) and to 2 (deep soil). It is seen that for periods up to ~ 0.3 sec. the Fourier amplitudes, FS(T), on s_L = 0 (rock) sites are higher than those with s_L = 1 (stiff soil), or s_L = 2 (deep soil). Beyond ~ 0.3 sec., this trend is reversed up to periods of about 10 sec., a trend also indicated earlier in Figure I.6.2. The two figures (I.6.3 and I.6.4) show that local alluvium depth and local soil parameters have different characteristics at different period ranges and that both are significant but in a different way.

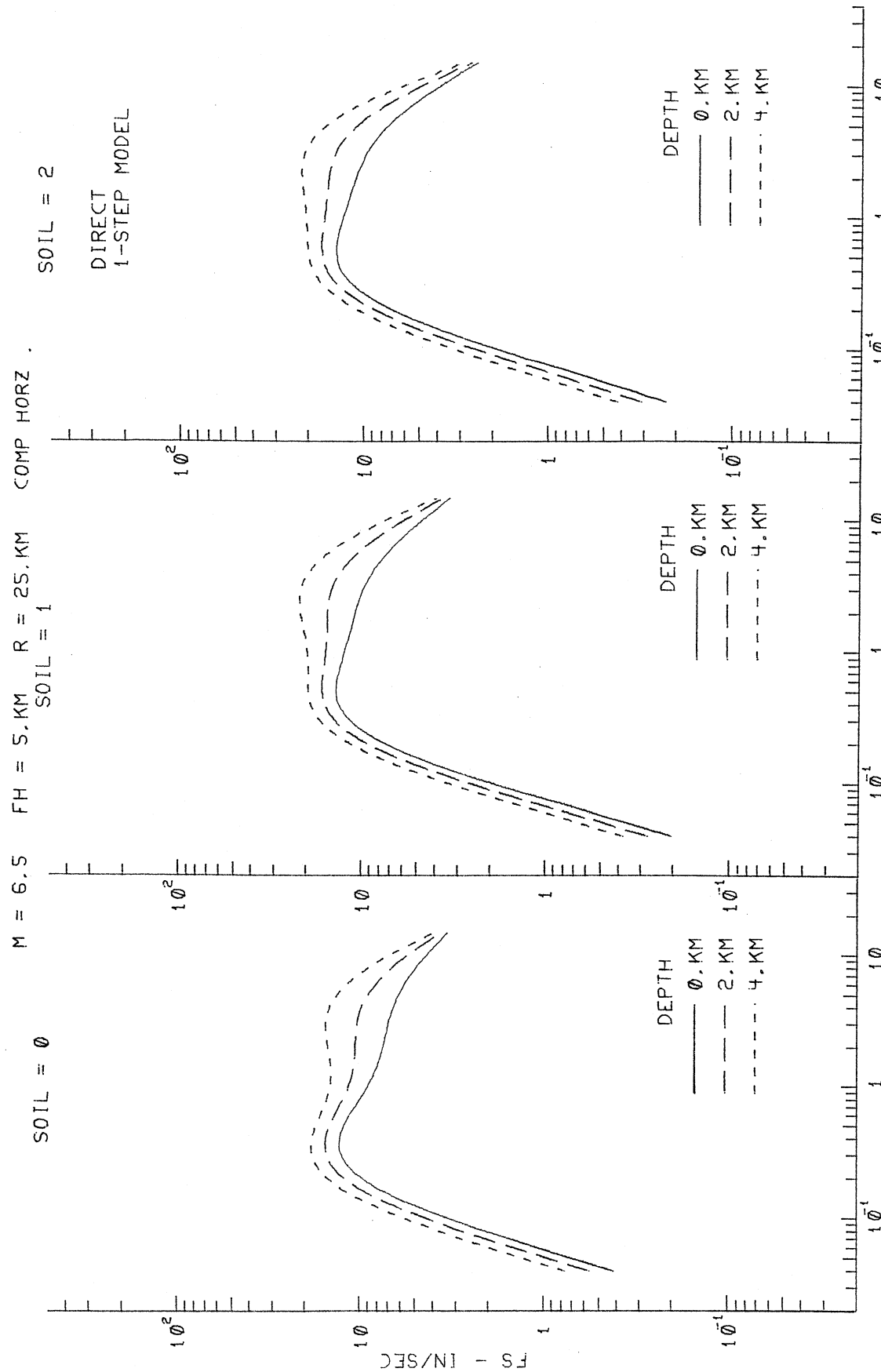
M = 6.5 FH = 5.KM R = 25.KM COMP HORZ .
SOIL = 0
SOIL = 1
SOIL = 2
DIRECT
1-STEP MODEL
DEPTH
0.KM
2.KM
4.KM
FS - IN/SEC
PERIOD - SEC

Figure I.6.3

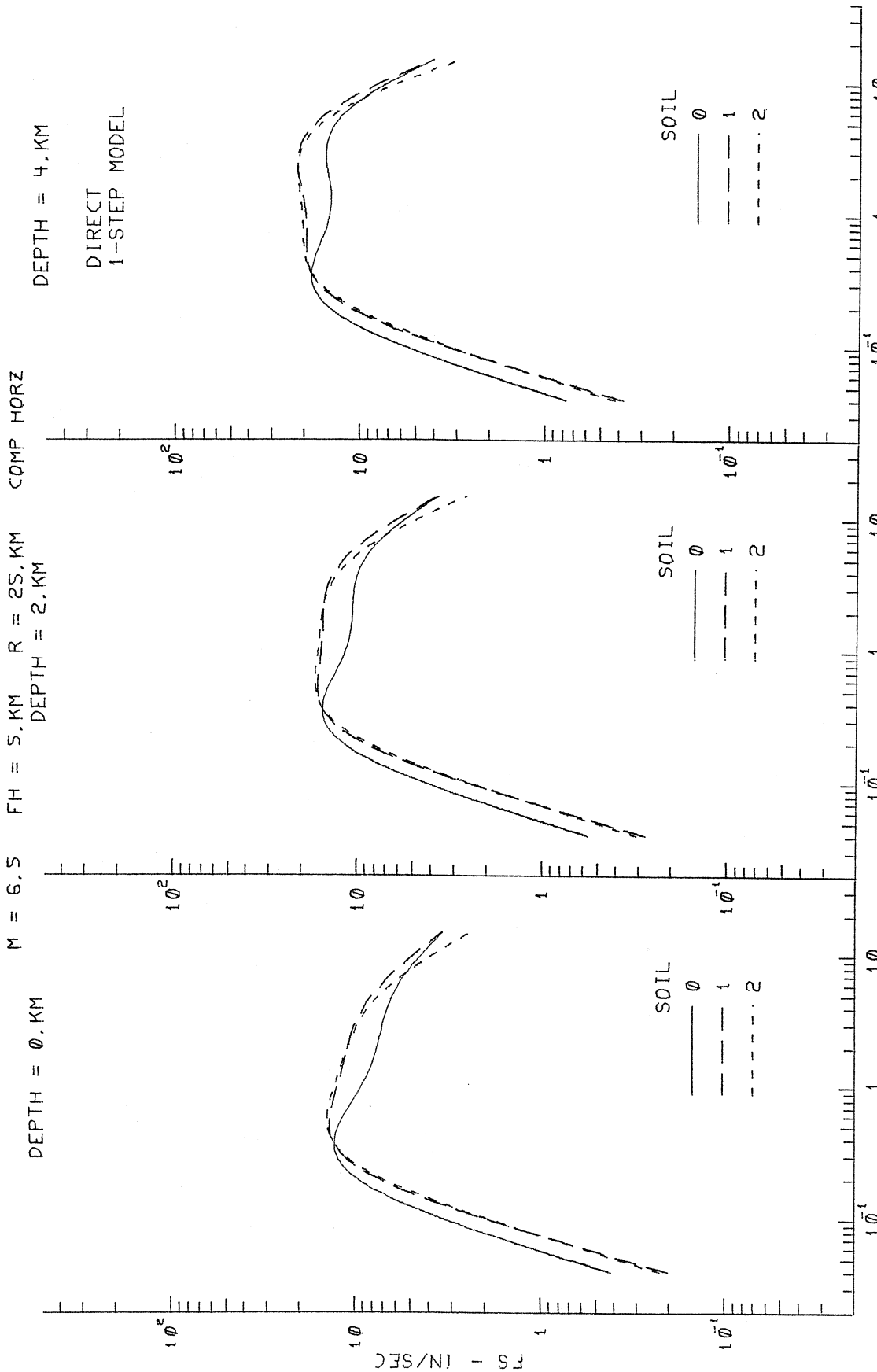
M = 6.5
FH = 5.KM
R = 25.KM
COMP HORZ
DEPTH = 0.KM
DEPTH = 2.KM
DEPTH = 4.KM
DIRECT
1-STEP MODEL
SOIL
0
1
2
FS - IN/SEC
PERIOD - SEC

Figure I.6.4

I.7 Actual Versus Estimated Fourier Spectra

Figures I.7.1 through I.7.9 show examples of how horizontal and vertical Fourier spectra computed from equation (I.4.2) compare with the actual Fourier spectra for the corresponding components of recorded strong-motion data at various sites. The various sites chosen here correspond to different combinations of the local soil and geological site classifications. Table I.7.1 shows the local soil classifications and depth of sediments at the chosen sites. The record reference names of the files used here (AG106,AJ141, etc.) correspond to our standard accelerogram file names in the uniform data base used here (Lee and Trifunac, 1987, EQINFOS Part 1). Table I.7.1 shows that for each soil classification (s_L = 0, 1 and 2), sites corresponding to small, medium and large alluvial depths have been chosen. In figures I.7.1 through I.7.9, the $\log_{10}FS(T)$ spectra were computed for the probability of exceedance (equation I.5.2) $p(\varepsilon,T)$ = 0.1, 0.5 and 0.9. The interval between the spectra for p = 0.1 and 0.9 then represents an estimate of the 80% confidence interval. At the top of each plot, the first line of the title identifies the record reference name, the location of the site and the year of the recording. The second line of title gives the parameters at the site that are used for the calculation of the estimated FS(T). This includes magnitude and focal depth of the earthquake, epicentral distance, local depth of alluvium and the local soil classification at the site. The left plot presents spectra for the two horizontal components of the recorded accelerations while the right plot shows the spectra for the vertical component. As can be seen from these figures, the agreement between the recorded and the estimated

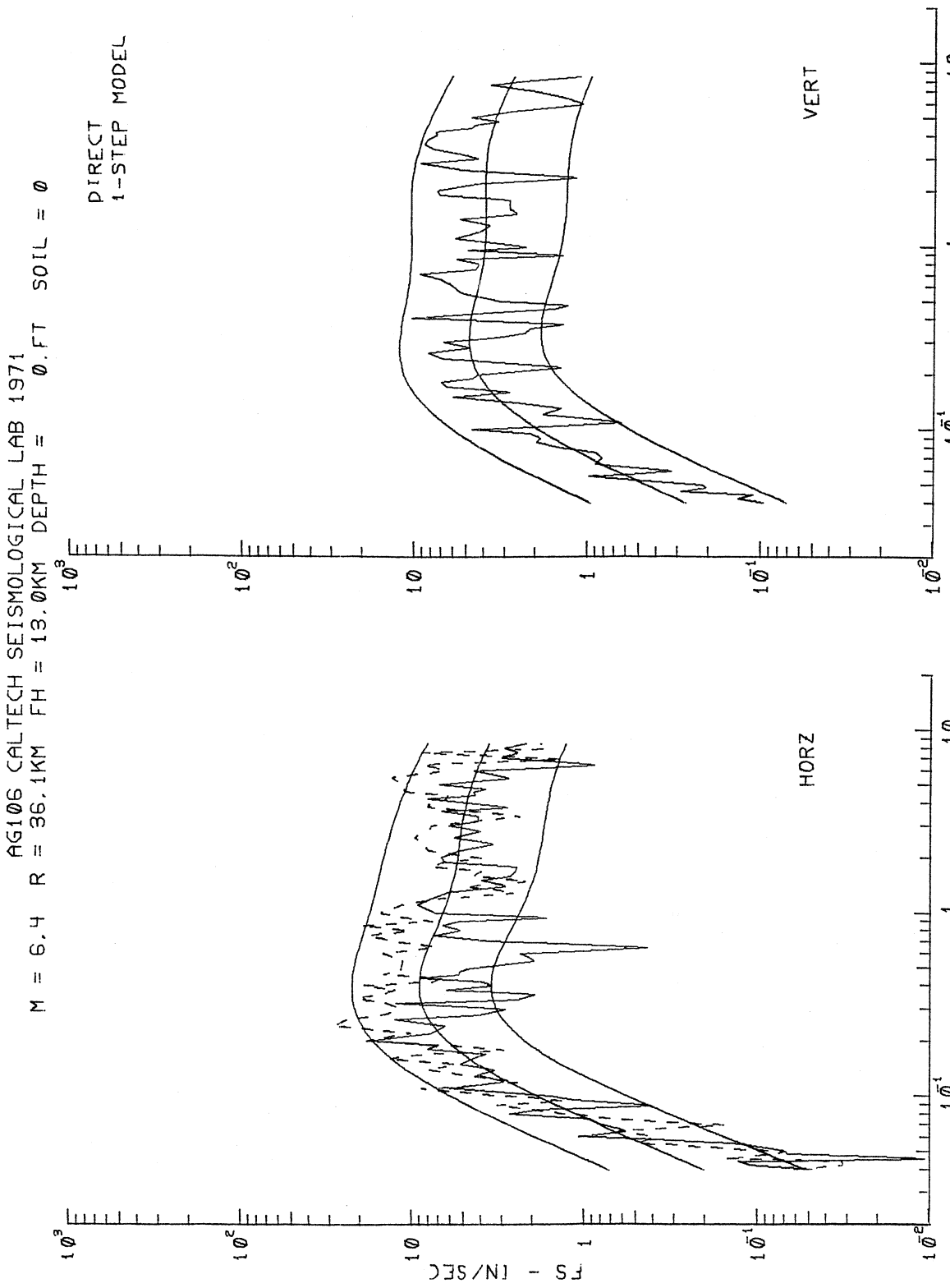
AG106 CALTECH SEISMOLOGICAL LAB 1971
M = 6.4 R = 36.1KM FH = 13.0KM DEPTH = 0.FT SOIL = 0
DIRECT
1-STEP MODEL
VERT
HORZ
FS - IN/SEC
PERIOD - SEC

Figure I.7.1

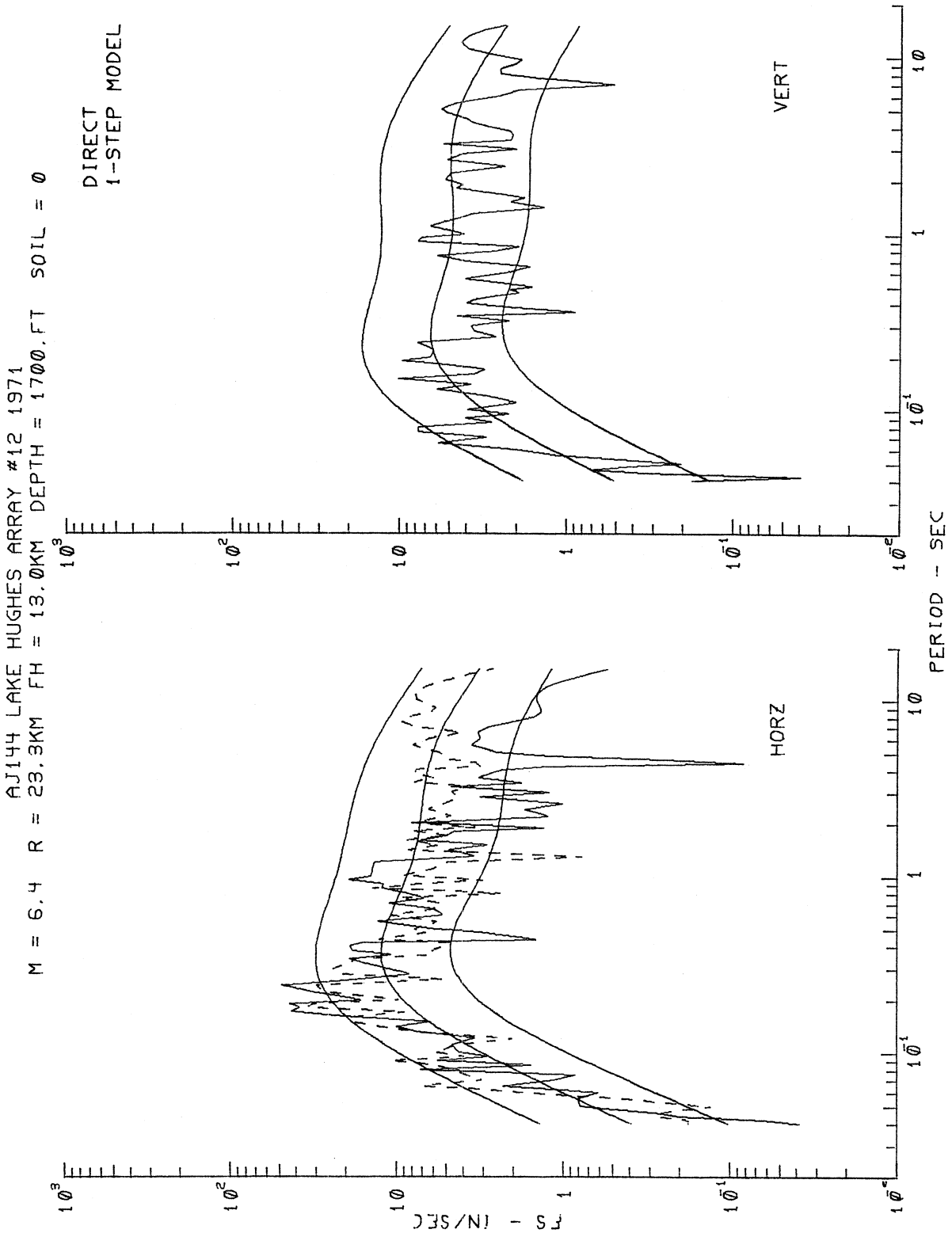
AJ144 LAKE HUGHES ARRAY #12 1971
M = 6.4 R = 23.3KM FH = 13.0KM DEPTH = 1700.FT SOIL = 0
DIRECT
1-STEP MODEL
VERT
HORZ
FS - IN/SEC
PERIOD - SEC

Figure I.7.2

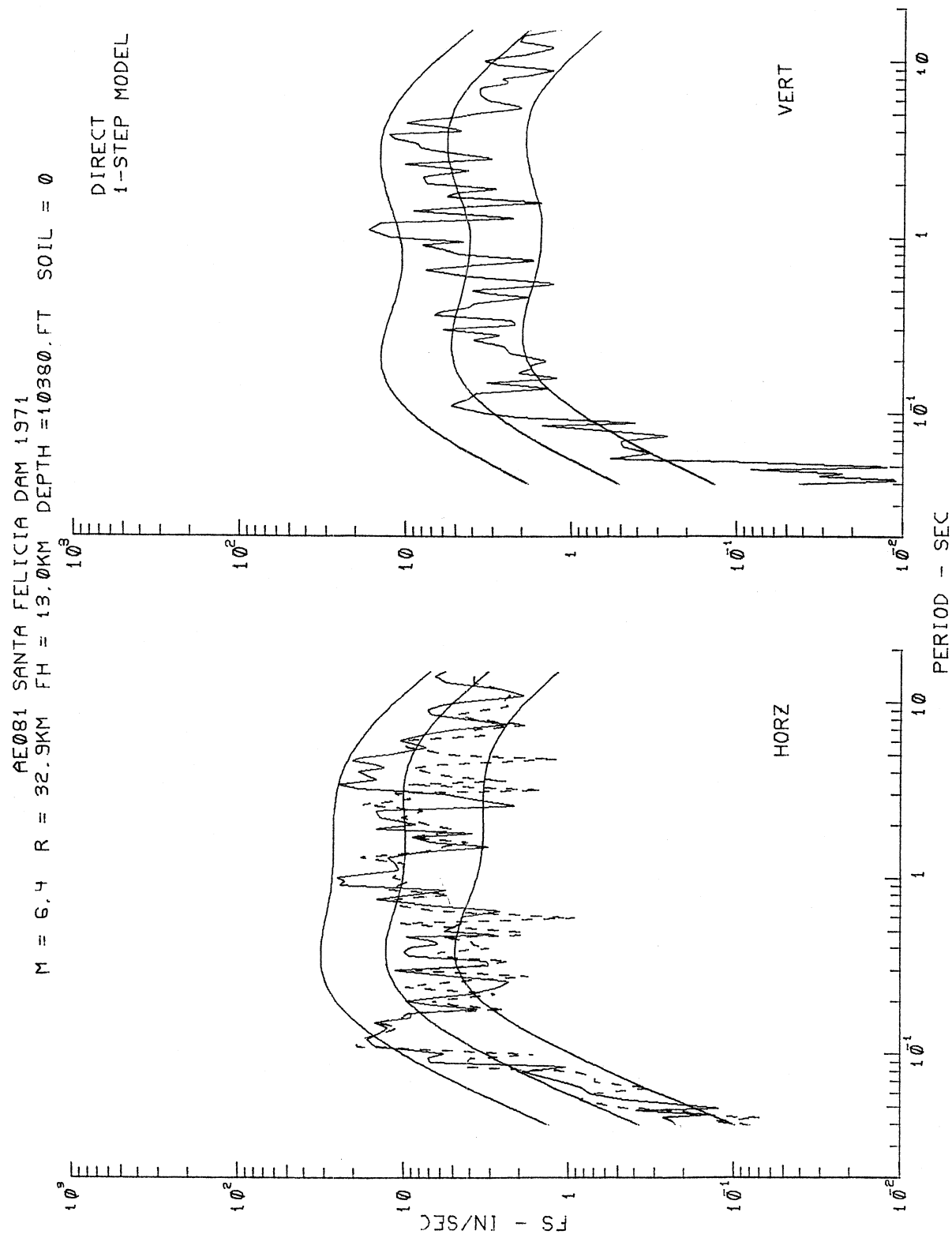
AE081 SANTA FELICIA DAM 1971
M = 6.4 R = 32.9KM FH = 13.0KM DEPTH =10380.FT SOIL = 0
DIRECT
1-STEP MODEL
VERT
HORZ
FS - IN/SEC
PERIOD - SEC

Figure I.7.3

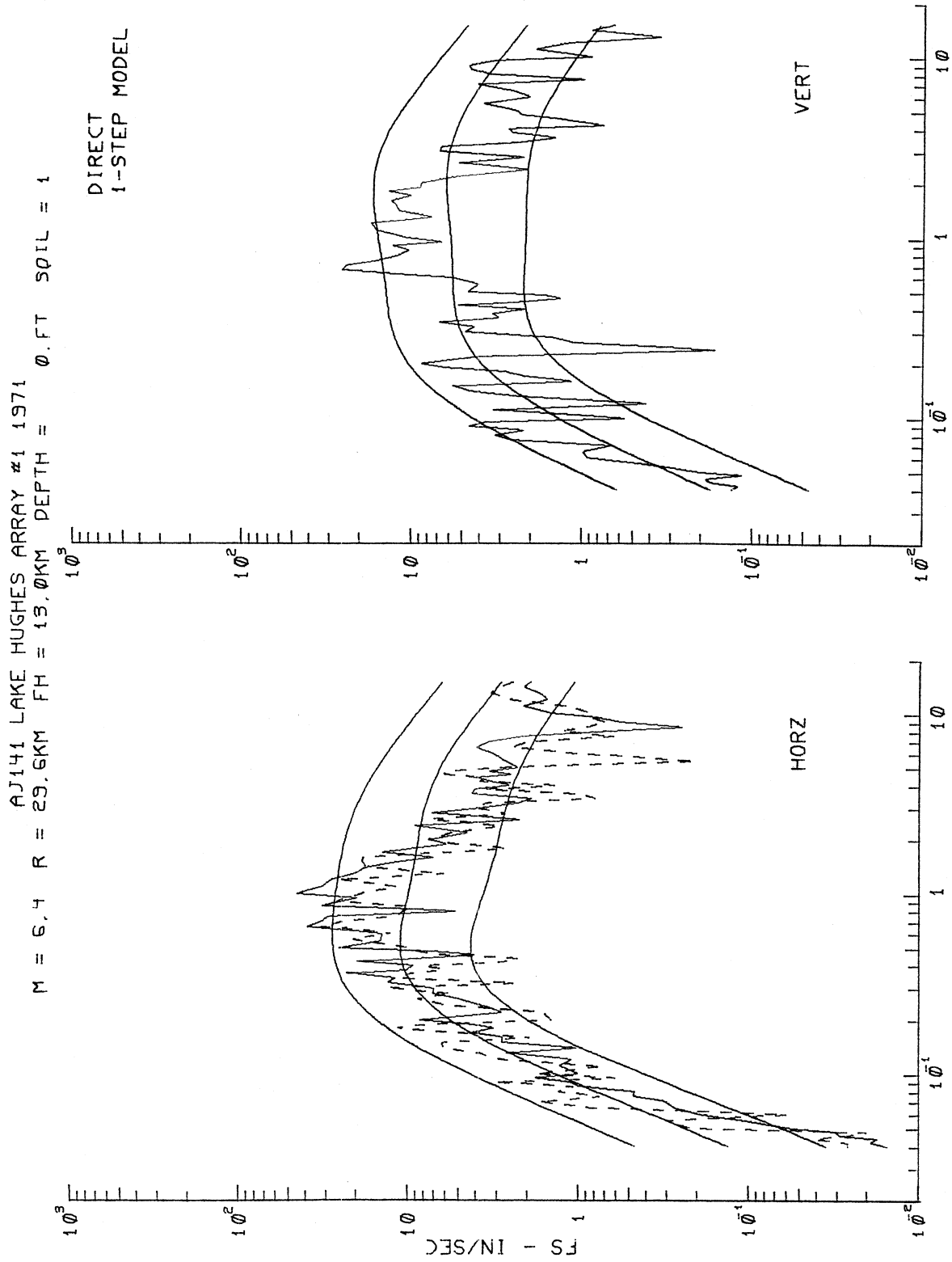
AJ141 LAKE HUGHES ARRAY #1 1971
M = 6.4 R = 29.6KM FH = 13.ØKM DEPTH = Ø.FT SOIL = 1
DIRECT
1-STEP MODEL
VERT
HORZ
FS - IN/SEC
PERIOD - SEC

Figure I.7.4

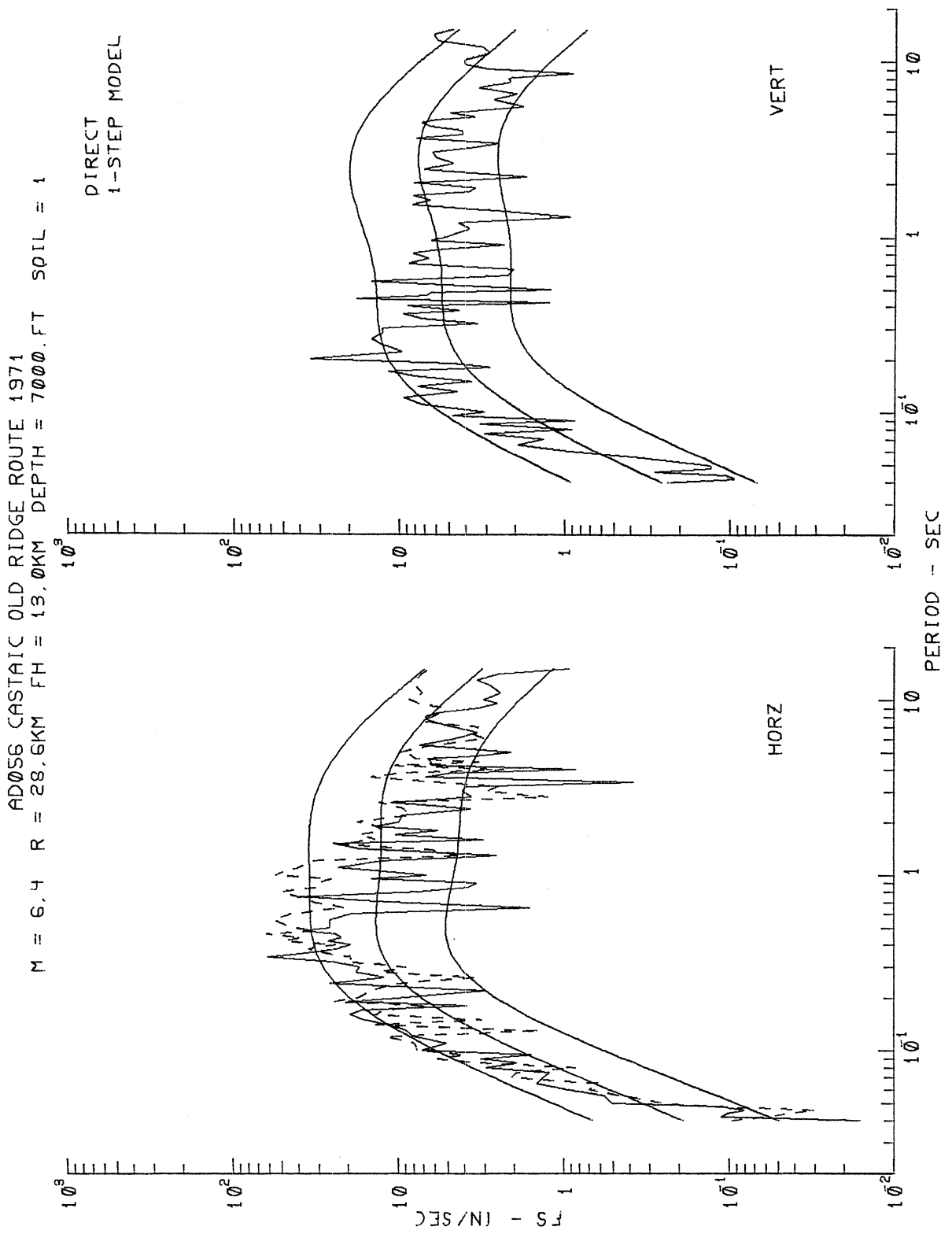
AD056 CASTAIC OLD RIDGE ROUTE 1971
M = 6.4 R = 28.6KM FH = 13.0KM DEPTH = 7000.FT SOIL = 1
DIRECT
1-STEP MODEL
VERT
HORZ
FS - IN/SEC
PERIOD - SEC

Figure I.7.5

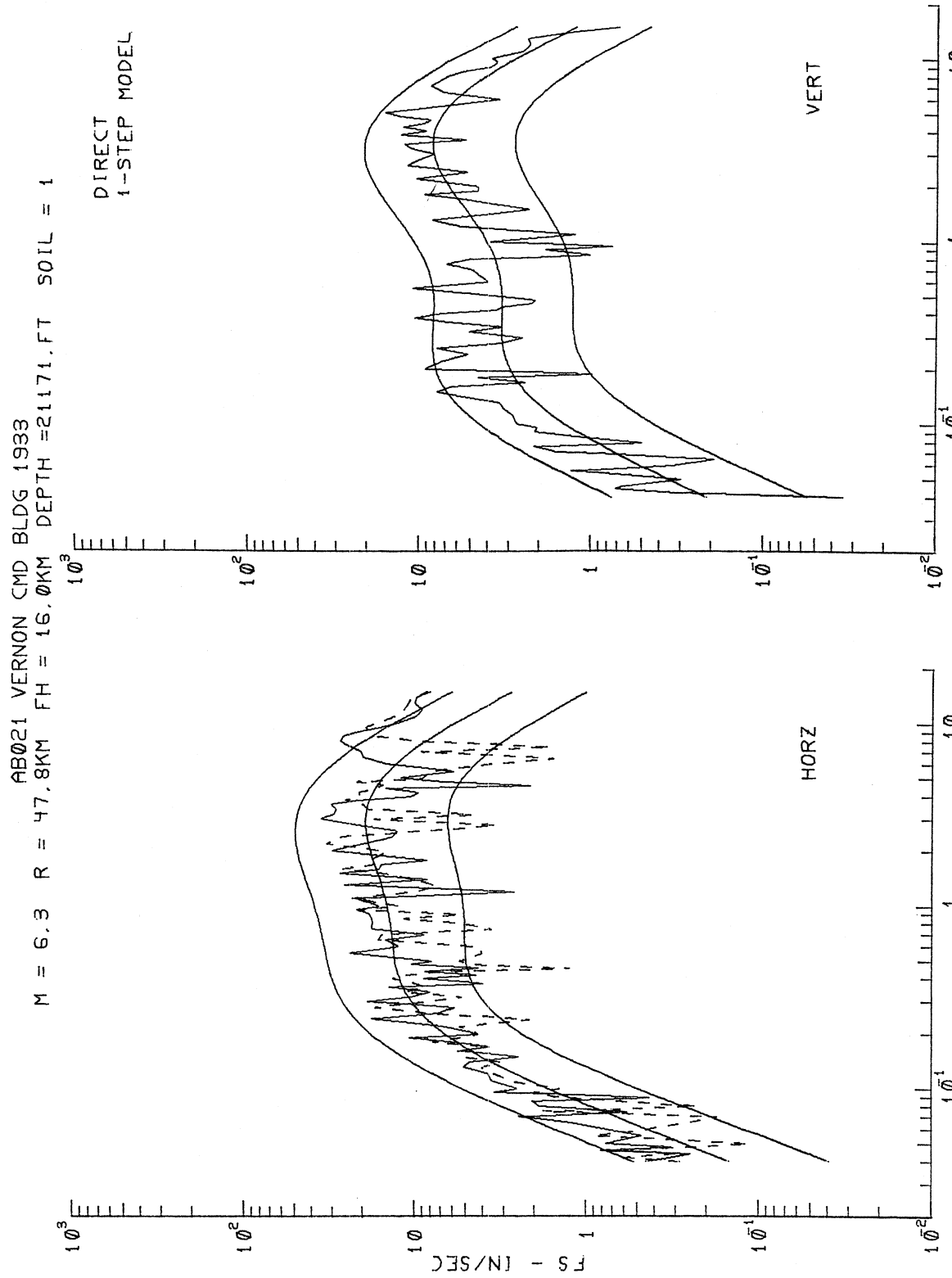
AB021 VERNON CMD BLDG 1933
M = 6.3 R = 47.8KM FH = 16.ØKM DEPTH =21171.FT SOIL = 1
DIRECT
1-STEP MODEL
HORZ
VERT
FS - IN/SEC
PERIOD - SEC

Figure I.7.6

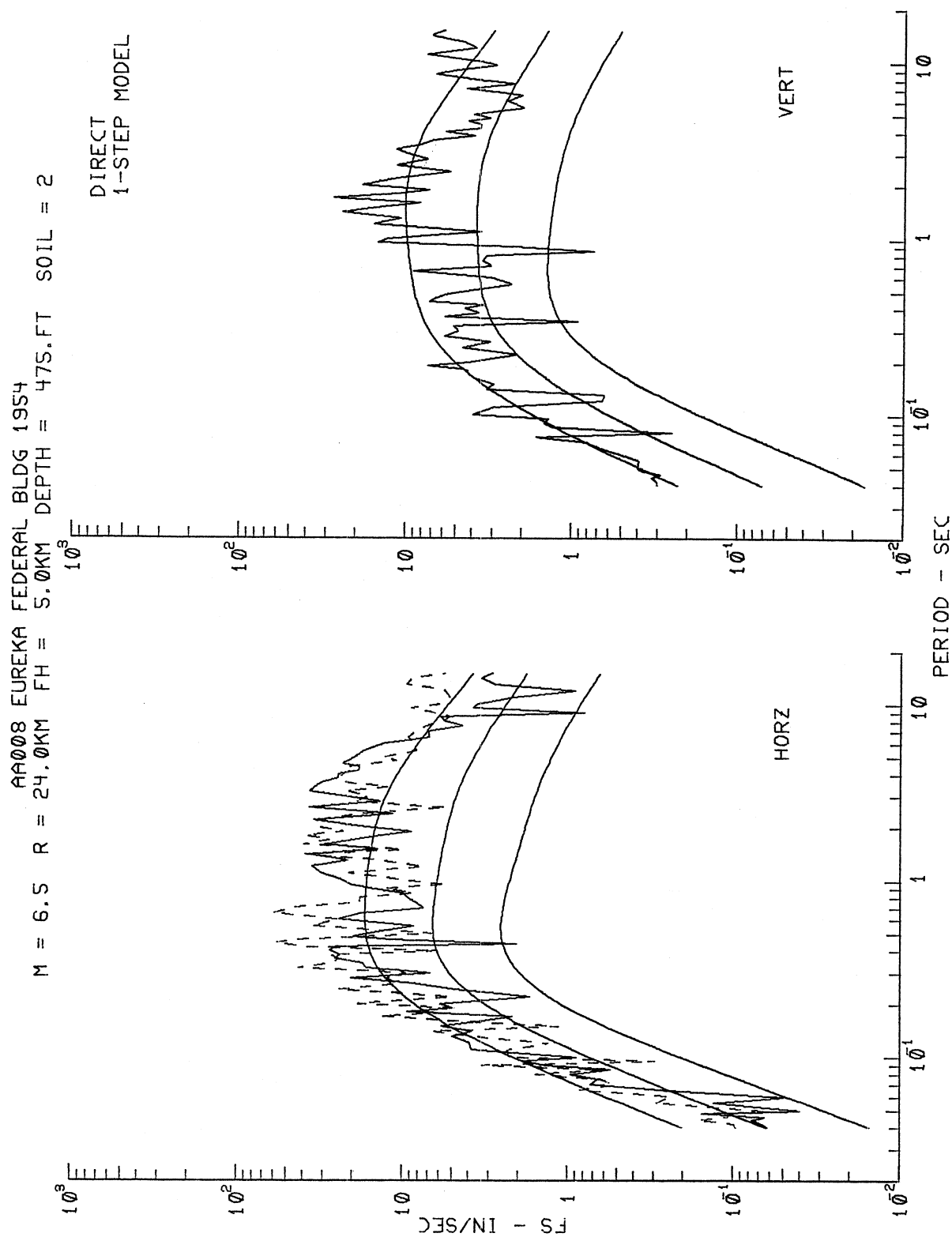
AA008 EUREKA FEDERAL BLDG 1954
M = 6.5 R = 24.0KM FH = 5.0KM DEPTH = 475.FT SOIL = 2
DIRECT
1-STEP MODEL
VERT
HORZ
FS - IN/SEC
PERIOD - SEC

Figure I.7.7

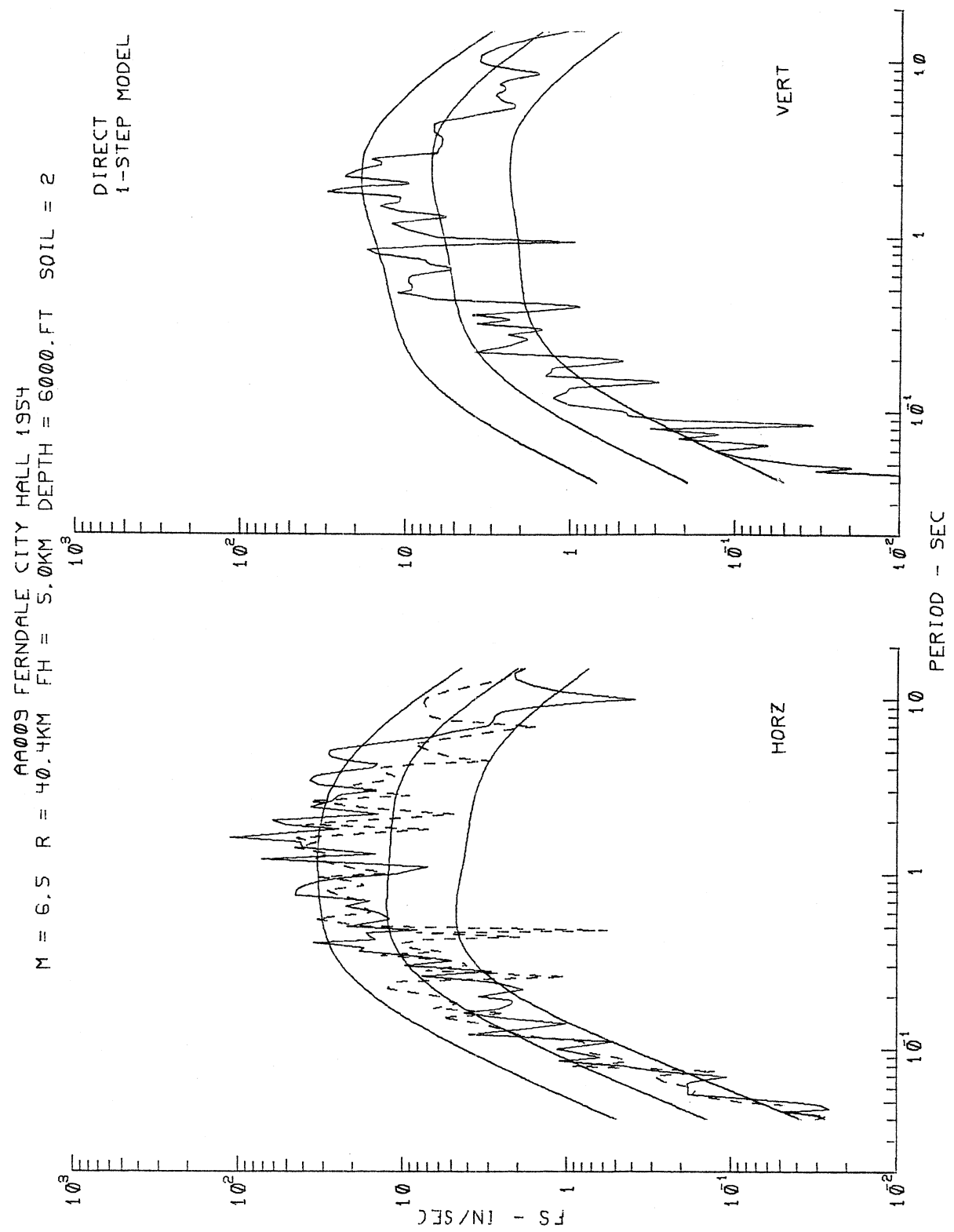
AA009 FERNDALE CITY HALL 1954
M = 6.5 R = 40.4KM FH = 5.0KM DEPTH = 6000.FT SOIL = 2
DIRECT
1-STEP MODEL
VERT
HORZ
FS - IN/SEC
PERIOD - SEC

Figure I.7.8

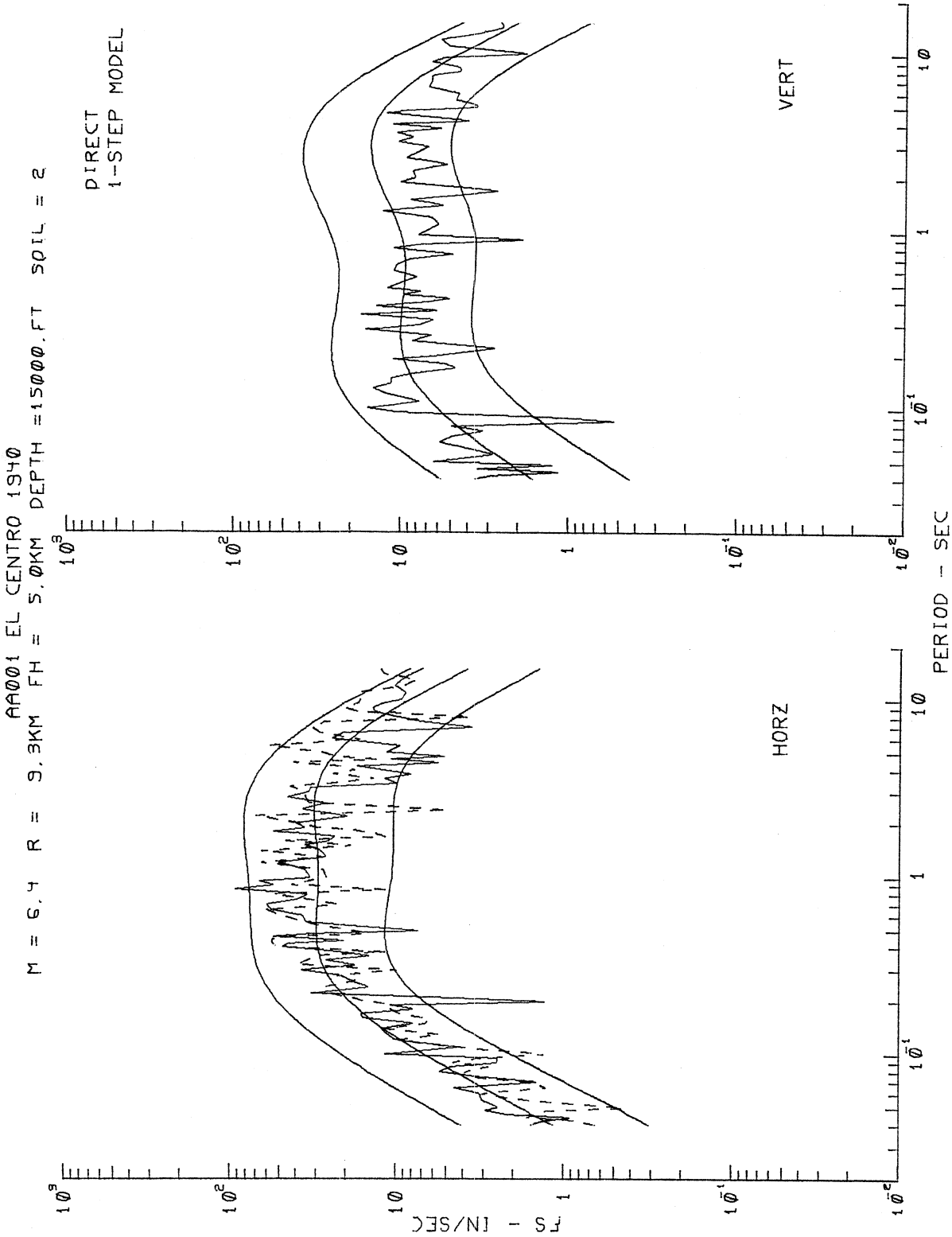
AA001 EL CENTRO 1940
M = 6.4 R = 9.3KM FH = 5.0KM DEPTH =15000.FT SOIL = 2
DIRECT
1-STEP MODEL
HORZ
VERT
FS - IN/SEC
PERIOD - SEC

Figure I.7.9

TABLE I.7.1

Alluvial Depth, h \ Soil	ROCK (s_L = 0)	STIFF SOIL (s_L = 1)	DEEP SOIL (s_L = 2)
SMALL	AG106 h = 0 ft.	AJ141 h = 0 ft.	AA008 h = 475 ft.
MEDIUM	AJ144 h = 1700 ft.	AD056 h = 6000 ft.	AA009 h = 6000 ft.
LARGE	AE081 h = 10380 ft.	AB021 h = 21171 ft.	AA001 h = 15000 ft.

spectra in each case is good. Comparing the last figure (Figure I.7.9) for El Centro, 1940, with the corresponding figures in our previous analysis (Trifunac and Lee, 1985a) for both the horizontal and vertical components it is seen that the 80% confidence interval in this analysis is narrower.

I.8 The Residue Two-Step Model

The previous sections in this part have dealt with the direct, "1-step," model where the scaling of Fourier spectra in terms of M, R, H, S, h, s_L and v has been performed in one step, with the soil indicator variables included in the regression equation directly. Here we consider another alternative in which our previous regression model (equation (I.1.1)) which doesn't include soil classification may have already been used and the scaling functions $\hat{b}_1(T)$ through $\hat{b}_6(T)$ estimated. Let $\log_{10}\hat{FS}(T)$ be such estimated Fourier amplitudes,

$$\log_{10}FS(T) = M_< + \mathcal{A}tt(\Delta,M,T) + \hat{b}_1(T)M_{<>} + \hat{b}_2(T)h + \hat{b}_3(T)v + \hat{b}_4(T)hv + \hat{b}_5(T) + \hat{b}_6(T)M^2_{<>} \quad . \tag{I.8.1}$$

To study the influence that the additional soil classification may have on the Fourier spectral amplitudes, the residues with respect to our previous regression model can first be calculated:

$$\varepsilon(T) = \log_{10}FS(T) - \log_{10}\hat{FS}(T) \quad , \tag{I.8.2}$$

with $\log_{10}FS(T)$ representing the actual Fourier amplitudes. The residues at each site where soil classification is available can then be fitted by the equation

$$\varepsilon(T) = b_7^{(1)}(T)S_L^{(1)} + b_7^{(2)}(T)S_L^{(2)} + b_8(T) \tag{I.8.3}$$

where $S_L^{(1)}$ and $S_L^{(2)}$ are the indicator variables for s_L as defined previously, $b_7^{(1)}(T)$ and $b_7^{(2)}(T)$ are the corresponding scaling functions and $b_8(T)$ is a new additional constant coefficient. Equation (I.8.2) can now be combined with equation (I.8.1) to become:

$$\log_{10}\hat{FS}(T) = M_{<} + \mathcal{A}tt(\Delta,M,T) +$$

$$\hat{c}_1(T)M_{<>} + \hat{c}_2(T)h + \hat{c}_3(T)v + \hat{c}_4(T)hv + \hat{c}_5(T) + \hat{c}_6(T)M_{<>}^2 +$$

$$\hat{c}_7^{(1)}(T)S_L^{(1)} + \hat{c}_7^{(2)}(T)S_L^{(2)} \quad , \qquad \text{(I.8.3)}$$

where $\hat{c}_i(T) = \hat{b}_i(T)$ except for the scaling function $\hat{c}_5(T)$ for the constant 1, which is given by

$$\hat{c}_5(T) = \hat{b}_5(T) + \hat{b}_8(T) \quad . \qquad \text{(I.8.4)}$$

The variance of $\hat{c}_5(T)$, $\hat{\sigma}_{c5}(T)$, is given by the root-mean-square (R.M.S.) of the variances of $\hat{b}_5(T)$ and $\hat{b}_8(T)$:

$$\hat{\sigma}_{c5}(T) = (\hat{\sigma}_{b5}^2(T) + \hat{\sigma}_{b8}^2(T))^{\frac{1}{2}} \quad . \qquad \text{(I.8.5)}$$

This procedure will be referred to as the residue "2-step" model in contrast with the direct "1-step" model presented earlier. The regression analyses and subsequent plots can now be repeated for the "MAG-DEPTH-SOIL" model as given in Part I.8 of this work. Figures I.8.1 through I.8.16 are an identical set of plots for the "2-step" model as Figures I.5.1 through I.7.9 for the direct "1-step model." Table I.8.1 shows the correspondence of the figure numbers, in these two models.

Comparisons of the corresponding figures of the direct "1-step" model and the residue "2-step" model show a lot of similarity between the two analyses. The shapes of the scaling functions are very similar, the residues for the nine probability levels have almost identical widths, and the estimated FS amplitudes are also very similar. One advantage that the residue "2-step" model has over the direct "1-step" model is that in the "2-step" model, the first step of regression (equation

TABLE I.8.1
FIGURE NUMBERS OF THE MAG-DEPTH-SOIL MODEL

Figure Description	Direct 1-step Model	Residue 2-step Model
Scaling Functions	I.5.1	I.8.1
Residue Levels	I.5.2	I.8.2
Residue Statistics	I.5.3	I.8.3
Estimated FS	I.6.1-I.6.4	I.8.4-I.8.7
Actual vs. Estimated FS	I.7.1-I.7.9	I.8.8-I.8.16

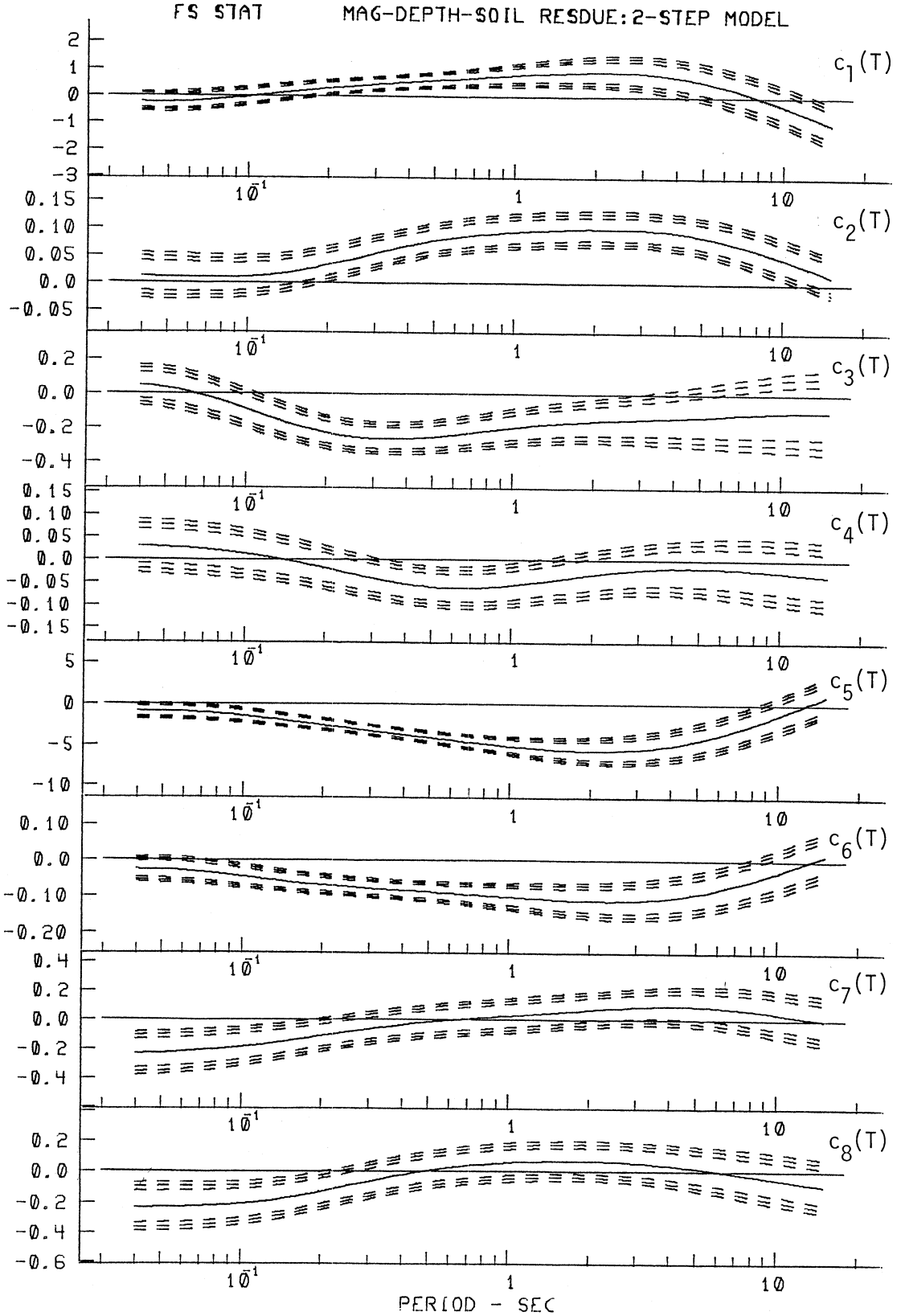
FS STAT
MAG-DEPTH-SOIL RESDUE:2-STEP MODEL
$c_1(T)$
$c_2(T)$
$c_3(T)$
$c_4(T)$
$c_5(T)$
$c_6(T)$
$c_7(T)$
$c_8(T)$
PERIOD - SEC

Figure I.8.1

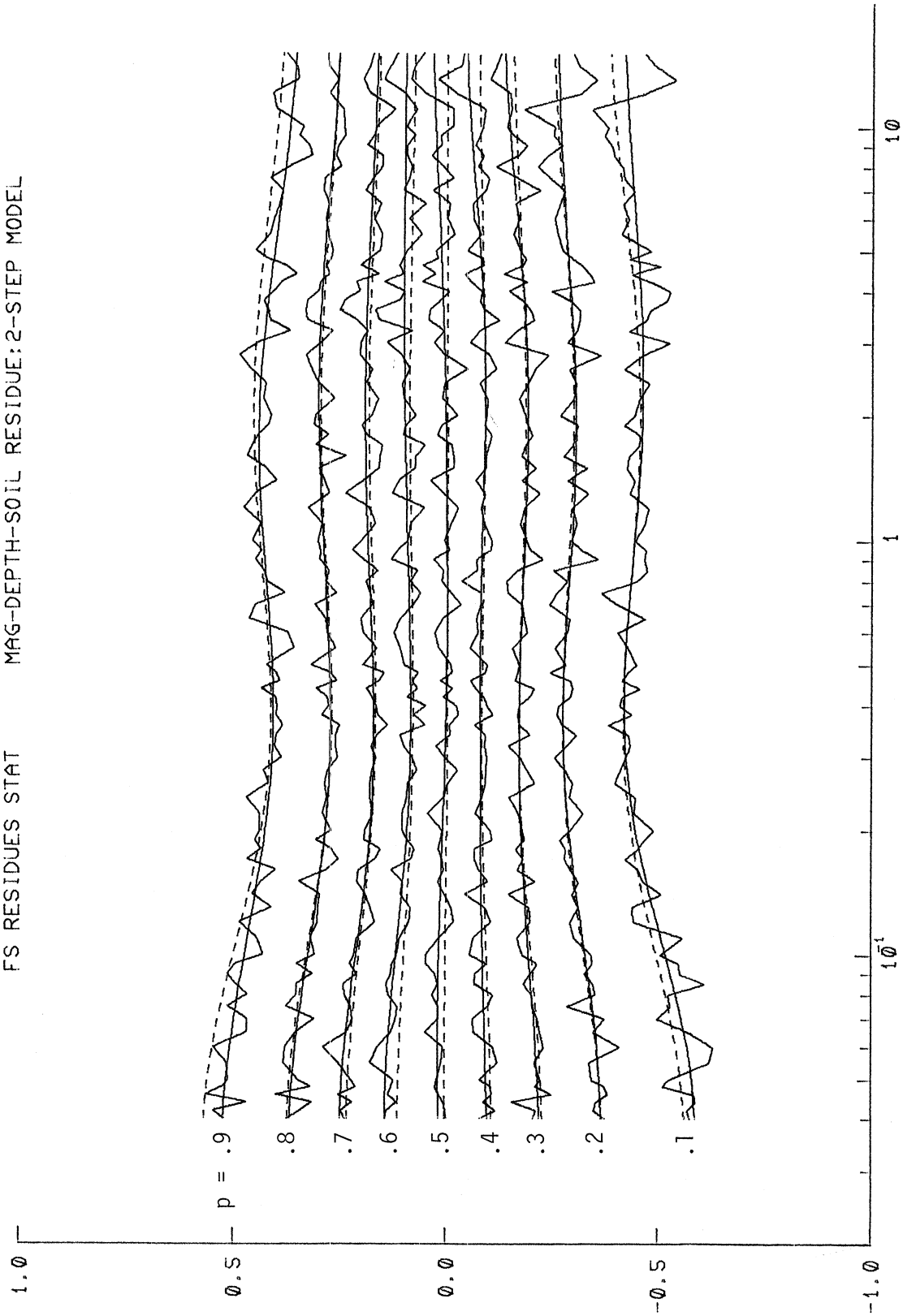
FS RESIDUES STAT
MAG-DEPTH-SOIL RESIDUE; 2-STEP MODEL
1.0
0.5
0.0
-0.5
-1.0
p = .9
.8
.7
.6
.5
.4
.3
.2
.1
10^-1
1
10

Figure I.8.2

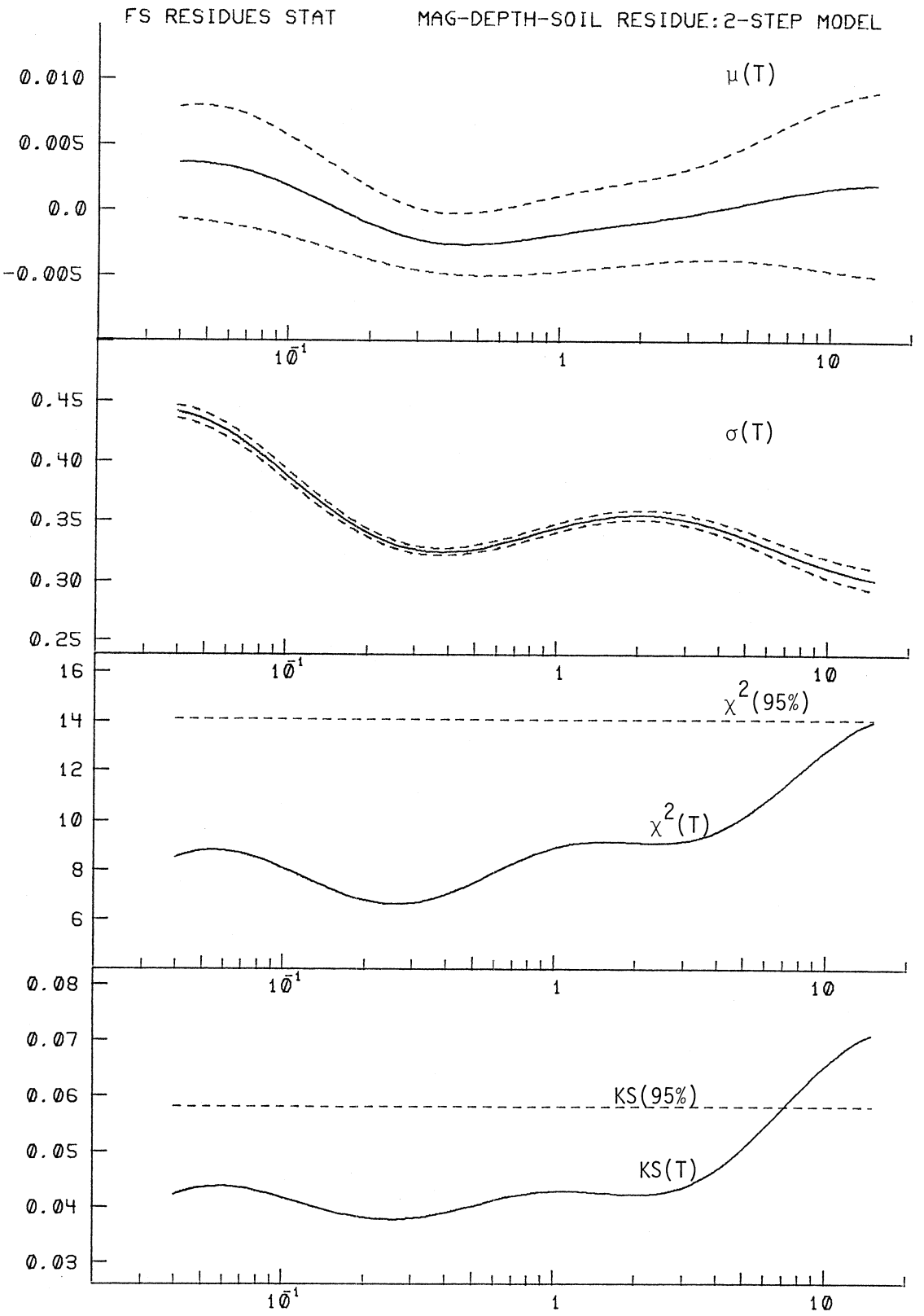
FS RESIDUES STAT
MAG-DEPTH-SOIL RESIDUE: 2-STEP MODEL
μ(T)
0.010
0.005
0.0
-0.005
σ(T)
0.45
0.40
0.35
0.30
0.25
χ²(95%)
χ²(T)
16
14
12
10
8
6
KS(95%)
KS(T)
0.08
0.07
0.06
0.05
0.04
0.03
10⁻¹
1
10

Figure I.8.3

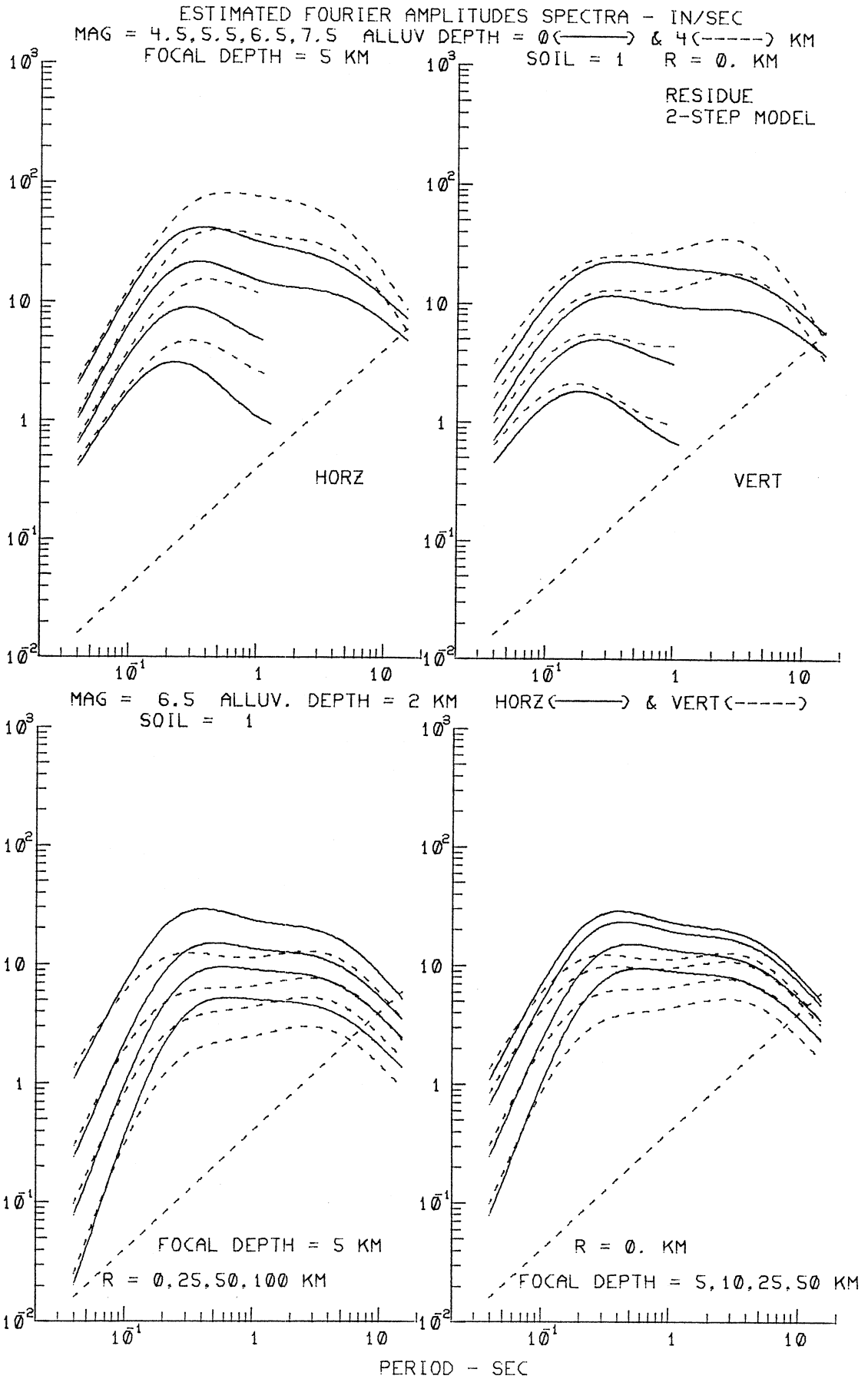
ESTIMATED FOURIER AMPLITUDES SPECTRA - IN/SEC
MAG = 4.5,5.5,6.5,7.5 ALLUV DEPTH = 0(———) & 4(-----) KM
FOCAL DEPTH = 5 KM
SOIL = 1 R = 0. KM
RESIDUE
2-STEP MODEL
HORZ
VERT
MAG = 6.5 ALLUV. DEPTH = 2 KM
HORZ(———) & VERT(-----)
SOIL = 1
FOCAL DEPTH = 5 KM
R = 0,25,50,100 KM
R = 0. KM
FOCAL DEPTH = 5,10,25,50 KM
PERIOD - SEC

Figure I.8.4

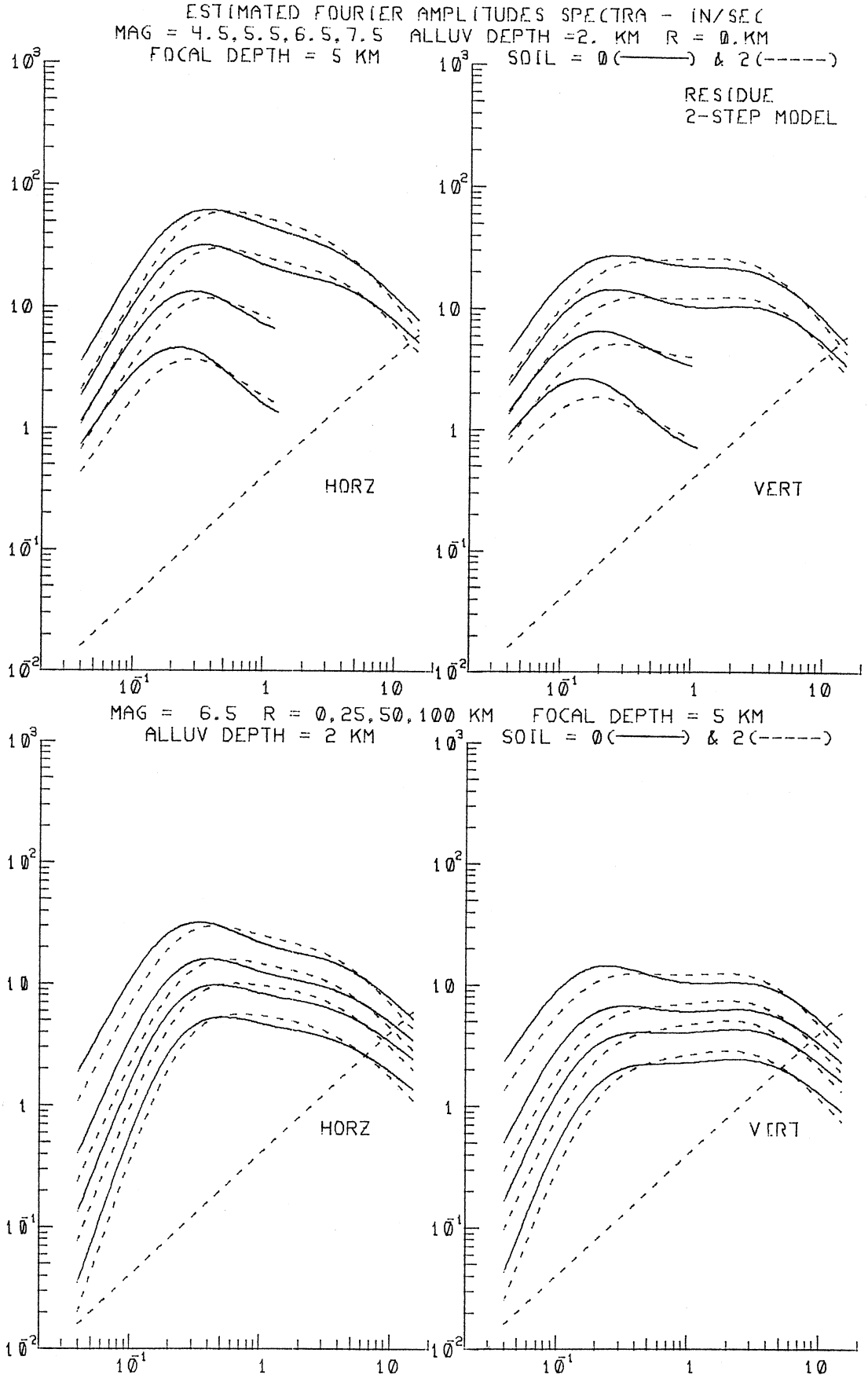
ESTIMATED FOURIER AMPLITUDES SPECTRA - IN/SEC
MAG = 4.5,5.5,6.5,7.5 ALLUV DEPTH =2. KM R = 0.KM
FOCAL DEPTH = 5 KM
SOIL = 0(———) & 2(-----)
RESIDUE
2-STEP MODEL
HORZ
VERT
MAG = 6.5 R = 0,25,50,100 KM FOCAL DEPTH = 5 KM
ALLUV DEPTH = 2 KM
SOIL = 0(———) & 2(-----)
HORZ
VERT

Figure I.8.5

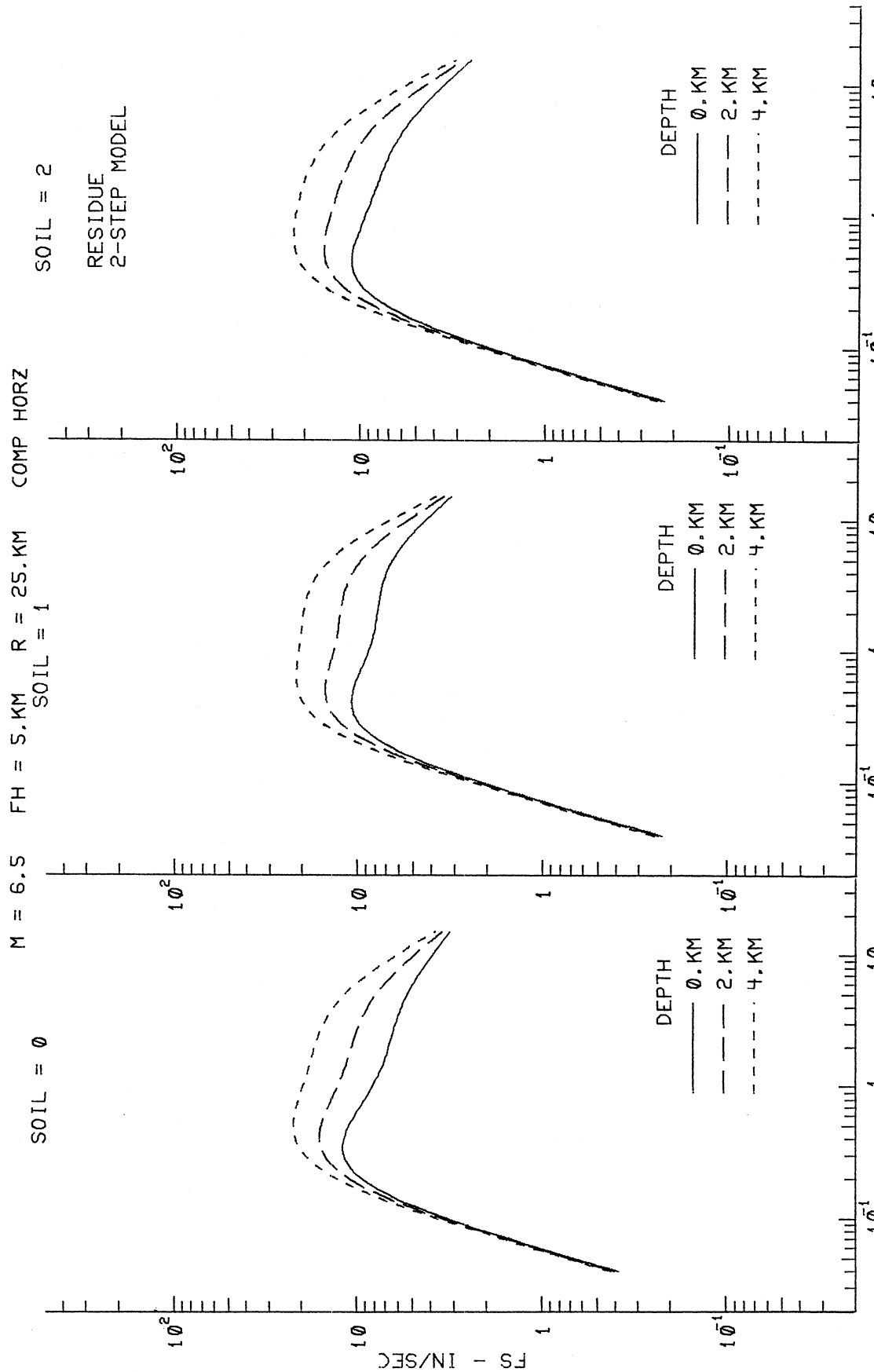
M = 6.5 FH = 5.KM R = 25.KM COMP HORZ
SOIL = 0
SOIL = 1
SOIL = 2
RESIDUE
2-STEP MODEL
DEPTH
0.KM
2.KM
4.KM
FS - IN/SEC
PERIOD - SEC
10^2
10
1
10^-1

Figure I.8.6

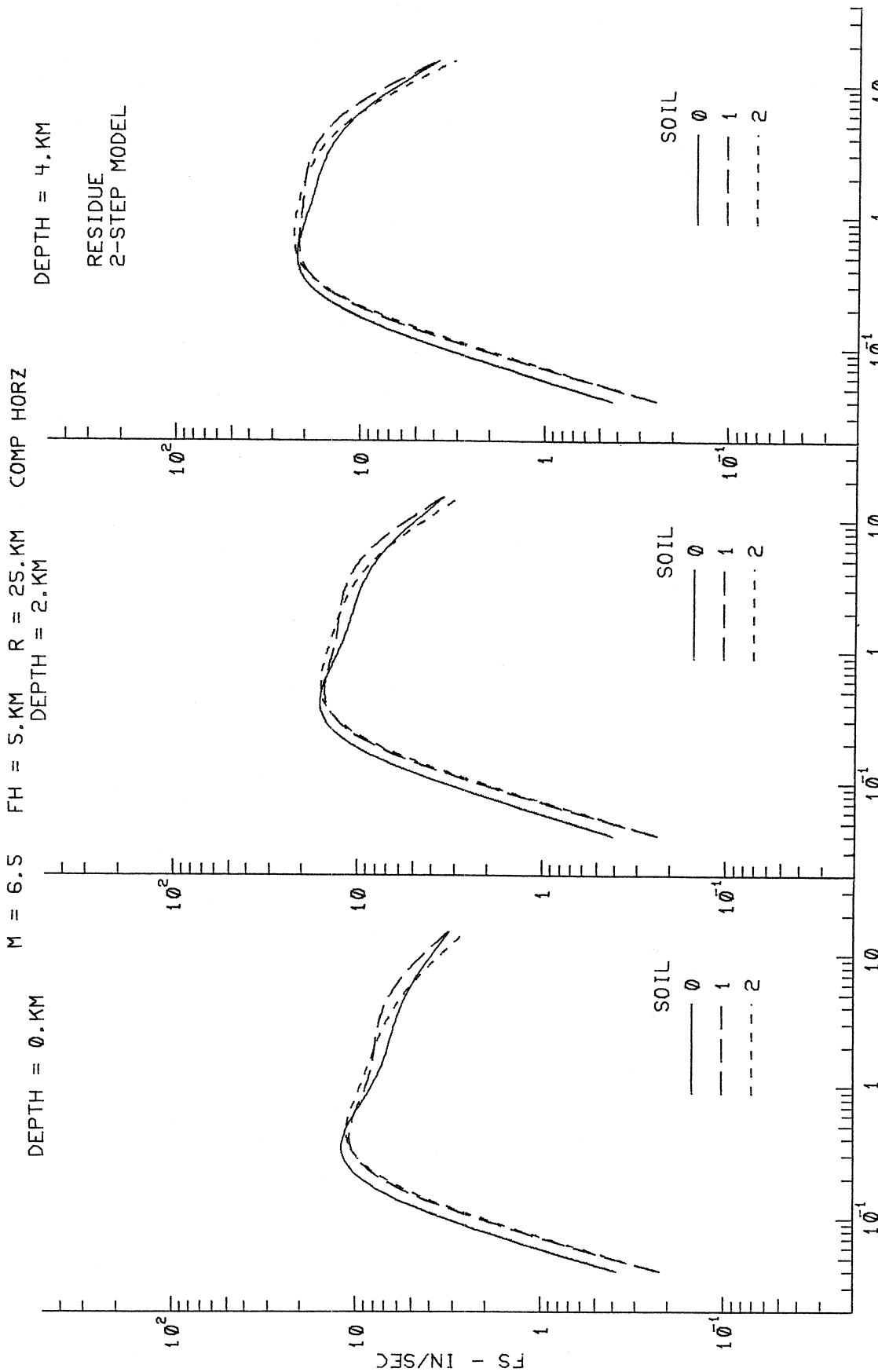
M = 6.5 FH = 5.KM R = 25.KM COMP HORZ
RESIDUE
2-STEP MODEL
DEPTH = 0.KM
DEPTH = 2.KM
DEPTH = 4.KM
SOIL
0
1
2
FS - IN/SEC
PERIOD - SEC
10^2
10
1
10^-1

Figure I.8.7

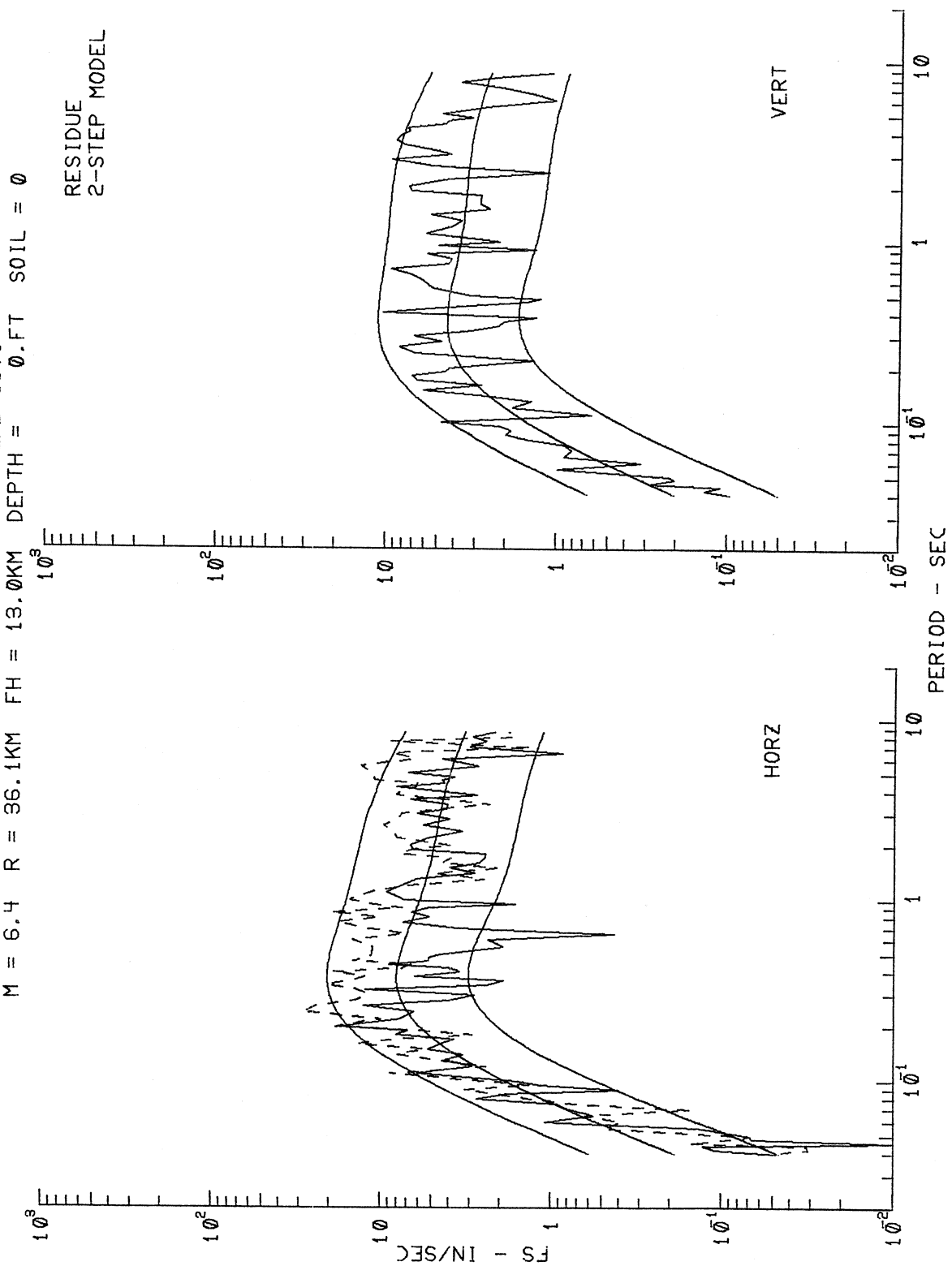
AG106 CALTECH SEISMOLOGICAL LAB 1971
M = 6.4 R = 36.1KM FH = 13.0KM DEPTH = 0.FT SOIL = 0
RESIDUE
2-STEP MODEL
VERT
HORZ
FS - IN/SEC
PERIOD - SEC

Figure I.8.8

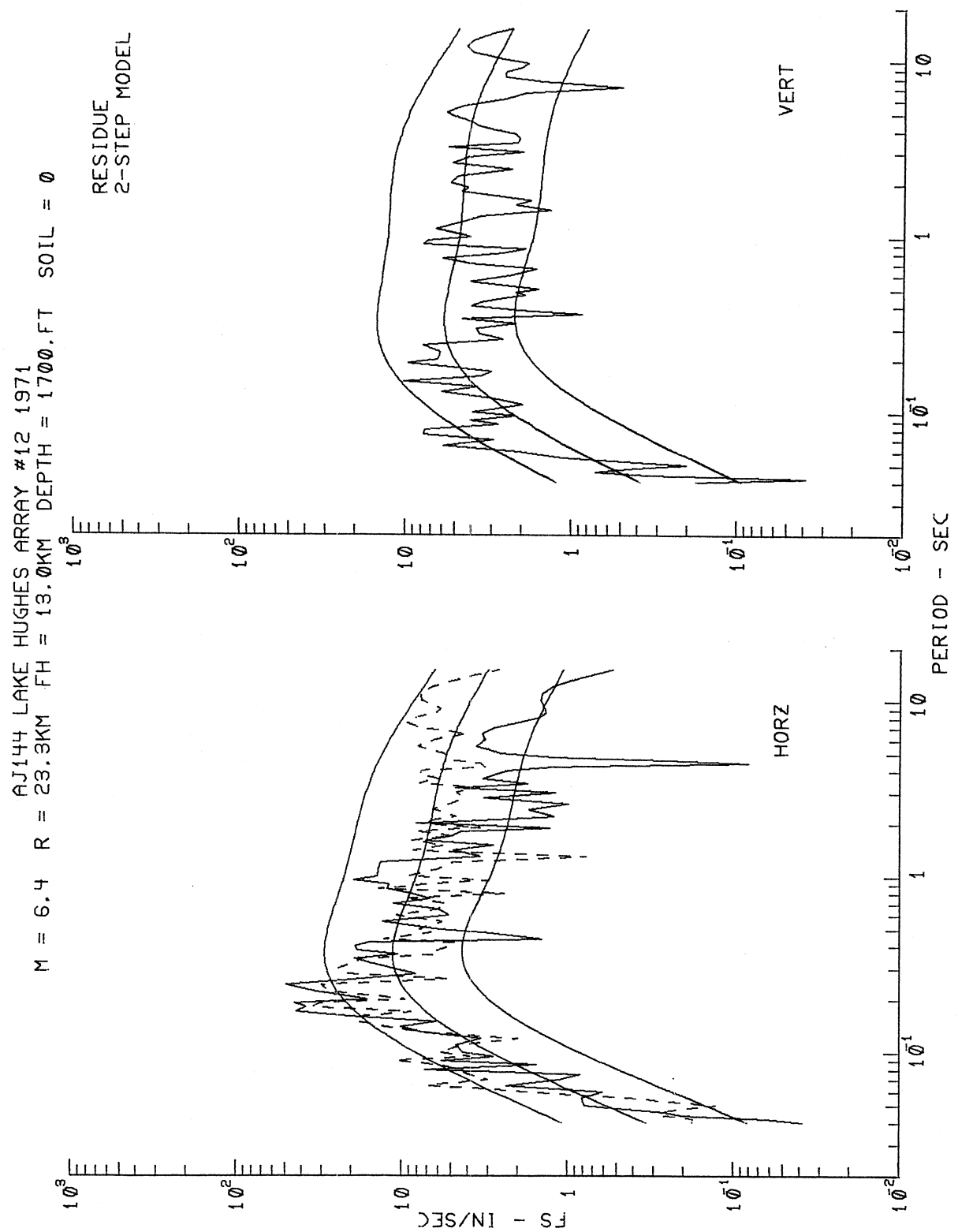
AJ144 LAKE HUGHES ARRAY #12 1971
M = 6.4 R = 23.3KM FH = 13.ØKM DEPTH = 17ØØ.FT SOIL = Ø
RESIDUE
2-STEP MODEL
HORZ
VERT
FS - IN/SEC
PERIOD - SEC

Figure I.8.9

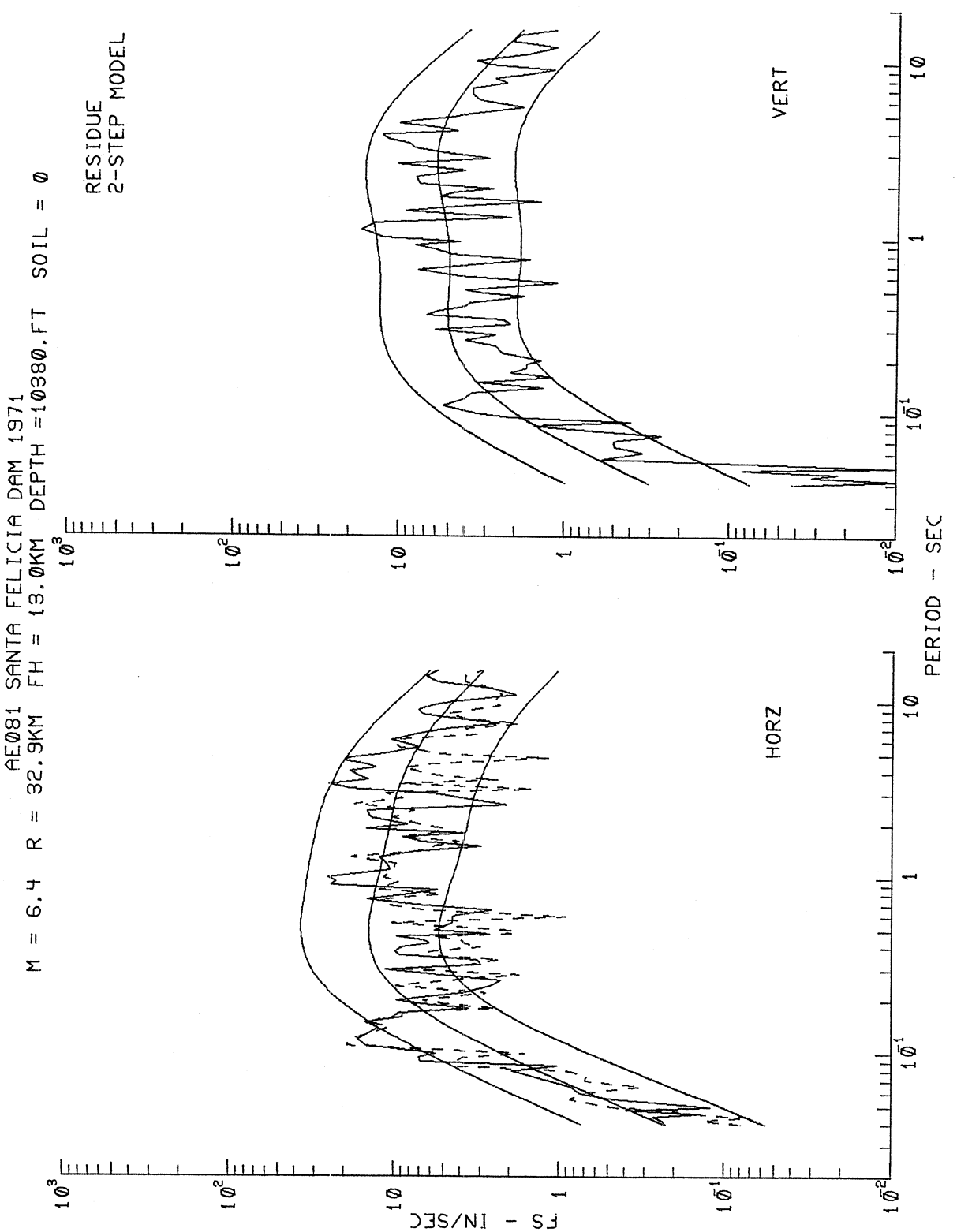
AE081 SANTA FELICIA DAM 1971
M = 6.4 R = 32.9KM FH = 13.0KM DEPTH =10380.FT SOIL = 0
RESIDUE
2-STEP MODEL
HORZ
VERT
FS - IN/SEC
PERIOD - SEC

Figure I.8.10

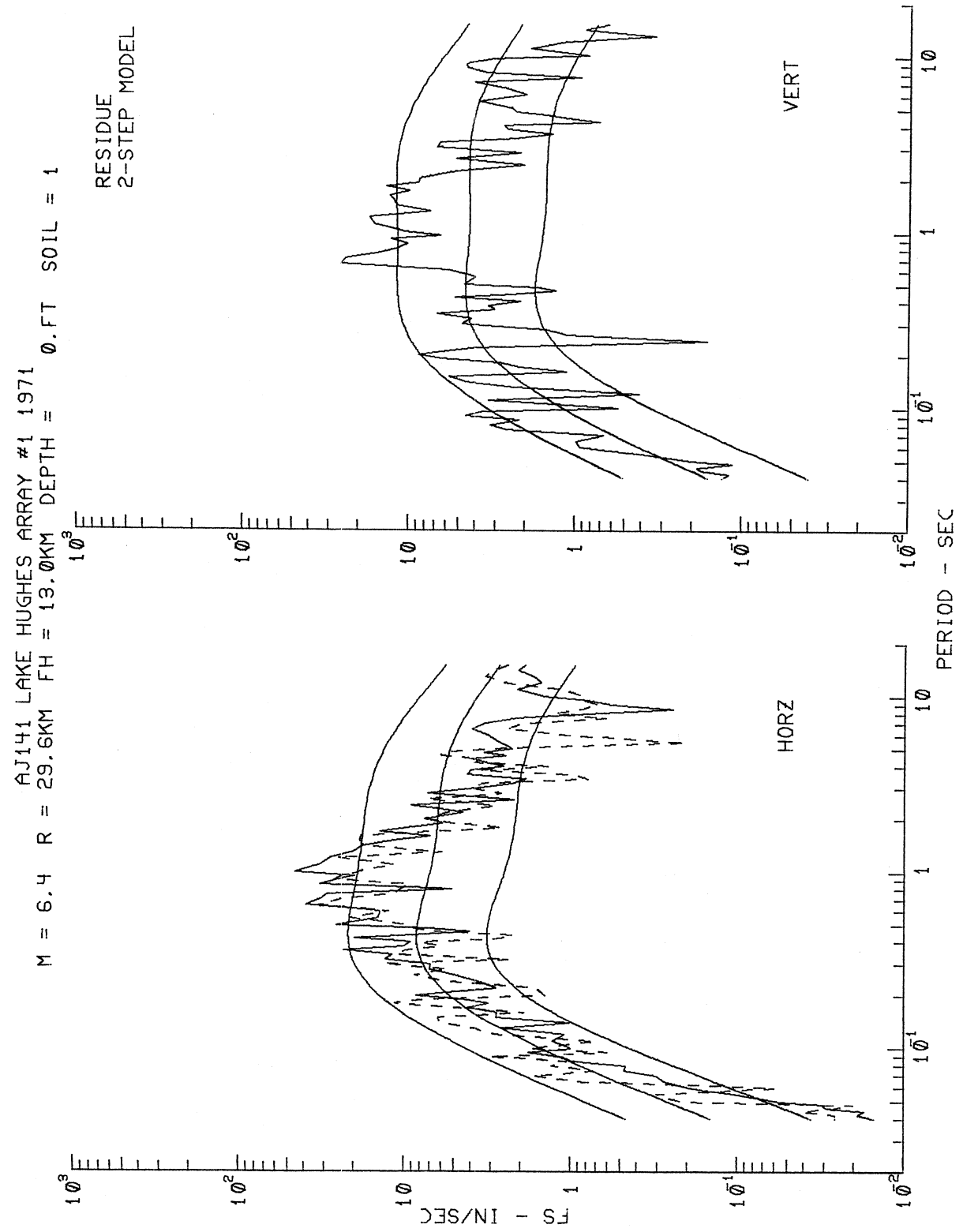
M = 6.4 R = 29.6KM FH = 13.0KM DEPTH = 0.FT SOIL = 1
AJ141 LAKE HUGHES ARRAY #1 1971
RESIDUE
2-STEP MODEL
VERT
HORZ
FS - IN/SEC
PERIOD - SEC

Figure I.8.11

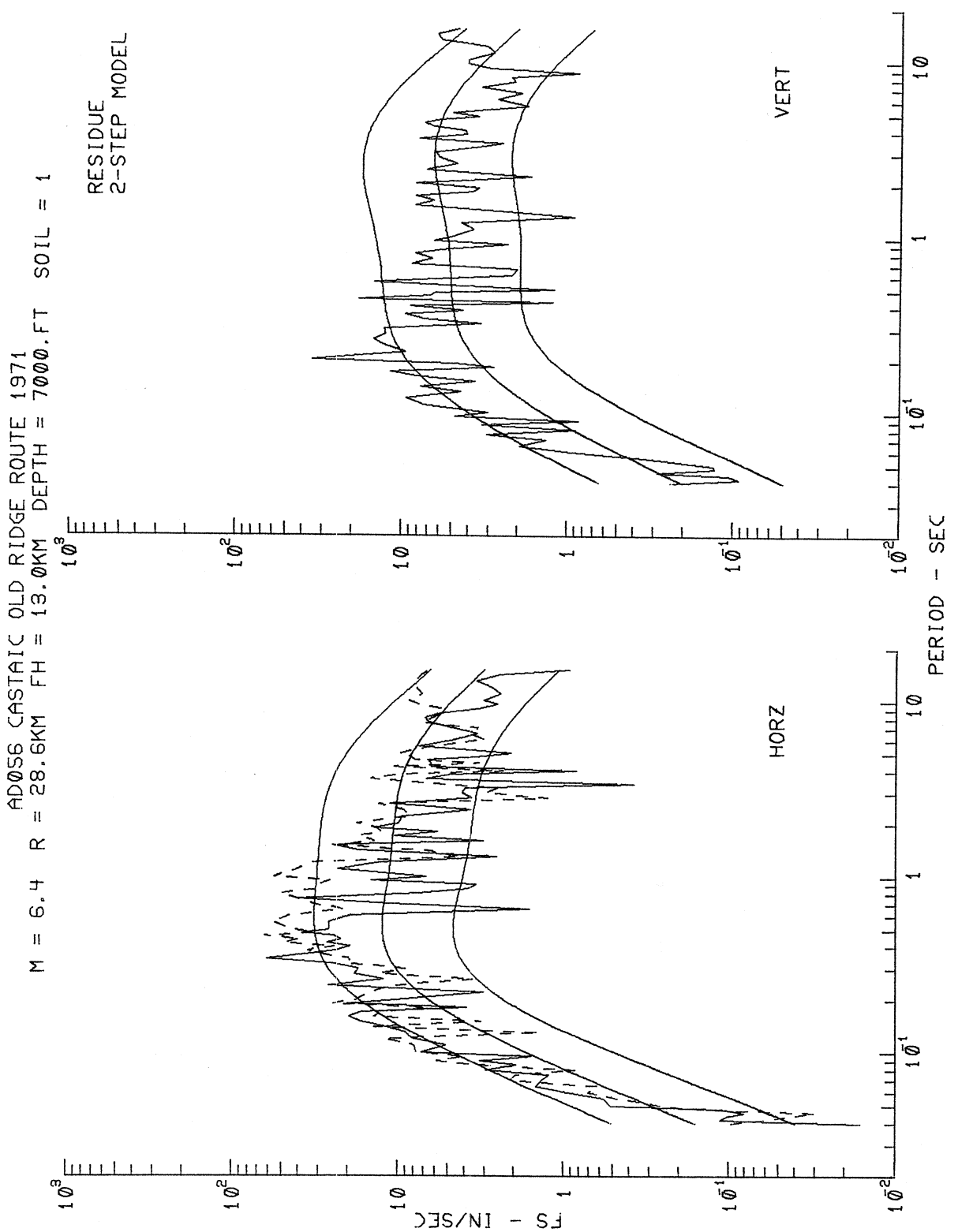
M = 6.4 R = 28.6KM FH = 13.0KM DEPTH = 7000.FT SOIL = 1
AD056 CASTAIC OLD RIDGE ROUTE 1971
RESIDUE
2-STEP MODEL
VERT
HORZ
FS - IN/SEC
PERIOD - SEC

Figure I.8.12

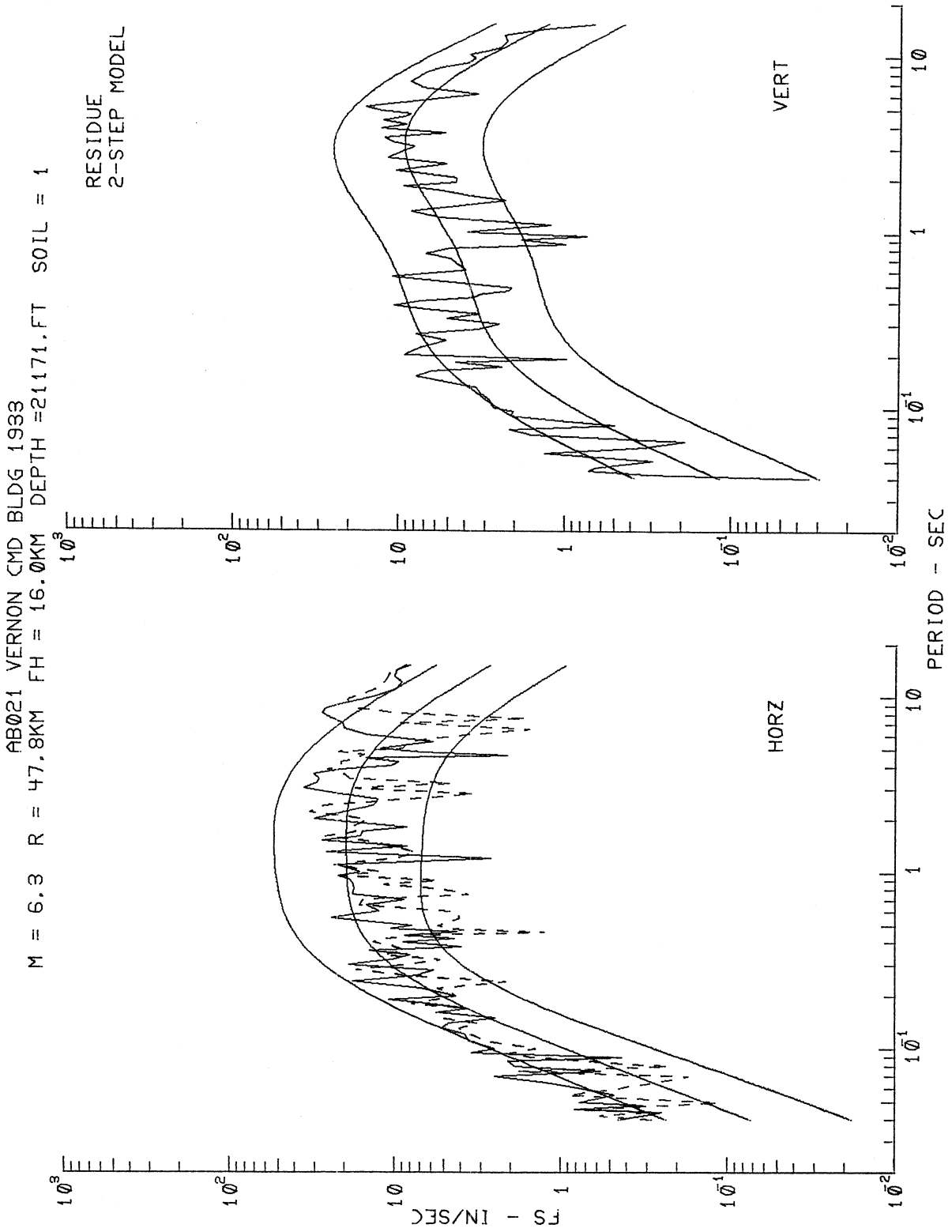
AB021 VERNON CMD BLDG 1933
M = 6.3 R = 47.8KM FH = 16.ØKM DEPTH =21171.FT SOIL = 1
RESIDUE
2-STEP MODEL
HORZ
VERT
FS - IN/SEC
PERIOD - SEC

Figure I.8.13

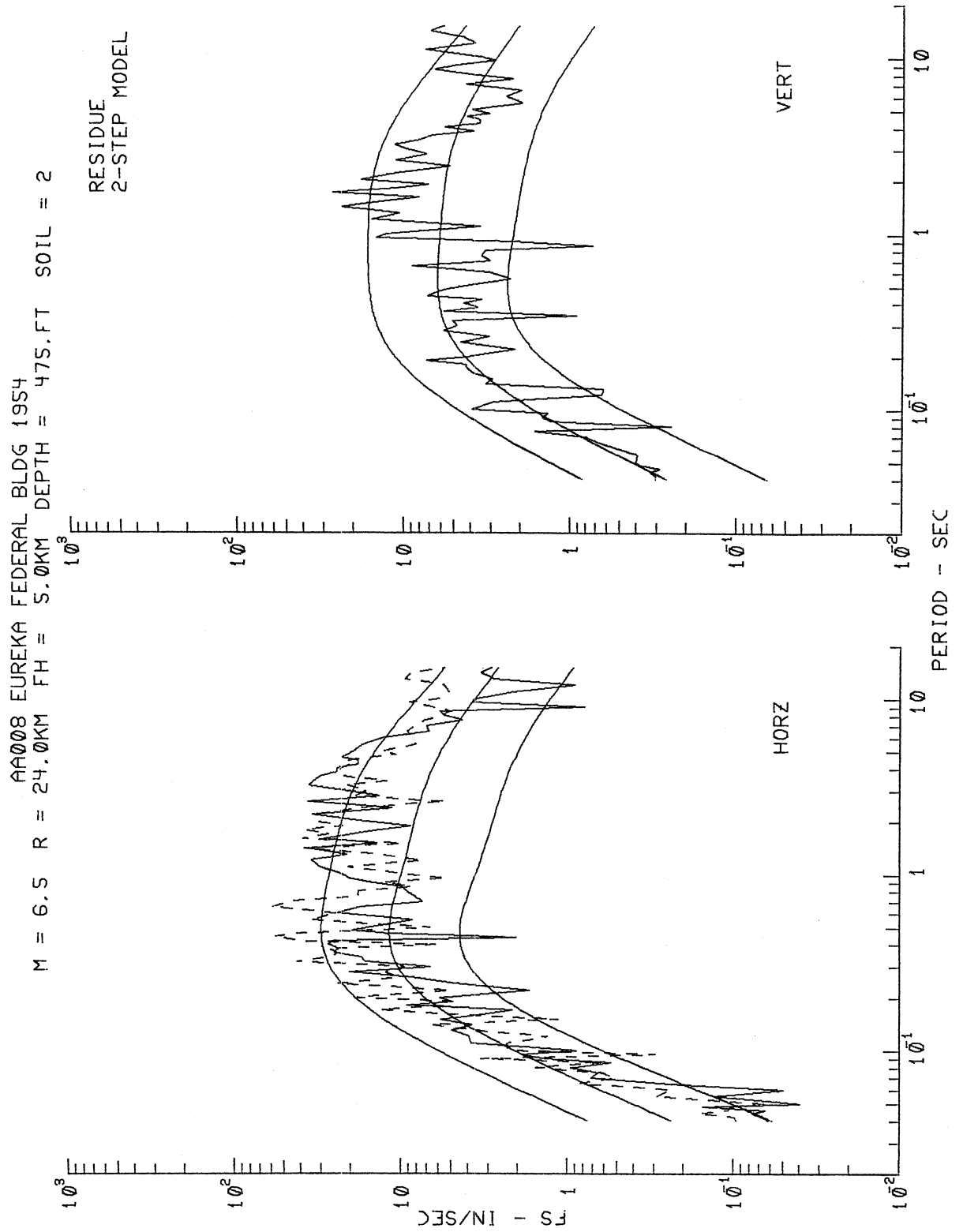
AA008 EUREKA FEDERAL BLDG 1954
M = 6.5 R = 24.0KM FH = 5.0KM DEPTH = 475.FT SOIL = 2
RESIDUE
2-STEP MODEL
VERT
HORZ
FS - IN/SEC
PERIOD - SEC

Figure I.8.14

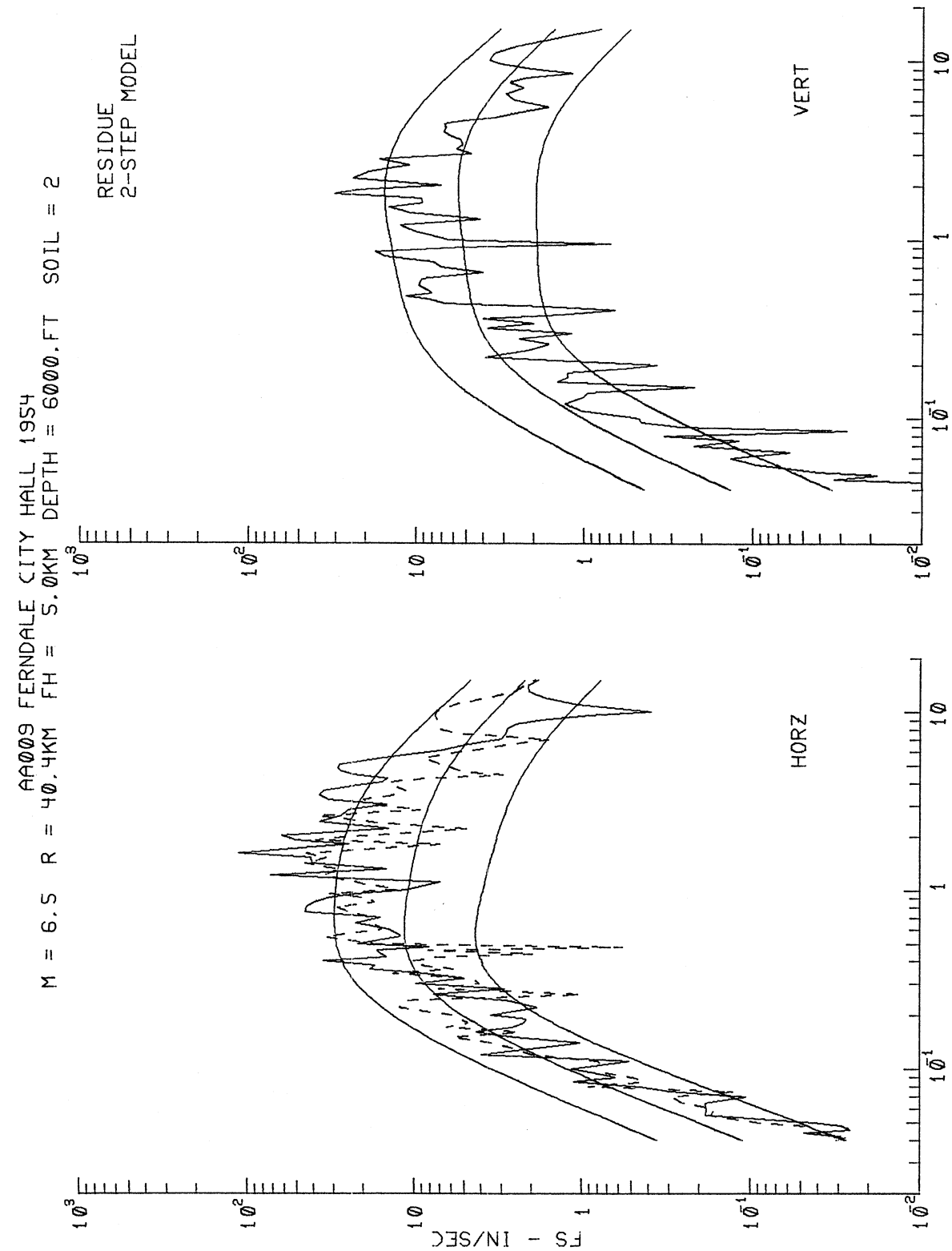
AA009 FERNDALE CITY HALL 1954
M = 6.5 R = 40.4KM FH = 5.0KM DEPTH = 6000.FT SOIL = 2
RESIDUE
2-STEP MODEL
VERT
HORZ
FS - IN/SEC
PERIOD - SEC

Figure I.8.15

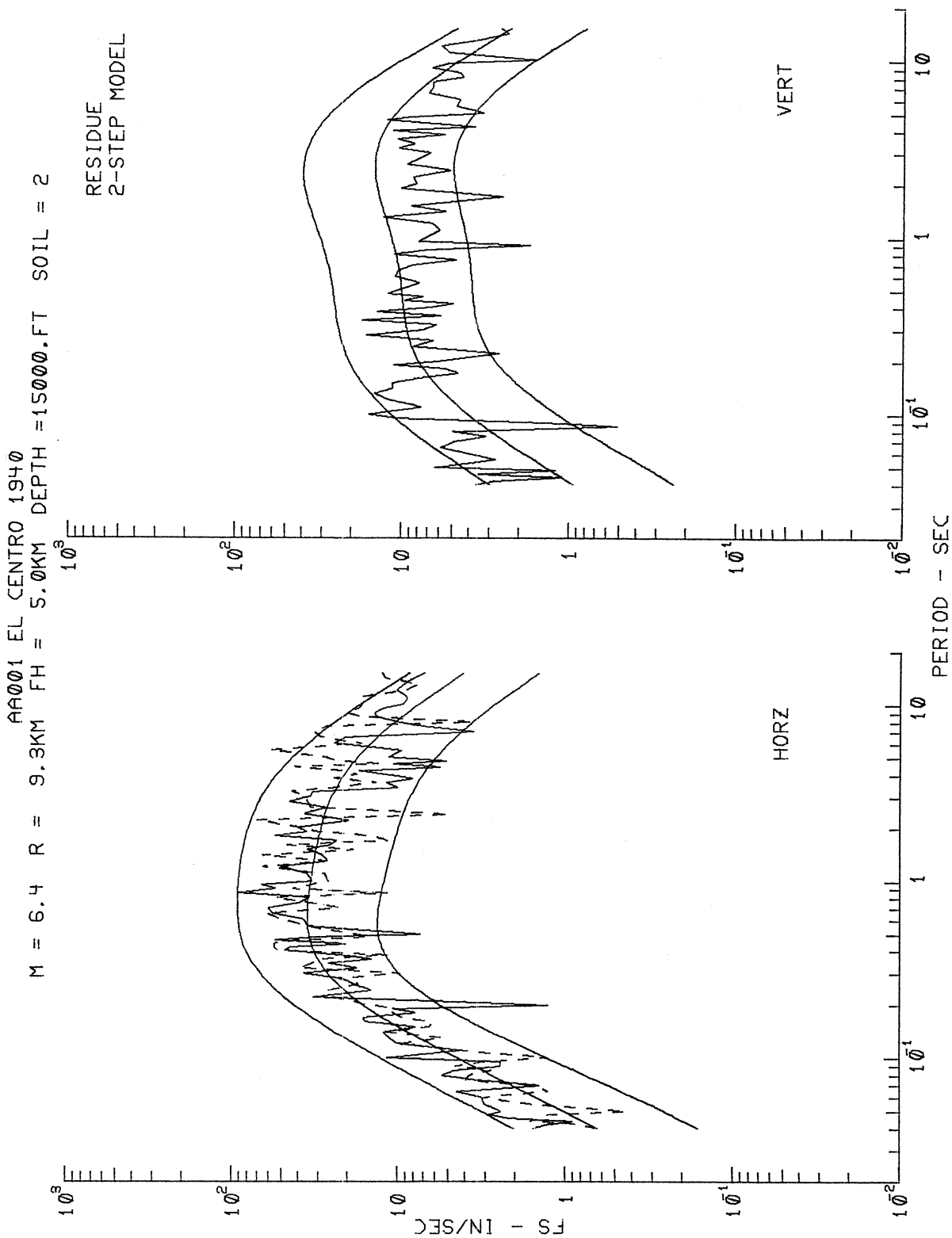
AA001 EL CENTRO 1940
M = 6.4 R = 9.3KM FH = 5.0KM DEPTH =15000.FT SOIL = 2
RESIDUE
2-STEP MODEL
HORZ
VERT
FS - IN/SEC
PERIOD - SEC

Figure I.8.16

TABLE I.8.2

$$\log_{10} FS(T) = M_{<} + \mathcal{A}tt(\Delta, M, T) +$$

$$c_1(T)M_{<>} + c_2(T)h + c_3(T)v + c_4(T)hv + c_5(T) + c_6(T)M_{<>}^2 +$$

$$c_7^{(1)}(T)S_L^{(1)} + c_7^{(2)}(T)S_L^{(2)}$$

MAG-DEPTH-SOIL RESIDUES: 2-STEP MODEL

PERIOD, T(SEC)	.040	.065	.11	.19	.34	.50	.90	1.60	2.80	4.40	7.50	14.0
COEFFICIENTS:												
$c_1(T)$	-.237	-.192	.019	.267	.468	.579	.750	.890	.879	.662	.095	-.907
$c_2(T)$	.012	.010	.013	.031	.060	.078	.093	.099	.099	.091	.065	.021
$c_3(T)$	.044	-.003	-.116	-.223	-.267	-.255	-.208	-.169	-.148	-.135	-.114	-.101
$c_4(T)$	.028	.022	.008	-.017	-.048	-.061	-.059	-.040	-.022	-.017	-.021	-.034
$c_5(T)$	-1.026	-1.115	-1.683	-2.540	-3.517	-4.156	-5.058	-5.673	-5.615	-4.792	-2.785	.618
$c_6(T)$	-.027	-.032	-.049	-.068	-.081	-.088	-.099	-.110	-.112	-.099	-.061	.008
$c_7^{(1)}(T)$	-.236	-.216	-.177	-.116	-.049	-.015	.021	.056	.086	.094	.070	.003
$c_7^{(2)}(T)$	-.237	-.227	-.202	-.138	-.046	.006	.053	.069	.059	.031	-.021	-.088
M_{min}	.000	.000	.194	1.970	2.877	3.285	3.778	4.041	3.939	3.356	.775	.000
M_{max}	14.500	14.500	10.392	9.342	9.023	8.958	8.814	8.583	8.419	8.426	8.967	14.500
RESIDUES:												
p =.1	-.587	-.562	-.508	-.452	-.421	-.421	-.440	-.458	-.462	-.453	-.436	-.420
p =.2	-.366	-.352	-.323	-.292	-.276	-.278	-.293	-.304	-.300	-.288	-.272	-.261
p =.3	-.220	-.209	-.192	-.177	-.172	-.174	-.183	-.191	-.188	-.176	-.156	-.136
p =.4	-.098	-.091	-.086	-.082	-.081	-.081	-.083	-.089	-.090	-.082	-.064	-.047
p =.5	.018	.020	.016	.009	.002	-.001	-.001	.001	.006	.013	.023	.034
p =.6	.144	.135	.114	.093	.084	.085	.091	.097	.101	.102	.101	.099
p =.7	.249	.235	.206	.180	.170	.174	.184	.191	.191	.186	.175	.165
p =.8	.368	.351	.317	.286	.272	.274	.287	.299	.300	.291	.274	.256
p =.9	.524	.502	.466	.428	.407	.410	.428	.441	.433	.413	.384	.358
RESIDUE STATISTICS:												
$\mu(T)$	.004	.003	.001	-.001	-.002	-.003	-.002	-.001	-.000	.000	.001	.002
$\sigma(T)$	.441	.421	.381	.343	.325	.327	.342	.354	.353	.341	.321	.302
$X^2(T)$	8.493	8.751	7.898	6.863	6.793	7.493	8.776	9.191	9.162	9.803	11.673	13.876
KS(T)	.042	.044	.041	.038	.038	.040	.043	.043	.043	.048	.059	.071

(I.8.1)) can be performed on a larger database including sites where information on soil classification is absent. It is only in the second step (equation (I.8.3) that regression has to be performed on that part of the database for the sites with available soil classification. Thus as more information on soil site classification becomes available, only the second step of iteration needs to be repeated to update the scaling functions. As for the direct "1-step" model, the regression analysis can be performed only on that part of the database for sites with soil classification. Every time this part of the database is updated, the whole regression has to be repeated.

Finally, Table I.8.2 presents scaling functions, residue levels and residue statistics at 12 discrete periods for the "2-step" model and corresponds to Table I.5.1 for the "1-step" model.

This completes the presentation of the Part I analysis of the scaling of FS(T) in terms of M, R, H, S, h, s_L and v.

PART II: SCALING OF FOURIER SPECTRA IN TERMS OF M, R, H, S, s, s_L and v

II.1 The New Scaling Relation

Part II of this work continues the description of the new empirical model for scaling Fourier Amplitude Spectra of strong ground motion in terms of earthquake magnitude, source-to-station "representative" distance, local site geology and local soil classification. Part I of this work characterizes the local geology by the approximate overall depth of sedimentary deposits beneath the recording station, h. As pointed out in our previous analyses (Trifunac and Lee, 1985a), while the alluvial depth at each recording station represents a well defined quantitative site characterization, in many instances, little may be known about such depth at some sites and so the scaling of FS(T) amplitudes there using depth, h, would be impossible. The qualitative site characterization in terms of s = 0 (sites on sediments), s = 1 (intermediate sites) and s = 2 (sites on basement rock), thus remains a useful approach to the scaling of FS(T) amplitudes.

The previous scaling relation using site condition, s, is of the form (Trifunac and Lee, 1985a)

$$\log_{10}FS(T) = M_< + \mathcal{A}tt(\Delta,M,T) + b_1(T)M_{<>} + b_2(T)s + b_3(T)v + b_5(T) + b_6(T)M^2_{<>} \quad , \qquad (II.1.1)$$

with all the parameters defined as before. Here the variable for site condition, s, has been treated as a quantitative variable in the scaling relation. To include the soil classification in the regression analysis, the regression equation of FS(T) to be used will now take the form:

$$\log_{10}FS(T) = M_{<} + \mathcal{A}tt(\Delta,M,T) +$$

$$b_1(T)M_{<>} + b_2^{(1)}(T)S^{(1)} + b_2^{(2)}(T)S^{(2)} + b_3(T)v +$$

$$b_4^{(1)}(T)S^{(1)}v + b_4^{(2)}(T)S^{(2)}v + b_5(T) + b_6(T)M_{<>}^2 +$$

$$b_7^{(1)}(T)S_L^{(1)} + b_7^{(2)}(T)S_L^{(2)} \quad . \qquad \text{(II.1.2)}$$

Here, as in Part I, $S_L^{(1)}$ and $S_L^{(2)}$ are the indicator variables used to characterize the soil classification at the site (equation I.3.3). $S^{(1)}$ and $S^{(2)}$ represent a new pair of indicator variables for local site conditions:

$$S^{(1)} = \begin{cases} 1 & \text{if } s = 1 \ , \\ 0 & \text{otherwise} \ , \end{cases}$$

and

$$S^{(2)} = \begin{cases} 1 & \text{if } s = 2 \ , \\ 0 & \text{otherwise} \ . \end{cases} \qquad \text{(II.1.3)}$$

As in the case for soil classification, (section I.3), the use of the indicator variables $S^{(1)}$ and $S^{(2)}$ instead of s (in our previous analyses), is due to the fact that s, unlike h, is a qualitative variable which takes on the discrete values of 0, 1 and 2 for the three distinct types of geological site classifications. The additional terms $b_4^{(i)}(T)S^{(i)}v$ together with $b_2^{(i)}(T)S^{(i)}$, for i = 1 and 2 will result in the coefficients characterizing the site condition, s, to be component dependent, so that for horizontal (v = 0) and vertical (v = 1) components, this takes the form (for i = 1, 2):

$$b_2^{(i)}(T)S^{(i)} + b_4^{(i)}(T)S^{(i)}v = \begin{cases} b_2^{(i)}(T)S^{(i)} & v = 0 \ , \\ (b_2^{(i)}(T) + b_4^{(1)}(T))S^{(i)} & v = 1 \ . \end{cases}$$

The scaling functions $b_1(T)$ through $b_7^{(2)}(T)$ have been determined through the regression analysis of the new database of 1482 components of spectral amplitudes, FS(T), at 91 discrete periods T ranging from 0.04 sec. to 15 sec. As in Part I of this work, the data were first screened for possible bias in the model. All procedures in data preparation, selection, and the procedures of the regression analysis employed here are identical to those in Part I of this work. The computed coefficients at each period T resulting from linear regression will be denoted by $\hat{b}_1(T)$ thorugh $\hat{b}_7^{(2)}(T)$, respectively.

Much of the presentation to follow in this and in the subsequent sections will be similar to the corresponding sections in Part I of this work. The reader may refer to the corresponding sections in Part I for a more comprehensive discussion and description of various procedures.

Substituting the fitted coefficients into equation (II.1.2) gives $\hat{FS}(T)$, the estimated spectral amplitudes, where

$$\begin{aligned}\log_{10}\hat{FS}(T) = {} & M + \mathcal{A}tt(\Delta,M,T) + \\ & \hat{b}_1(T)M + \hat{b}_2^{(1)}(T)S^{(1)} + \hat{b}_2^{(2)}(T)S^{(2)} + \\ & \hat{b}_3(T)v + \hat{b}_4^{(1)}(T)S^{(1)}v + \hat{b}_4^{(2)}(T)S^{(2)}v + \hat{b}_5(T) + \\ & \hat{b}_6(T)M^2 + \hat{b}_7^{(1)}(T)S_L^{(1)} + \hat{b}_7^{(2)}(T)S_L^{(2)} \quad . \end{aligned} \tag{II.1.4}$$

As before, equation (II.1.4) applies only in the range $M_{min} \leq M \leq M_{max}$, where for each period, T:

$$M_{min}(T) = -\hat{b}_1(T)/(2\hat{b}_6(T)) \quad , \text{ and}$$

$$M_{max}(T) = -(1+\hat{b}_1(T))/(2\hat{b}_6(T)) \quad , \qquad \text{(II.1.5)}$$

and equation (II.1.4) is then modified to:

$$\log_{10}\hat{FS}(T) = M_{<} + \mathcal{A}tt(\Delta,M,T) +$$
$$\hat{b}_1(T)M_{<>} + \hat{b}_2^{(1)}(T)S^{(1)} + \hat{b}_2^{(2)}(T)S^{(2)} +$$
$$\hat{b}_3(T)v + \hat{b}_4^{(1)}(T)S^{(1)}v + \hat{b}_4^{(2)}(T)S^{(2)}v + \hat{b}_5(T) +$$
$$\hat{b}_6(T)M_{<>}^2 + \hat{b}_7^{(1)}(T)S_L^{(1)} + \hat{b}_7^{(2)}(T)S_L^{(2)} \quad , \qquad \text{(II.1.6)}$$

with

$$M_{<} = \min(M,M_{max})$$

$$M_{<>} = \max(M_{min},M_{<}) = \begin{cases} M_{min} & M \leq M_{min} \\ M & M_{min} \leq M \leq M_{max} \\ M_{max} & M > M_{max} \end{cases} \quad .$$

(II.1.7)

The residues $\varepsilon(T) = \log_{10}(FS(T)) - \log_{10}(\hat{FS}(T))$ describing the distribution of the recorded FS(T) about the estimated $\hat{FS}(T)$ are next calculated. As in the previous part, $\varepsilon(T)$ can be described by a normal distribution funciton with mean $\mu(T)$ and standard deviation $\sigma(T)$.

II.2 The Regression Coefficients

Figure II.2.1 shows the smoothed coefficients $\hat{b}_1(T)$, $\hat{b}_2^{(1)}(T)$, $\hat{b}_2^{(2)}(T)$, $\hat{b}_3(T)$, $\hat{b}_4^{(1)}(T)$, $\hat{b}_4^{(2)}(T)$, $\hat{b}_5(T)$, $\hat{b}_6(T)$, $\hat{b}_7^{(1)}(T)$ and $\hat{b}_7^{(2)}(T)$ (solid lines) together with the estimates of their 80%, 90% and 95% confidence intervals (dashed lines). Comparison of this figure with the corresponding figure I.5.1 in Part I shows that the scaling functions $\hat{b}_1(T)$, $\hat{b}_3(T)$, $\hat{b}_5(T)$, $\hat{b}_6(T)$, $\hat{b}_7^{(1)}(T)$ and $\hat{b}_7^{(2)}(T)$ in both figures are almost identical. These functions correspond to the same parameters, M, v, 1, M^2, $S_L^{(1)}$ and $S_L^{(2)}$, respectively, in the respective scaling relations. Their similarity thus demonstrates the consistancy between the two scaling models. The functions $\hat{b}_2^{(1)}(T)$ and $\hat{b}_2^{(2)}(T)$, for $S^{(1)}$ (s = 1) and $S^{(2)}$ (s = 2), in Figure II.2.1 are both opposite in sign when compared to the corresponding function $b_2(T)$ for alluvial depth h in Figure I.5.1. This again shows consistency since s = 2 (for basement rock sites) corresponds to alluvial depth h = 0 km. Similar observation can be made for the functions $b_4^{(1)}(T)$ and $b_4^{(2)}(T)$ for $S_L^{(1)}v$ and $S_L^{(2)}v$, when compared with the corresponding function $b_4(T)$ for hv.

Figure II.2.2 shows the plot of the residuals corresponding to $p^*(\varepsilon,T)$ = 0.1 through 0.9 for $\log_{10}FS(T)$. Refer to the Figure I.5.2 in Part I for a more detailed description of each of the nine sets of curves. It is of interest to compare these figures, since they both illustrate the spread of the observed data about their corresponding models, being different only in the method for characterization of the local site geology. As in our previous analyses (Trifunac and Lee, 1985a) the resemblance of the two figures demonstrates that with other factors being identical the uncertainties associated with the characterization

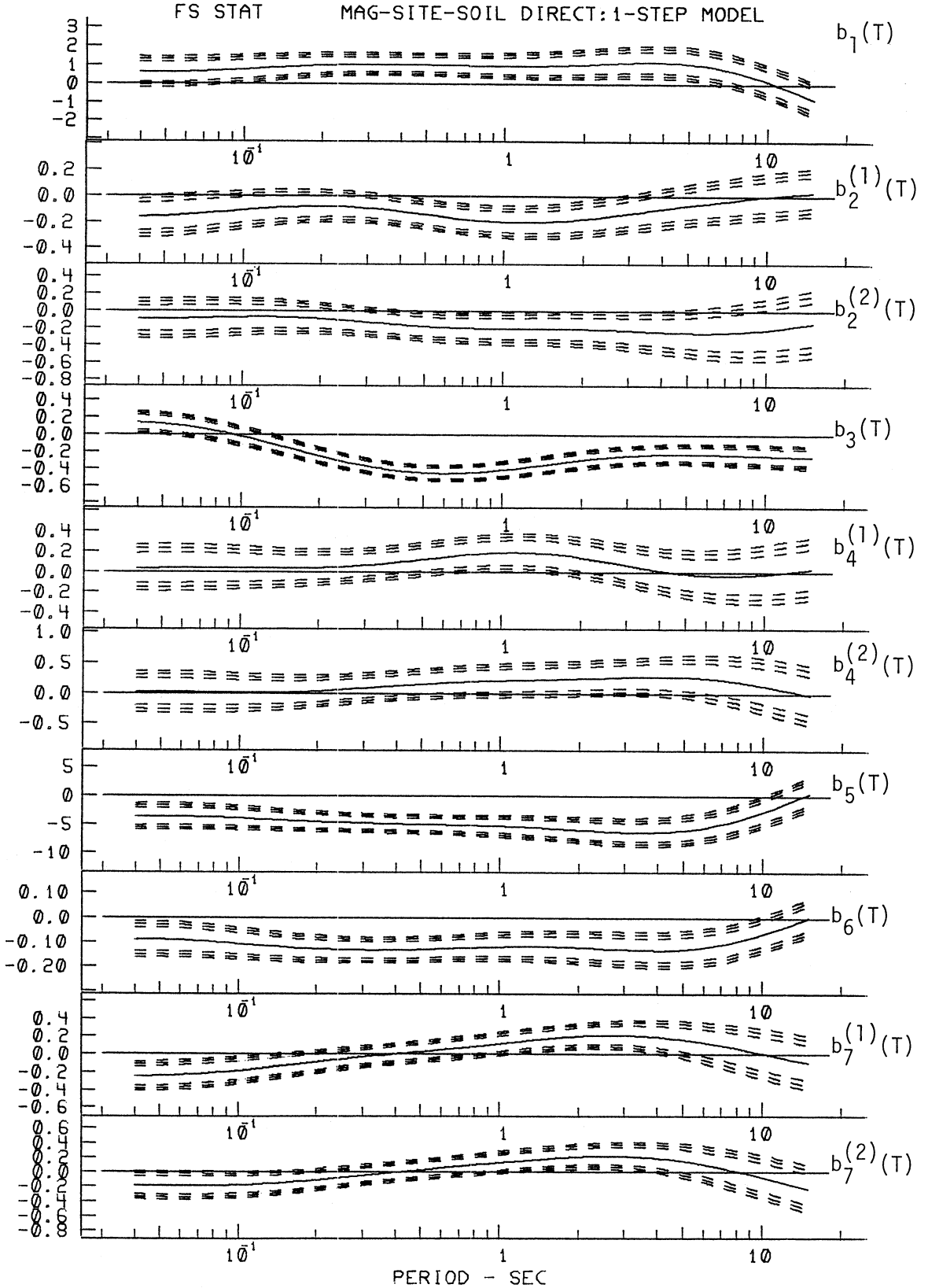
FS STAT
MAG-SITE-SOIL DIRECT: 1-STEP MODEL
$b_1(T)$
$b_2^{(1)}(T)$
$b_2^{(2)}(T)$
$b_3(T)$
$b_4^{(1)}(T)$
$b_4^{(2)}(T)$
$b_5(T)$
$b_6(T)$
$b_7^{(1)}(T)$
$b_7^{(2)}(T)$
PERIOD - SEC

Figure II.2.1

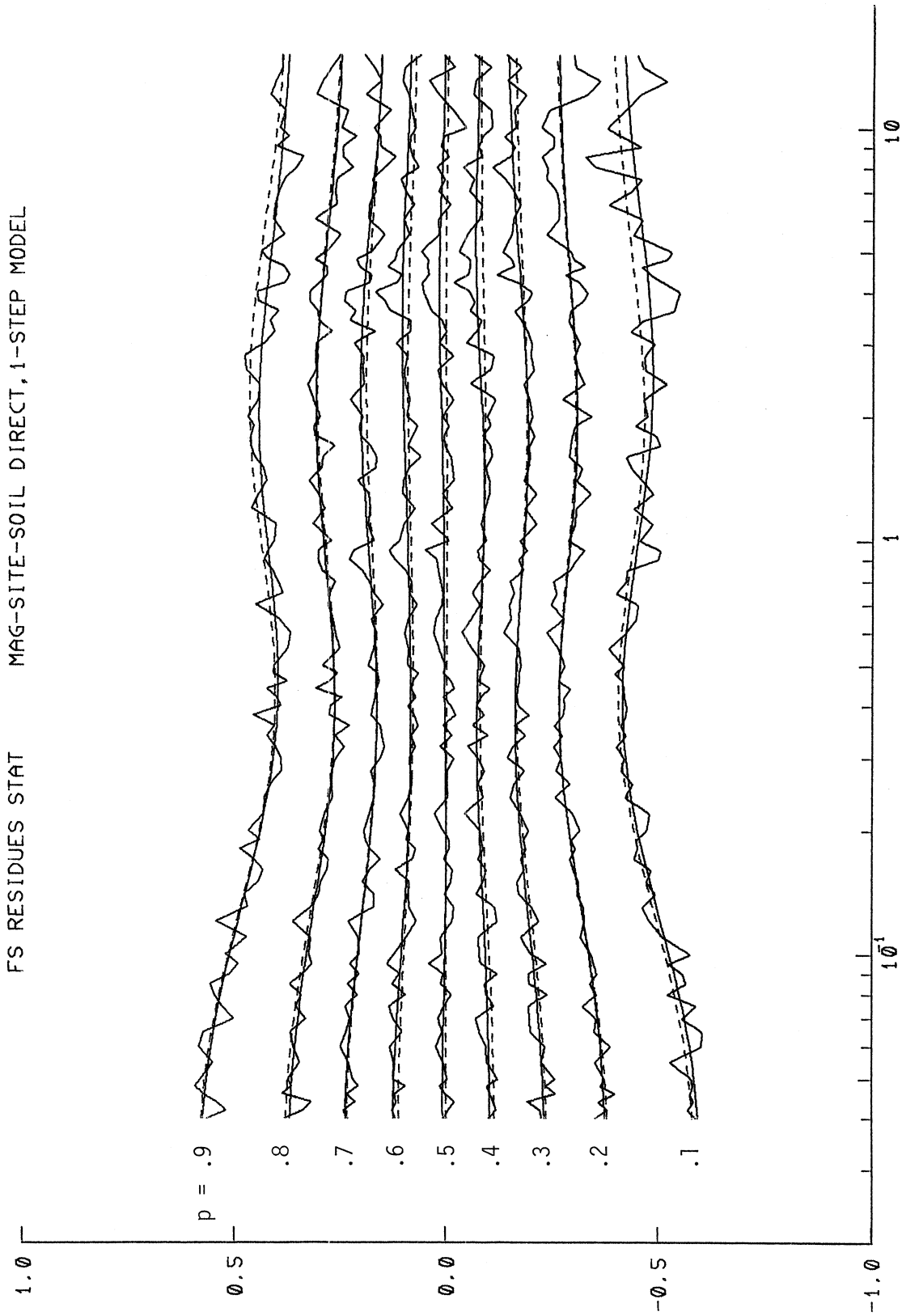
FS RESIDUES STAT
MAG-SITE-SOIL DIRECT,1-STEP MODEL
1.0
0.5
0.0
-0.5
-1.0
p = .9
.8
.7
.6
.5
.4
.3
.2
.1
10^1
1
10

Figure II.2.2

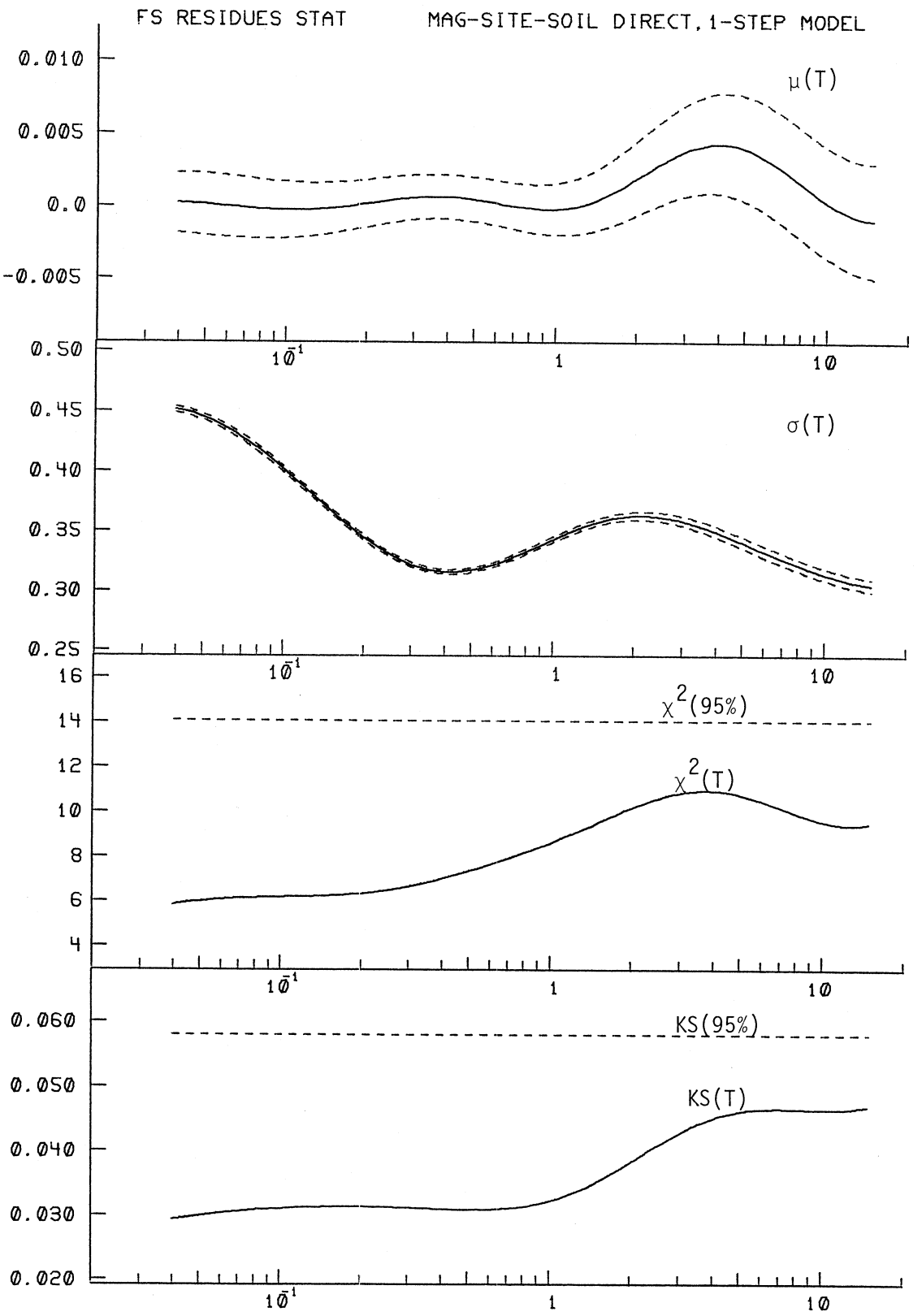
FS RESIDUES STAT
MAG-SITE-SOIL DIRECT, 1-STEP MODEL
μ(T)
σ(T)
χ²(95%)
χ²(T)
KS(95%)
KS(T)
0.010
0.005
0.0
-0.005
0.50
0.45
0.40
0.35
0.30
0.25
16
14
12
10
8
6
4
0.060
0.050
0.040
0.030
0.020
10⁻¹
1
10

Figure II.2.3

TABLE II.2.1

$$\log_{10} FS(T) = M_{<} + \mathcal{A}tt(\Delta,M,T) + b_1(T)M_{<>} + b_2^{(1)}(T)S^{(1)} + b_2^{(2)}(T)S^{(2)} + b_3(T)v + b_4^{(1)}S^{(1)}v + b_4^{(2)}(T)S^{(2)}v + b_5(T) + b_6(T)M_{<>}^2 + b_7^{(1)}(T)S_L^{(1)} + b_7^{(2)}(T)S_L^{(2)}$$

MAG-SITE-SOIL DIRECT:1-STEP MODEL

PERIOD, T(SEC)	.040	.065	.11	.19	.34	.50	.90	1.60	2.80	4.40	7.50	14.0
COEFFICIENTS:												
$b_1(T)$	.604	.629	.797	.971	1.039	1.017	.953	.990	1.138	1.140	.661	-.656
$b_2^{(1)}(T)$	-.161	-.138	-.100	-.077	-.101	-.141	-.193	-.191	-.138	-.082	-.025	.031
$b_2^{(2)}(T)$	-.092	-.086	-.070	-.086	-.145	-.183	-.207	-.205	-.225	-.251	-.245	-.157
$b_3(T)$	.140	.084	-.052	-.233	-.397	-.450	-.429	-.333	-.250	-.224	-.234	-.260
$b_4^{(1)}(T)$	.036	.039	.038	.042	.078	.124	.186	.173	.080	-.001	-.036	.021
$b_4^{(2)}(T)$	.021	.015	.006	.030	.102	.154	.206	.236	.270	.280	.211	-.002
$b_5(T)$	-3.686	-3.675	-4.009	-4.473	-4.853	-5.012	-5.237	-5.705	-6.291	-6.203	-4.464	-.049
$b_6(T)$	-.090	-.094	-.110	-.127	-.134	-.130	-.120	-.119	-.129	-.133	-.103	-.011
$b_7^{(1)}(T)$	-.252	-.227	-.174	-.096	-.019	.026	.099	.178	.213	.180	.078	-.080
$b_7^{(2)}(T)$	-.183	-.187	-.174	-.117	-.027	.030	.113	.188	.218	.175	.034	-.209
M_{min}	3.367	3.351	3.615	3.815	3.891	3.906	3.968	4.168	4.411	4.295	3.220	.000
M_{max}	8.937	8.680	8.152	7.743	7.637	7.746	8.131	8.376	8.287	8.063	8.088	14.500
RESIDUES:												
p =.1	-.590	-.566	-.514	-.455	-.417	-.416	-.443	-.474	-.482	-.469	-.442	-.417
p =.2	-.373	-.360	-.329	-.292	-.267	-.267	-.287	-.305	-.301	-.288	-.273	-.263
p =.3	-.230	-.219	-.199	-.175	-.162	-.163	-.179	-.190	-.184	-.170	-.154	-.143
p =.4	-.103	-.099	-.091	-.079	-.071	-.074	-.084	-.086	-.075	-.067	-.068	-.073
p =.5	.008	.006	.002	.000	.003	.006	.007	.011	.018	.020	.014	.007
p =.6	.126	.118	.103	.090	.085	.086	.092	.100	.107	.107	.099	.089
p =.7	.239	.228	.204	.180	.166	.168	.184	.201	.204	.195	.175	.157
p =.8	.369	.353	.323	.288	.266	.267	.287	.307	.307	.293	.271	.252
p =.9	.574	.549	.501	.444	.403	.398	.419	.442	.440	.422	.398	.376
RESIDUE STATISTICS:												
$\mu(T)$	.000	-.000	-.000	.000	.001	.000	-.000	.001	.004	.004	.002	-.001
$\sigma(T)$	.451	.432	.394	.348	.318	.317	.338	.360	.360	.346	.324	.306
$X^2(T)$	5.835	6.112	6.207	6.337	6.811	7.359	8.415	9.706	10.795	10.921	10.105	9.457
KS(T)	.029	.031	.031	.031	.031	.031	.032	.036	.042	.046	.047	.047

of local geology in terms of the site conditions s = 0, 1 and 2, are not much greater than those associated with the site characterization in terms of the alluvial depth, h.

Figure II.2.3 shows the plot of the statistical parameters in the description of the residues, namely, $\hat{\mu}(T)$, $\hat{\sigma}(T)$, $\chi^2(T)$ and KS(T), from top to bottom. Note that in the entire period range from T = 0.04 sec. to T = 15 sec., both the χ^2 and KS tests again (as in Part I) fail to reject the hypothesis that the distribution is normal, with 95% confidence.

Table II.2.1 gives, for 12 periods between T = 0.04 sec. and T = 14 sec., the regression coefficients, $\hat{b}_1(T)$, $\hat{b}_2^{(1)}(T)$, $\hat{b}_2^{(2)}(T)$, $\hat{b}_3(T)$, $\hat{b}_4^{(1)}(T)$, $\hat{b}_4^{(2)}(T)$, $\hat{b}_5(T)$, $\hat{b}_6(T)$, $\hat{b}_7^{(1)}(T)$, $\hat{b}_7^{(2)}(T)$, $\hat{M}_{min}(T)$, $\hat{M}_{max}(T)$, the nine residue levels corresponding to $p^*(\varepsilon,T)$ = 0.1 through 0.9, the coefficients $\hat{\mu}(T)$, $\hat{\sigma}(T)$ of the normal distribution and finally the $\chi^2(T)$ and KS(T) statistics.

II.3 Examples of Estimated Fourier Spectra

Figure II.3.1 presents four sets of plots of estimated FS(T) spectra using equation (II.1.6). The top two sets are examples of FS(T) computed for magnitudes M = 4.5, 5.5, 6.5 and 7.5 at epicentral distance R = 0, focal depth H = 5 km, for soil parameter S_L = 1 (stiff soil), for $p(\varepsilon,T)$ = 0.5 (see equation I.5.2 of Part I), and for the horizontal and vertical motions. The solid lines in both figures correspond to the geologic site condition s = 2 (rock), while the dashed lines correspond to s = 0 (alluvium). The diagonal dashed lines represent the average Fourier amplitudes of digitization noise. The lower left plot illustrates the effect of epicentral distance R on the changes of spectral amplitudes for magnitudes M = 6.5, focal depth H = 5 km, site condition s = 0, soil classification s_L = 1, $p(\varepsilon,T)$ = 0.5 and for horizontal (solid lines) and vertical (dashed lines) components. Four sets of curves corresponding to R = 0, 25, 50 and 100 km are presented. The lower right plot illustrates the effect of focal depth H on the changes of spectral amplitudes.

The trends of the computed FS(T) amplitudes in Figure II.3.1 are in many ways similar to those presented in Figure I.6.1 of Part I for the magnitude-depth model. The local geologic conditions in terms of s = 2, 1 and 0, here, correspond to small, intermediate and large alluvial depths in the model using h in Part I.

Figure II.3.2 presents another four plots of estimated FS(T) to illustrate the effects of local soil conditions on FS(T). This figure is very similar to the corresponding figure, Figure I.6.1 of Part I in the MAG-DEPTH-SOIL Model. As in the case of the magnitude-depth-soil model in Part I, it is observed that for periods up to ~ 0.3 sec., the

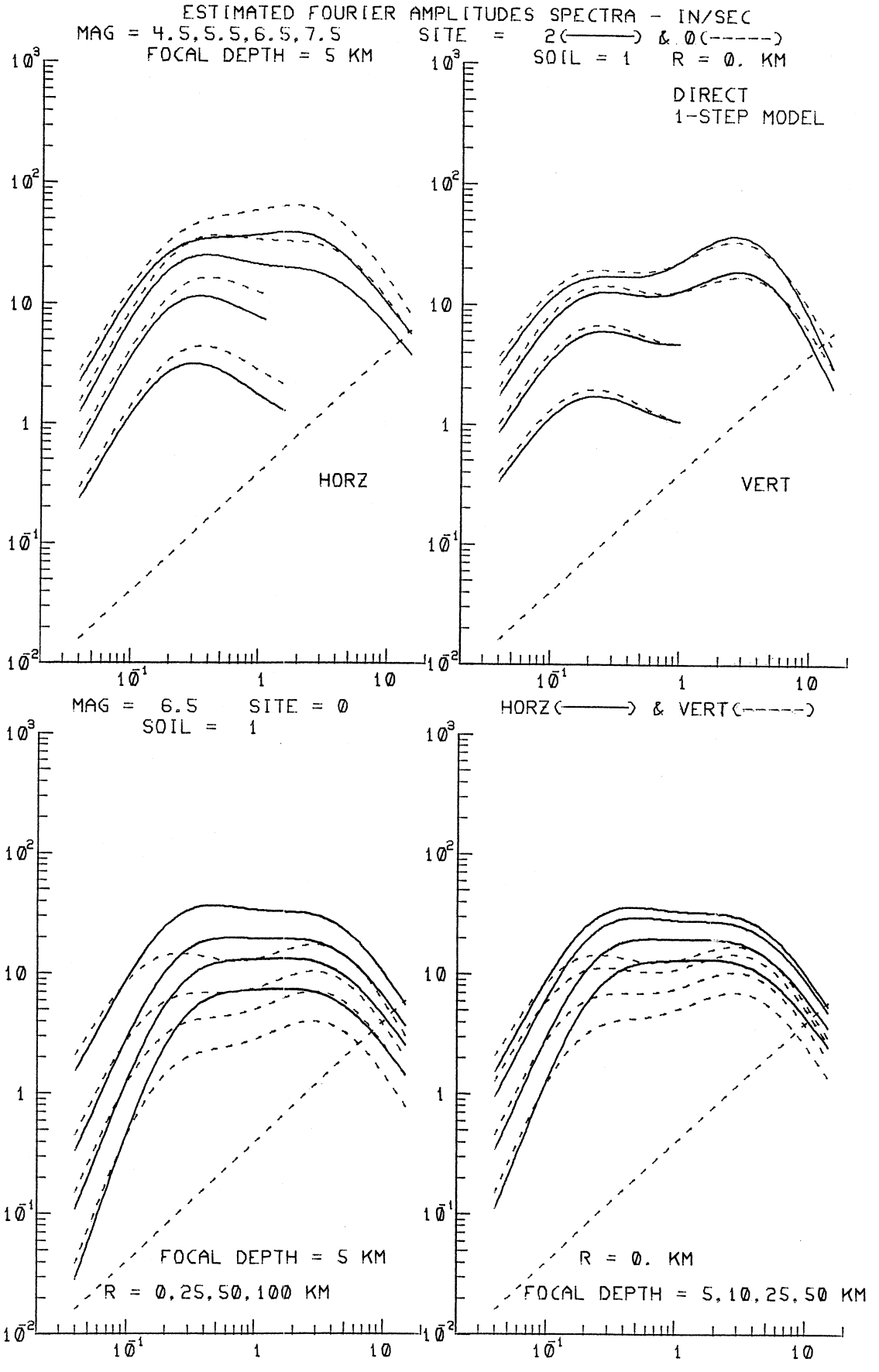
ESTIMATED FOURIER AMPLITUDES SPECTRA - IN/SEC
MAG = 4.5, 5.5, 6.5, 7.5
FOCAL DEPTH = 5 KM
SITE = 2(———) & 0(- - - -)
SOIL = 1
R = 0. KM
DIRECT
1-STEP MODEL
HORZ
VERT
MAG = 6.5
SOIL = 1
SITE = 0
HORZ(———) & VERT(- - - -)
FOCAL DEPTH = 5 KM
R = 0, 25, 50, 100 KM
R = 0. KM
FOCAL DEPTH = 5, 10, 25, 50 KM
PERIOD - SEC

Figure II.3.1

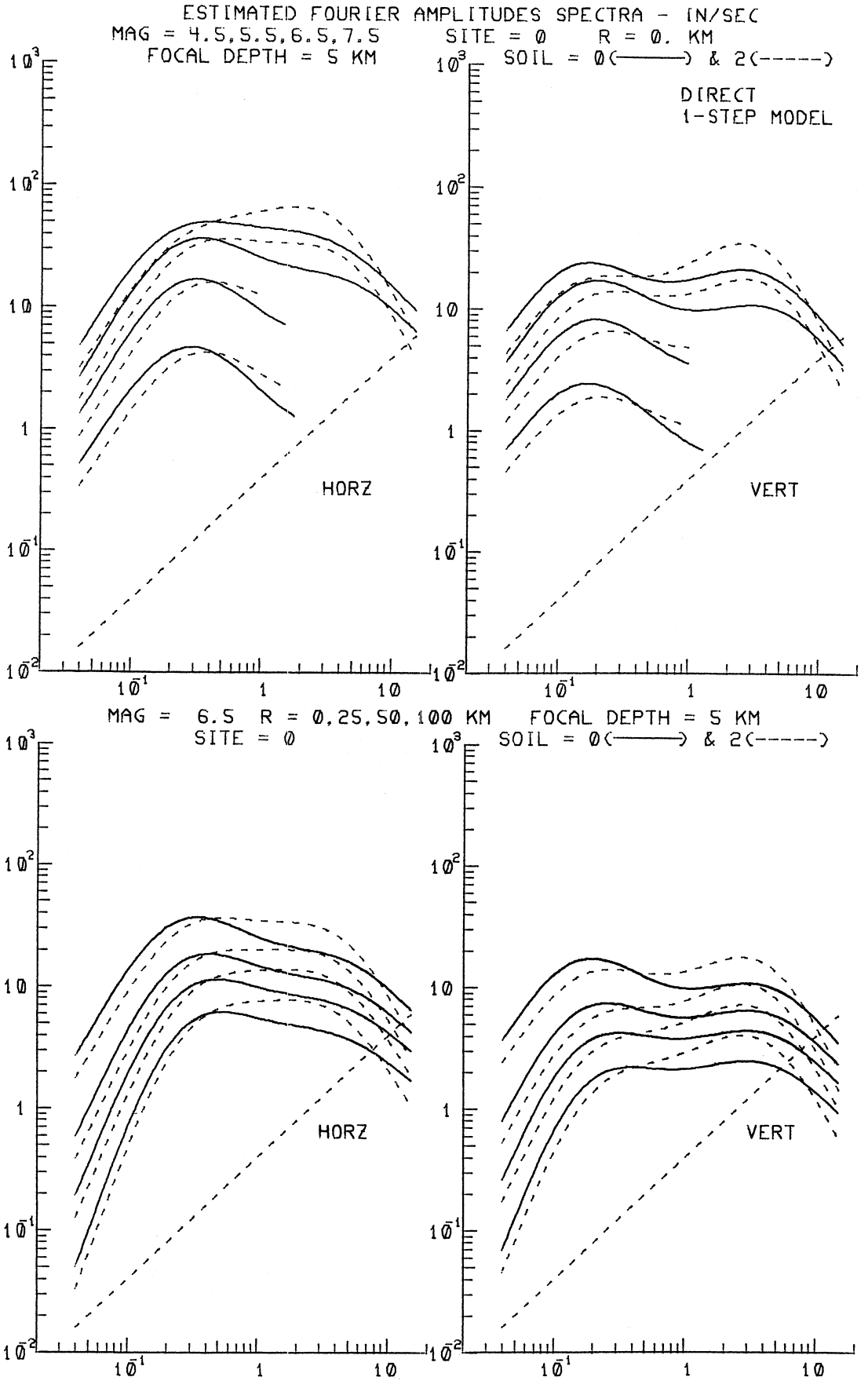
ESTIMATED FOURIER AMPLITUDES SPECTRA - IN/SEC
MAG = 4.5,5.5,6.5,7.5
FOCAL DEPTH = 5 KM
SITE = 0
R = 0. KM
SOIL = 0(———) & 2(-----)
DIRECT
1-STEP MODEL
HORZ
VERT
MAG = 6.5
R = 0,25,50,100 KM
FOCAL DEPTH = 5 KM
SITE = 0
SOIL = 0(———) & 2(-----)
HORZ
VERT
PERIOD - SEC

Figure II.3.2

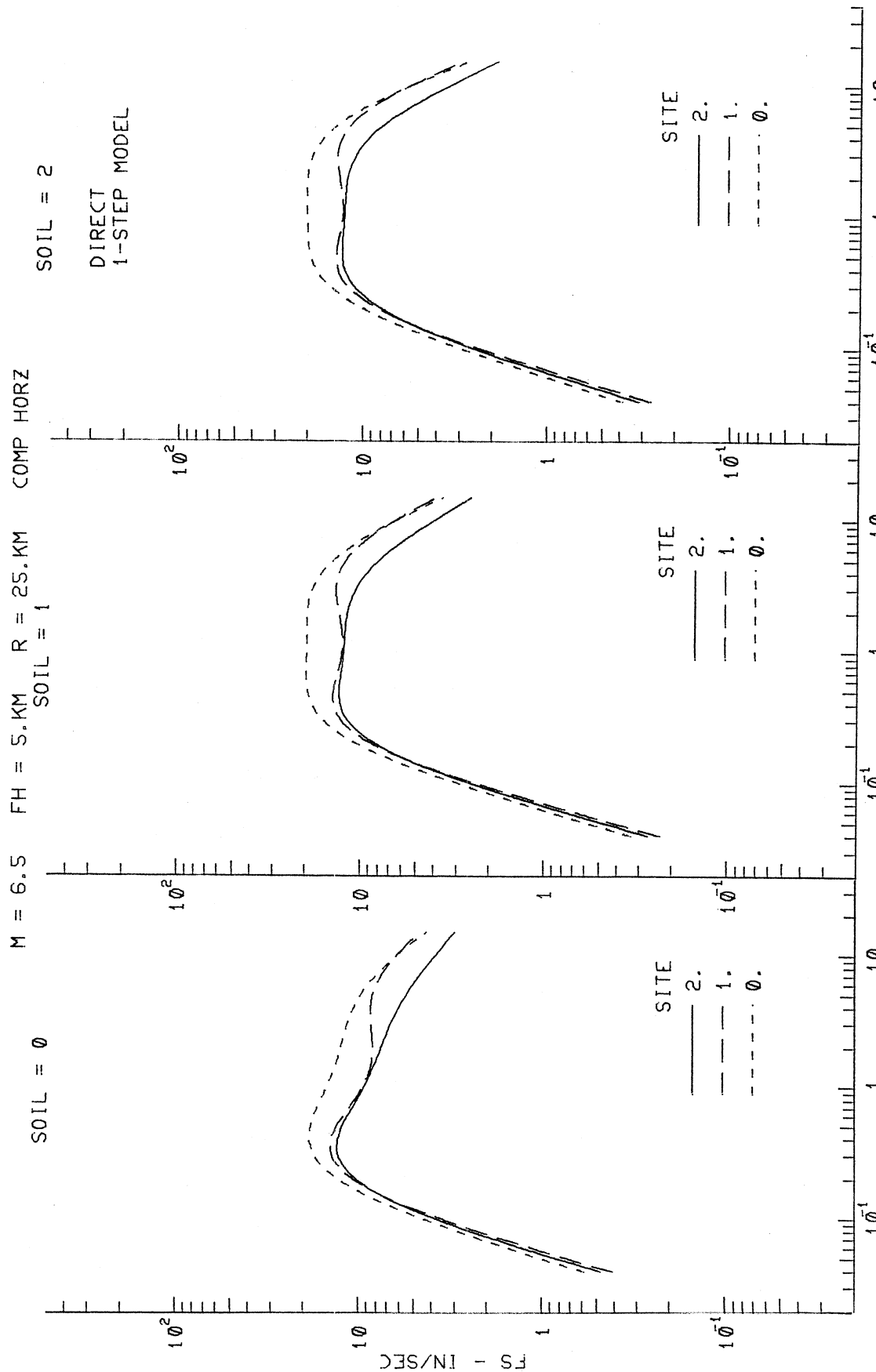
M = 6.5 FH = 5.KM R = 25.KM COMP HORZ
SOIL = 0
SOIL = 1
SOIL = 2
DIRECT
1-STEP MODEL
SITE
2.
1.
0.
FS - IN/SEC
PERIOD - SEC

Figure II.3.3

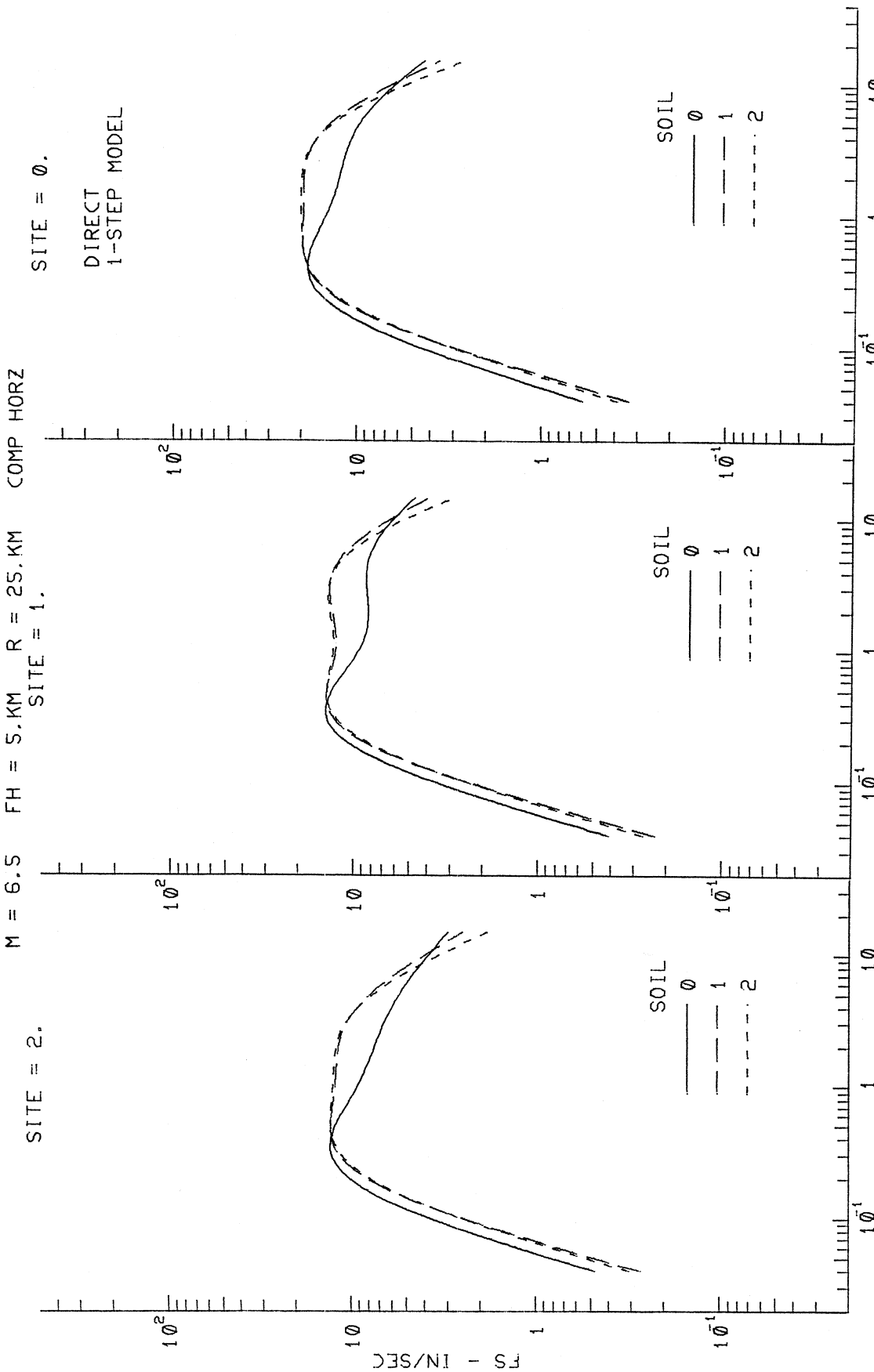
M = 6.5 FH = 5.KM R = 25.KM COMP HORZ
DIRECT
1-STEP MODEL
SITE = 0.
SITE = 1.
SITE = 2.
SOIL
0
1
2
FS - IN/SEC
PERIOD - SEC

Figure II.3.4

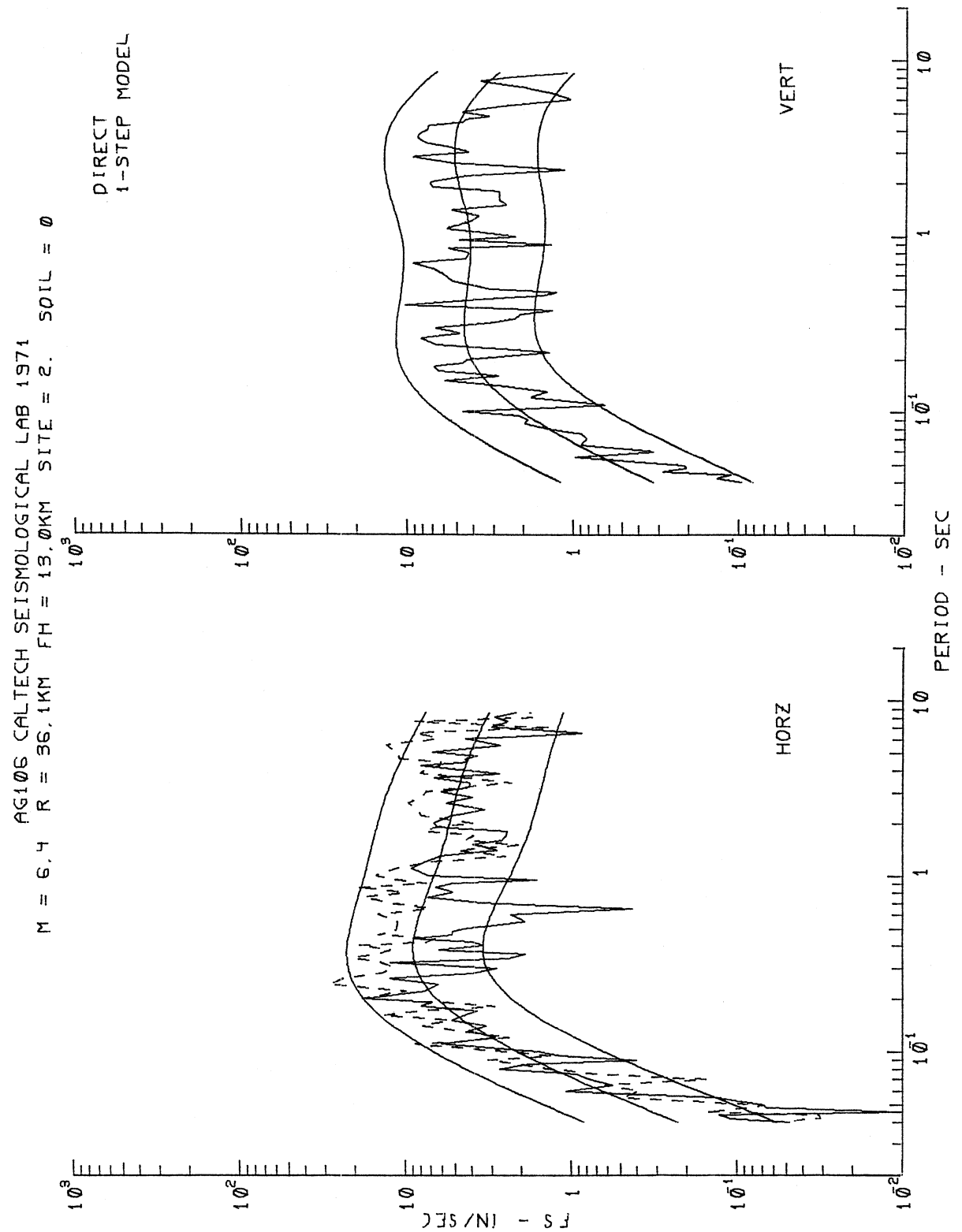
AG106 CALTECH SEISMOLOGICAL LAB 1971
M = 6.4 R = 36.1KM FH = 13.0KM SITE = 2. SOIL = 0
DIRECT
1-STEP MODEL
VERT
HORZ
FS - IN/SEC
PERIOD - SEC

Figure II.3.5

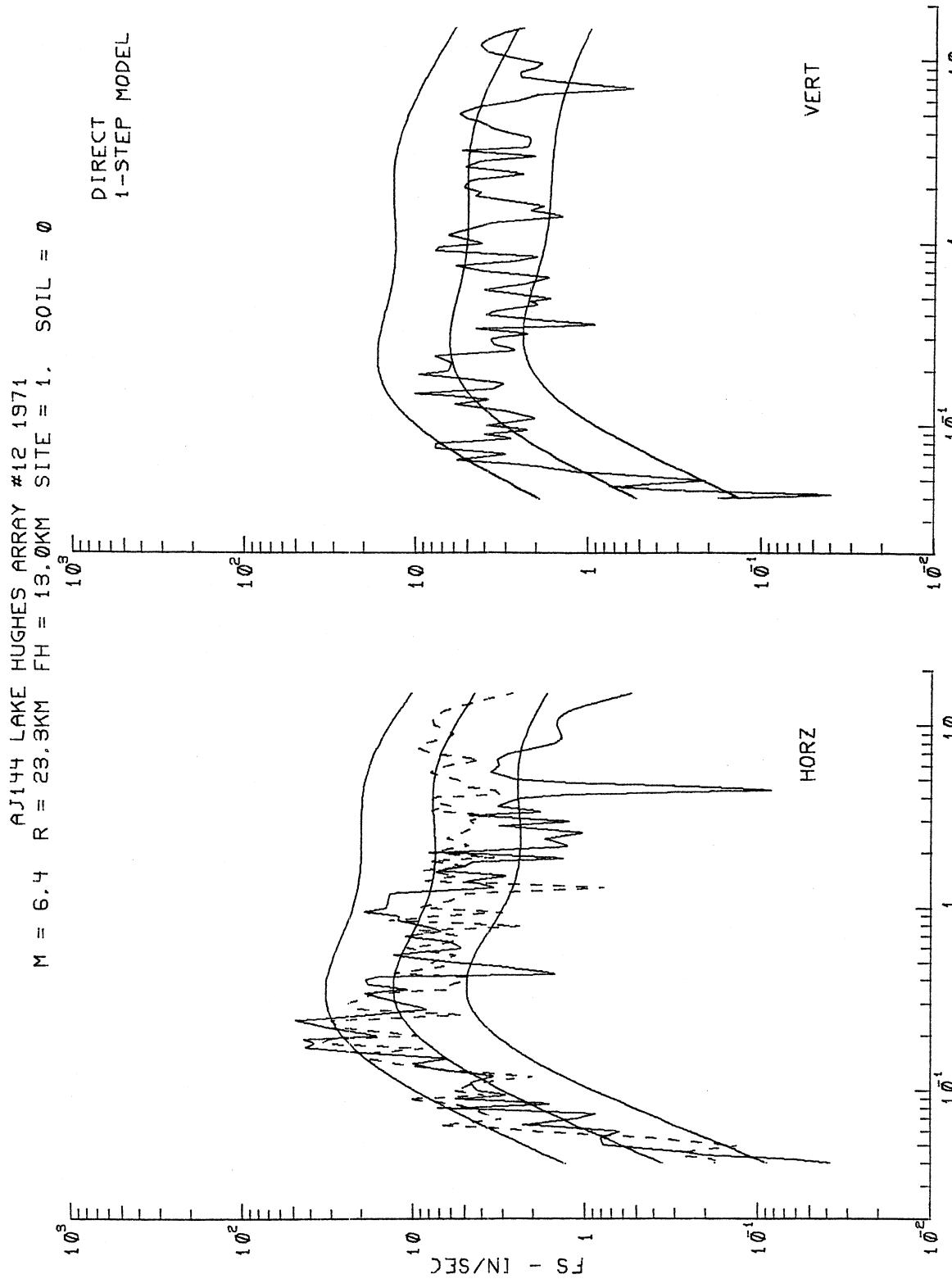
AJ144 LAKE HUGHES ARRAY #12 1971
M = 6.4 R = 23.3KM FH = 13.0KM SITE = 1. SOIL = 0
DIRECT
1-STEP MODEL
HORZ
VERT
FS - IN/SEC
PERIOD - SEC

Figure II.3.6

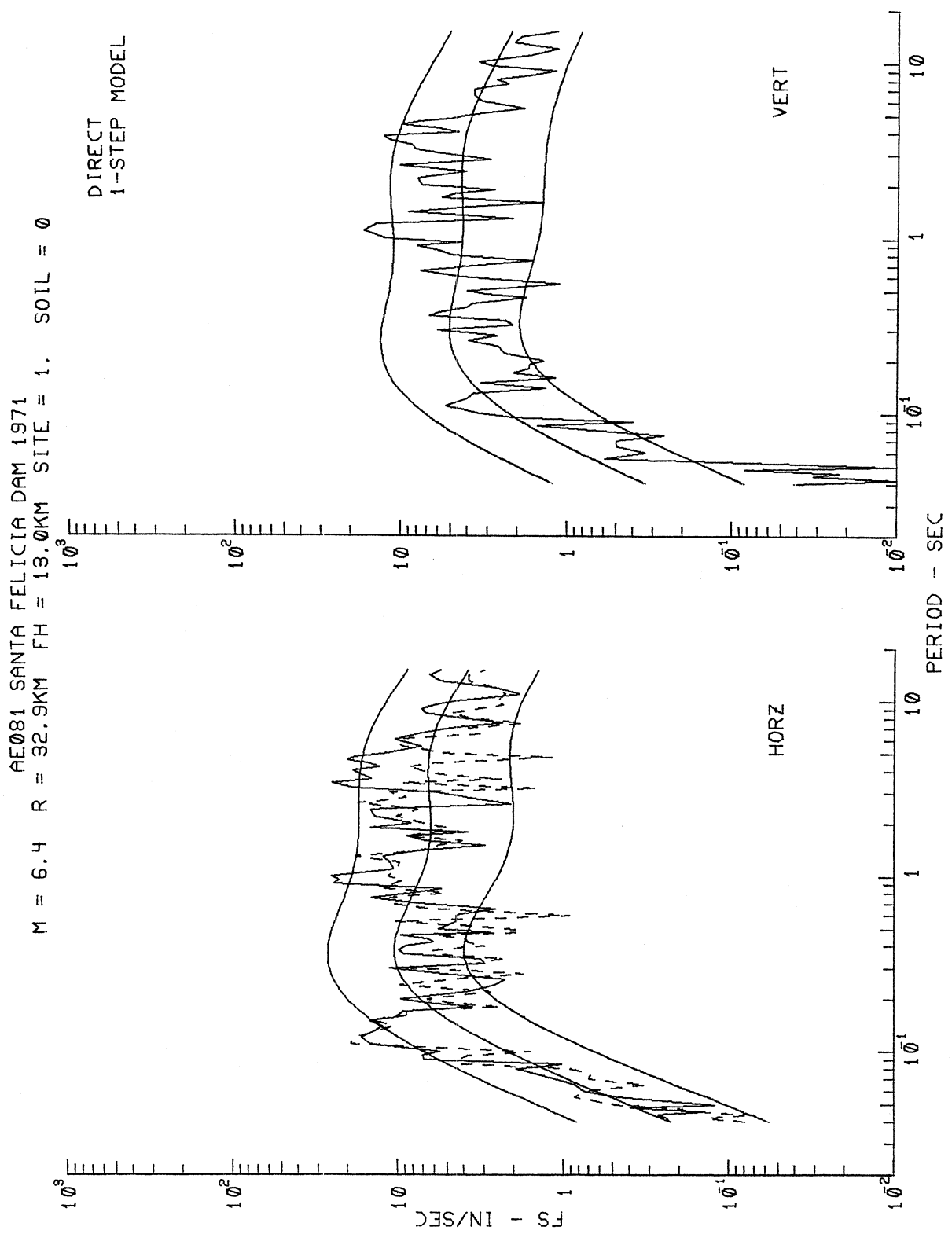
AE081 SANTA FELICIA DAM 1971
M = 6.4 R = 32.9KM FH = 13.0KM SITE = 1. SOIL = 0
DIRECT
1-STEP MODEL
VERT
HORZ
FS - IN/SEC
PERIOD - SEC

Figure II.3.7

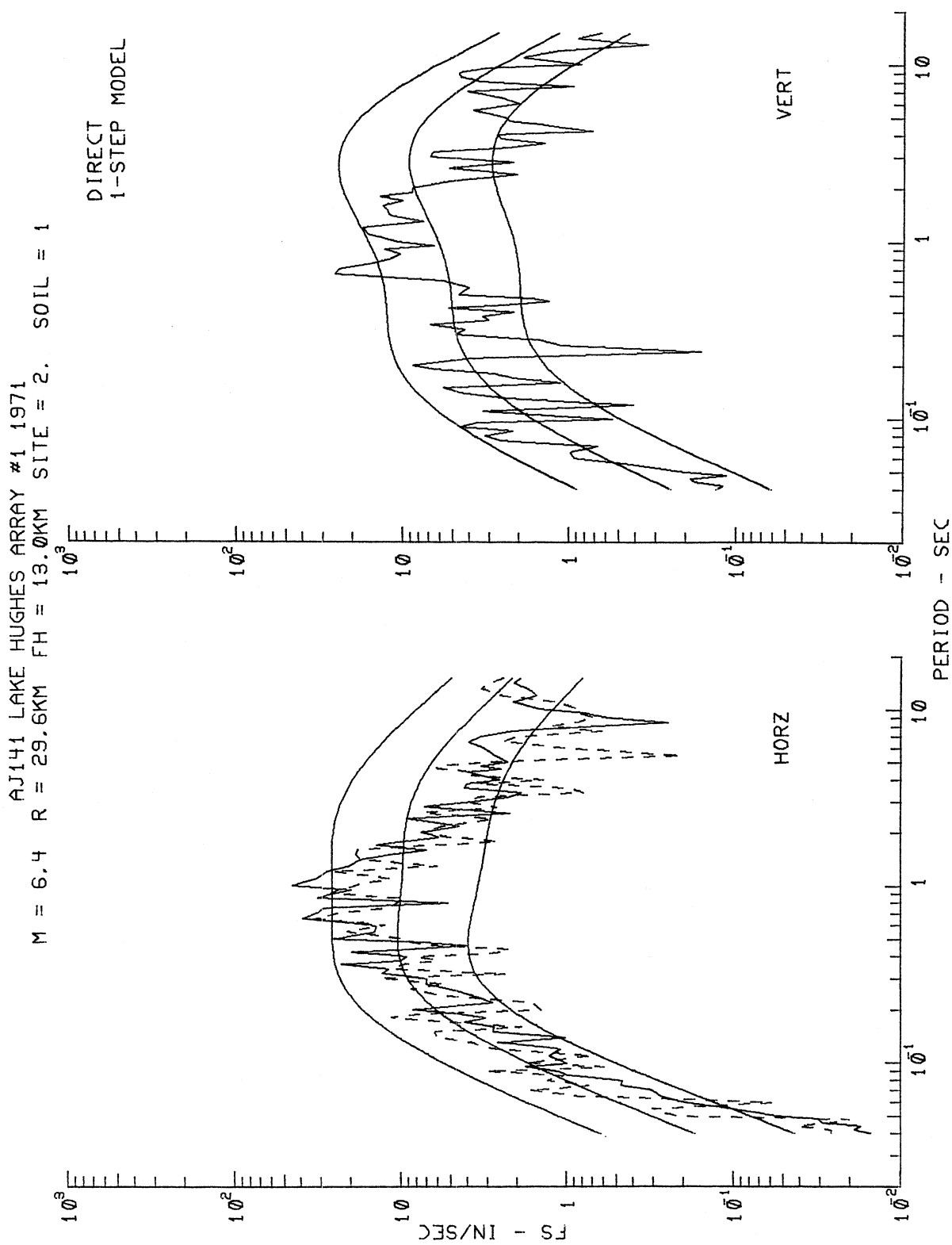
AJ141 LAKE HUGHES ARRAY #1 1971
M = 6.4 R = 29.6KM FH = 13.0KM SITE = 2. SOIL = 1
DIRECT
1-STEP MODEL
HORZ
VERT
FS - IN/SEC
PERIOD - SEC

Figure II.3.8

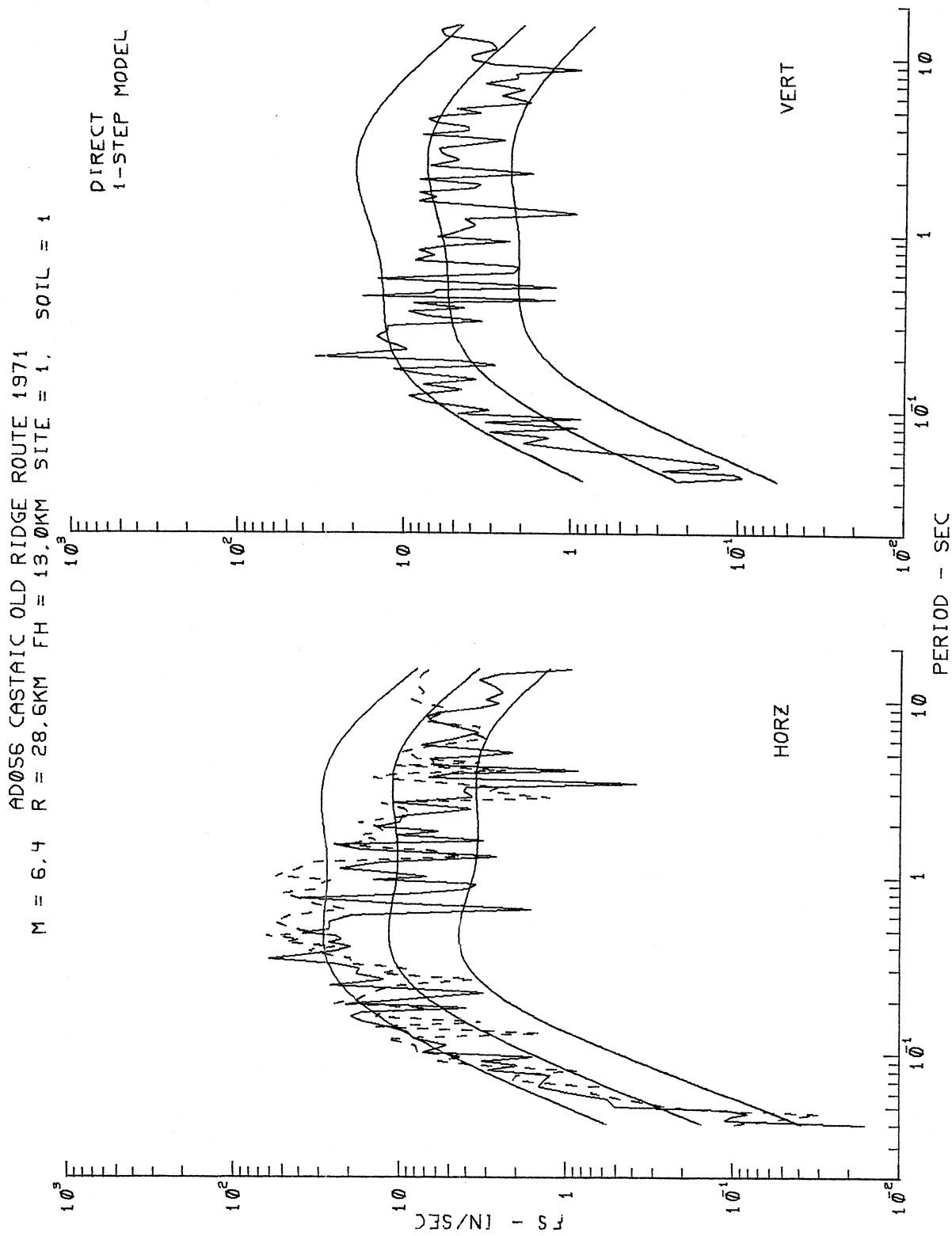
AD056 CASTAIC OLD RIDGE ROUTE 1971
M = 6.4 R = 28.6KM FH = 13.0KM SITE = 1, SOIL = 1
DIRECT
1-STEP MODEL
VERT
HORZ
FS - IN/SEC
PERIOD - SEC

Figure II.3.9

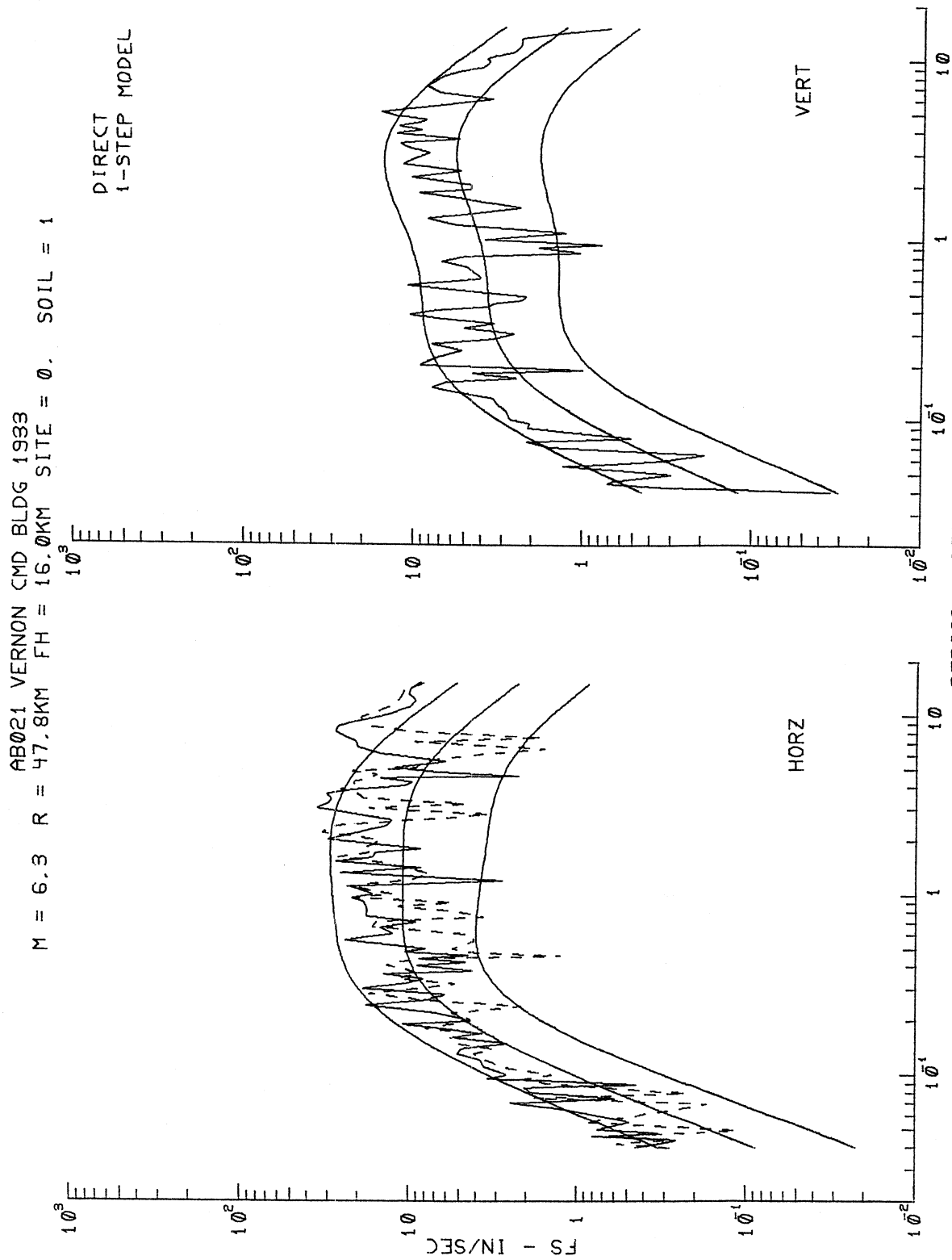

Figure II.3.10

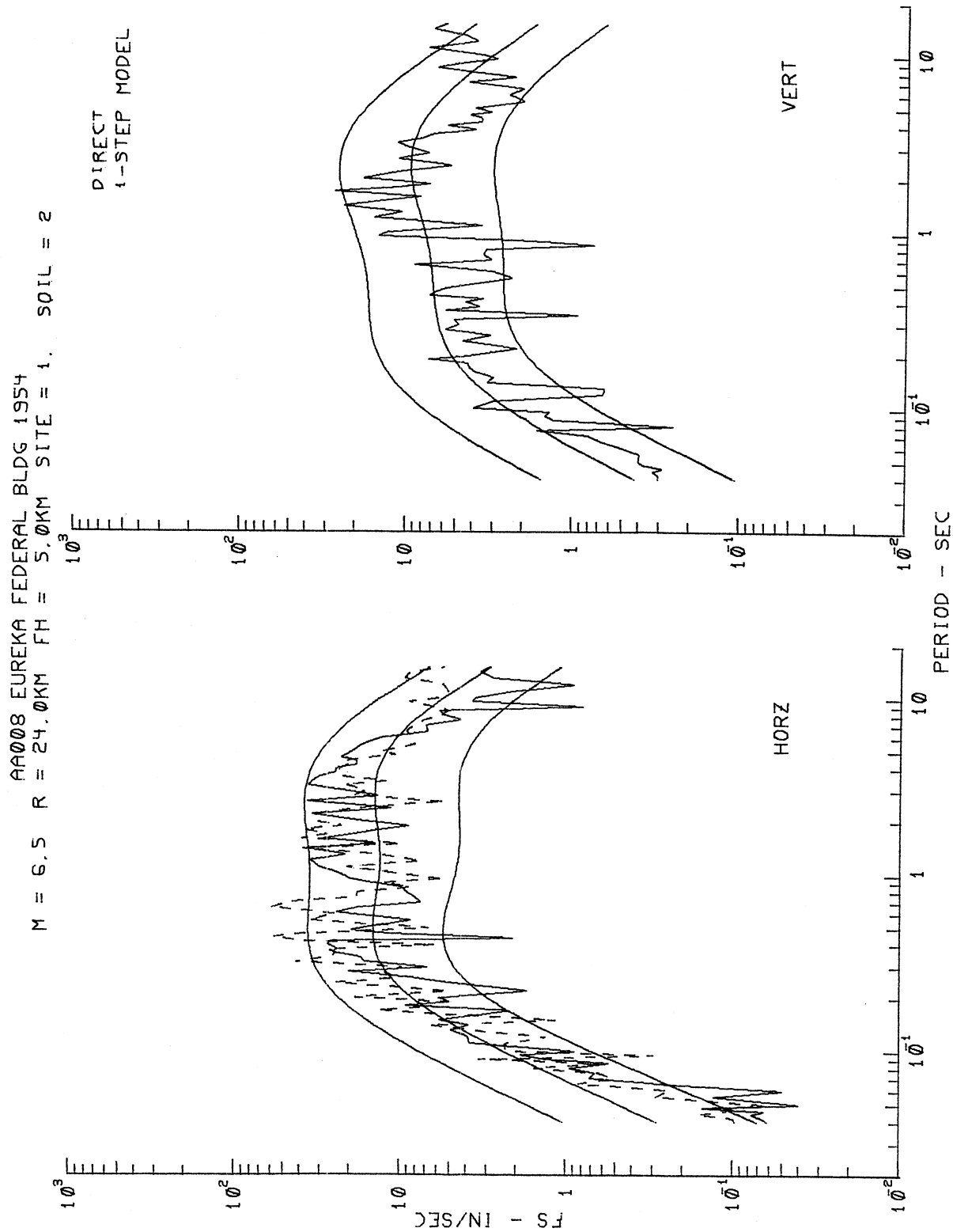

Figure II.3.11

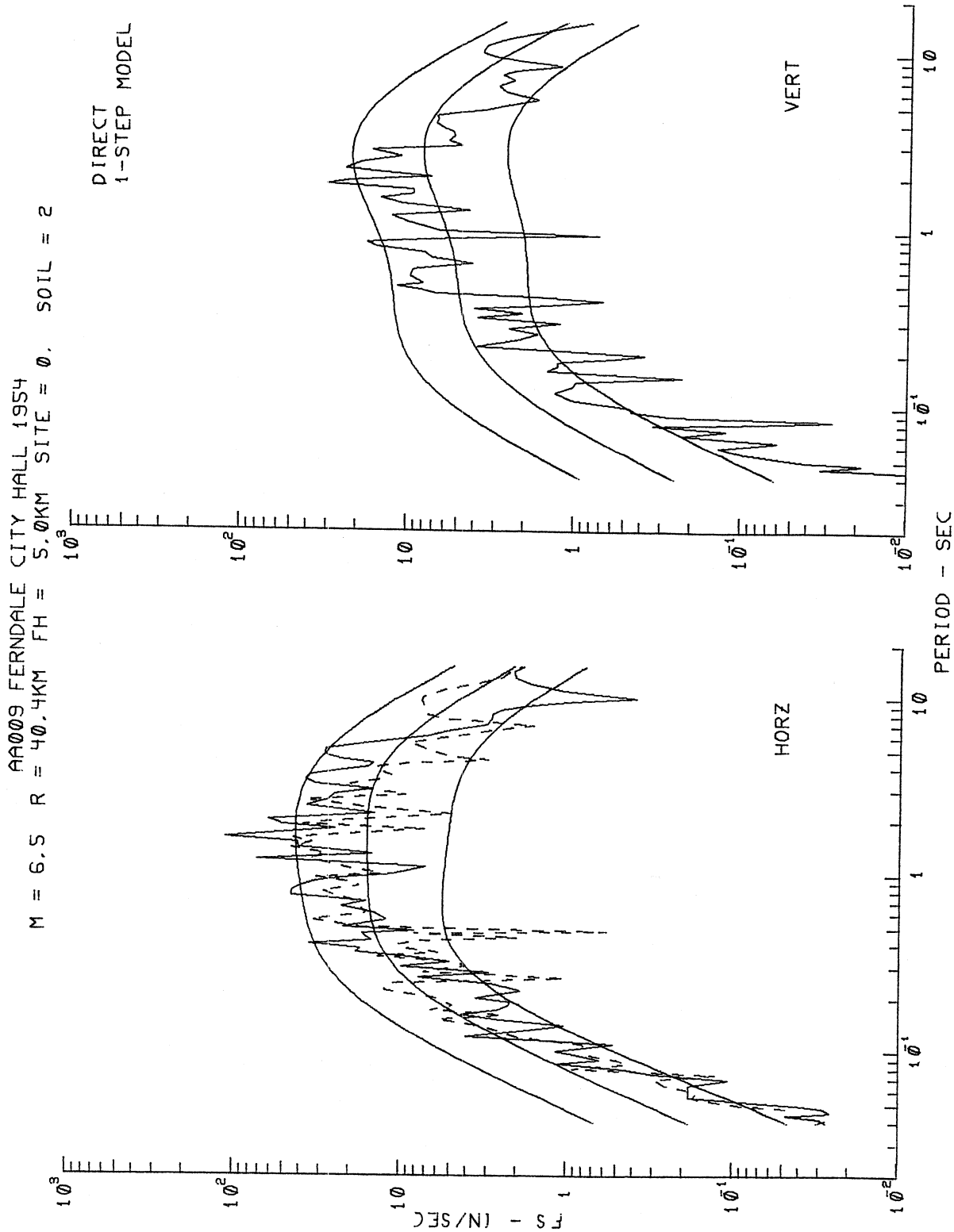

Figure II.3.12

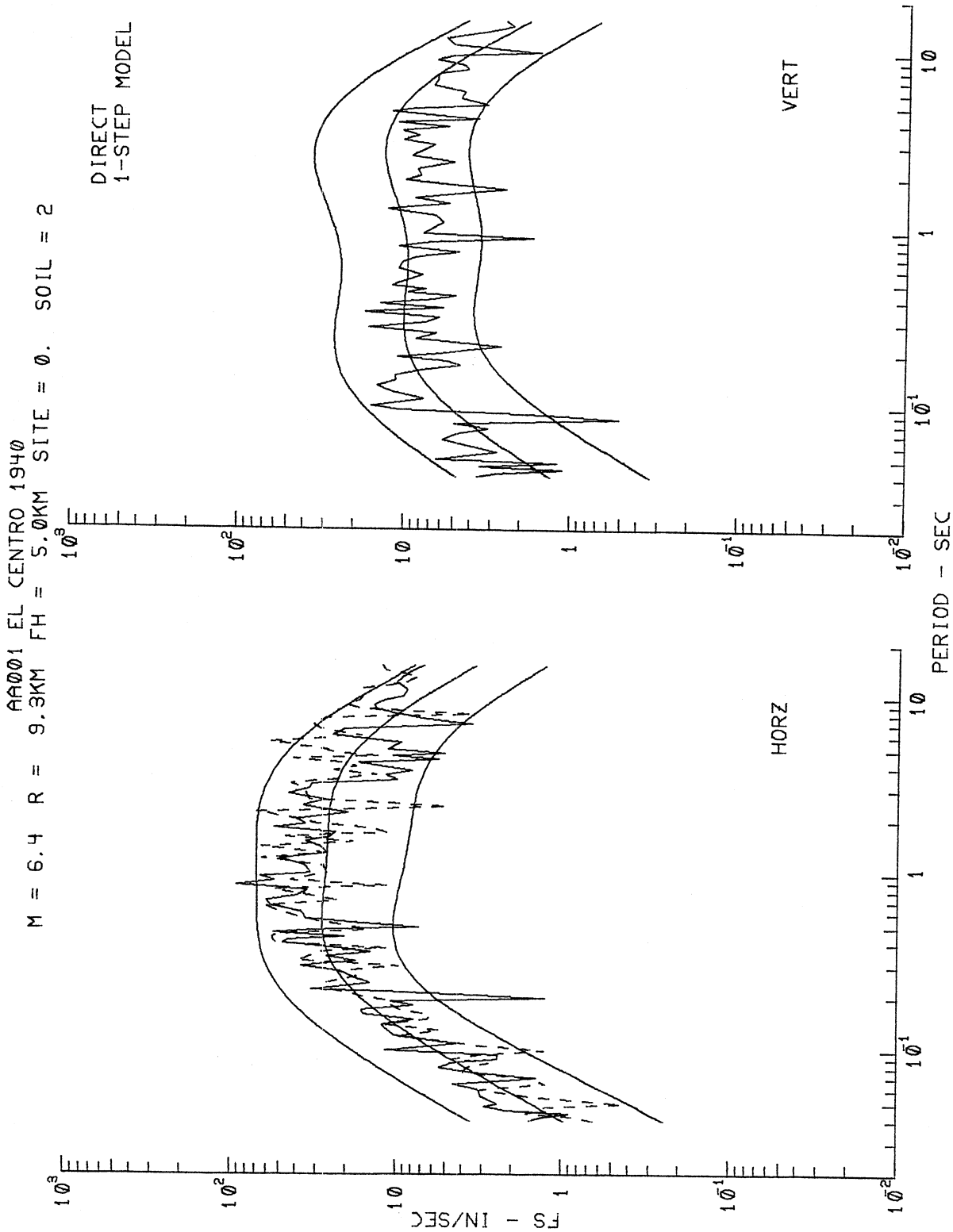

Figure II.3.13

TABLE II.3.1

Geologic Site Conditions \ Soil	"ROCK" (s_L = 0)	STIFF SOIL (s_L = 1)	DEEP SOIL (s_L = 2)
Rock or Intermediate (s = 2 or 1)	AG106 s = 2	AJ141 s = 2	AA008 s = 1
Intermediate (s = 1)	AJ144 s = 1	AD056 s = 1	AA009 s = 0
Intermediate or Alluvium (s = 1 or 0)	AE081 s = 1	AB021 s = 0	AA001 s = 0

spectral amplitudes FS(T) at rock sites (s_L = 0) are higher than those at deep soil sites (s_L = 2). Beyond ~ 0.3 sec., this trend is reversed up to the periods of about 10 sec., so that within this intermediate period range the Fourier amplitudes at deep soil sites are slightly higher than those at the rock sites.

Figures II.3.3 and II.3.4 (as Figure I.6.3 and I.6.4 of Part I) compare the differences in the effects of local geologic site conditions and of local soil classification on FS(T). Similar conclusions can be drawn here as for the model using alluvium depth in Part I.

Figures II.3.5 through II.3.13 present nine examples of how the horizontal and vertical Fourier amplitudes computed from equation (II.1.2) compare with the actual Fourier spectra for the corresponding components of recorded strong-motion data at various sites. The same nine sites have been used here as for the magnitude-depth-soil model in Part I. Table II.3.1 shows the soil (s_L) and the geological site (s) parameters at the chosen sites.

Table II.3.1 shows that for each soil classification s_L = 0, 1 and 2, we attemted to find the sites corresponding to the geological site conditions s = 2 (rock), s = 1 (intermediate) and s = 0 (alluvium). The exceptions are the sites corresponding to s_L = 0 (rock) and s = 1 (AE081) and s_L = 2 (deep soil) and s = 0 (AA009), since such combinations of s and s_L do not exist in the data base. As in the case of the model which was discussed in Part I (Figures I.7.1 to I.7.9), the agreement between the actual and estimated FS(T) amplitudes is good.

II.4 The Residue Two Step Model

As in Part I of this work, the residue, two-step procedure, for the MAG-SITE-SOIL model will be presented here briefly. The first step of this procedure is to scale the Fourier spectra in terms of all the parameters except for soil site classification:

$$\log_{10}\hat{FS}(T) = M_{<} + \mathcal{A}tt(\Delta,M,T) + \hat{b}_1(T)M_{<>} + \hat{b}_2^{(1)}(T)S^{(1)} + \hat{b}_2^{(2)}(T)S^{(2)} + \hat{b}_3(T)v + \hat{b}_4^{(1)}(T)S^{(1)}v + \hat{b}_4^{(2)}(T)S^{(T)}v + \hat{b}_5(T) + \hat{b}_6(T)M_{<>}^2 \quad . \tag{II.4.1}$$

The residues, $\varepsilon(T) = \log_{10}FS(T) - \log_{10}\hat{FS}(T)$, at each site where soil classification is available are then fitted by the equation

$$\varepsilon(T) = b_7^{(1)}(T)S_L^{(1)} + b_7^{(2)}(T)S_L^{(2)} + b_8(T) \quad . \tag{II.4.2}$$

Combining equations (II.4.1) and II.4.2) gives

$$\log_{10}\hat{FS}(T) = M_{<} + \mathcal{A}tt(\Delta,M,T) + \hat{c}_1(T)M_{<>} + \hat{c}_2^{(1)}(T)S^{(1)} + \hat{c}_2^{(2)}(T)S^{(2)} + \hat{c}_5(T) + \hat{c}_6(T)M_{<>}^2 + c_7^{(1)}(T)S_L^{(1)} + c_7^{(2)}(T)S_L^{(2)} \quad , \tag{II.4.3}$$

where $\hat{c}_i(T) = \hat{b}_i(T)$, except for $\hat{c}_5(T)$, with

$$\hat{c}_5(T) = \hat{b}_5(T) + \hat{b}_8(T) \quad , \tag{II.4.4}$$

as in Section I.8, Part I of this work. The regression analyses and all subsequent plots can thus be reprated systematically, analogous to those

TABLE II.4.1
FIGURE NUMBERS OF THE MAG-SITE-SOIL MODEL

Figure Description	Direct 1-step Model	Residue 2-step Model
Scaling Functions	II.2.1	II.4.1
Residues	II.2.2	II.4.2
Residue Statistics	II.2.3	II.4.3
Estimated FS	II.3.1-II.3.4	II.4.4-II.4.7
Actual versus Estimated FS	II.3.5-II.3.13	II.4.8-II.4.16

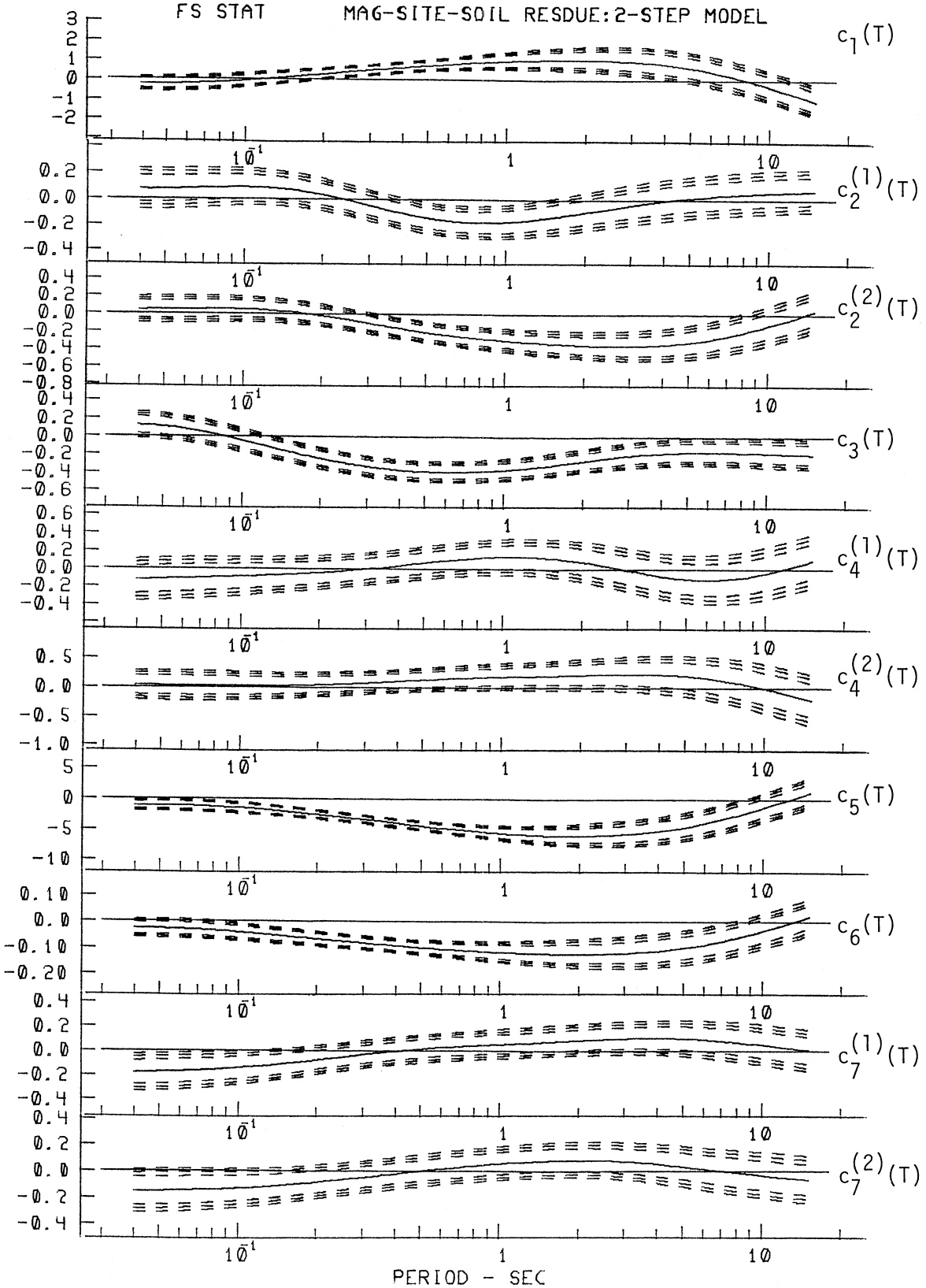
FS STAT
MAG-SITE-SOIL RESDUE:2-STEP MODEL
$c_1(T)$
$c_2^{(1)}(T)$
$c_2^{(2)}(T)$
$c_3(T)$
$c_4^{(1)}(T)$
$c_4^{(2)}(T)$
$c_5(T)$
$c_6(T)$
$c_7^{(1)}(T)$
$c_7^{(2)}(T)$
PERIOD - SEC

Figure II.4.1

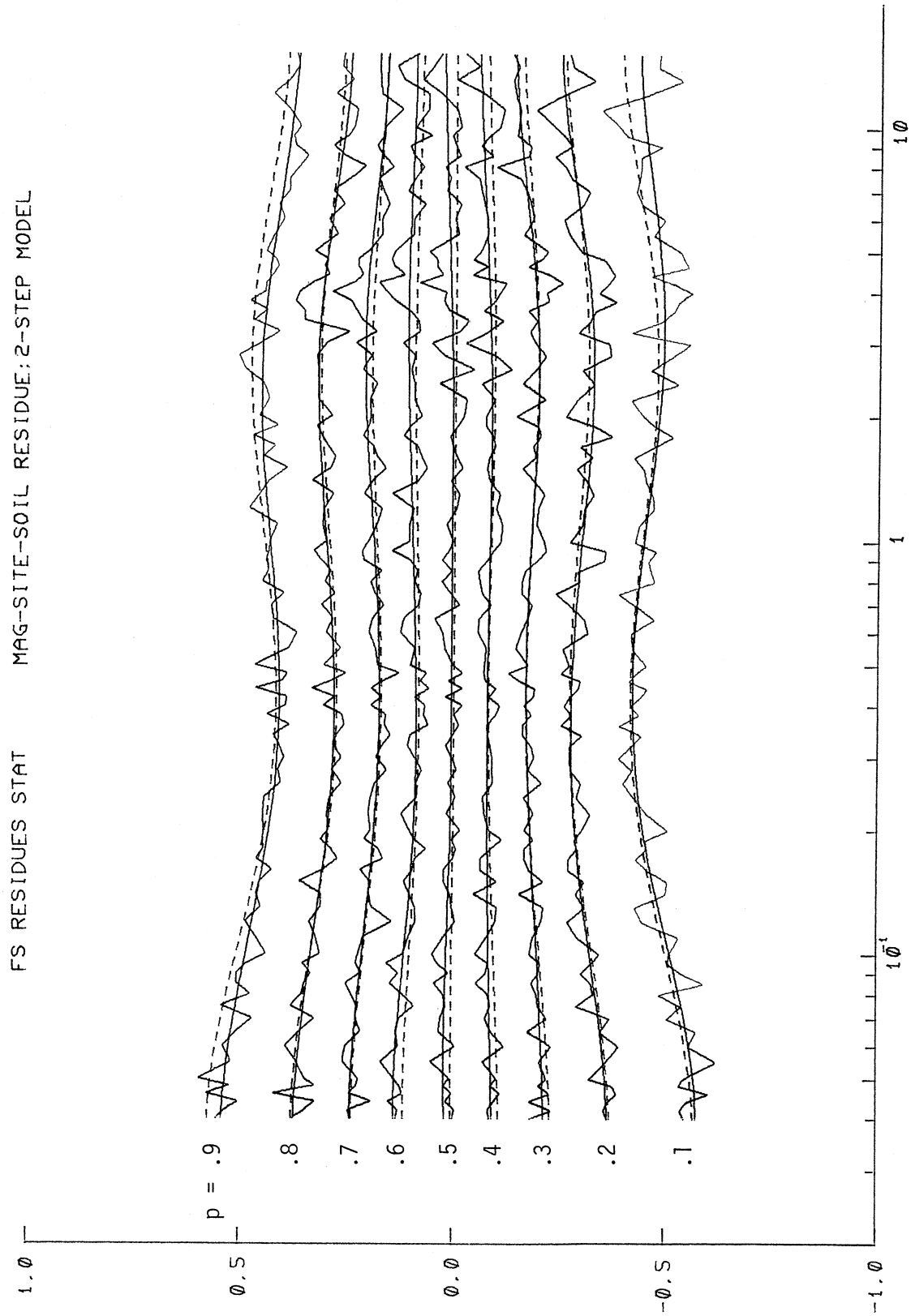
FS RESIDUES STAT
MAG-SITE-SOIL RESIDUE: 2-STEP MODEL
1.0
0.5
0.0
-0.5
-1.0
p = .9
.8
.7
.6
.5
.4
.3
.2
.1
10⁻¹
1
10

Figure II.4.2

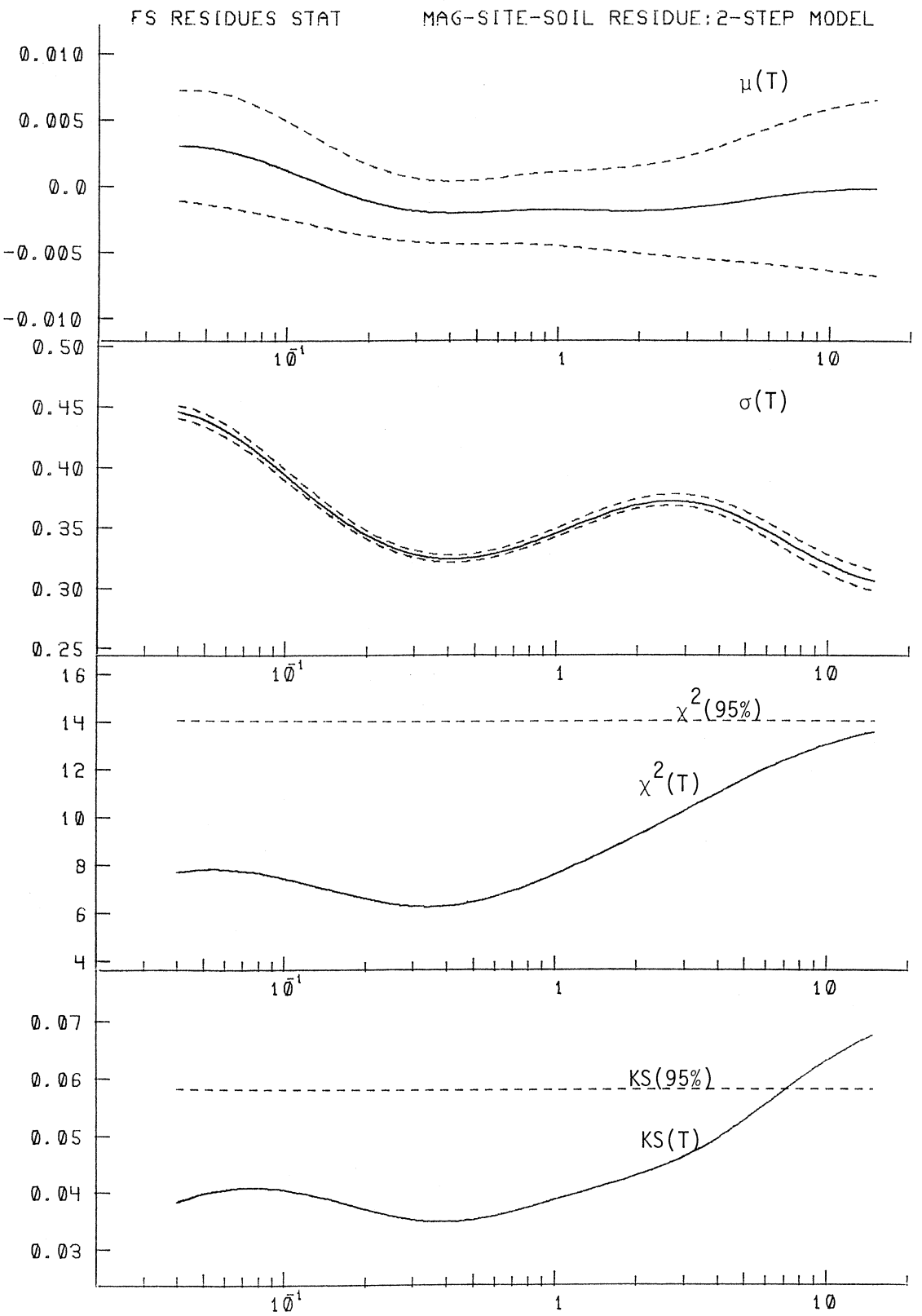
FS RESIDUES STAT
MAG-SITE-SOIL RESIDUE:2-STEP MODEL
μ(T)
σ(T)
χ²(95%)
χ²(T)
KS(95%)
KS(T)

Figure II.4.3

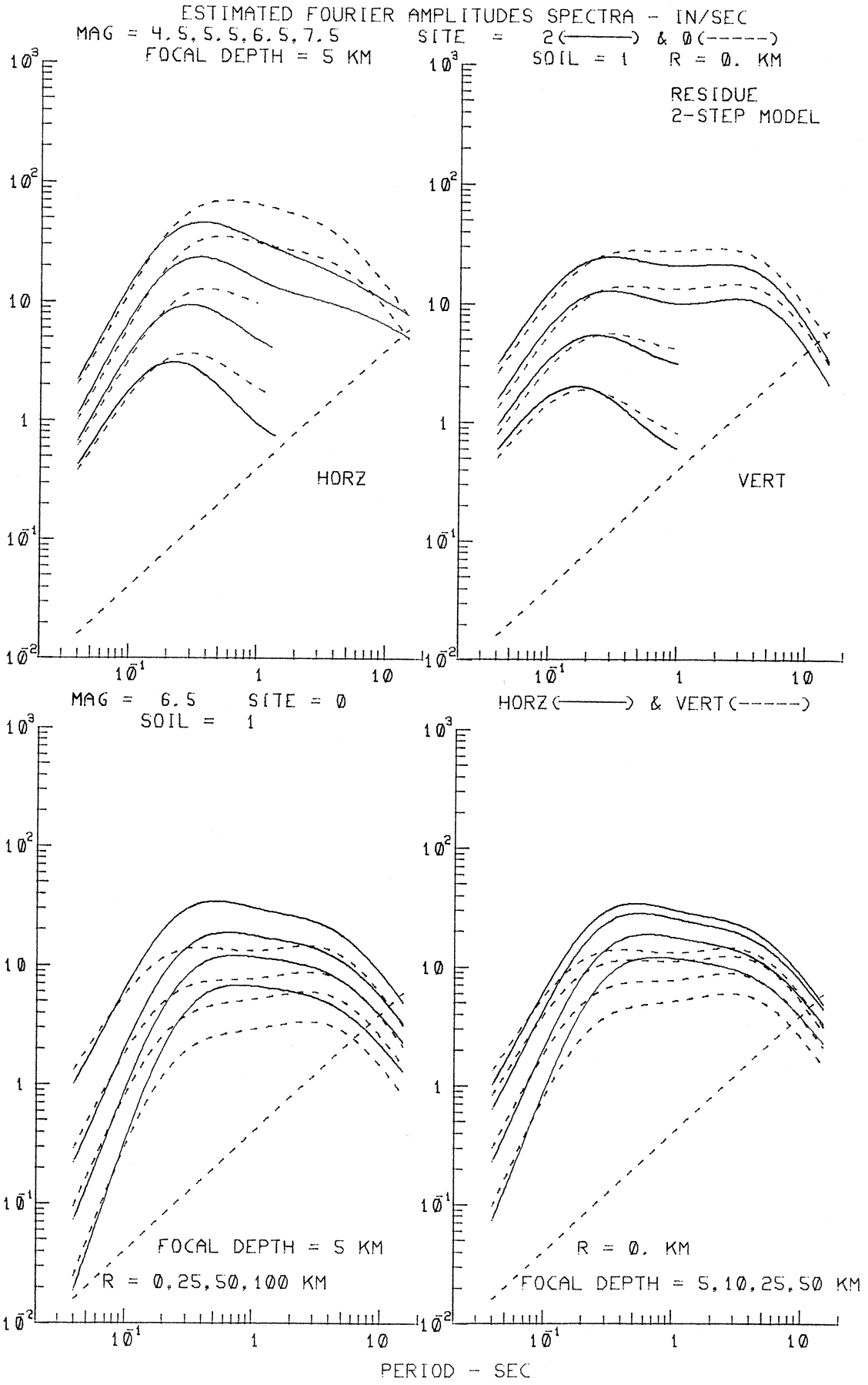
ESTIMATED FOURIER AMPLITUDES SPECTRA - IN/SEC
MAG = 4.5, 5.5, 6.5, 7.5
FOCAL DEPTH = 5 KM
SITE = 2(———) & 0(-----)
SOIL = 1 R = 0. KM
RESIDUE
2-STEP MODEL
HORZ
VERT
MAG = 6.5 SITE = 0
SOIL = 1
HORZ(———) & VERT(-----)
FOCAL DEPTH = 5 KM
R = 0, 25, 50, 100 KM
R = 0. KM
FOCAL DEPTH = 5, 10, 25, 50 KM
PERIOD - SEC

Figure II.4.4

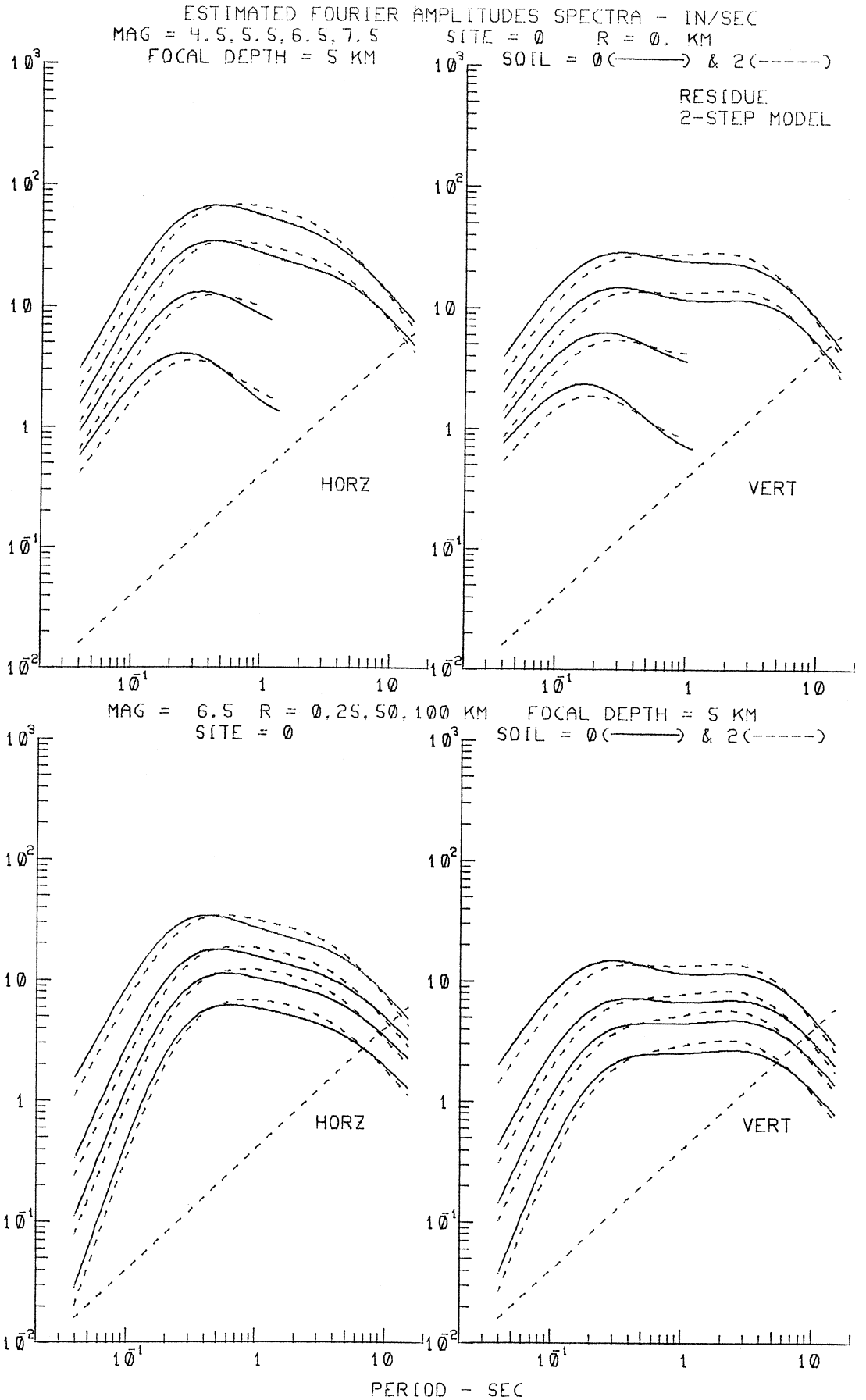
ESTIMATED FOURIER AMPLITUDES SPECTRA - IN/SEC
MAG = 4.5, 5.5, 6.5, 7.5
FOCAL DEPTH = 5 KM
SITE = 0
R = 0. KM
SOIL = 0(——) & 2(- - - -)
RESIDUE
2-STEP MODEL
HORZ
VERT
MAG = 6.5
R = 0, 25, 50, 100 KM
FOCAL DEPTH = 5 KM
SITE = 0
SOIL = 0(——) & 2(- - - -)
HORZ
VERT
PERIOD - SEC

Figure II.4.5

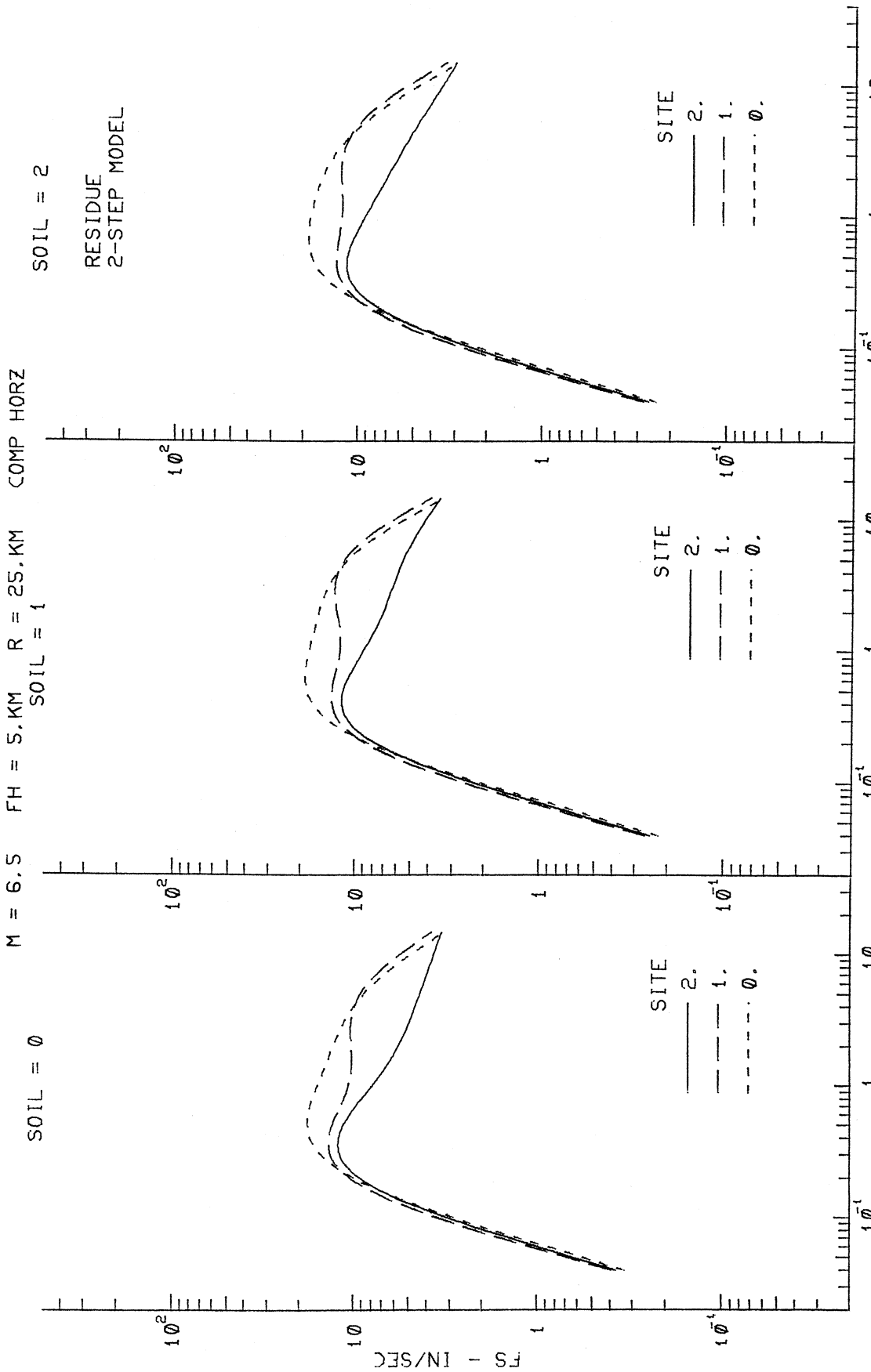
M = 6.5 FH = 5.KM R = 25.KM COMP HORZ
RESIDUE
2-STEP MODEL
SOIL = 0
SOIL = 1
SOIL = 2
SITE
2.
1.
0.
FS - IN/SEC
PERIOD - SEC

Figure II.4.6

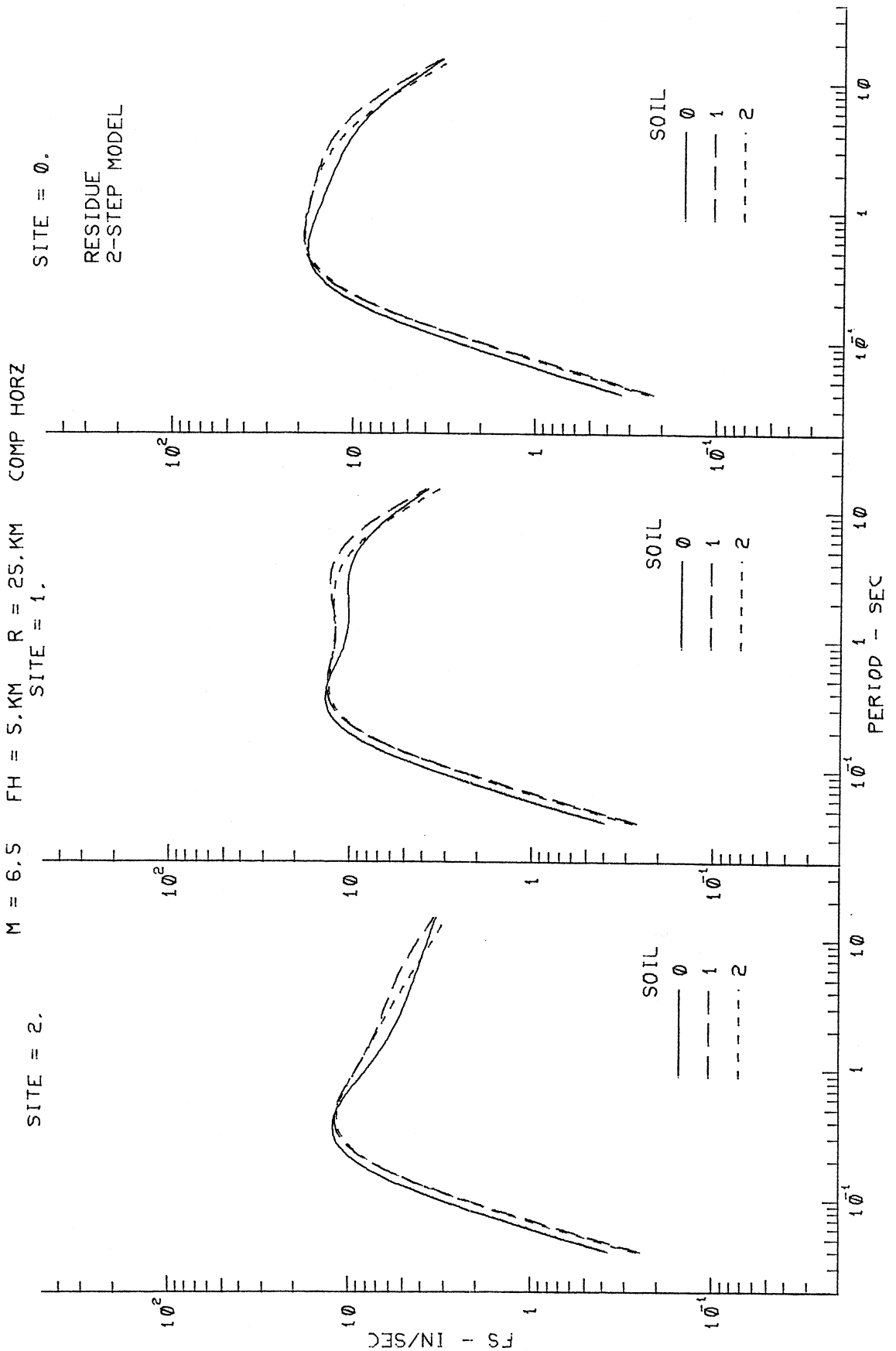
M = 6.5 FH = 5.KM R = 25.KM COMP HORZ
RESIDUE
2-STEP MODEL
SITE = 0.
SITE = 1.
SITE = 2.
SOIL
0
1
2
FS - IN/SEC
PERIOD - SEC

Figure II.4.7

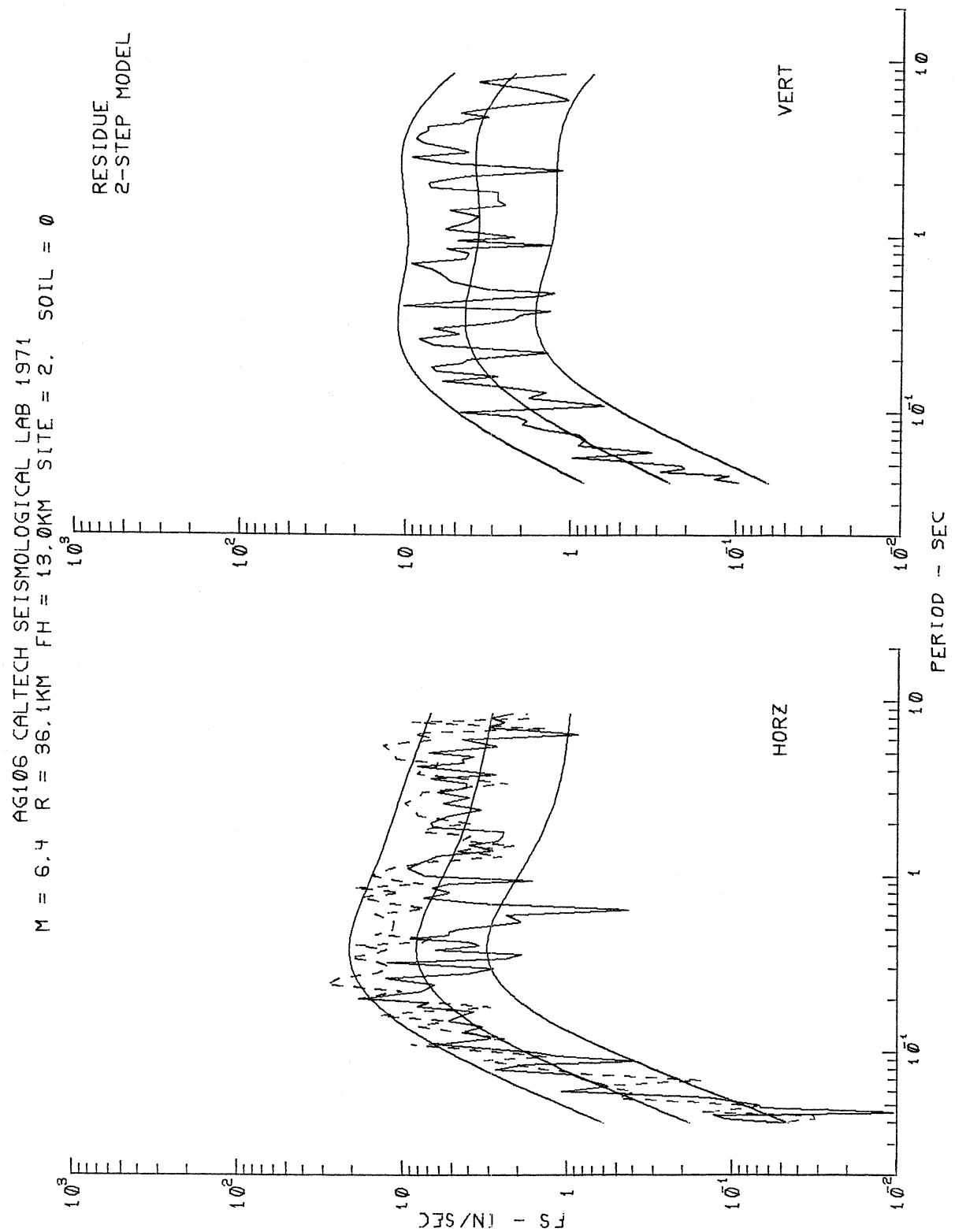
AG106 CALTECH SEISMOLOGICAL LAB 1971
M = 6.4 R = 36.1KM FH = 13.0KM SITE = 2. SOIL = 0
RESIDUE
2-STEP MODEL
VERT
HORZ
FS - IN/SEC
PERIOD - SEC

Figure II.4.8

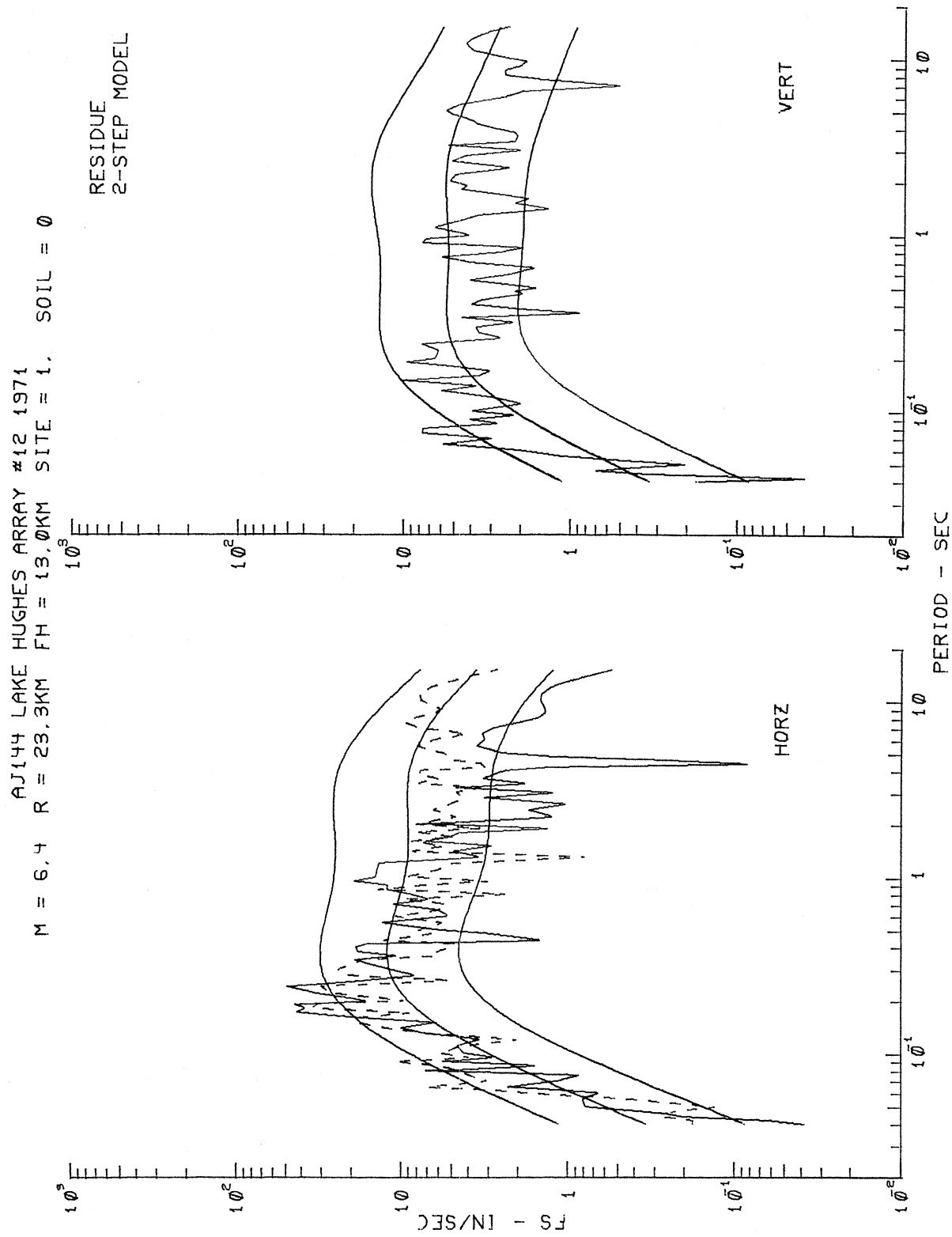
AJ144 LAKE HUGHES ARRAY #12 1971
M = 6.4 R = 23.3KM FH = 13.ØKM SITE = 1. SOIL = Ø
RESIDUE
2-STEP MODEL
VERT
HORZ
FS - IN/SEC
PERIOD - SEC

Figure II.4.9

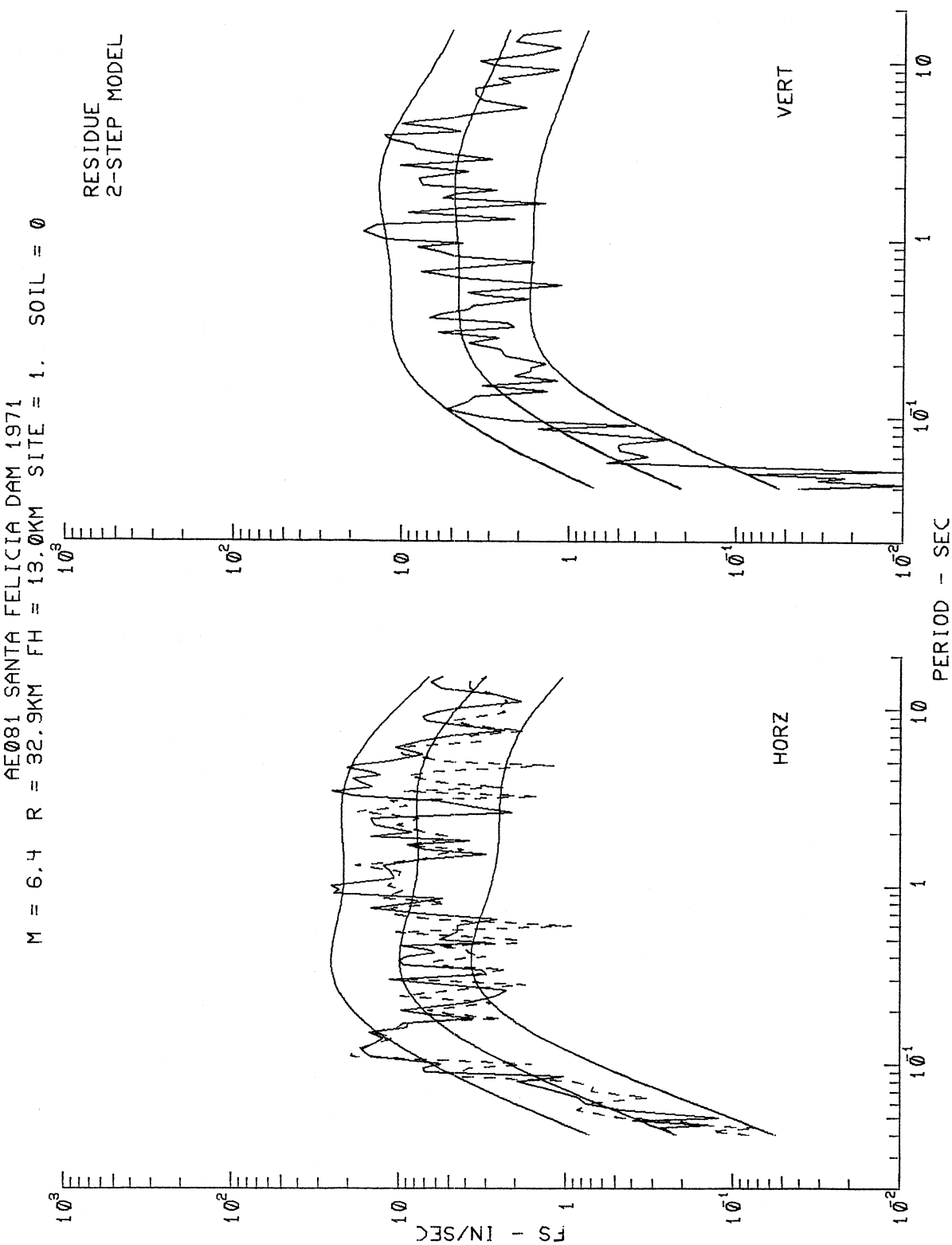

Figure II.4.10

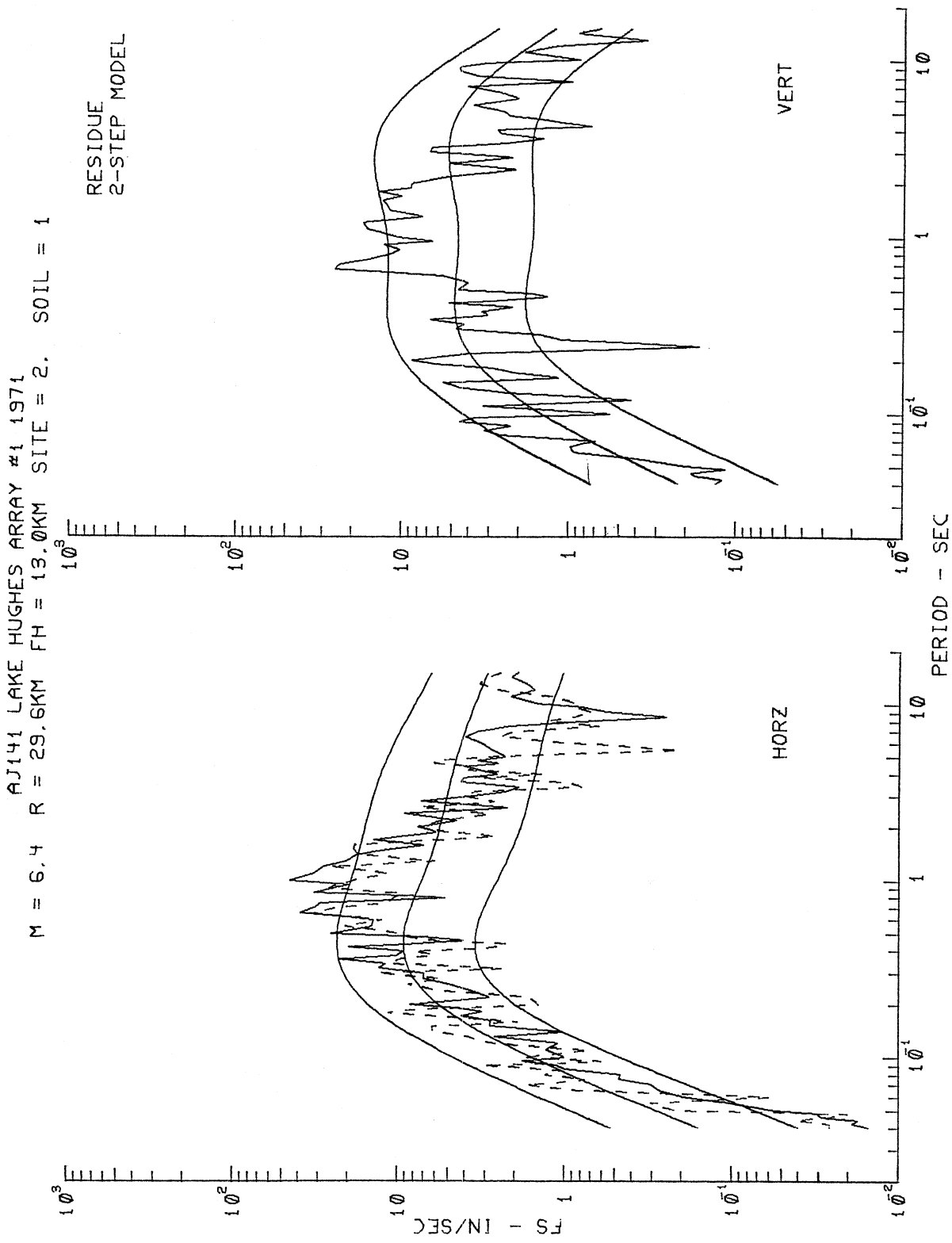

Figure II.4.11

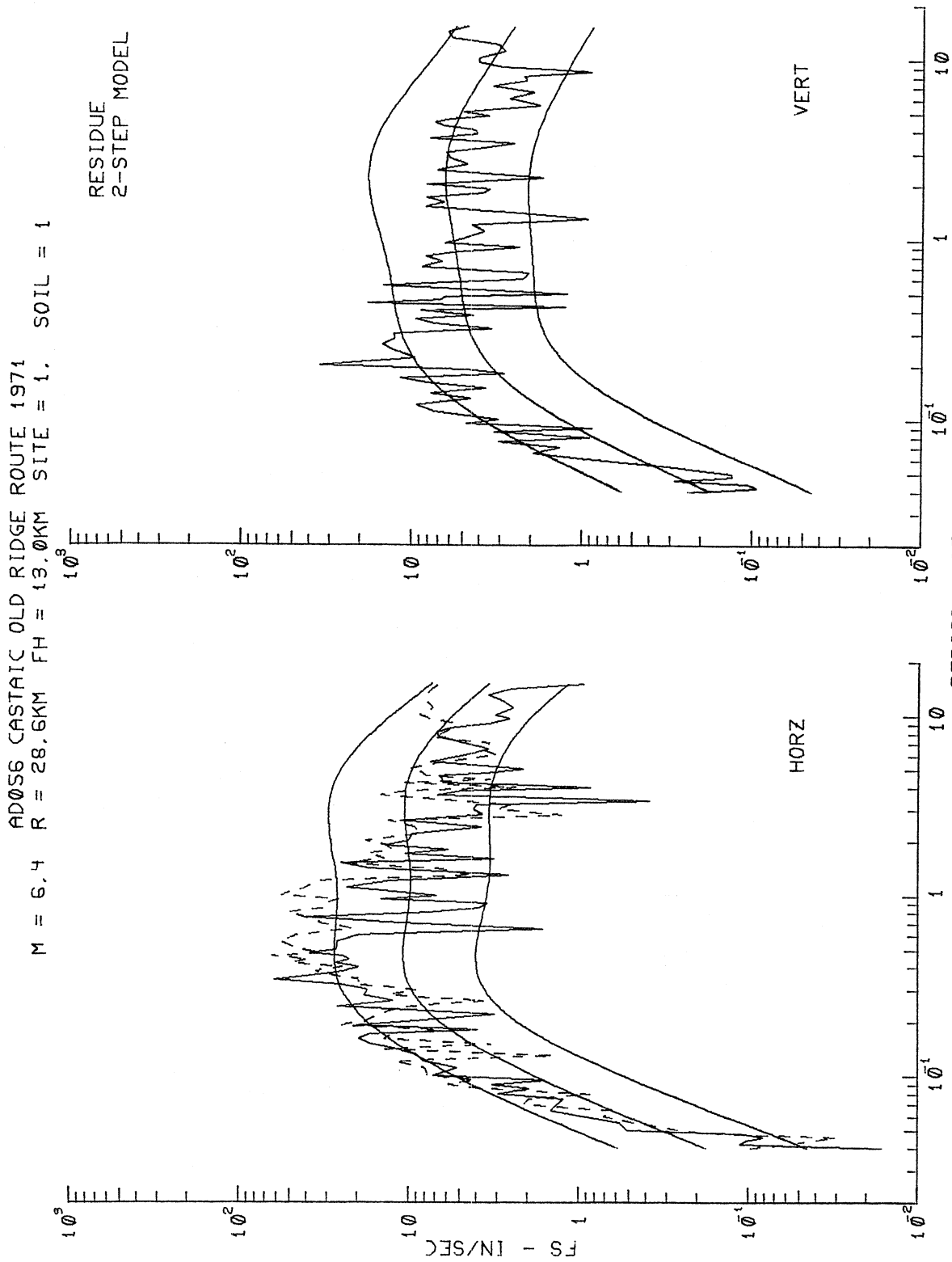

Figure II.4.12

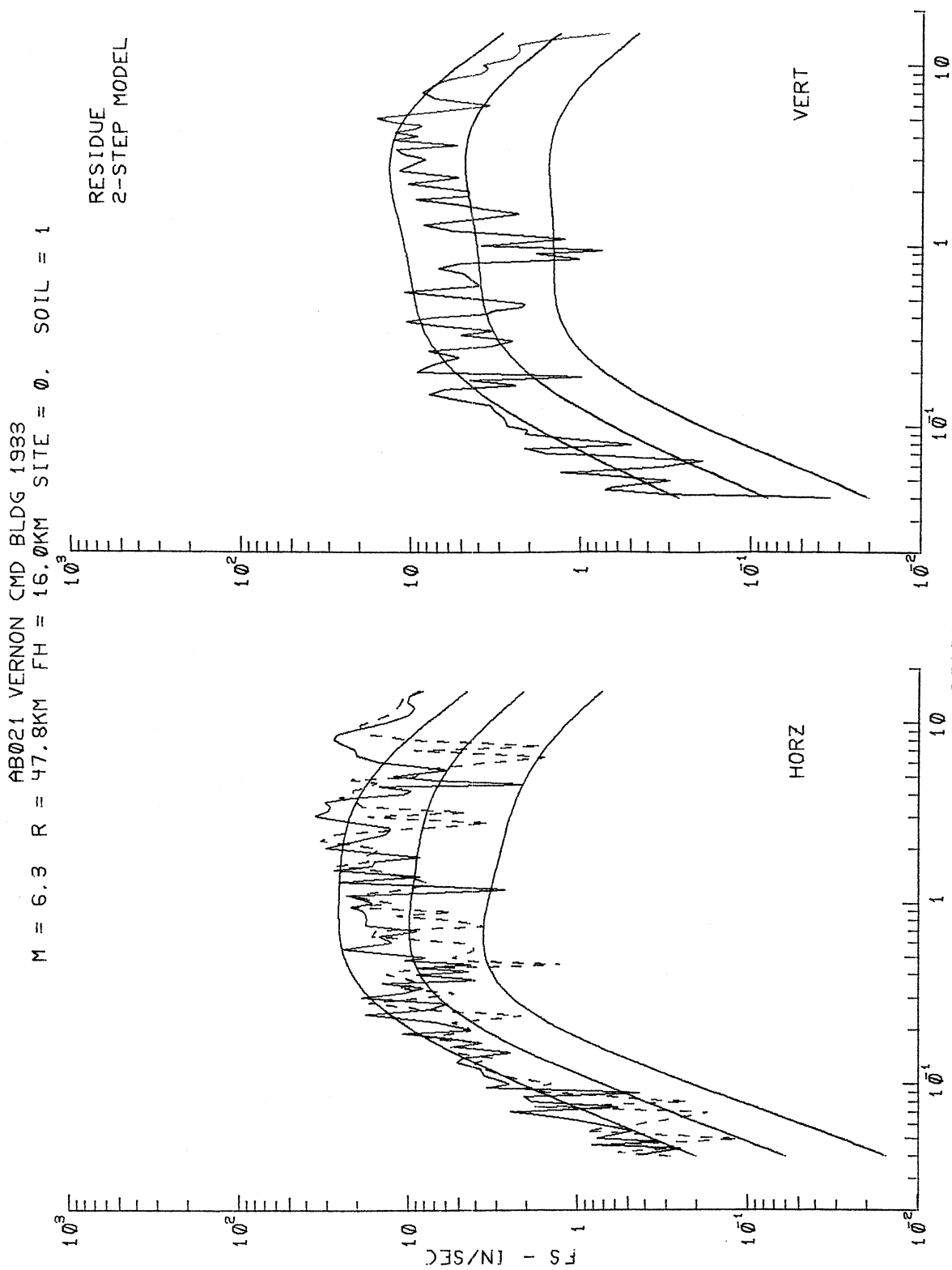

Figure II.4.13

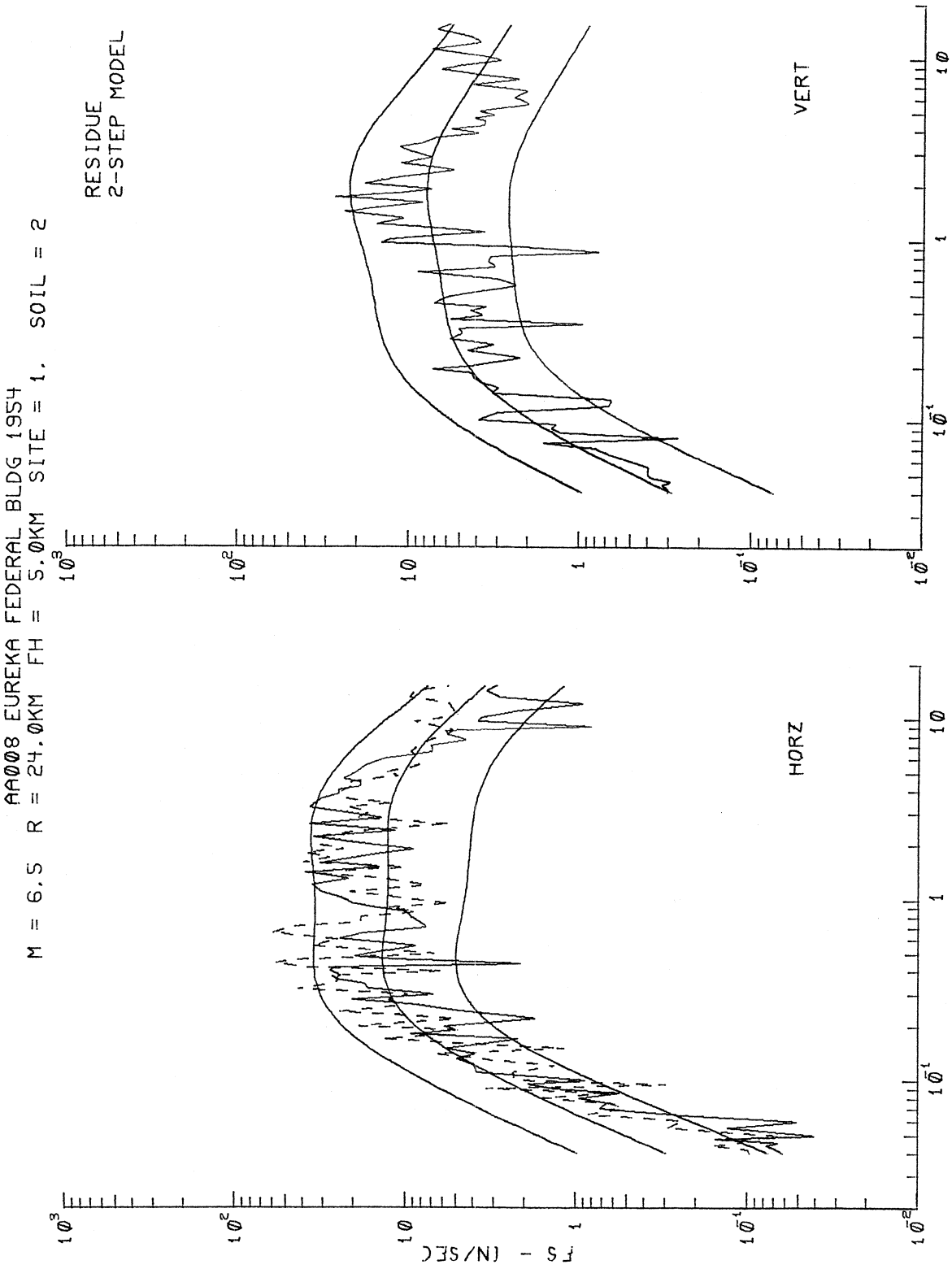

Figure II.4.14

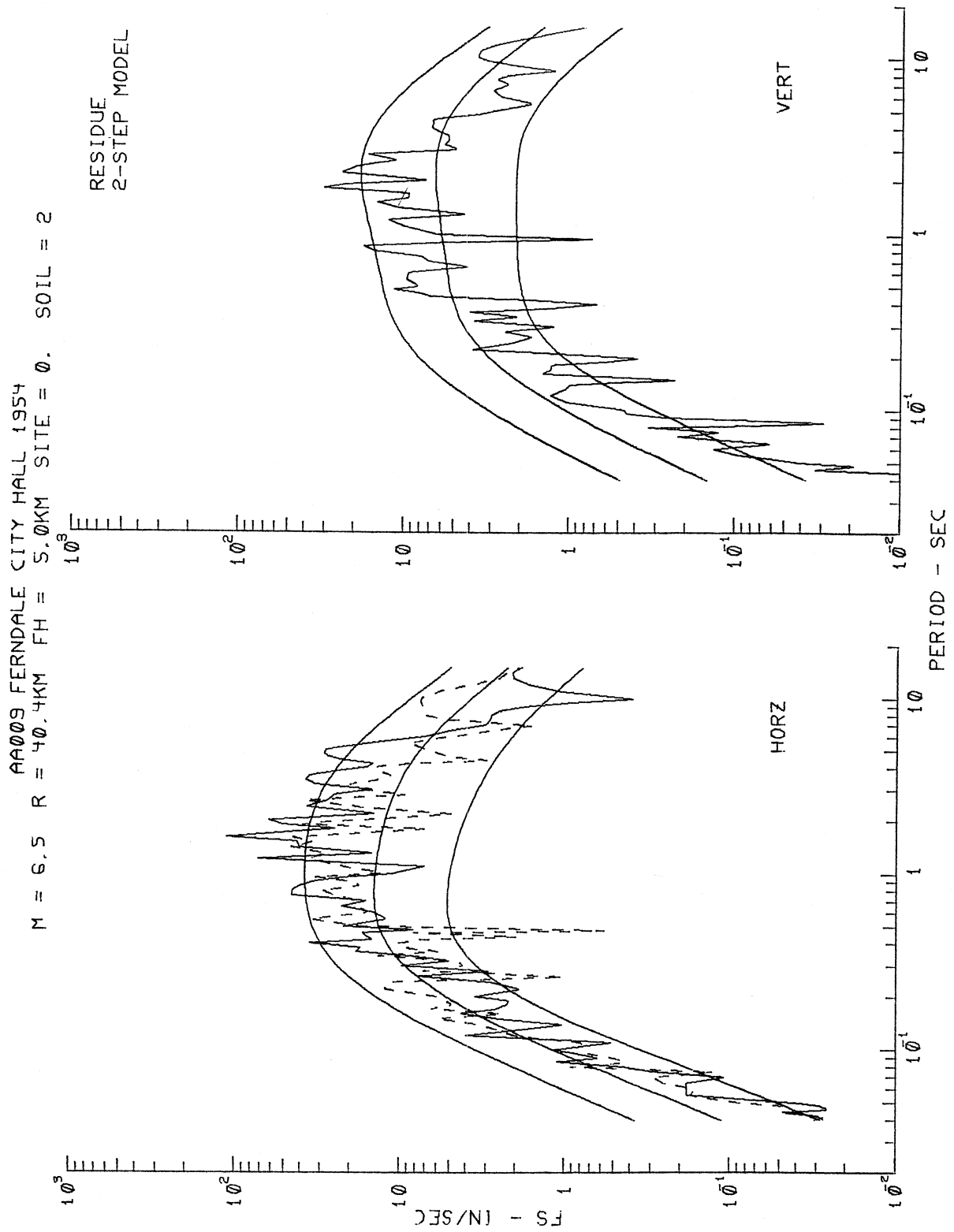

Figure II.4.15

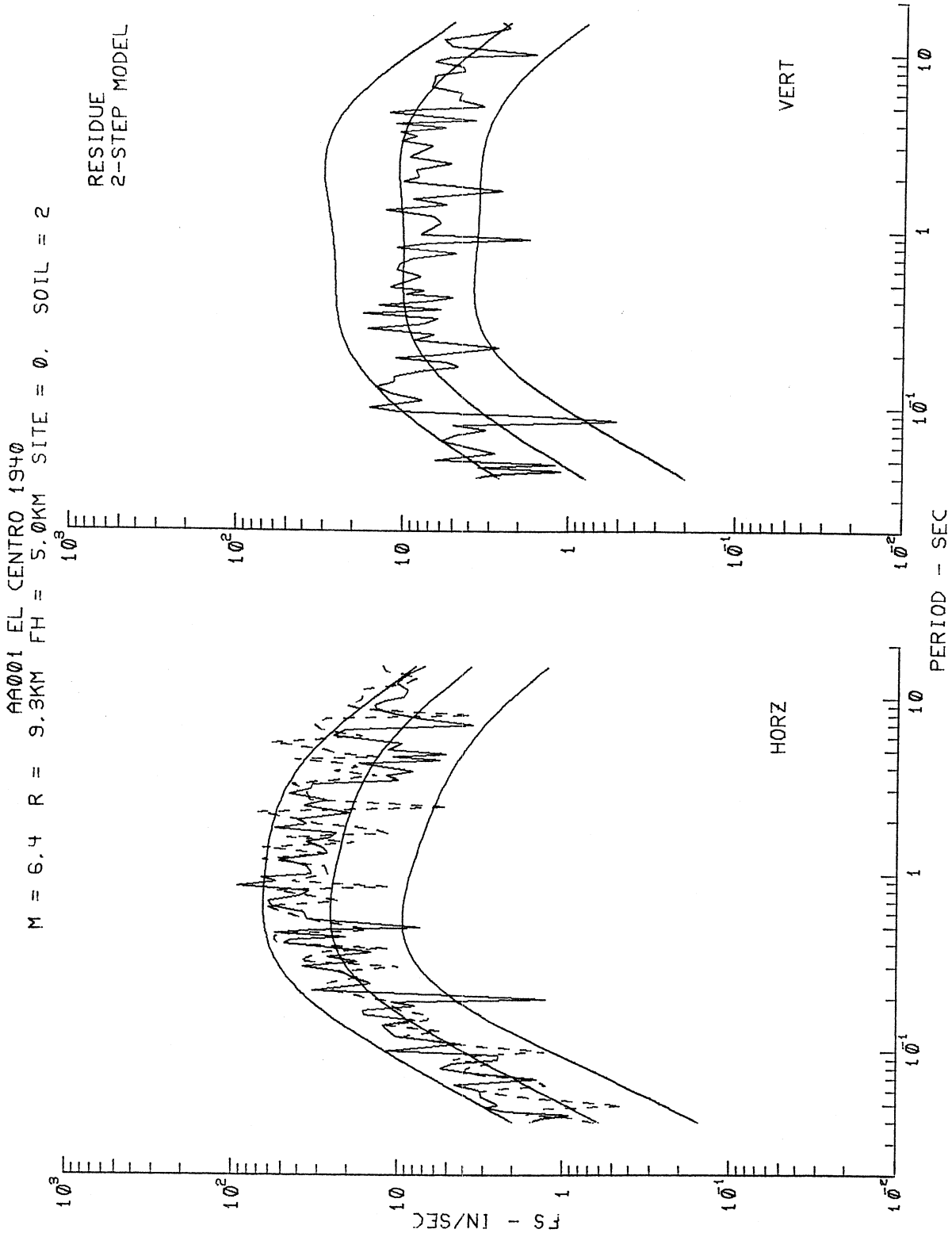

Figure II.4.16

TABLE II.4.2

$$\log_{10} FS(T) = M_< + \mathcal{A}tt(\Delta,M,T) + c_1(T)M_{<>} + c_2^{(1)}(T)S^{(1)} + c_2^{(2)}(T)S^{(2)} + c_3(T)v + c_4^{(1)}(T)S^{(1)}v + c_4^{(2)}(T)S^{(2)}v + c_5(T) + c_6(T)M_{<>}^2 + c_7^{(1)}(T)S_L^{(1)} + c_7^{(2)}(T)S_L^{(2)}$$

MAG-SITE-SOIL RESIDUES:2-STEP MODEL

PERIOD, T(SEC)	.040	.065	.11	.19	.34	.50	.90	1.60	2.80	4.40	7.50	14.0
COEFFICIENTS:												
$c_1(T)$	-.230	-.200	-.015	.250	.544	.727	.948	1.049	.992	.758	.160	-.945
$c_2^{(1)}(T)$	.073	.081	.089	.039	-.077	-.146	-.179	-.128	-.051	.002	.042	.068
$c_2^{(2)}(T)$	.044	.051	.047	-.015	-.133	-.209	-.288	-.337	-.360	-.334	-.222	.010
$c_3(T)$	.123	.062	-.076	-.232	-.351	-.389	-.378	-.303	-.217	-.174	-.169	-.193
$c_4^{(1)}(T)$	-.129	-.107	-.083	-.048	.012	.064	.129	.116	.005	-.092	-.104	.068
$c_4^{(2)}(T)$	.032	.021	.019	.038	.087	.127	.176	.211	.233	.217	.101	-.178
$c_5(T)$	-1.156	-1.197	-1.680	-2.522	-3.655	-4.442	-5.446	-5.941	-5.740	-4.879	-2.839	.733
$c_6(T)$	-.027	-.031	-.046	-.065	-.086	-.100	-.115	-.121	-.119	-.105	-.066	.012
$c_7^{(1)}(T)$	-.180	-.166	-.137	-.084	-.020	.014	.049	.077	.100	.103	.077	.011
$c_7^{(2)}(T)$	-.151	-.144	-.127	-.089	-.034	.002	.050	.081	.078	.046	-.005	-.058
M_{min}	.000	.000	.000	1.919	3.151	3.654	4.139	4.328	4.152	3.598	1.212	.000
M_{max}	14.500	14.500	10.987	9.593	8.943	8.679	8.506	8.453	8.340	8.346	8.775	14.500
RESIDUES:												
p =.1	-.575	-.553	-.504	-.453	-.425	-.424	-.444	-.474	-.492	-.487	-.461	-.435
p =.2	-.366	-.349	-.317	-.289	-.278	-.281	-.299	-.320	-.328	-.314	-.280	-.250
p =.3	-.215	-.207	-.196	-.182	-.173	-.172	-.181	-.194	-.197	-.187	-.163	-.141
p =.4	-.094	-.089	-.085	-.083	-.082	-.082	-.086	-.089	-.086	-.079	-.068	-.057
p =.5	.018	.019	.012	.006	.004	.004	.004	.003	.006	.011	.019	.027
p =.6	.137	.128	.109	.092	.086	.088	.095	.102	.109	.108	.101	.092
p =.7	.238	.227	.205	.184	.172	.172	.183	.200	.208	.201	.179	.158
p =.8	.370	.353	.323	.293	.277	.278	.293	.312	.317	.303	.272	.243
p =.9	.540	.516	.474	.432	.407	.407	.425	.447	.450	.433	.400	.368
RESIDUE STATISTICS:												
$\mu(T)$	.003	.002	.001	-.001	-.002	-.002	-.002	-.002	-.002	-.001	-.000	-.000
$\sigma(T)$	.446	.425	.386	.347	.326	.326	.342	.364	.373	.363	.335	.308
$X^2(T)$	7.685	7.786	7.356	6.705	6.332	6.526	7.451	8.731	10.132	11.310	12.547	13.515
KS(T)	.038	.041	.040	.037	.035	.035	.038	.042	.046	.051	.059	.067

in I.8, for the MAG-SITE-SOIL model given here in Part II. Figures II.4.1 through II.4.16 represent an identical sequence of plots for the residue 2-step model as the sequence for the direct 1-step model. Table II.4.1 shows the corresponding figure numbers in the two models.

Finally, Table II.4.2 presents the scaling functions, residues and residue statistics at 12 discrete periods for the 2-step model as did Table II.2.1 for the 1-step model.

This completes the presentation of Part II of the scaling of FS(T) in terms of M, R, H, S, s, S_L and v.

PART III: SCALING OF FOURIER SPECTRA IN TERMS OF M.M.I., h, s_L and v

III.1 The Scaling Relation

Parts I and II of this work presented the empirical model for scaling of the Fourier amplitude spectra of strong earthquake ground motion in terms of earthquake magnitude, source-to-station "representative" distance, characterization of local geology and soil classification at the recording site. Parts III and IV of this work will continue with the scaling of Fourier amplitude spectra but in terms of Modified Mercalli Intensity (M.M.I.) at the site and its local geological and soil classification.

As pointed out in our previous analyses (Trifunac and Lee, 1985a), the scaling of Fourier amplitude spectra, FS(T), in terms of earthquake intensity at a site will likely remain a common engineering practice for years to come, in spite of all the shortcomings associated with such qualitative and descriptive scaling of strong earthquake ground motion. Our previous analysis used the following scaling relation for the database of 438 records with 1314 components:

$$\log_{10}[FS(T)] = b_1(T)\hat{I}_{MM} + b_2(T)h + b_3(T)v + b_4(T) \quad , \tag{III.1.1}$$

where $\hat{I}_{MM}$ is the estimated M.M.I level at the site, or the reported M.M.I. level, if available. The new database has many records from the earthquakes after 1972, which have magnitudes typically below 6. The M.M.I. levels for these earthquakes are not well documented or are not available for many recording sites. For these sites, the M.M.I. levels have been estimated. Lee and Trifunac (1985) used the original database of 57 earthquakes and 186 stations where the reported M.M.I. levels are

documented and performed the regression analysis of M.M.I. levels, I_{MM}, with earthquake magnitudes, M, representative source-to-station distance, Δ, and local site geology, in the form

$$I_{MM} = 1.5\ M - A - B\ell n\Delta - C\Delta/100 - Ds \quad . \qquad \text{(III.1.2)}$$

The coefficients were estimated and are $\hat{A} = -1.12$, $\hat{B} = 0.856$, $\hat{C} = 1.50$ and $\hat{D} = 0.260$. Then the estimated M.M.I. level at a site, $\hat{I}_{MM}$, is given by

$$\hat{I}_{MM} = 1.5\ M - \hat{A} - \hat{B}\ell n\Delta - \hat{C}\Delta/100 - Ds \quad . \qquad \text{(III.1.3)}$$

To include the local soil classification at each site in the regression analysis, equation (III.1.1) is modified to:

$$\log_{10}FS(T) = b_1(T)\hat{I}_{MM} + b_2(T)h + b_3(T)v + b_4(T)hv + b_5(T) + b_6^{(1)}(T)S_L^{(1)} + b_6^{(2)}(T)S_L^{(2)} \quad . \qquad \text{(III.1.4)}$$

With $S_L^{(1)}$ and $S_L^{(2)}$ representing the indicator variables for soil classification as before. Also, the terms $b_2(T)h + b_4(T)hv$ are used so that the coefficients characterizing the effects of alluvial depth are component dependent. In the above equation, the M.M.I. level $\hat{I}_{MM}$ is used as a quantitative variable. The fact that M.M.I. levels are discrete, and take on values of positive integers 1 through 12, indicates that $\hat{I}_{MM}$ should be replaced by indicator variables, one at each level. This would be consistent with the use of indicator variables for the local geologic site conditions and for the soil classification. However, the number of data points at each M.M.I. level is very nonuniform and is small or zero for higher M.M.I. levels. The use of indicator variables

for M.M.I. levels with the existing database would only result in a poor fit. So, for the time being the M.M.I. levels I_{MM}, will be considered as a quantitative variable.

The scaling functions $b_1(T)$ through $b_5(T)$, $b_6^{(1)}(T)$ and $b_6^{(2)}(T)$ have been determined through the regression analysis of the new database of 1482 components of spectral amplitudes, FS(T), at 91 discrete periods T ranging from 0.04 sec. to 15 sec. As in all previous analyses, the data are first screened to minimize possible bias in the model. The only difference now is that an additional category, namely, the local classification, is included in this selection. The coefficients, at each period T, resulting from linear regression are denoted by $\hat{b}_1(T)$, $\hat{b}_2(T)$, $\hat{b}_3(T)$, $\hat{b}_4(T)$, $\hat{b}_5(T)$, $\hat{b}_6^{(1)}$, and $\hat{b}_6^{(2)}(T)$ respectively.

III.2 Results of the Regression Analysis

Figure III.2.1 shows the smooth coefficients $\hat{b}_1(T)$, $\hat{b}_2(T)$, $\hat{b}_3(T)$, $\hat{b}_4(T)$, $\hat{b}_5(T)$, $\hat{b}_6^{(1)}(T)$ and $\hat{b}_6^{(2)}(T)$ (solid lines) and the corresponding estimates of their 80%, 90% and 95% confidence intervals, represented by the dashed lines. Substituting these coefficients into equation (III.1.4) gives:

$$\log_{10}\hat{FS}(T) = \hat{b}_1(T)\hat{I}_{MM} + \hat{b}_2(T)h + \hat{b}_3(T)v + \hat{b}_4(T)hv + \hat{b}_5(T) + \hat{b}_6^{(1)}(T)S_L^{(1)} + \hat{b}_6^{(2)}(T)S_L^{(2)} \quad , \qquad \text{(III.2.1)}$$

where $\log_{10}\hat{FS}(T)$ represents the estimate of the logarithm of the Fourier amplitude spectrum at period T for this MMI-DEPTH-SOIL model. We recall equation (I.4.2) in Part I of this work:

$$\log_{10}\hat{FS}(T) = M_< + \mathcal{A}tt(\Delta,M,T) + \hat{b}_1(T)M_{<>} + \hat{b}_2(T)h + \hat{b}_3(T)v + \hat{b}_4(T)hv + \hat{b}_5(T) + \hat{b}_6(T)M_{<>}^2 + \hat{b}_7^{(1)}(T)S_L^{(1)} + b_7^{(2)}(T)S_L^{(2)} \quad , \qquad \text{(III.2.2)}$$

for the MAG-DEPTH-SOIL model, and note the resemblance in shape of the functions $\hat{b}_1(T)$ for both equations. The same holds true for the scaling functions $\hat{b}_2(T)$ for h, $\hat{b}_3(T)$ for v and $\hat{b}_4(T)$ for hv in both equations. This is also in agreement with our previous analyses (Trifunac and Lee, 1985a,b), even though equation (III.2.1) has simpler form compared to equation (III.2.2).

With FS(T) being the Fourier amplitude spectrum calculated from the recorded accelerograms, the residuals, $\varepsilon(T)$, are calculated as in Parts I and II of this work, from

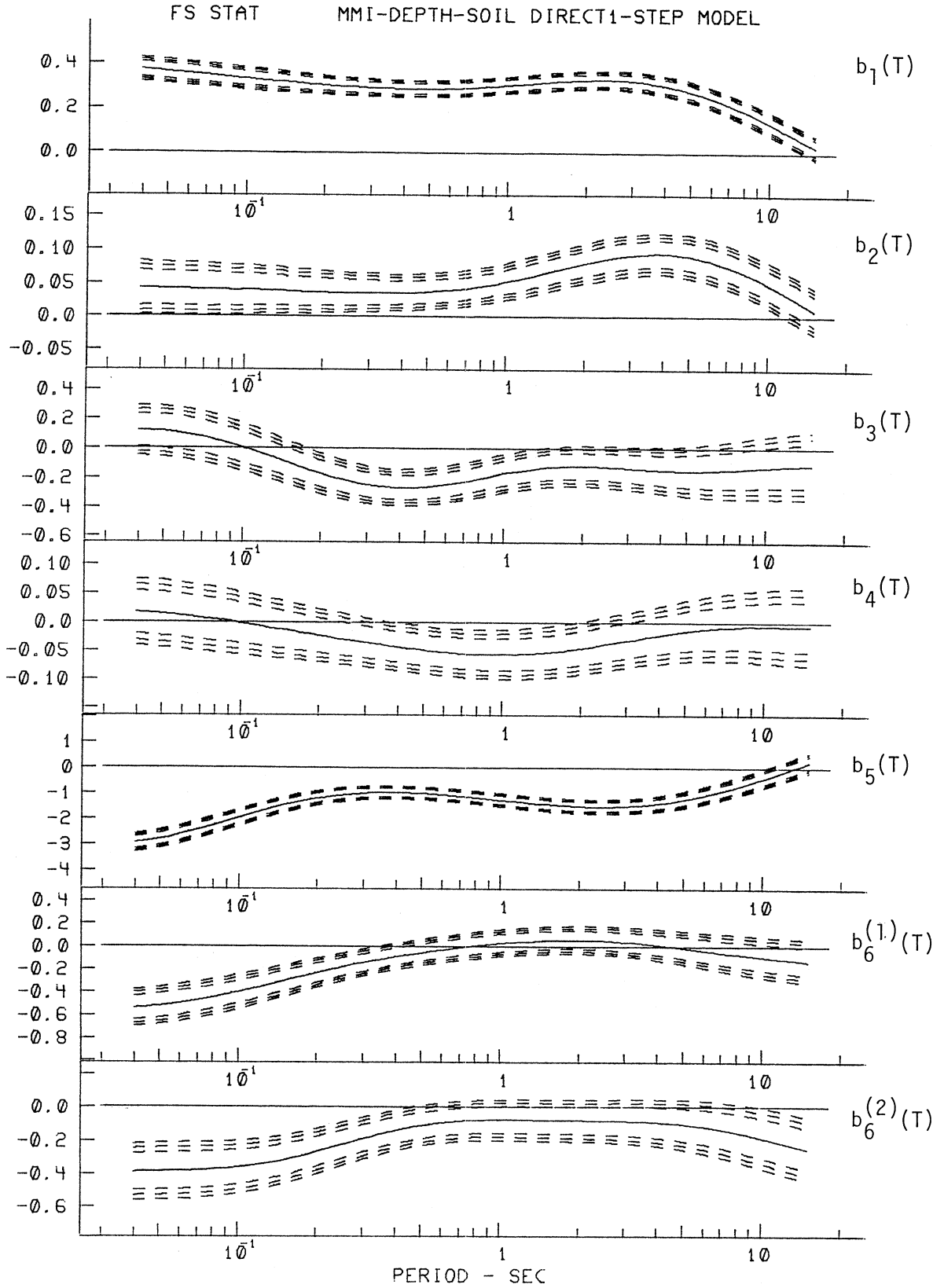

Figure III.2.1

$$\varepsilon(T) = \log_{10}FS(T) - \log_{10}\hat{FS}(T) \quad . \qquad \text{(III.2.3)}$$

As in the previous parts of this work, it is assumed here that the residuals, $\varepsilon(T)$, can again be described by a normal distribution function with mean $\mu(T)$ and standard deviation $\sigma(T)$. The probability $p(\varepsilon,T)$ at period T that

$$\log_{10}FS(T) - \log_{10}\hat{FS}(T) \leq \varepsilon(T) \qquad \text{(III.2.4)}$$

is thus given by (equation (I.5.2) of Part I):

$$p(\varepsilon,T) = \frac{1}{\sigma(T)\sqrt{2\pi}} \int_{-\infty}^{\varepsilon(T)} \exp\left[-\frac{1}{2}\left(\frac{x-\mu(T)}{\sigma(T)}\right)^2\right]dx \quad . \qquad \text{(III.2.5)}$$

For a given residue, $\varepsilon(T)$, at a particular period T, the actual probability $p^*(\varepsilon,T)$, that $\varepsilon(T)$ will not be exceeded, and the corresponding estimated probability $\hat{p}(\varepsilon,T)$, the Kolmogovor-Smirnov, KS(T), and the chi-square, $\chi^2(T)$ tests of fit are again all computed as in Part I of this report, where a complete description of the steps and formulae involved are also described.

Figure III.2.2 shows the plot of the residue levels corresponding to $p^*(\varepsilon,T) = 0.1$ through 0.9 for $\log_{10}FS(T)$. As in Parts I and II of this report, the nine sets of curves, plotted versus period T, from the bottom to the top of the plot correspond to the residue levels at each of the nine probabilities (0.1 through 0.9). At each of the nine probabilities, the rough solid curve represents the actual calculated residues at that particular level. The smoothed solid curve is obtained by smoothing the rough solid curve along the T-axis in logarithmic scale. The corresponding dashed curve is the estimated residue $\varepsilon(T)$ at the particular probability level using equation (III.2.5)

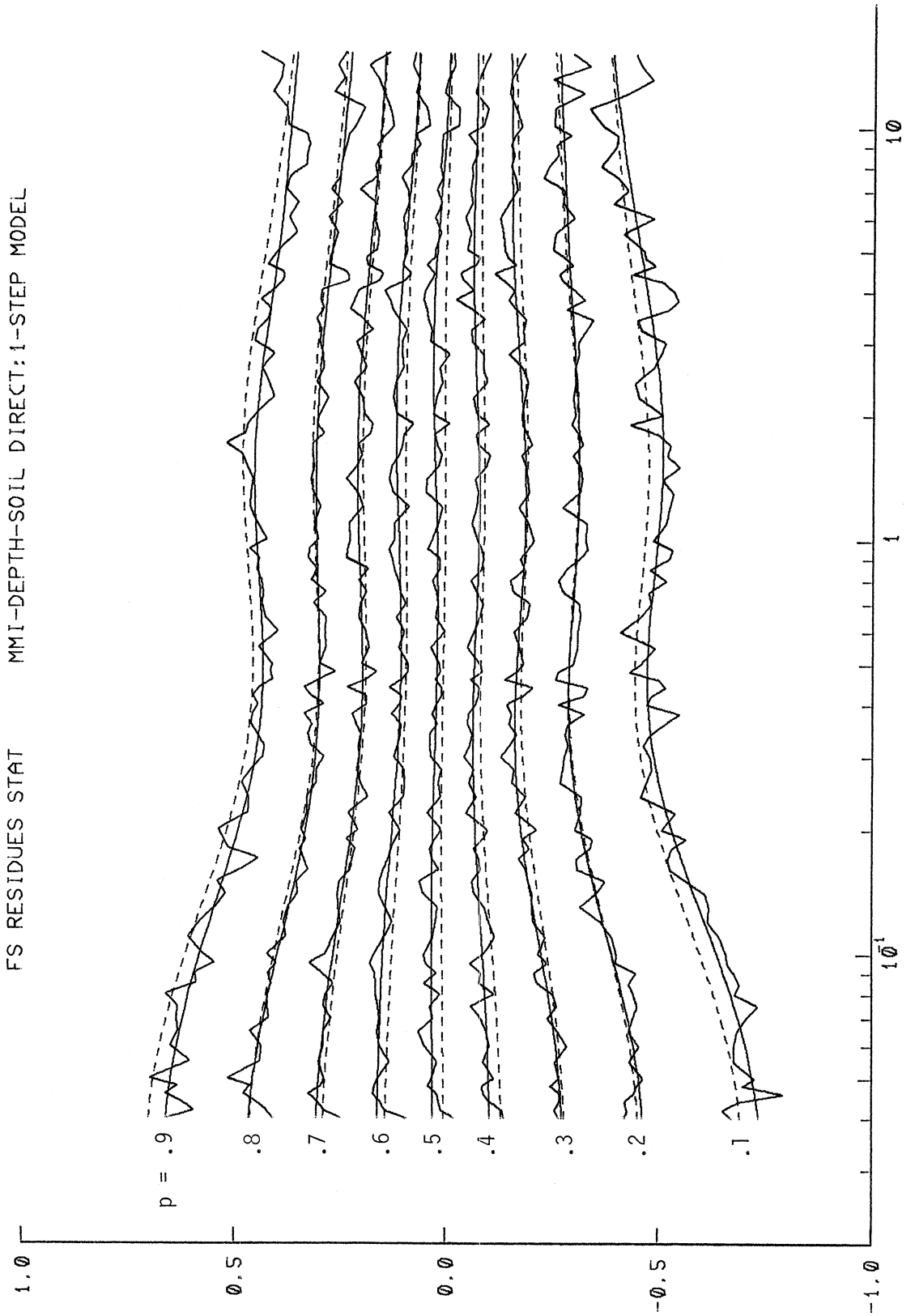

Figure III.2.2

It is of interest to compare this figure with the corresponding figure of the same MMI-DEPTH-SOIL model in the previous analyses (Figure III.2.2 of Trifunac and Lee, 1985a). The surface $p^*(\varepsilon,T)$ that resulted from the new MMI-DEPTH-SOIL model in the present analysis is slightly narrower in the ε-range when compared with the previous model. It is also of interest to compare this figure with the corresponding one in Part I of this work (Figure I.5.2) for the MAG-DEPTH-SOIL model, dealing with the scaling of FS(T) in terms of earthquake magnitude M and representative source to station distance Δ.

Note that the surfaces $p^*(\varepsilon,T)$ defined by the nine smooth curves represent the spread of the observed data about the models given here (equation (III.1.4)) and in Part I (equation (I.4.2)). The comparison shows that the MAG-DEPTH-SOIL model has a narrower spread, but that the uncertainties associated with the prediction of FS(T) using the MMI-DEPTH-SOIL model are certainly not much worse than those of the MAG-DEPTH-SOIL model of Part I.

Figure III.2.3 shows the statistical parameters used in the description of the residues: the mean, $\hat{\mu}(T)$, standard deviation, $\hat{\sigma}(T)$ the computed chi-square, $\chi^2(T)$ and Komolgorov-Smirnov, KS(T), statistics and their 95% confidence levels, as described in Part I of this work (Section I.5). Both the χ^2 and K-S tests fail to reject the hypothesis that the distribution is normal in the whole period range (0.04 sec. to 15 sec.)

Table III.2.1 gives, for 12 periods between T = 0.04 and 14 sec. the amplitudes of the seven smoothed regression coefficients, $b_1(T)$ through $b_6^{(2)}(T)$, the nine smoothed residual levels corresponding to $p^*(\varepsilon,T) = 0.1$ through 0.9, the smoothed coefficients $\hat{\mu}(T)$, $\hat{\sigma}(T)$, $\chi^2(T)$ and KS(T).

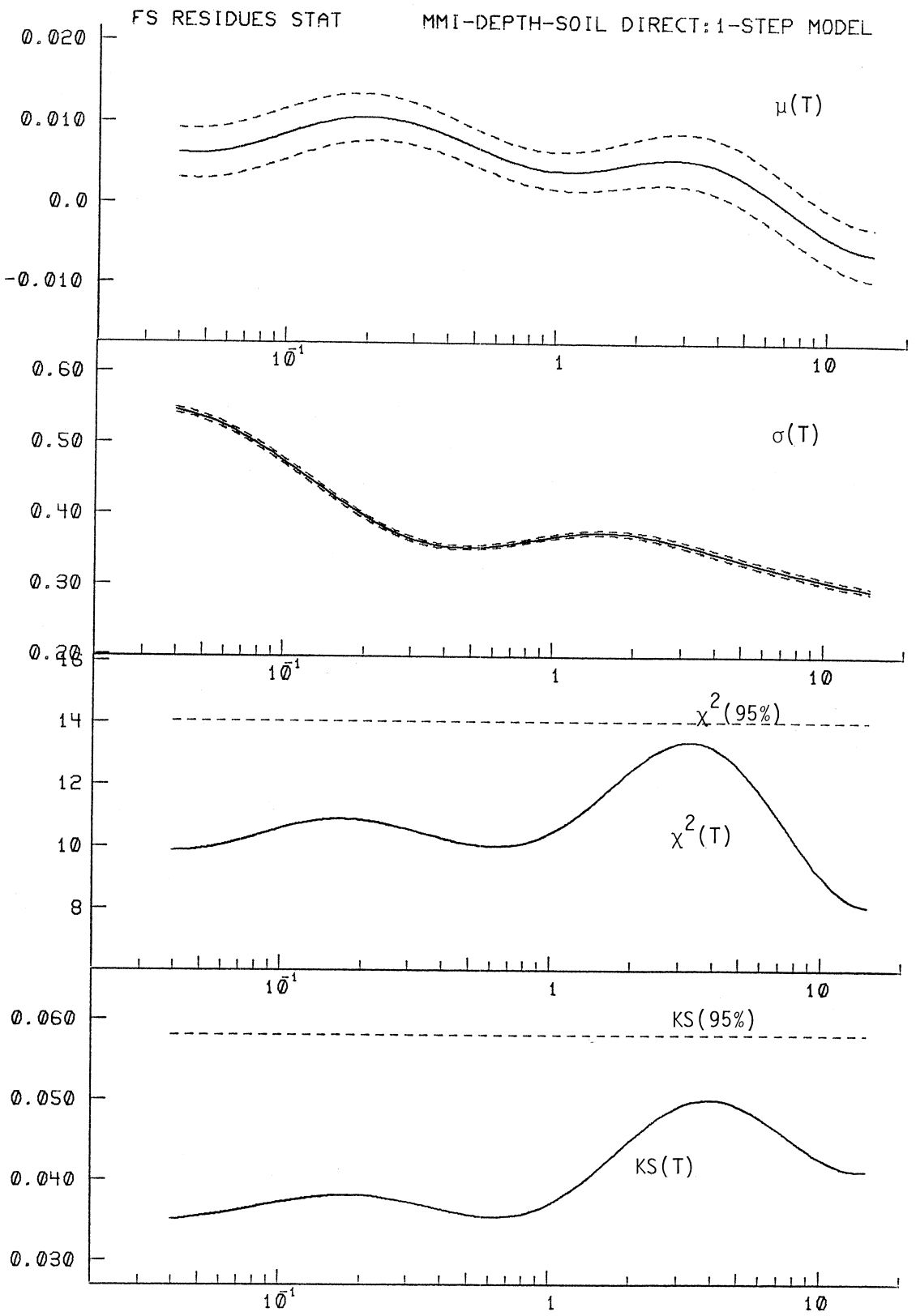

Figure III.2.3

TABLE III.2.1

$$\log_{10} FS(T) = b_1(T)\hat{I}_{MM} + b_2(T)h + b_3(T)v + b_4(T)hv + b_5(T) + b_6^{(1)}(T)S_L^{(1)} + b_6^{(2)}(T)S_L^{(2)}$$

MMI-DEPTH-SOIL DIRECT:1-STEP MODEL

PERIOD, T(SEC)	.040	.065	.11	.19	.34	.50	.90	1.60	2.80	4.40	7.50	14.0
COEFFICIENTS:												
$b_1(T)$	.374	.352	.328	.306	.291	.288	.302	.325	.329	.296	.205	.045
$b_2(T)$	.042	.041	.040	.037	.036	.038	.049	.071	.091	.093	.072	.016
$b_3(T)$	.119	.086	-.019	-.161	-.263	-.264	-.186	-.122	-.131	-.151	-.142	-.116
$b_4(T)$	.017	.008	-.006	-.022	-.039	-.049	-.057	-.051	-.034	-.019	-.009	-.008
$b_5(T)$	-2.956	-2.530	-1.833	-1.229	-.974	-1.005	-1.216	-1.449	-1.508	-1.321	-.794	.112
$b_6^{(1)}(T)$	-.540	-.486	-.380	-.247	-.119	-.052	.019	.057	.046	.004	-.060	-.127
$b_6^{(2)}(T)$	-.390	-.381	-.353	-.277	-.167	-.112	-.078	-.080	-.086	-.099	-.146	-.244
RESIDUES:												
p =.1	-.734	-.696	-.623	-.538	-.480	-.473	-.493	-.508	-.492	-.463	-.425	-.390
p =.2	-.462	-.435	-.380	-.322	-.290	-.289	-.305	-.311	-.300	-.287	-.275	-.263
p =.3	-.274	-.255	-.218	-.180	-.162	-.167	-.183	-.185	-.169	-.157	-.152	-.149
p =.4	-.104	-.098	-.085	-.070	-.063	-.066	-.076	-.076	-.067	-.062	-.065	-.069
p =.5	.032	.032	.033	.032	.026	.022	.022	.028	.033	.028	.012	-.002
p =.6	.162	.156	.146	.129	.112	.108	.112	.120	.118	.106	.087	.070
p =.7	.306	.290	.260	.226	.202	.199	.206	.212	.203	.188	.168	.150
p =.8	.465	.438	.388	.337	.305	.301	.307	.309	.297	.279	.255	.231
p =.9	.662	.630	.569	.496	.443	.434	.448	.455	.434	.407	.382	.360
RESIDUE STATISTICS:												
$\mu(T)$	.006	.007	.009	.011	.009	.007	.004	.005	.006	.004	-.001	-.006
$\sigma(T)$	.545	.517	.463	.401	.359	.352	.365	.374	.360	.340	.316	.295
$X^2(T)$	9.874	10.129	10.690	10.887	10.441	10.101	10.274	11.760	13.306	13.015	10.548	8.142
KS(T)	.035	.036	.037	.038	.037	.036	.036	.042	.049	.050	.046	.041

III.3 Examples of Estimated Fourier Spectra

Figure III.3.1 presents examples of the Fourier amplitude spectra, FS(T), computed from equation (III.2.1) for $p(\varepsilon,T) = 0.5$ for M.M.I. levels IV, VI, VIII, X and XII and for soil type $s_L = 1$. The left figure is for horizontal motion (v = 0) while the right one is for vertical motion (v = 1). The solid lines in both figures correspond to the local depth of sediments h = 0 km, while the dashed lines correspond to h = 4 km. The diagonal dashed lines at the bottom of each figure represent the average Fourier amplitudes of the digitization noise. The plot of each spectrum is presented only for the portion of the periods where the estimated spectral amplitudes are not distorted by the digitization noise. As in the corresponding plots for the MAG-DEPTH-SOIL model in Part I (Figure I.6.1), the effect of local geologic conditions (alluvium depth), is significant not just in the intermediate and long period ranges, but also in the short period range.

Figure III.3.2 presents another set of estimated FS(T) spectra to illustrate the effect of local soil conditions on FS(T). These are computed from equation (III.2.1) for $p(\varepsilon,T) = 0.5$ for M.M.I. levels IV, VI, VIII, X and XII, and for alluvium depth of h = 2 km. The left figure is for horizontal motion (v = 0) and the right one is for vertical motion (v = 1). The solid lines in both figures correspond to the local soil group $s_L = 0$ (rock), while the dashed line is for $s_L = 2$ (deep soil). It is observed that in the whole period range, the Fourier amplitudes FS(T) at rock sites ($s_L = 0$) are higher than those at deep soil, though the difference becomes less significant beyond the 1 sec. period. Earlier in both the MAG-DEPTH-SOIL and MAG-SITE-SOIL models of Parts I

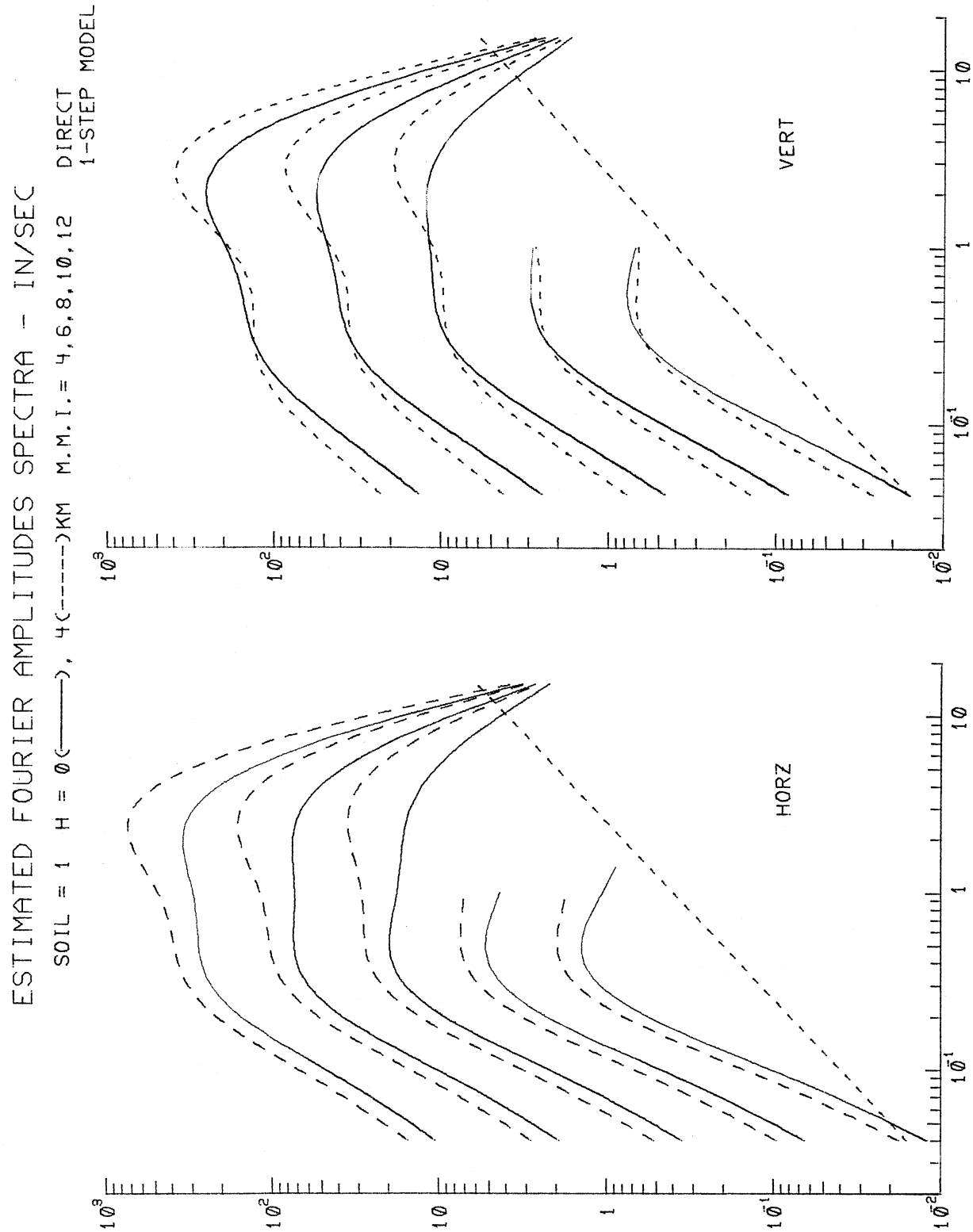

Figure III.3.1

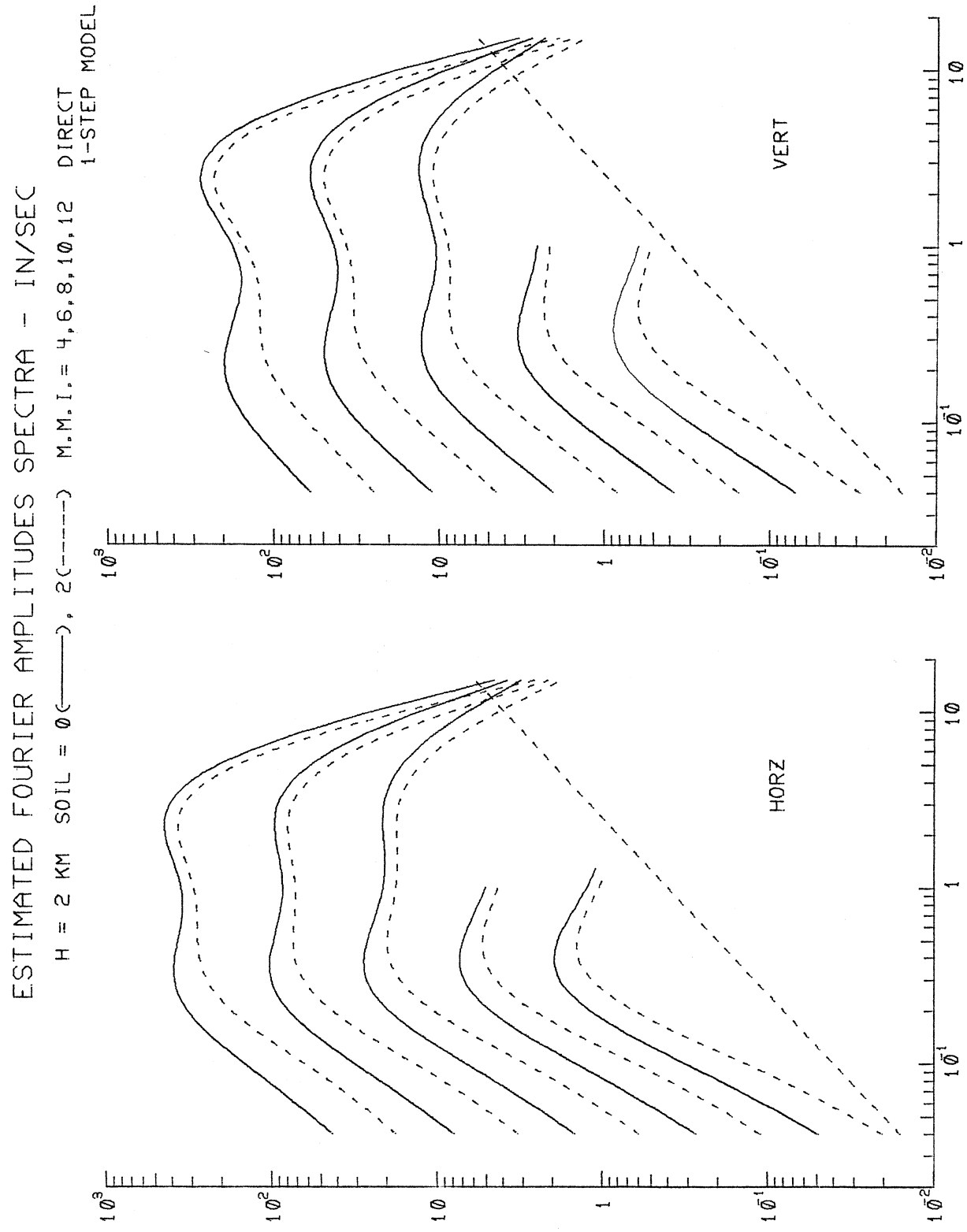

Figure III.3.2

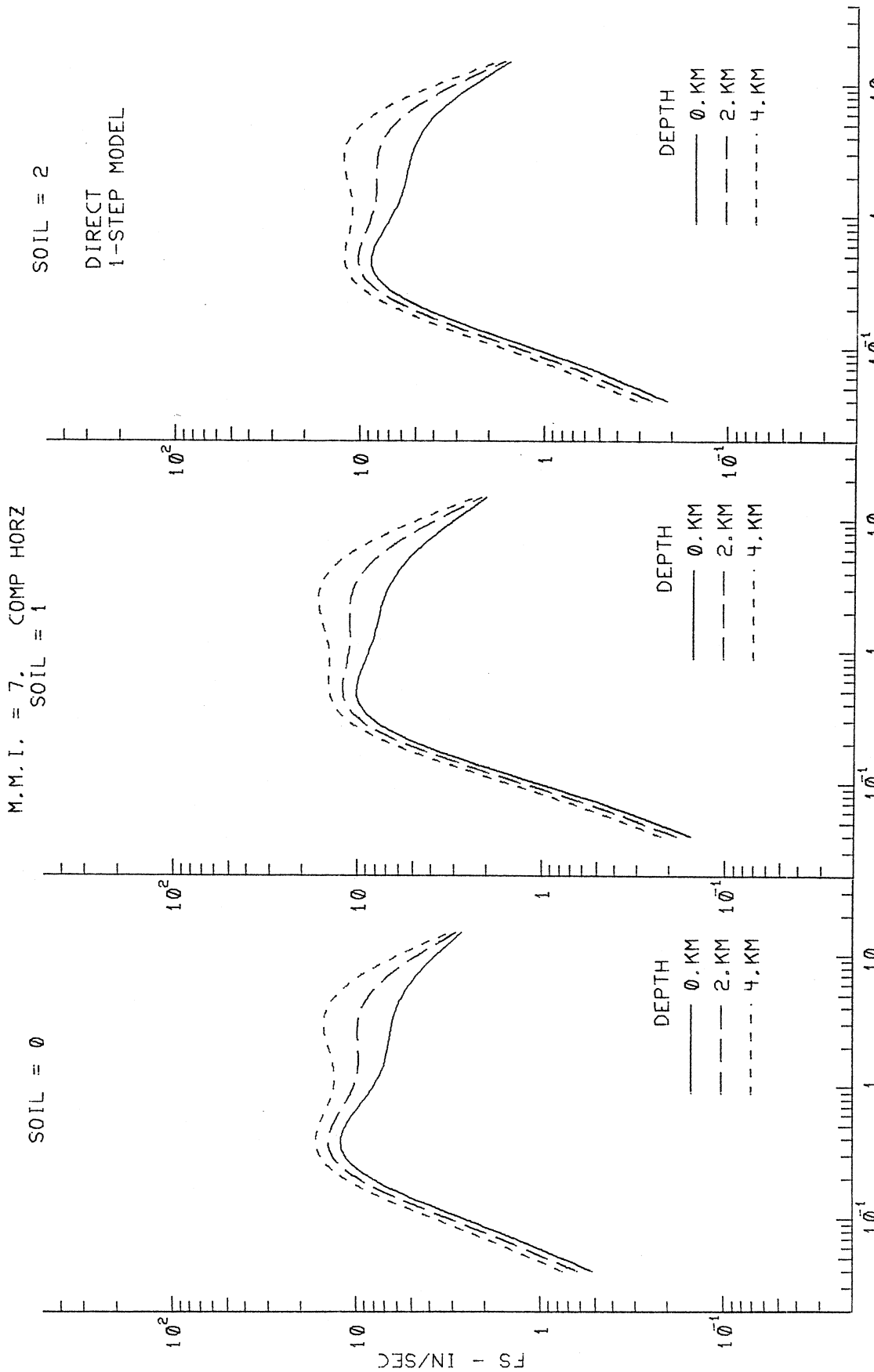

Figure III.3.3

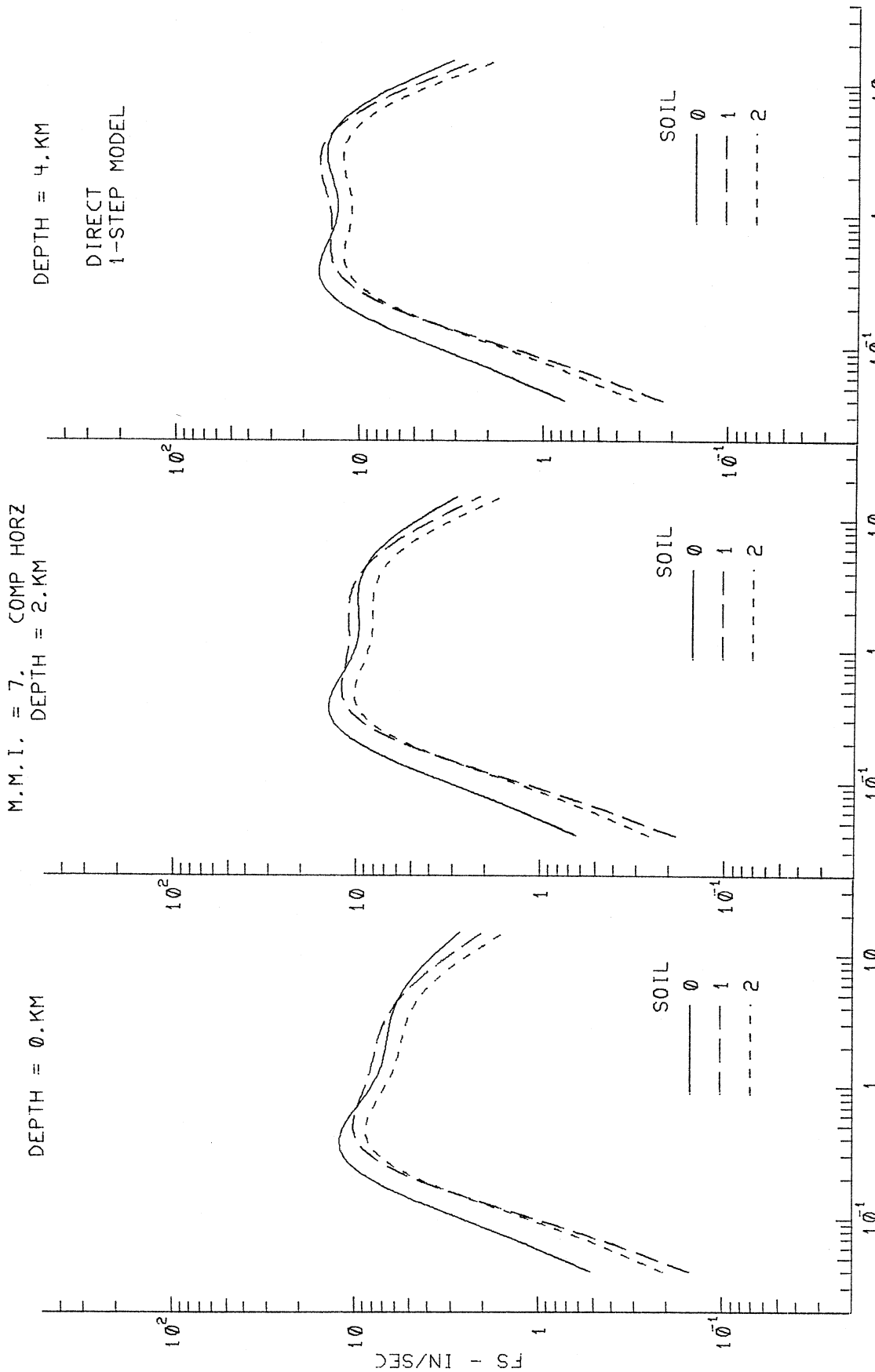

Figure III.3.4

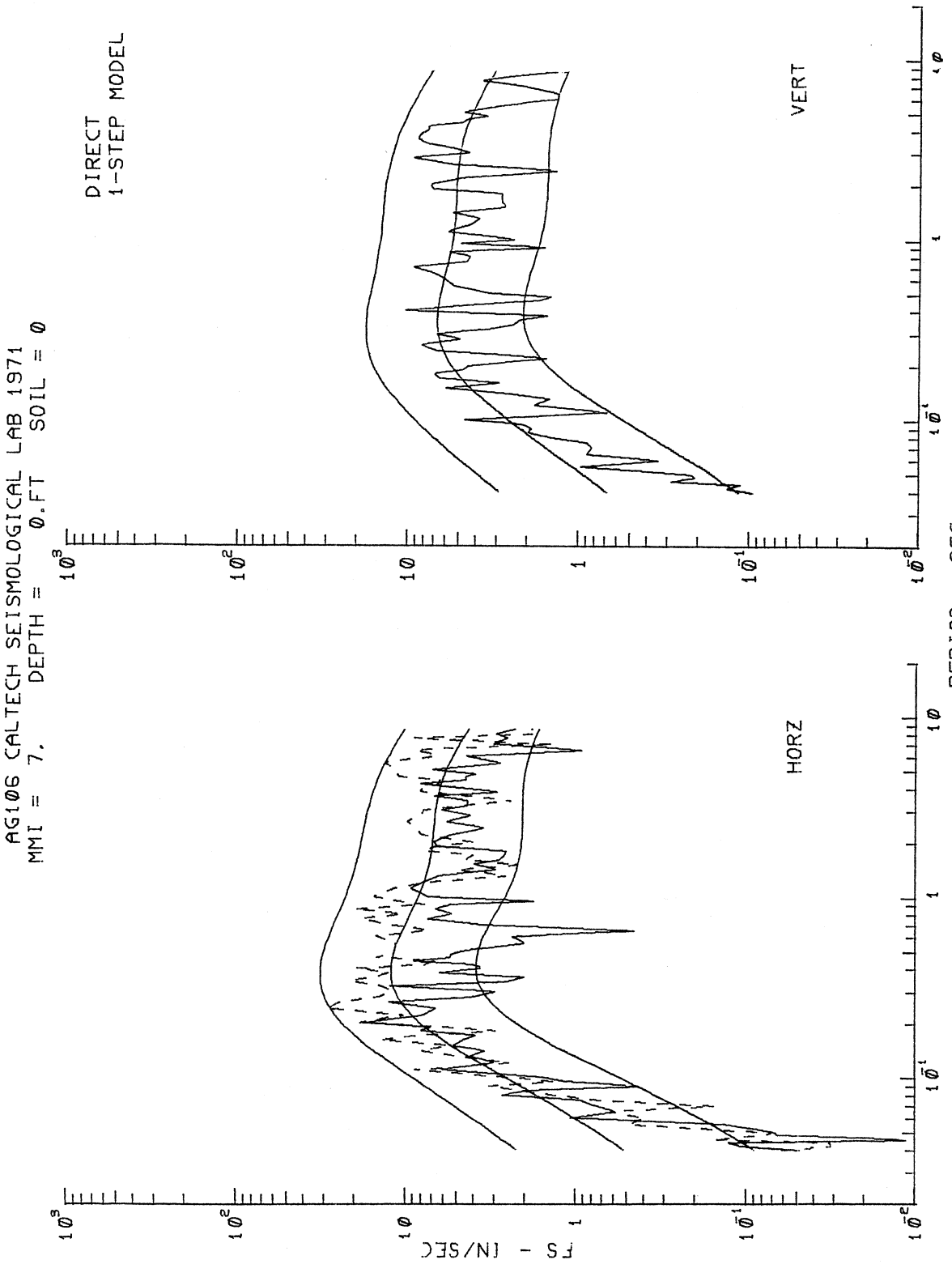

Figure III.3.5

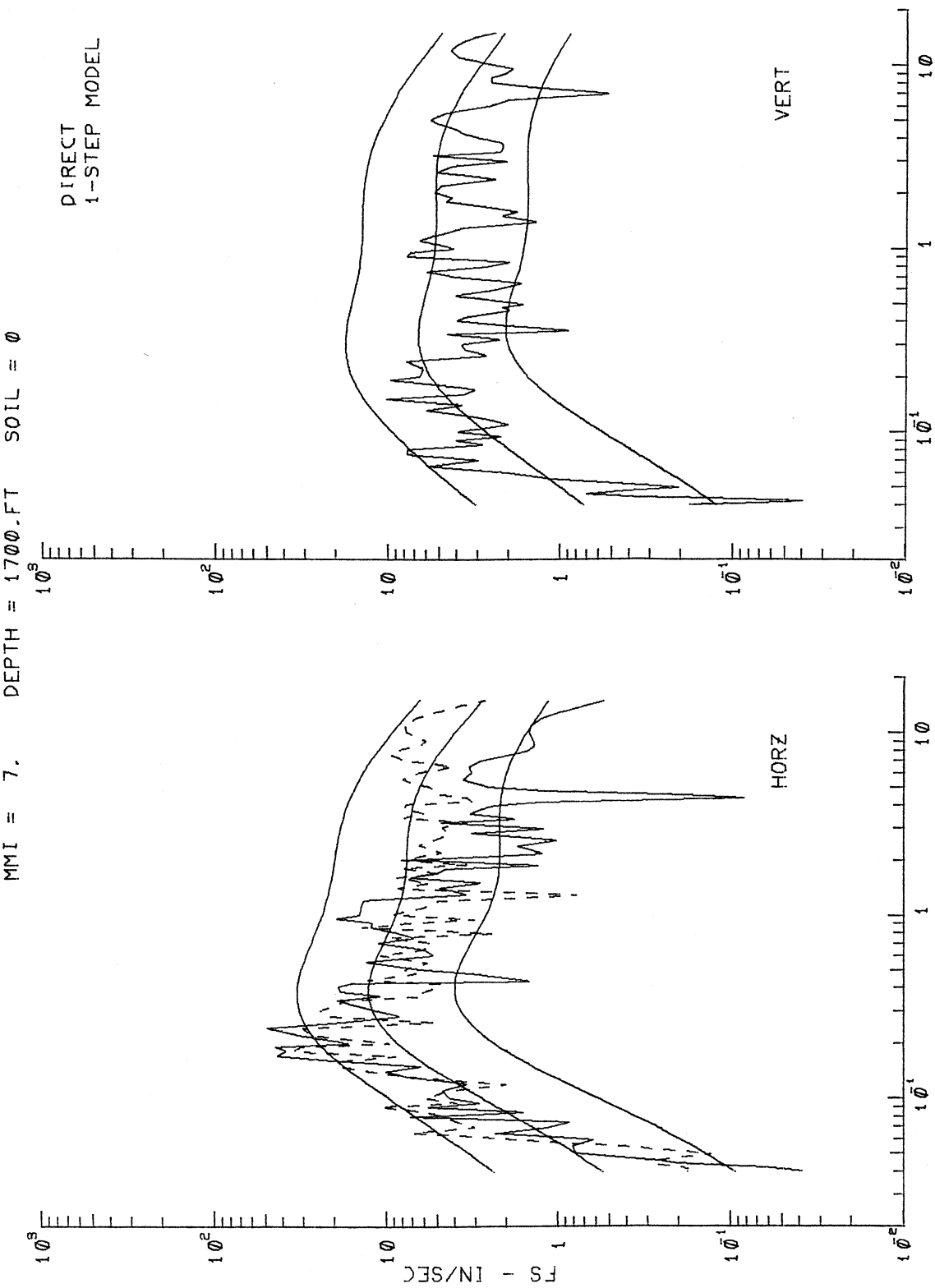

Figure III.3.6

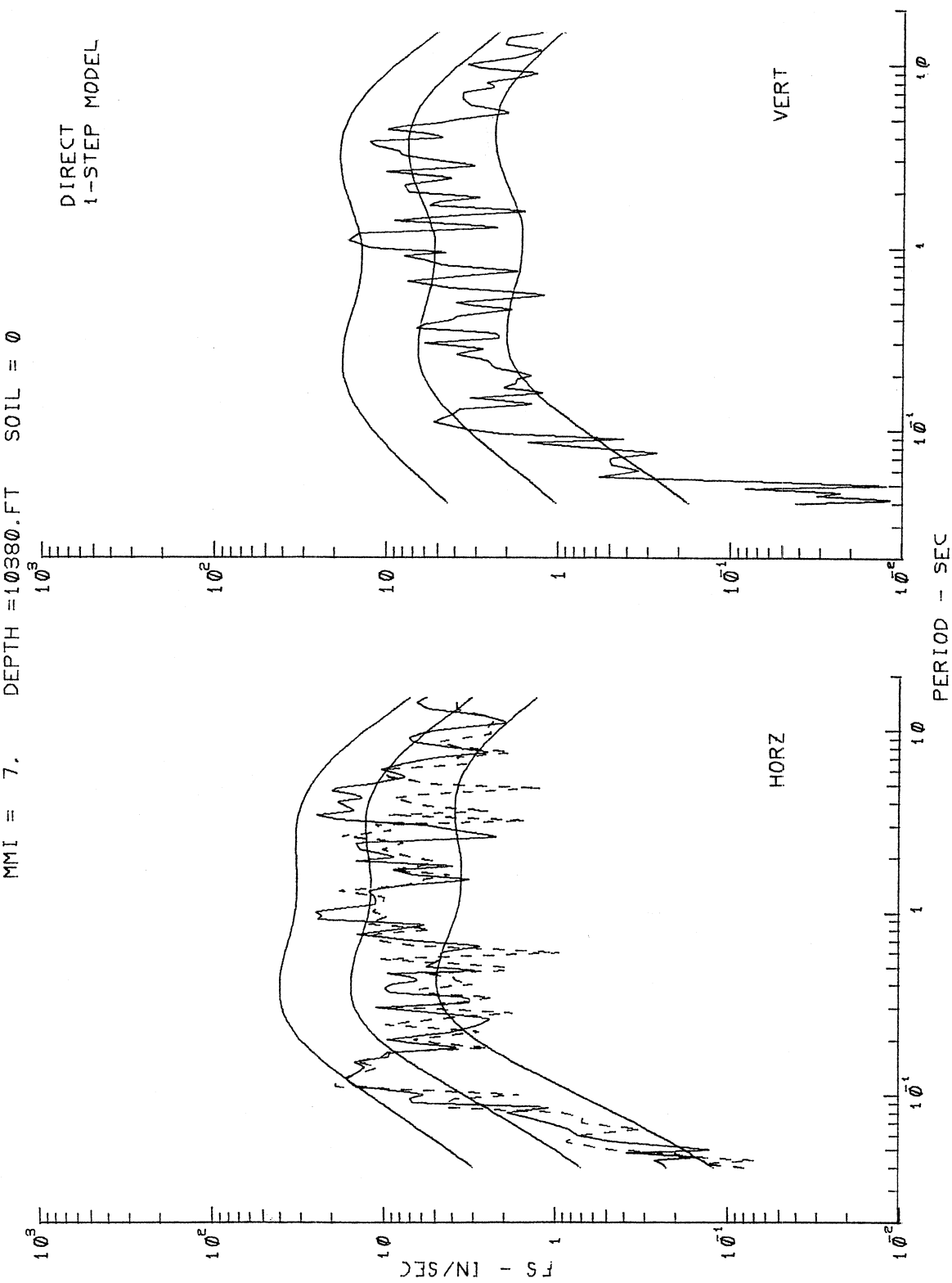

Figure III.3.7

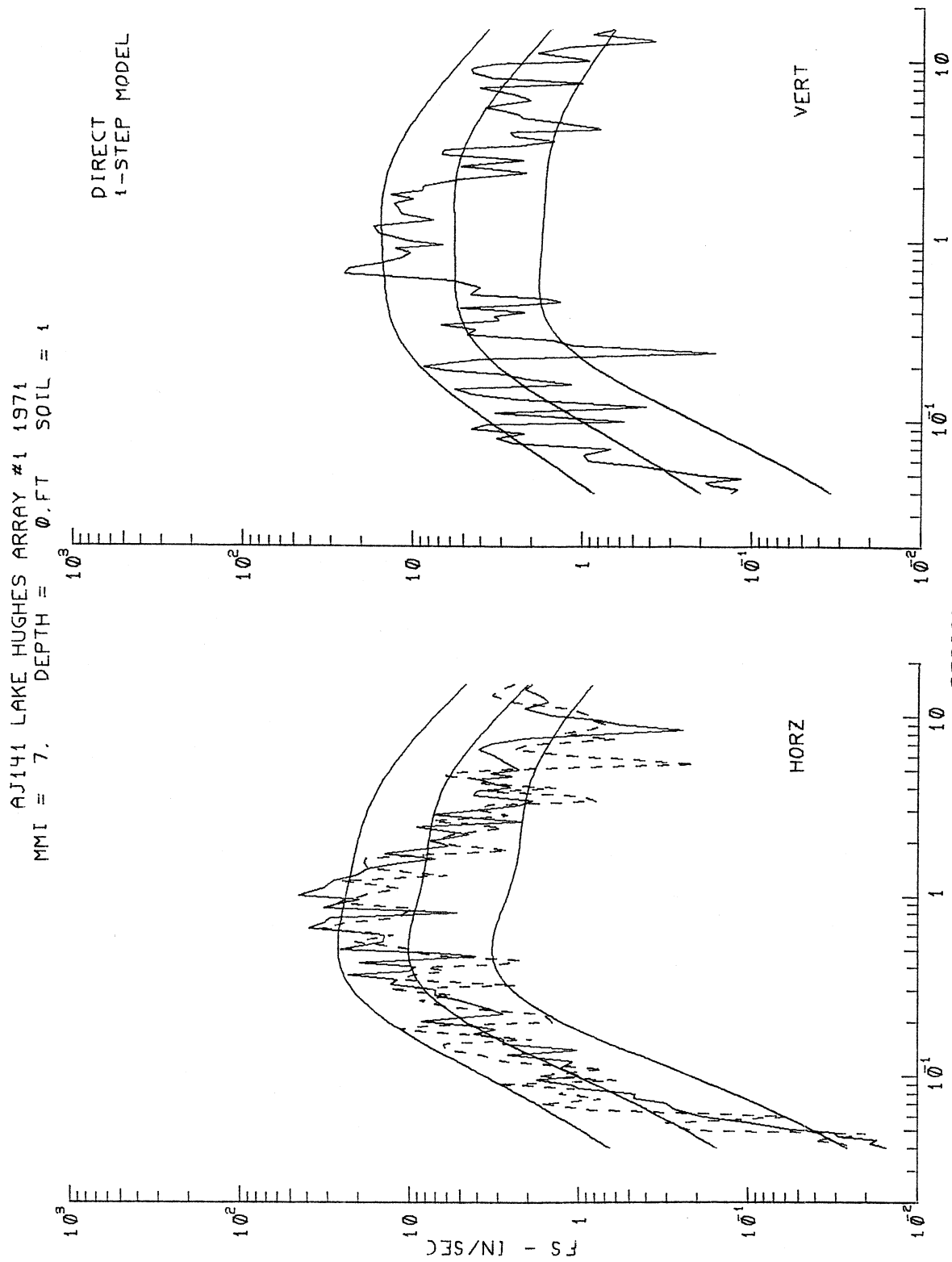

Figure III.3.8

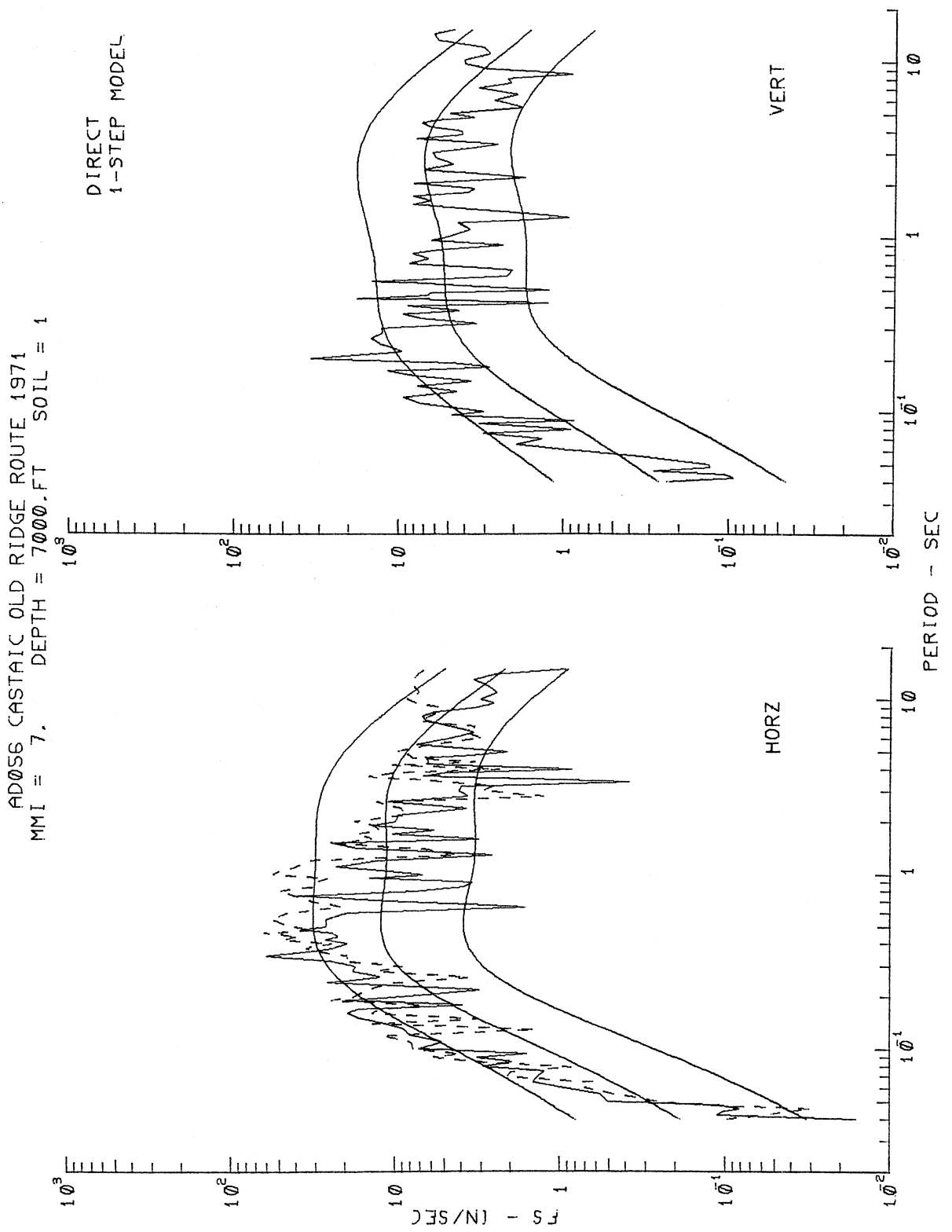

Figure III.3.9

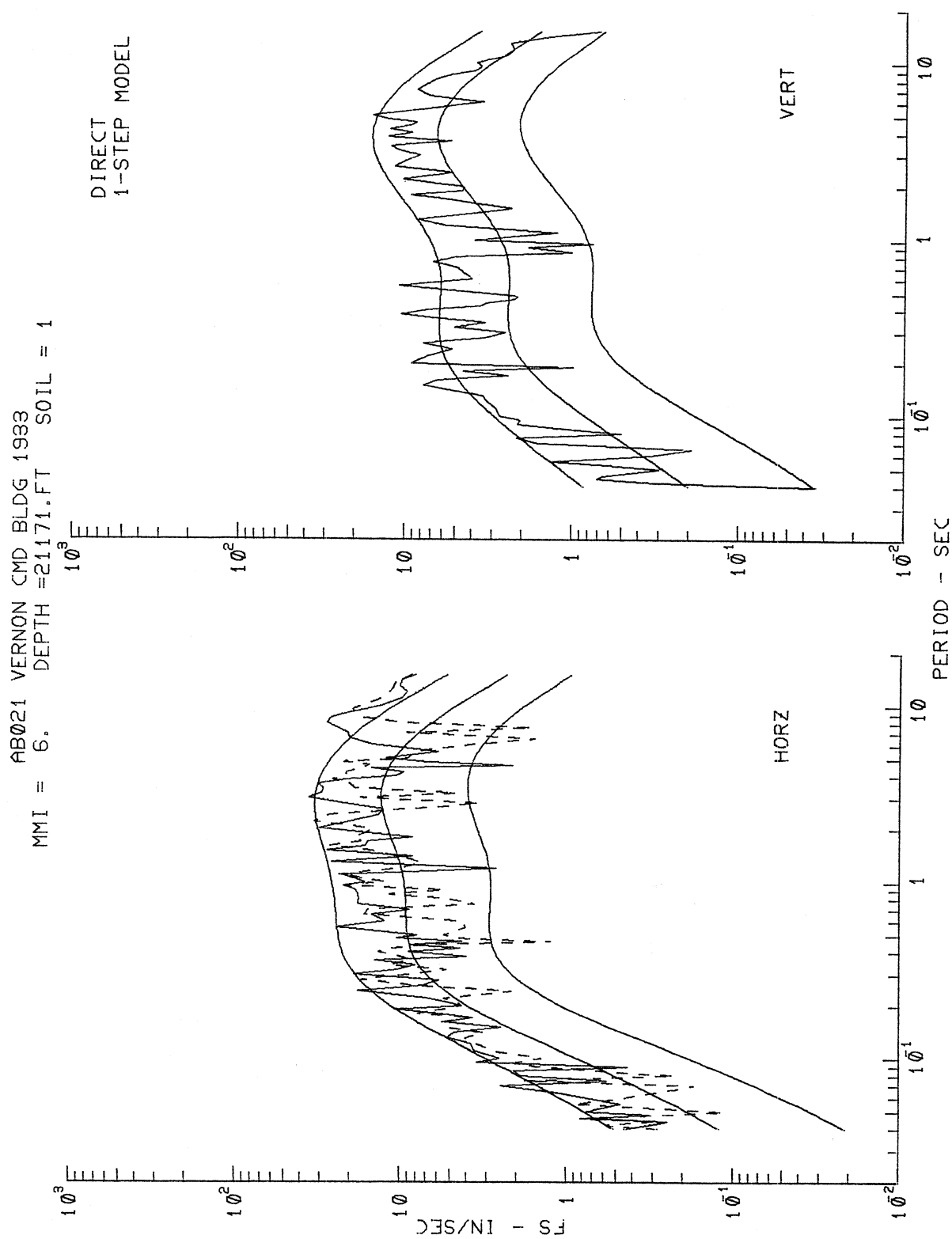

Figure III.3.10

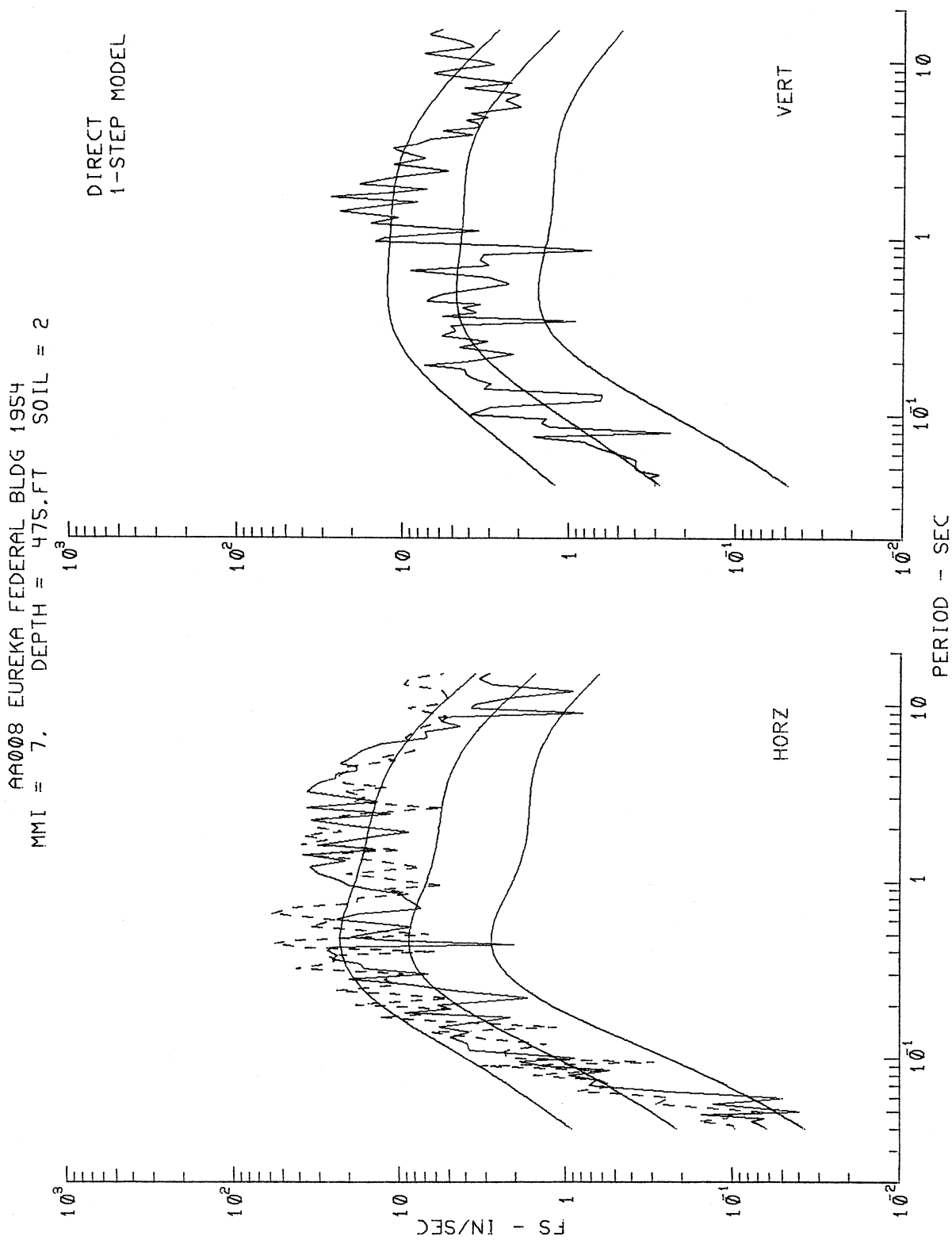

Figure III.3.11

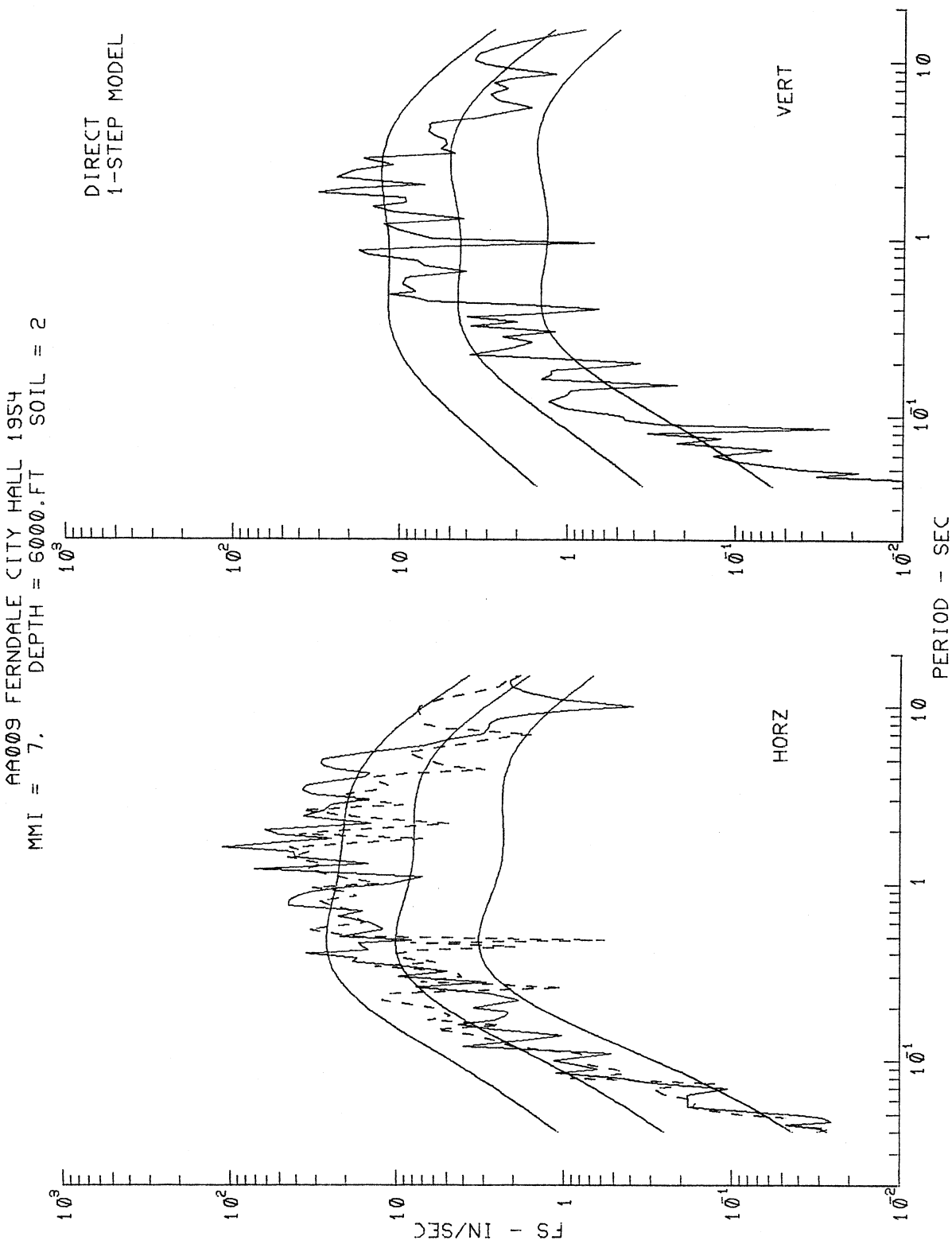

Figure III.3.12

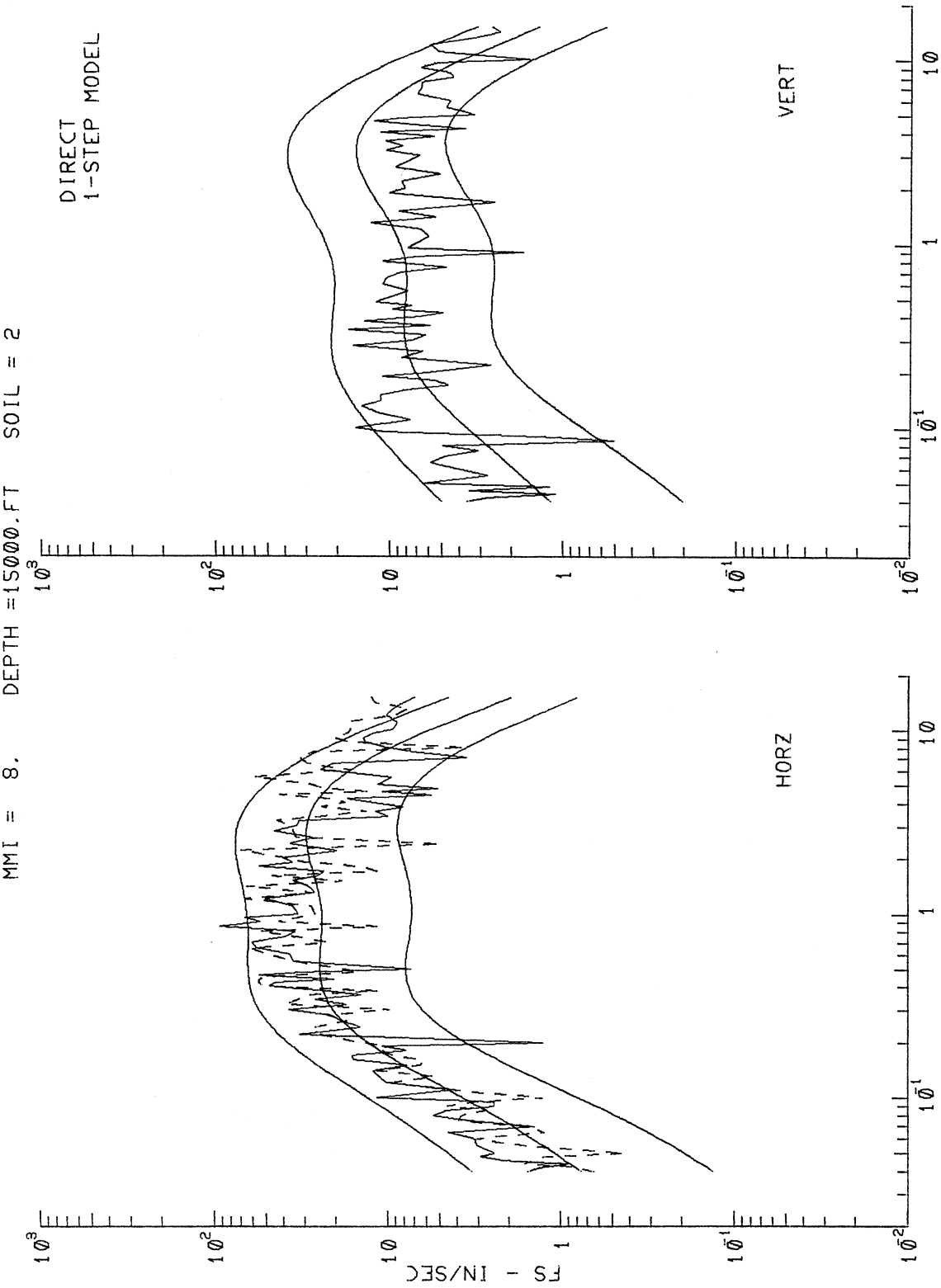

Figure III.3.13

and II this trend is observed only for periods up to ~ .35, beyond which the trend is reversed, though again the difference is less significant for long periods (Figures I.6.2 of Part I, Figures II.3.2 of Part II). The difference lies in the behavior of the scaling function for $S_L^{(2)}$ (deep soil) in both models. In the present model, the scaling function for $S_L^{(2)}$ (Figure III.2.1) starts out around -0.4 for short periods and gradually increases to and stays constant at ~ -0.1 in the middle period range. The scaling function for $S_L^{(2)}$ in the MAG-DEPTH-SOIL model of Part I, starts out around -0.25 for short periods, gradually increases, crosses the zero axis around T = 0.35 sec. and stays positive (around 0.15) in the middle period range.

Figures III.3.3 and III.3.4 (as did Figure I.6.3 and I.6.4 of Part I) compare the characteristics of the effects of the local geologic and soil classifications on FS(T) amplitudes. The same type of trends can be observed as in the MAG-DEPTH-SOIL model of Part I.

Figures III.3.5 through III.3.13 present the same nine examples (as in the previous parts) of how horizontal and vertical Fourier amplitudes computed from equation (III.2.1) compare with the corresponding spectra of recorded strong-motion data at various sites. Refer to Table I.7.1 for the various combinations of alluvium depths and soil classifications at each site. As in the previous models in Parts I and II, the agreement between the actual and estimated spectra is good.

III.4 The Residue Two-Step Model

Analogous to the previous parts of this work, a residue 2-step procedure for the MMI-DEPTH-SOIL model will next be presented. The first step of this procedure is to scale the Fourier spectra in terms of M.M.I., depth and component direction, but without soil classification:

$$\log_{10}\hat{FS}(T) = \hat{b}_1(T)I_{MM} + \hat{b}_2(T)h + \hat{b}_3(T)v + \hat{b}_4(T)hv + \hat{b}_5(T) \quad . \tag{III.4.1}$$

The residues, $\varepsilon(T) = \log_{10}FS(T) - \log_{10}\hat{FS}(T)$, at each site where soil classification is available are next fitted by the equation

$$\varepsilon(T) = b_6^{(1)}(T)S_L^{(1)} + b_6^{(2)}(T)S_L^{(2)} + b_7(T) \quad . \tag{III.4.2}$$

Combining equations (III.4.1) and (III.4.2) gives

$$\log_{10}\hat{FS}(T) = \hat{c}_1(T)I_{MM} + \hat{c}_2(T)h + \hat{c}_3(T)v + \hat{c}_4(T)hv + \hat{c}_5(T) + \hat{c}_6^{(1)}(T)S_L^{(1)} + \hat{c}_6^{(2)}(T)S_L^{(2)} \quad , \tag{III.4.3}$$

where $\hat{c}_i(T) = \hat{b}_i(T)$, except for $\hat{c}_5(T)$, with

$$\hat{c}_5(T) = \hat{b}_5(T) + \hat{b}_7(T) \quad , \tag{III.4.4}$$

as in Section I.8, Part I, of this work. The regression analyses and the subsequent plots can now be repeated for the MMI-DEPTH-SOIL model given in this Part III of this work. Figures III.4.1 through III.4.16 represent the figures for the residue 2-step model and correspond to those for the direct 1-step model. Table III.4.1 shows the corresponding figure numbers.

TABLE III.4.1
FIGURE NUMBERS OF THE MMI-DEPTH-SOIL MODEL

Figure Description	Direct 1-step Model	Residue 2-step Model
Scaling Functions	III.2.1	III.4.1
Residue Levels	III.2.2	III.4.2
Residue Statistics	III.2.3	III.4.3
Estimated FS	III.3.1-III.3.4	III.4.4-III.4.7
Actual versus Estimated FS	III.3.5-III.3.13	III.4.8-III.4.16

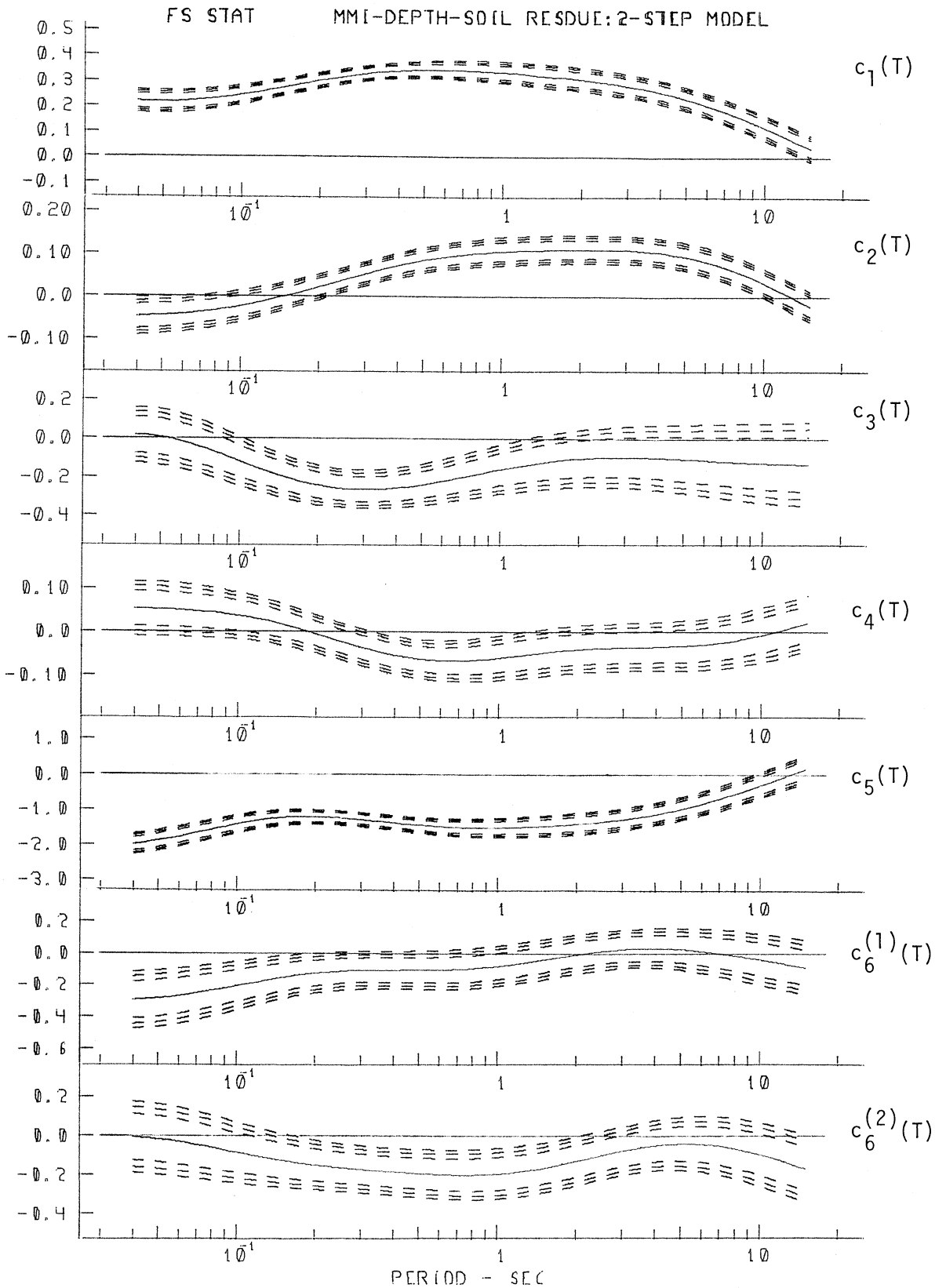

Figure III.4.1

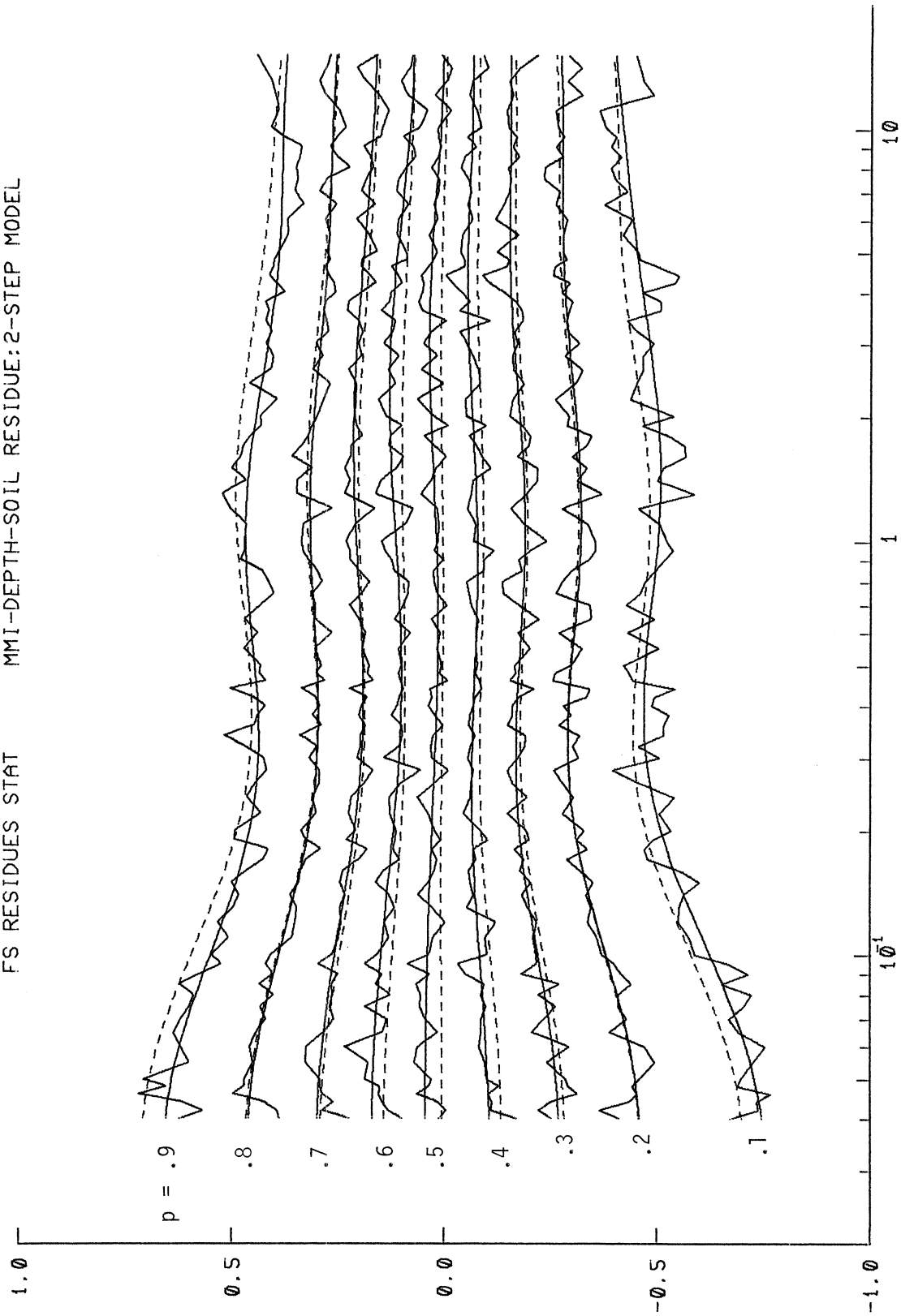
FS RESIDUES STAT
MMI-DEPTH-SOIL RESIDUE:2-STEP MODEL
1.0
0.5
0.0
-0.5
-1.0
p = .9
.8
.7
.6
.5
.4
.3
.2
.1
10^1
1
10

Figure II.4.2

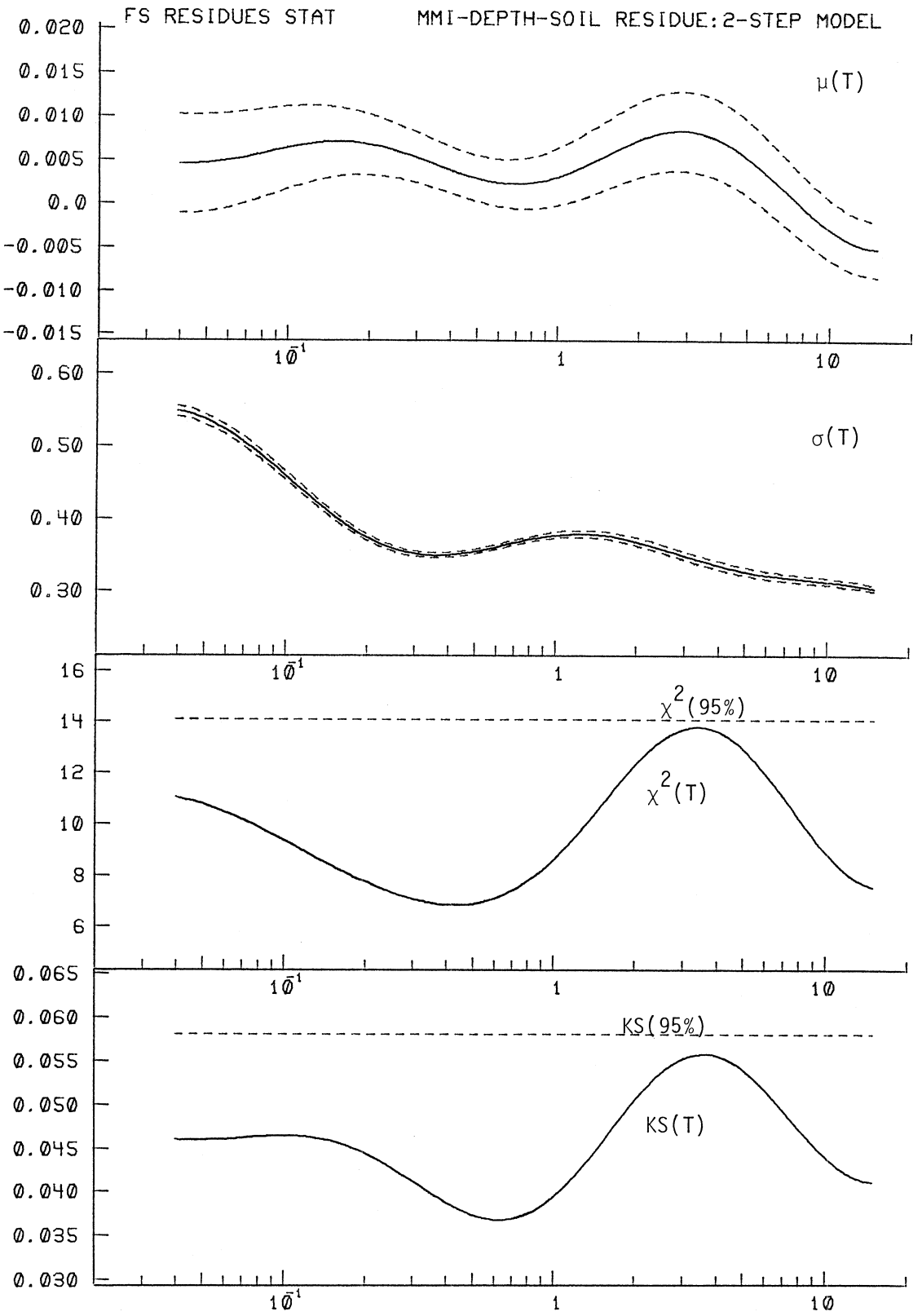

Figure III.4.3

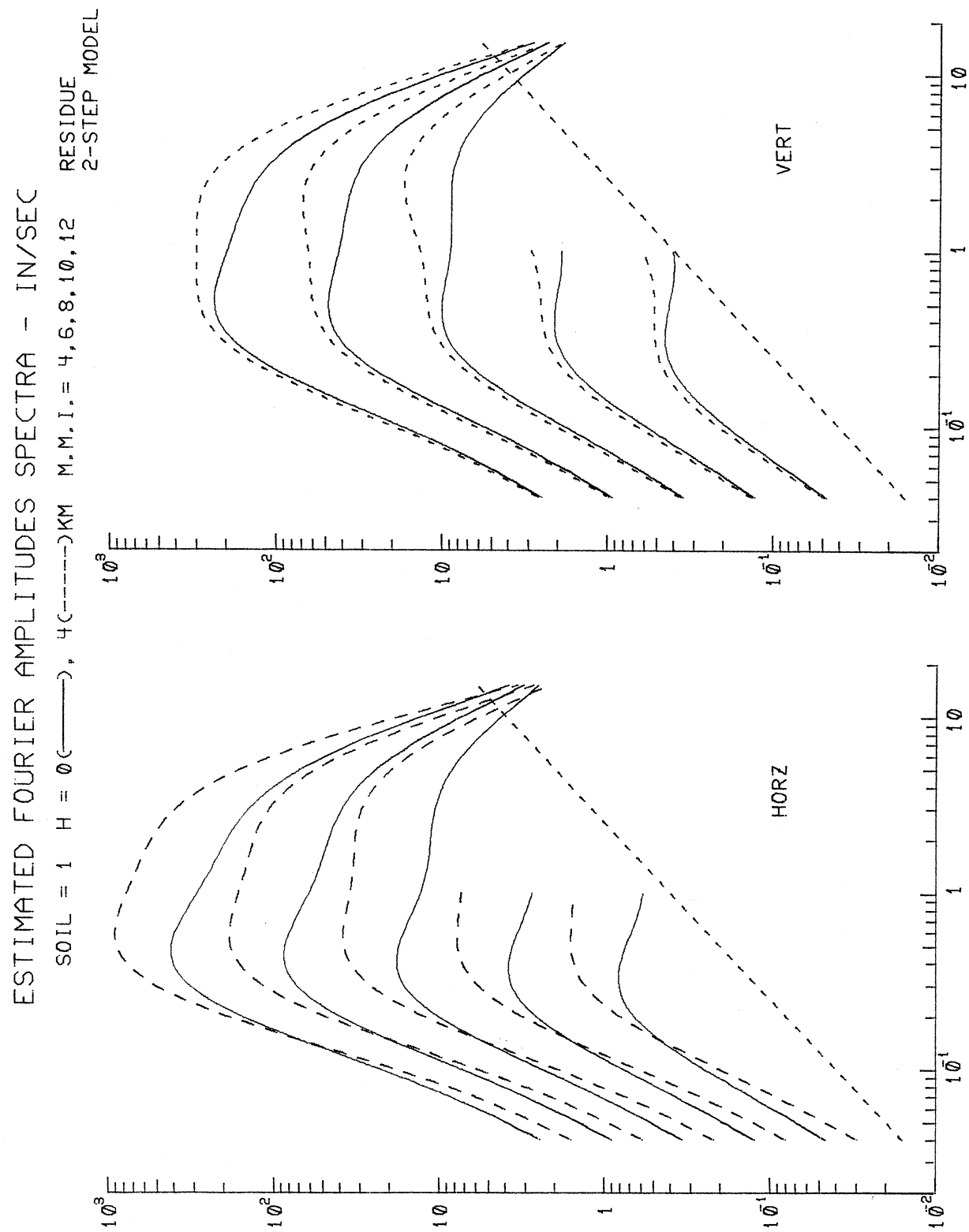

Figure III.4.4

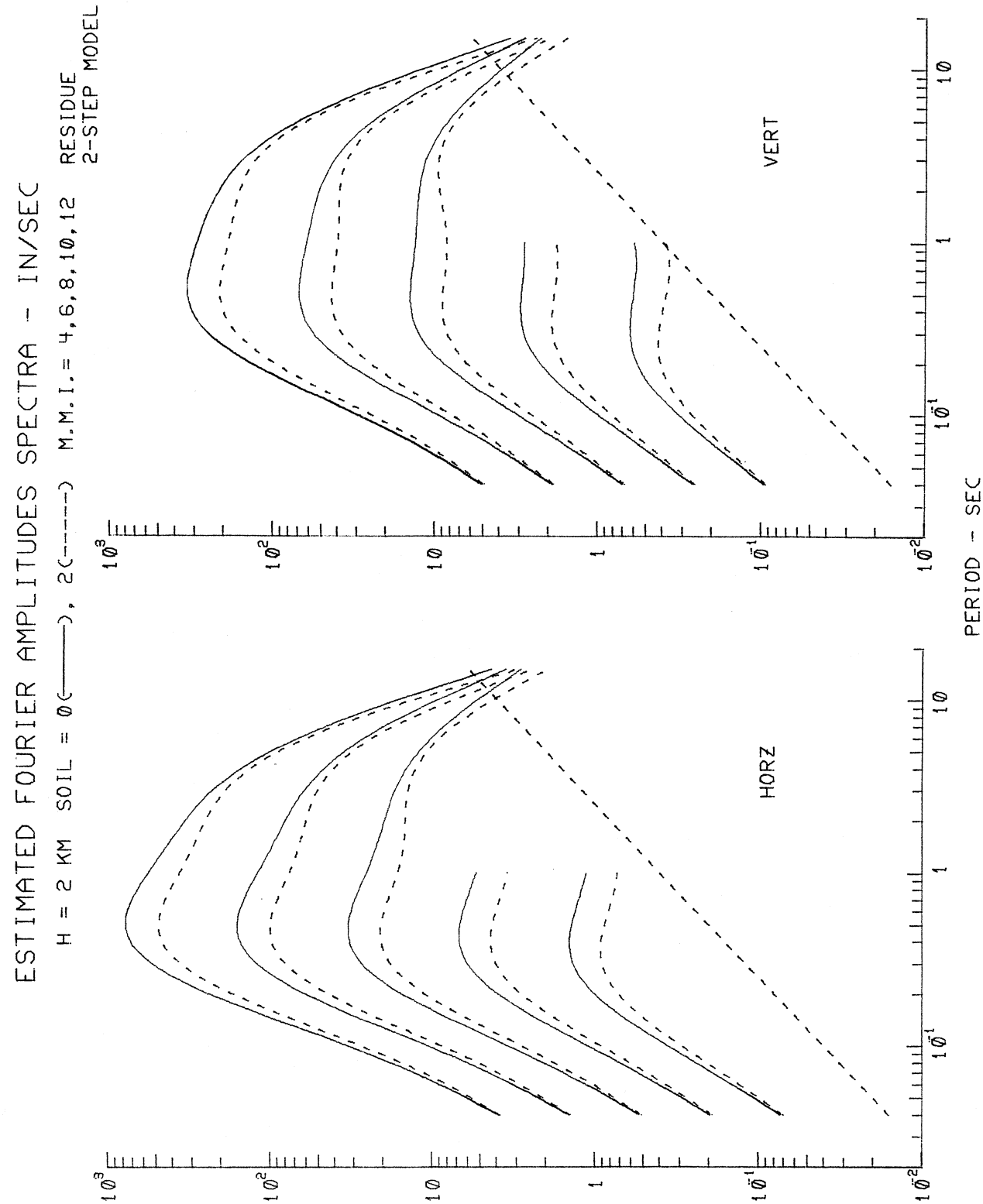

Figure III.4.5

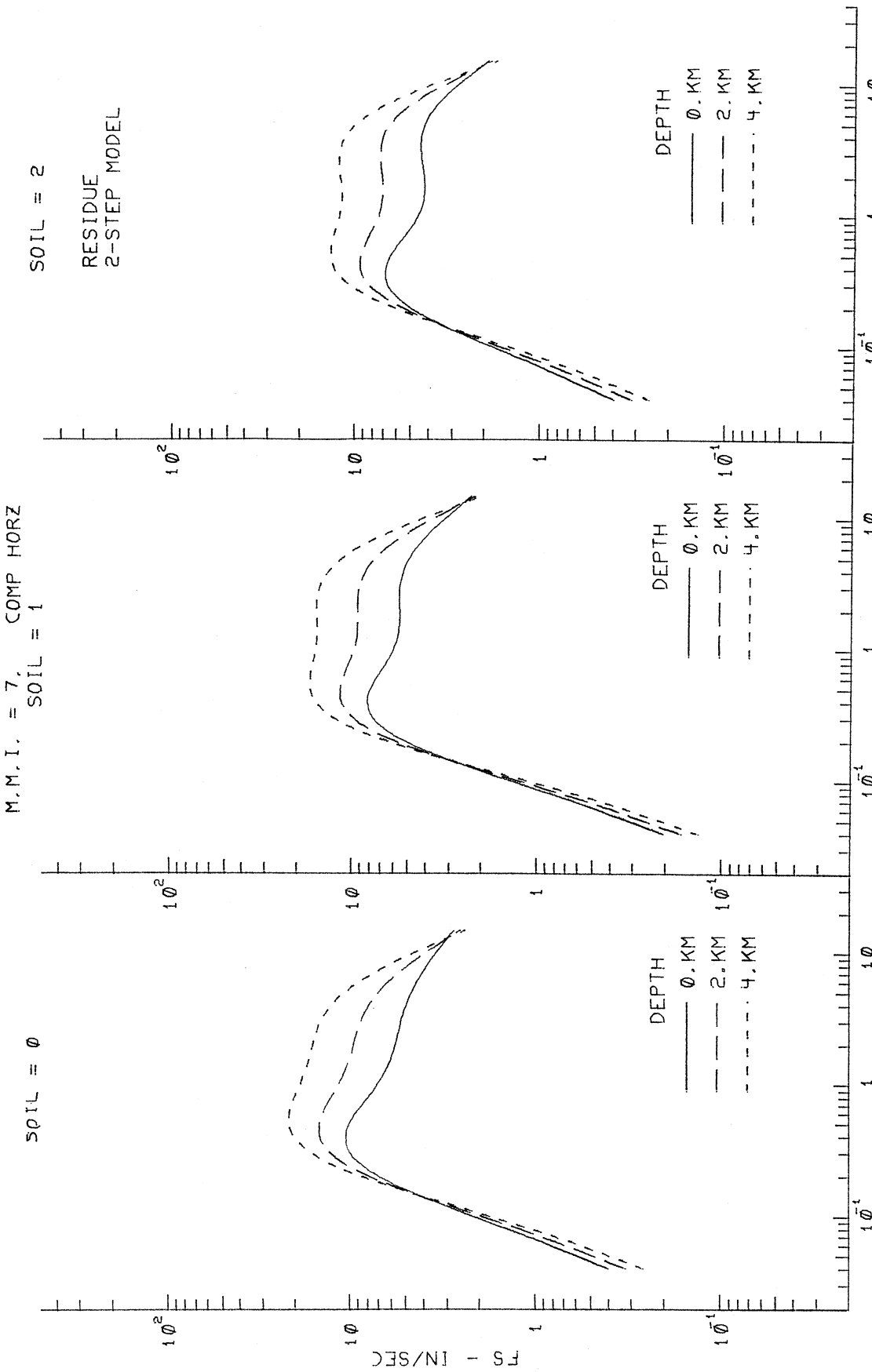

Figure III.4.6

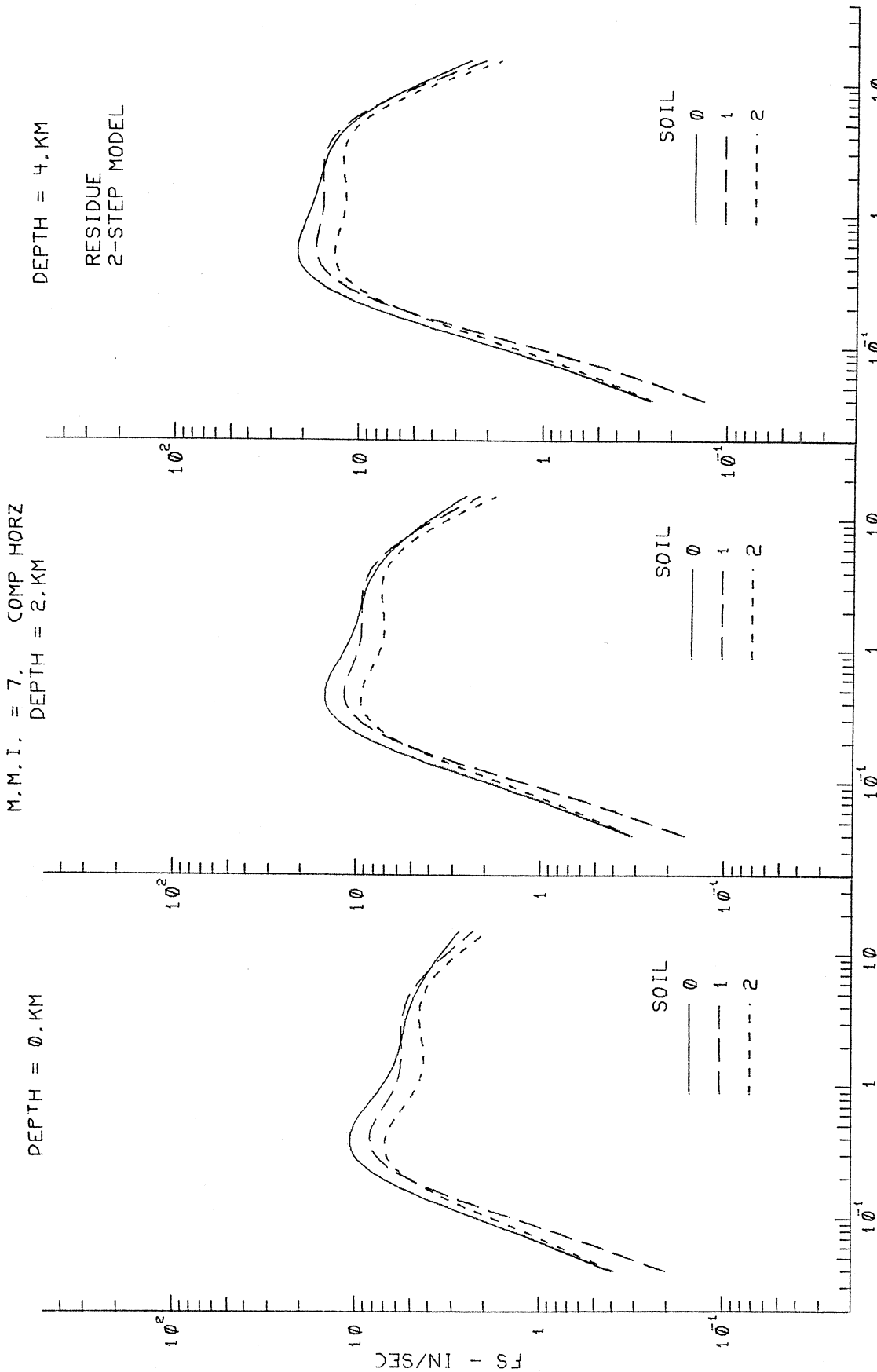

Figure III.4.7

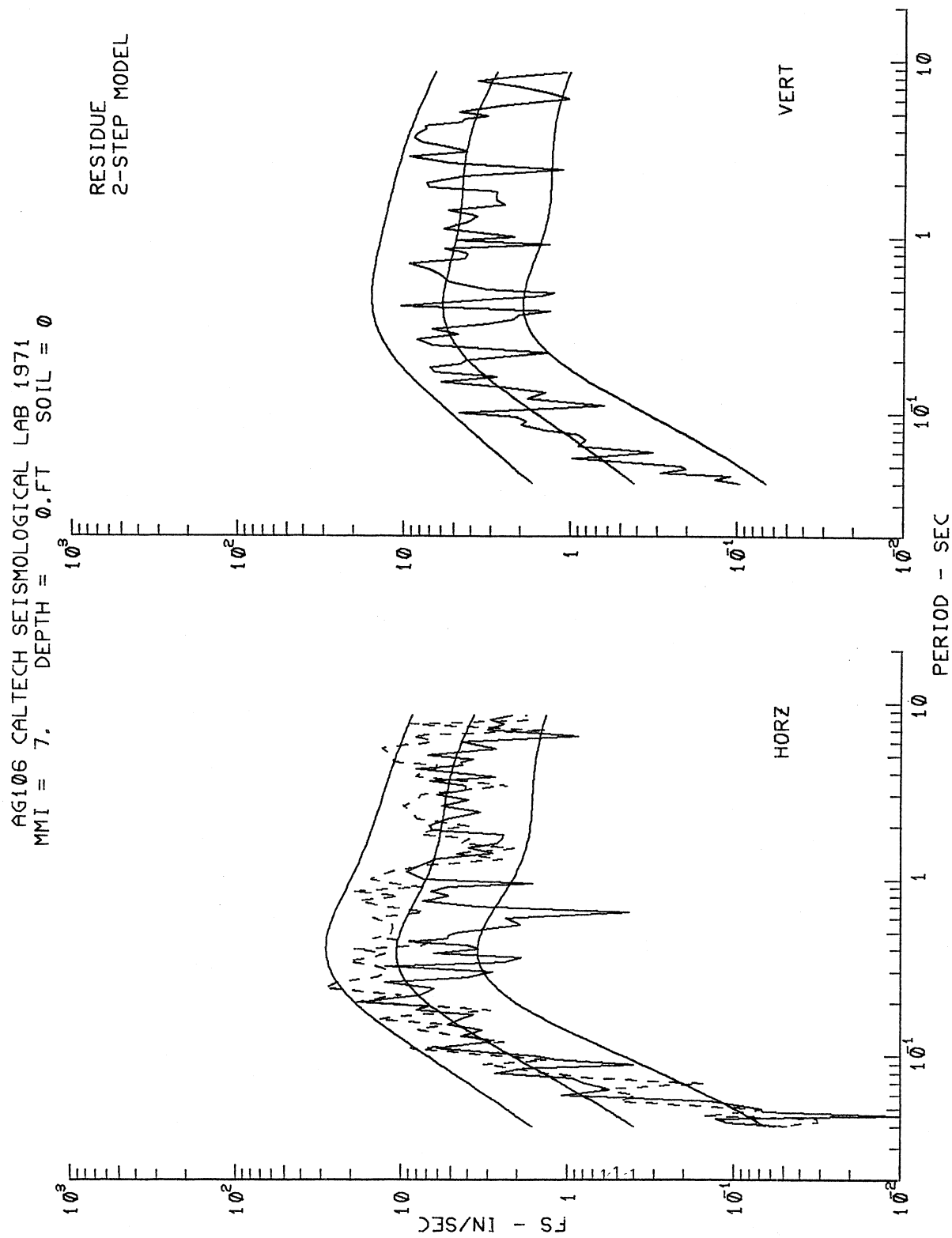

Figure III.4.8

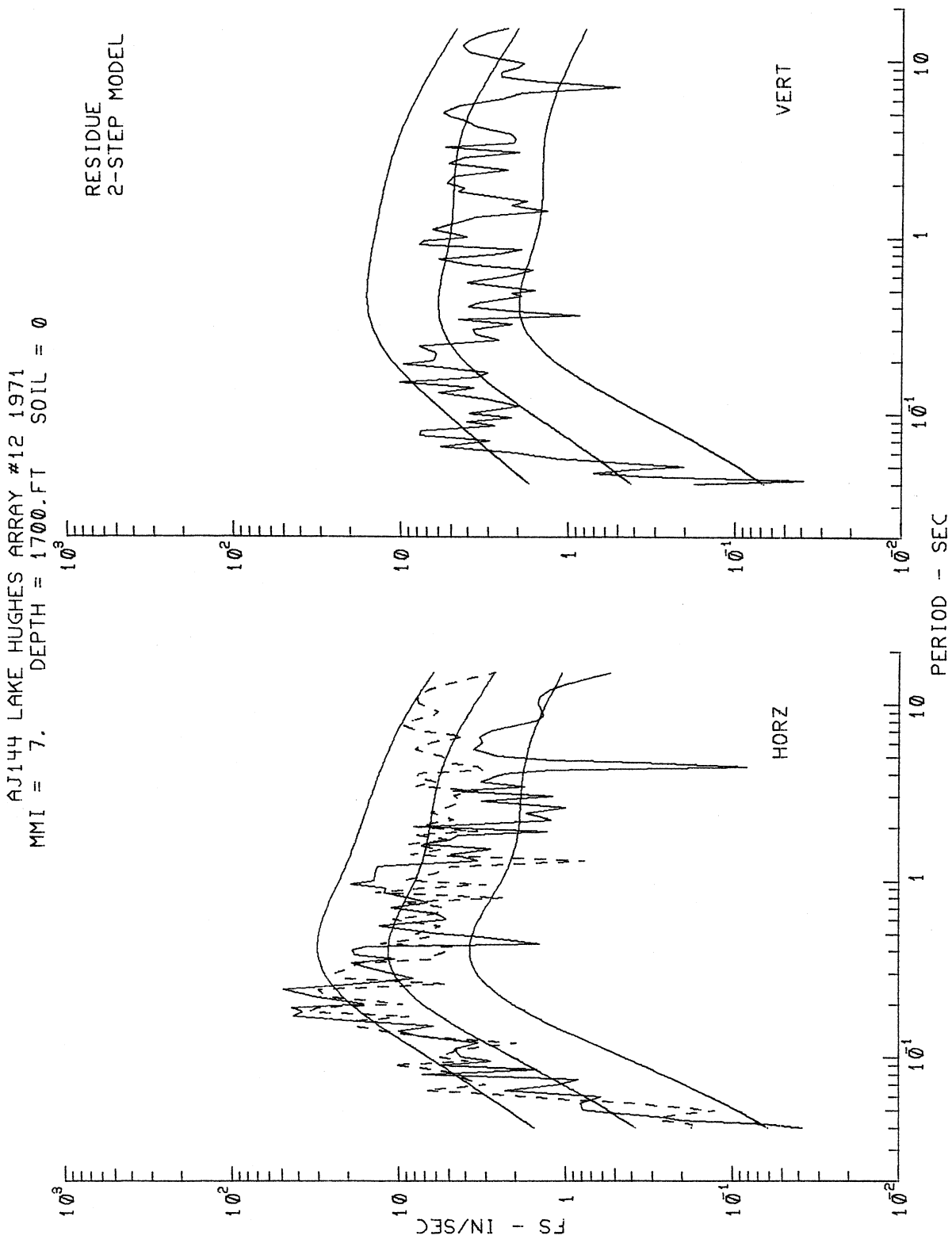

Figure III.4.9

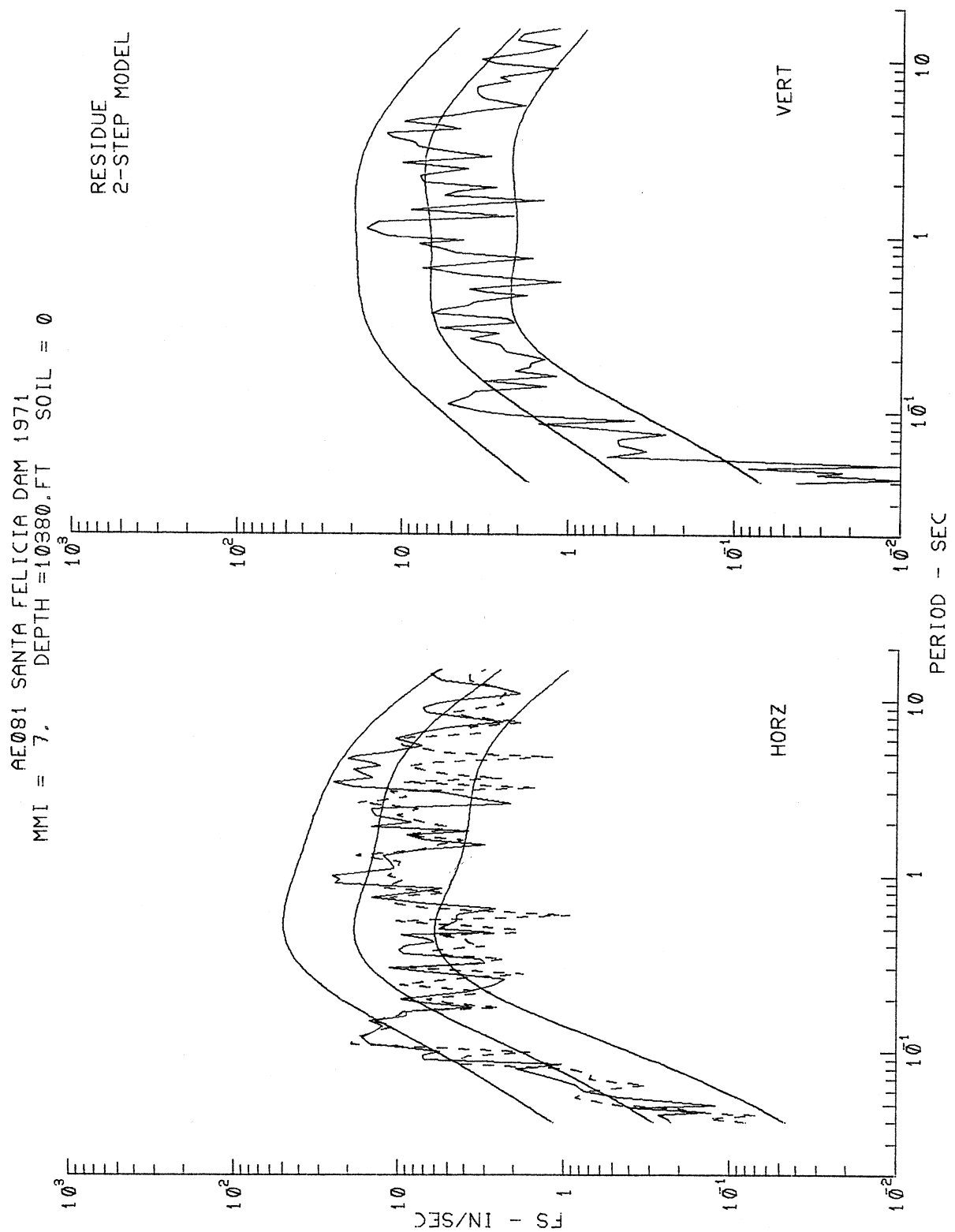

Figure III.4.10

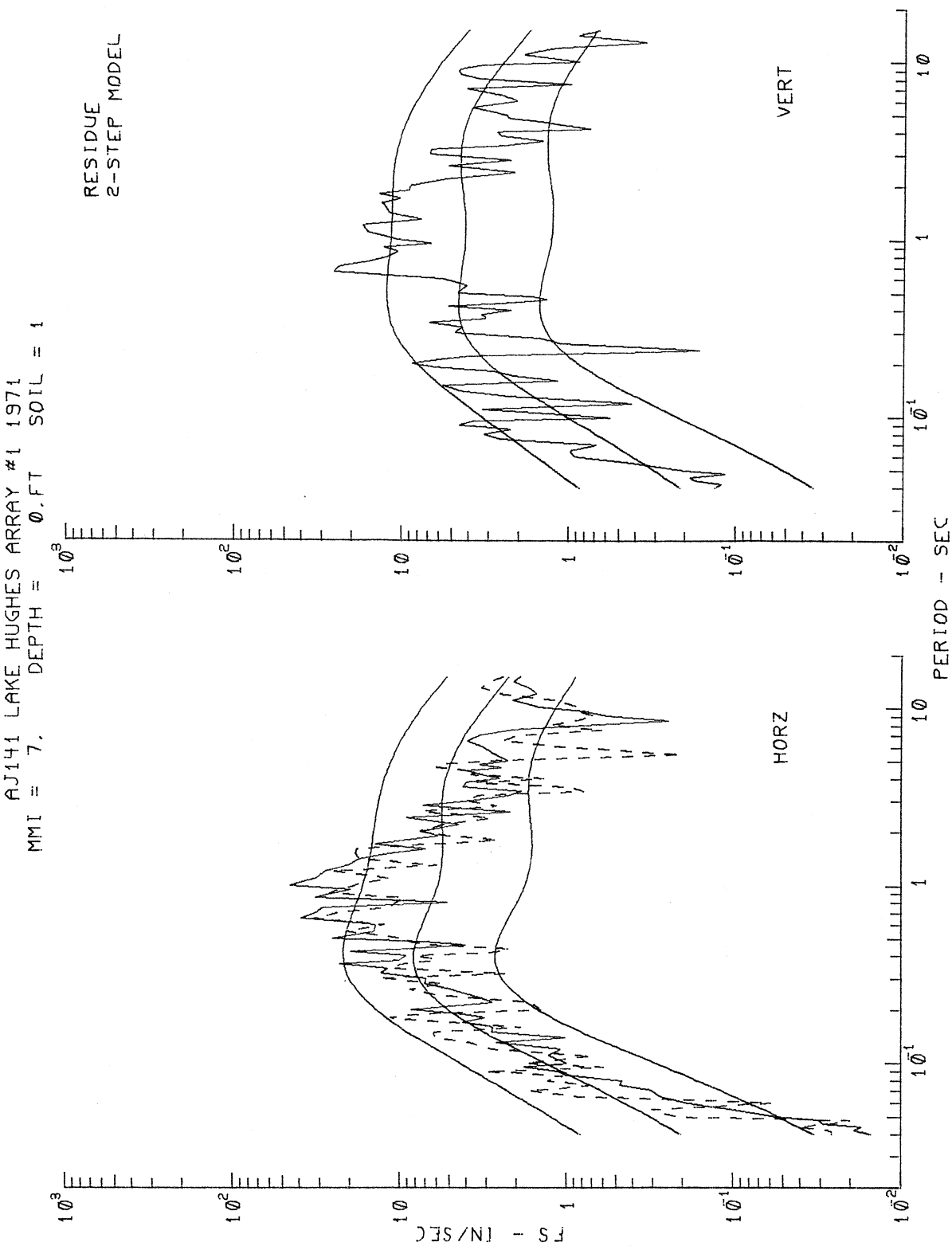

Figure III.4.11

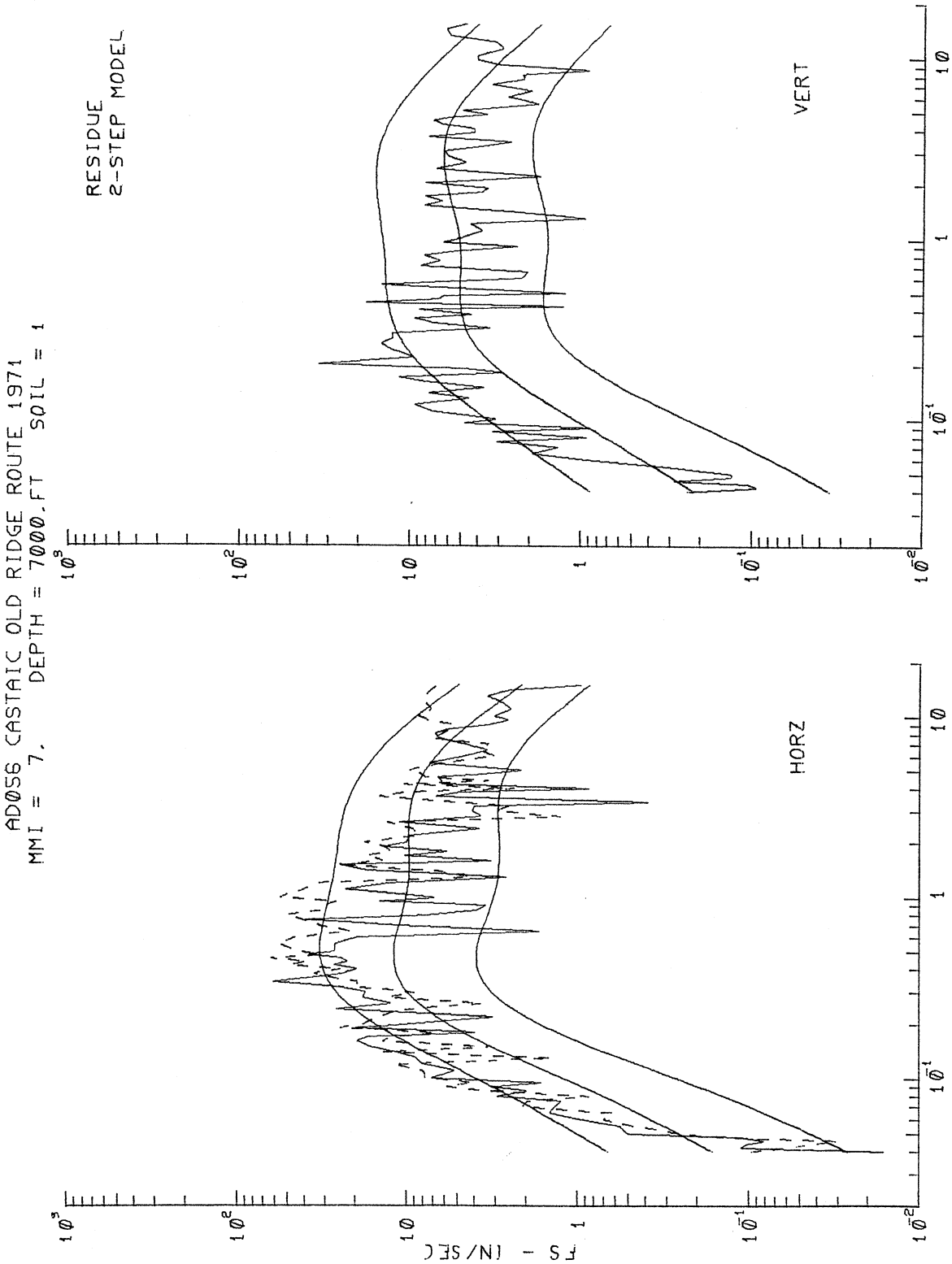

Figure III.4.12

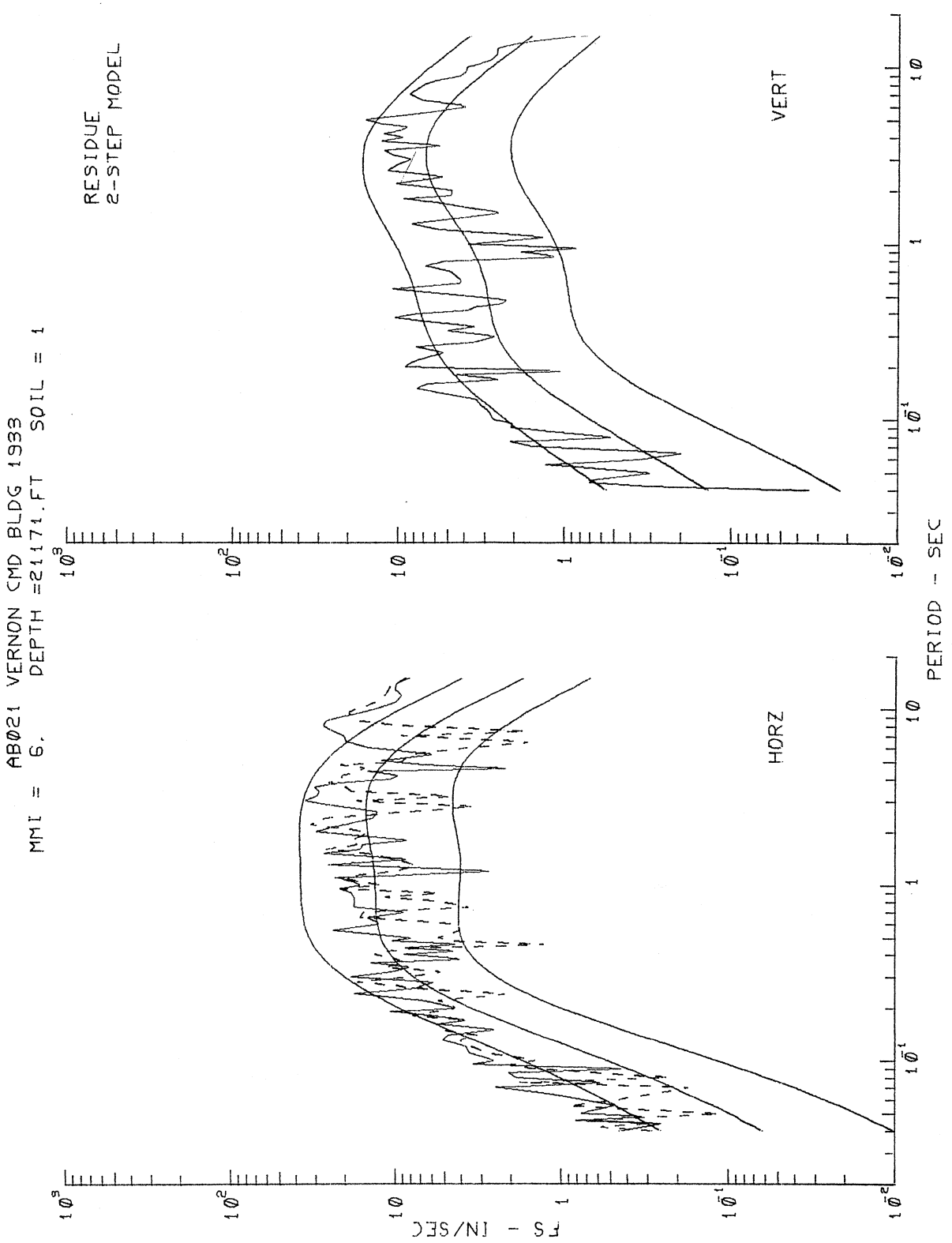

Figure III.4.13

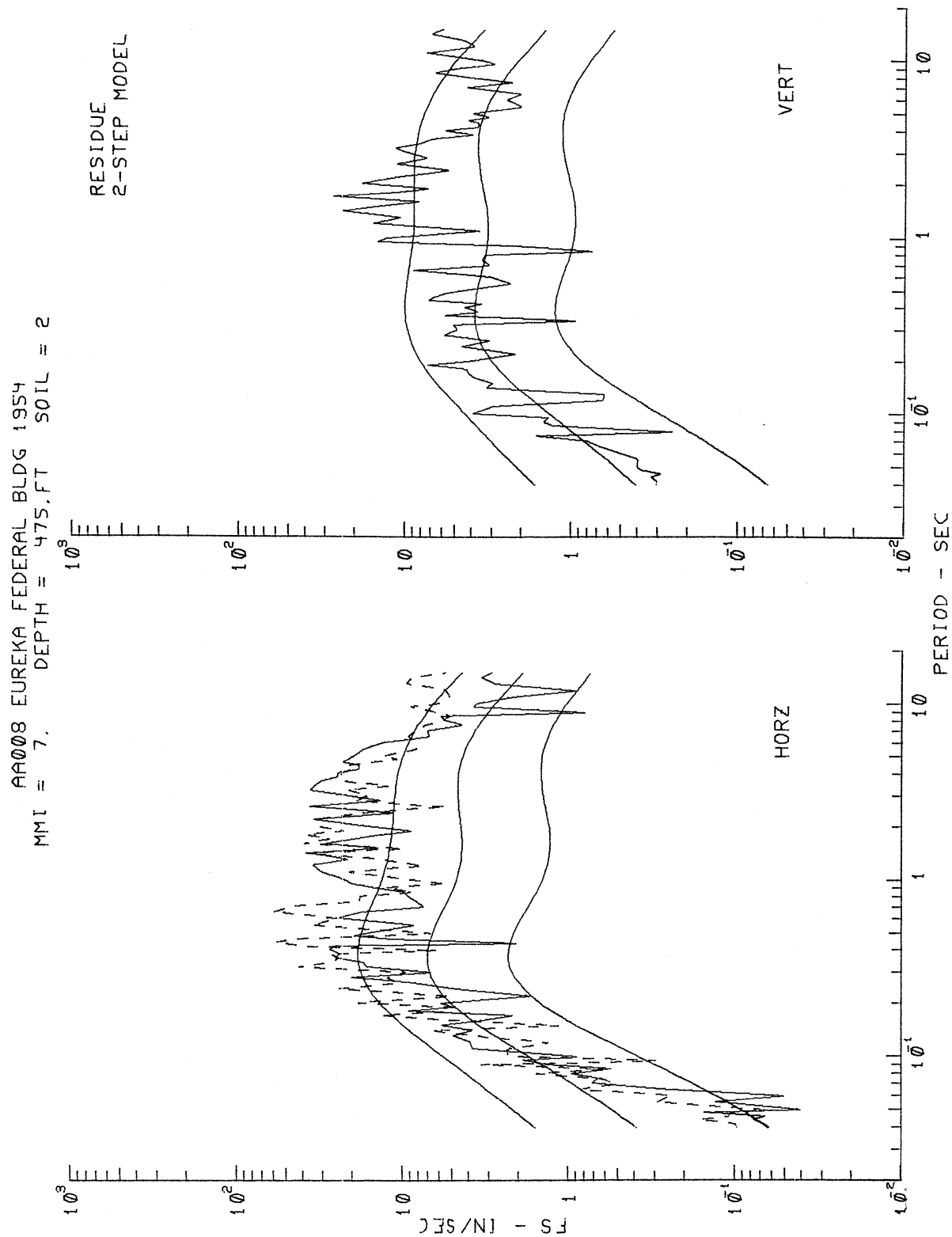

Figure III.4.14

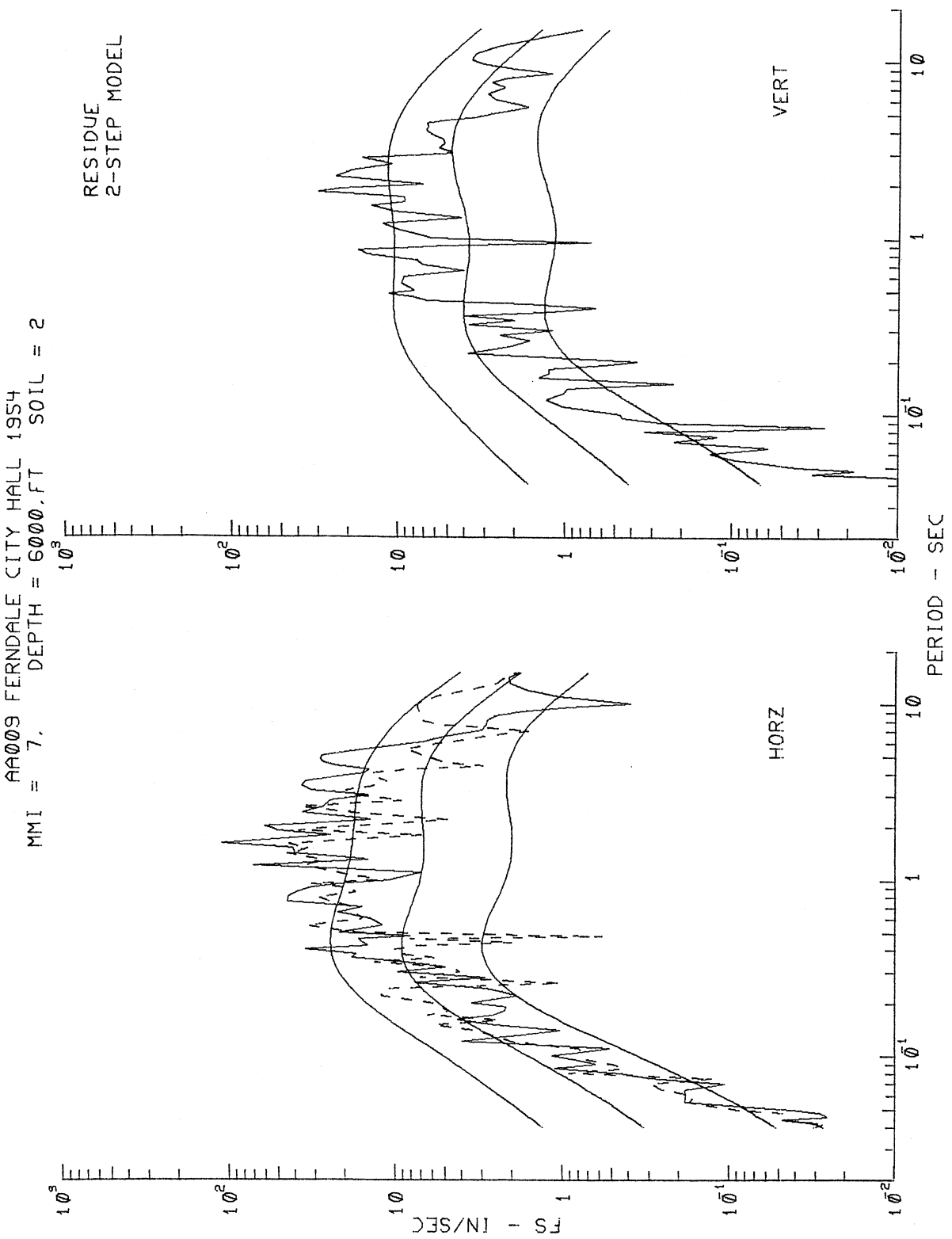

Figure III.4.15

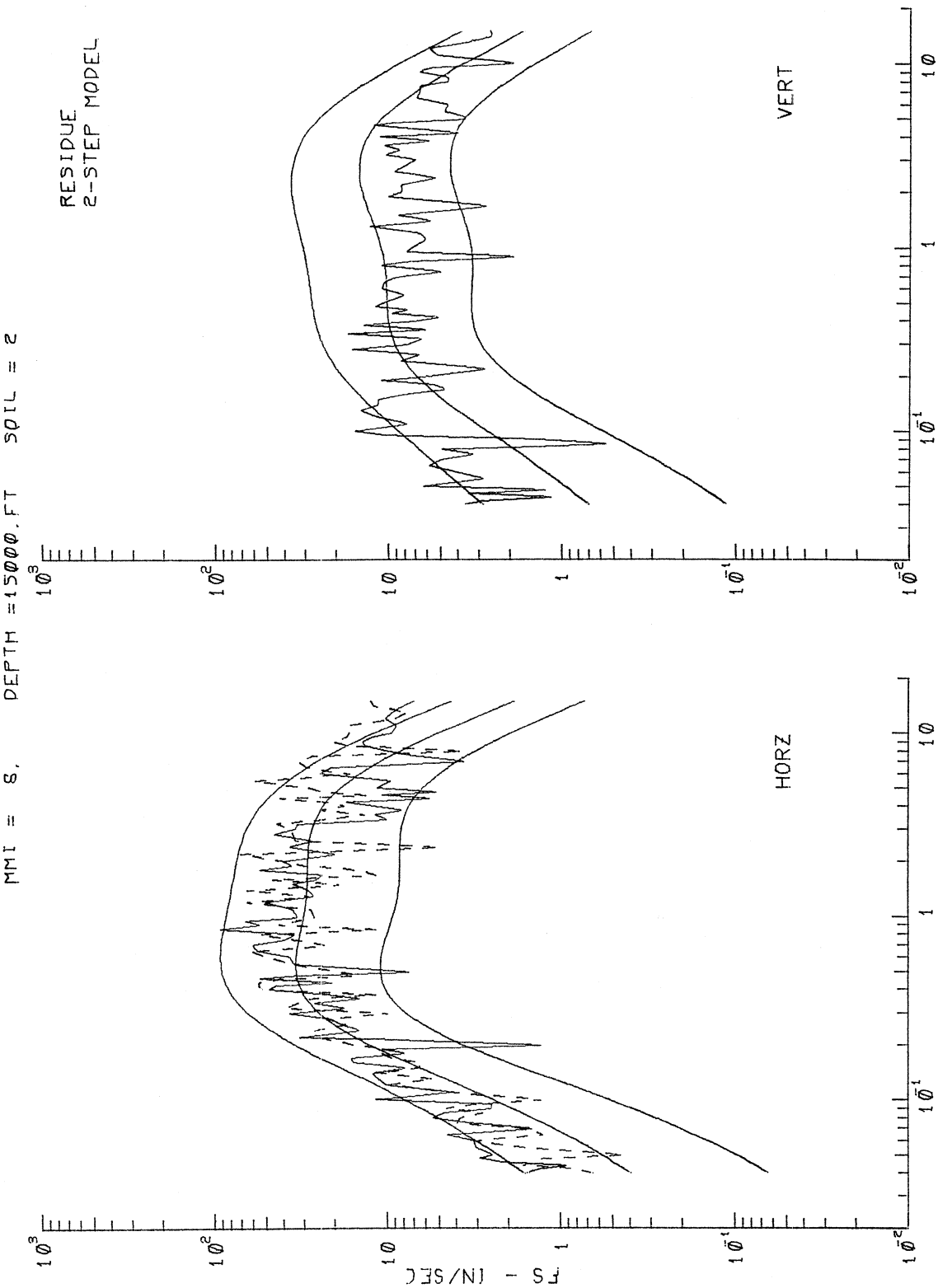

Figure III.4.16

TABLE III.4.2

$$\log_{10} FS(T) = c_1(T)\hat{I}_{MM} + c_2(T)h + c_3(T)v + c_4(T)hv + c_5(T) + c_6^{(1)}S_L^{(1)} + c_6^{(2)}(T)S_L^{(2)}$$

MMI-DEPTH-SOIL RESIDUES: 2-STEP MODEL

PERIOD, T(SEC)	.040	.065	.11	.19	.34	.50	.90	1.60	2.80	4.40	7.50	14.0
COEFFICIENTS:												
$c_1(T)$	.219	.221	.251	.296	.335	.344	.338	.317	.287	.247	.171	.049
$c_2(T)$	-.048	-.040	-.018	.018	.062	.085	.104	.111	.111	.100	.064	-.013
$c_3(T)$	.017	-.029	-.138	-.235	-.262	-.238	-.170	-.114	-.095	-.102	-.118	-.131
$c_4(T)$	.052	.048	.032	-.002	-.045	-.063	-.063	-.045	-.036	-.034	-.022	.014
$c_5(T)$	-2.001	-1.725	-1.371	-1.216	-1.333	-1.449	-1.520	-1.460	-1.304	-1.068	-.621	.082
$c_6^{(1)}(T)$	-.297	-.263	-.195	-.132	-.107	-.107	-.089	-.031	.023	.031	-.006	-.081
$c_6^{(2)}(T)$	-.007	-.039	-.097	-.147	-.178	-.193	-.198	-.157	-.086	-.046	-.059	-.156
RESIDUES:												
p =.1	-.745	-.698	-.607	-.516	-.470	-.472	-.497	-.506	-.486	-.459	-.431	-.404
p =.2	-.457	-.429	-.369	-.311	-.290	-.299	-.318	-.317	-.295	-.281	-.276	-.274
p =.3	-.268	-.250	-.213	-.179	-.169	-.176	-.188	-.183	-.165	-.154	-.153	-.155
p =.4	-.105	-.097	-.081	-.068	-.067	-.072	-.078	-.071	-.058	-.054	-.060	-.067
p =.5	.044	.042	.037	.029	.019	.015	.016	.027	.035	.032	.017	.003
p =.6	.170	.161	.144	.121	.103	.101	.111	.126	.128	.116	.093	.074
p =.7	.297	.282	.250	.214	.192	.191	.204	.214	.208	.194	.176	.162
p =.8	.460	.432	.377	.322	.296	.299	.313	.312	.293	.277	.266	.257
p =.9	.653	.612	.533	.461	.435	.445	.466	.456	.419	.393	.381	.373
RESIDUE STATISTICS:												
$\mu(T)$	.005	.005	.007	.007	.005	.003	.003	.006	.008	.007	.000	-.005
$\sigma(T)$	.548	.514	.445	.379	.350	.356	.376	.376	.353	.332	.319	.307
$X^2(T)$	11.049	10.325	9.130	7.849	6.947	6.891	8.187	11.114	13.591	13.422	10.632	7.661
KS(T)	.046	.046	.046	.045	.040	.037	.038	.047	.055	.055	.048	.041

Table III.4.2 presents the scaling functions, residue levels and the residue statistics at 12 discrete periods for the 2-step model. It corresponds to the Table III.2.1 for the 1-step model.

This completes the presentation of Part III of the scaling of FS(T) in terms of M.M.I., h, s_L and v.

PART IV: SCALING OF FOURIER SPECTRA IN TERMS OF MMI, s, v and s_L

IV.1 The Scaling Relation

Part IV of this report continues the description of the empirical scaling of Fourier amplitude spectra of strong ground motion in terms of Modified Mercalli Intensity (M.M.I.) at the site, and the local geological and soil classifications. As in Part II of this report, in this part we replace the depth of sedimentary deposits, h, by the corresponding local geological site parameter s (s = 0, 1 or 2). Treating the site parameter as an indicator variable, as in Part II, the scaling relation now takes the form

$$\log_{10}FS(T) = b_1(T)\hat{I}_{MM} + b_2^{(1)}(T)S^{(1)} + b_2^{(2)}S^{(2)} + b_3(T)v$$
$$+ b_4^{(1)}(T)S^{(1)}v + b_4^{(2)}(T)S^{(2)}v + b_5(T)$$
$$+ b_6^{(1)}(T)S_L^{(1)} + b_6^{(2)}(T)S_L^{(2)} \quad , \qquad \text{(IV.1.1)}$$

with all the parameters defined as before. $b_2^{(i)}(T)$ and $b_4^{(i)}(T)$, for i = 1 and 2, are now the scaling functions associated with the site parameters $S^{(i)}$ and $S^{(i)}v$ respectively.

As in all previous models in this work, the scaling functions $b_1(T)$ through $b_6^{(2)}(T)$ are determined from the regression analysis of the new database of 1482 components of spectral amplitudes, FS(T) at 91 discrete periods T ranging from 0.04 sec. to 15 sec. the data are first screened and selected as before to reduce the possible bias in the model. All procedures in data preparation, selection and the steps of regression analysis employed here are identical to those in Part III of this work.

The resulting scaling functions at each period T will be denoted by $\hat{b}_1(T)$ through $\hat{b}_6(T)$, respectively.

Much of the presentation in the following will be very similar to the corresponding sections in Part III of this work. The reader can simply refer to the corresponding sections of Part III for a more detailed description. Substituting the fitted scaling functions in equation (IV.1.1) gives $\hat{FS}(T)$, the estimated spectral amplitudes, where

$$\log_{10}\hat{FS}(T) = \hat{b}_1(T)\hat{I}_{MM} + \hat{b}_2^{(1)}(T)S^{(1)} + \hat{b}_2^{(2)}(T)S^{(2)} + \hat{b}_3(T)v$$
$$+ \hat{b}_4^{(1)}(T)S^{(1)}v + \hat{b}_4^{(2)}(T)S^{(2)}v + \hat{b}_5(T)$$
$$+ \hat{b}_6^{(1)}(T)S_L^{(1)} + \hat{b}_6^{(2)}(T)S_L^{(2)} \quad . \qquad \text{(IV.1.2)}$$

The residues $\varepsilon(T) = \log_{10}(FS(T)) - \log_{10}(\hat{FS}(T))$ describing the distribution of the recorded FS(T) about the estimated FS(T) are next calculated. We assume again that $\varepsilon(T)$ is described by a normal distribution function with mean, $\mu(T)$, and standard deviation, $\sigma(T)$.

IV.2 The Regression Coefficients

Figure IV.2.1 shows the smoothed coefficients $\hat{b}_1(T)$ through $\hat{b}_6^{(2)}(T)$ (solid lines) together with the estimates of their 80%, 90% and 95% confidence intervals (dashed lines). Comparison of this figure with the corresponding Figure III.2.1 of the MMI-DEPTH-SOIL model, in Part III, shows that the functions $\hat{b}_1(T)$, $\hat{b}_3(T)$, $\hat{b}_5(T)$, $\hat{b}_6^{(1)}(T)$ and $\hat{b}_6^{(2)}(T)$ in both figures are similar. These functions correspond to the same scaling parameters: I_{MM}, v, l, $S_L^{(1)}$ and $S_L^{(2)}$, and their similarity again demonstrates the stability and consistency of the two regression models.

Figure IV.2.2 shows the plot of the residuals corresponding to $p^*(\varepsilon,T) = 0.1$ through 0.9 for $\log_{10}FS(T)$. Refer to the same Figure III.2.2 in Part III of this work for a description of these curves. The resemblance of these two figures (Figures IV.2.2 and III.2.2) again demonstrates that the uncertainties associated with the characterization of local site geology in terms of site conditions (s = 0, 1 or 2) are not much greater than those associated with characterization in terms of the alluvium depth.

Figure IV.2.3 shows the plot of the statistical parameters employed in the description of the residues, namely, $\hat{\mu}(T)$, $\hat{\sigma}(T)$, $\chi^2(T)$ and KS(T). Both the chi-squared and the Kolmogorov-Smirnov tests again fail to reject the hypothesis that the distribution is normal, at the 95% level of confidence. Table IV.2.1 gives, for 12 periods between T = 0.4 sec. and 14 sec., the nine coefficients $\hat{b}_1(T)$ through $\hat{b}_6^{(2)}(T)$, the nine residue levels corresponding to $p^*(\varepsilon,T) = 0.1$ through 0.9, and the smooth coefficients $\hat{\mu}(T)$, $\hat{\sigma}(T)$, $\chi^2(T)$ and KS(T).

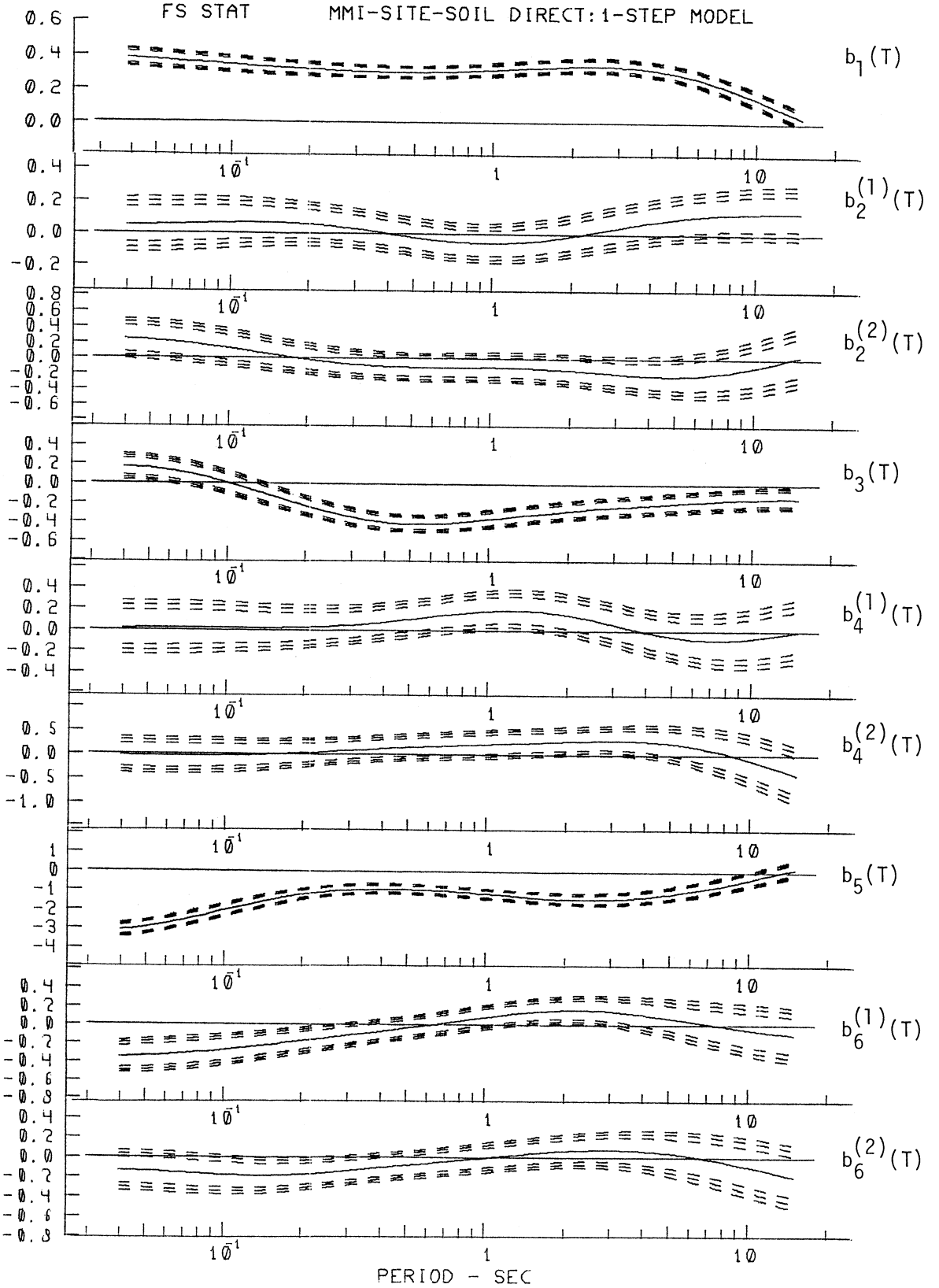
FS STAT
MMI-SITE-SOIL DIRECT: 1-STEP MODEL
$b_1(T)$
$b_2^{(1)}(T)$
$b_2^{(2)}(T)$
$b_3(T)$
$b_4^{(1)}(T)$
$b_4^{(2)}(T)$
$b_5(T)$
$b_6^{(1)}(T)$
$b_6^{(2)}(T)$
PERIOD - SEC

Figure IV.2.1

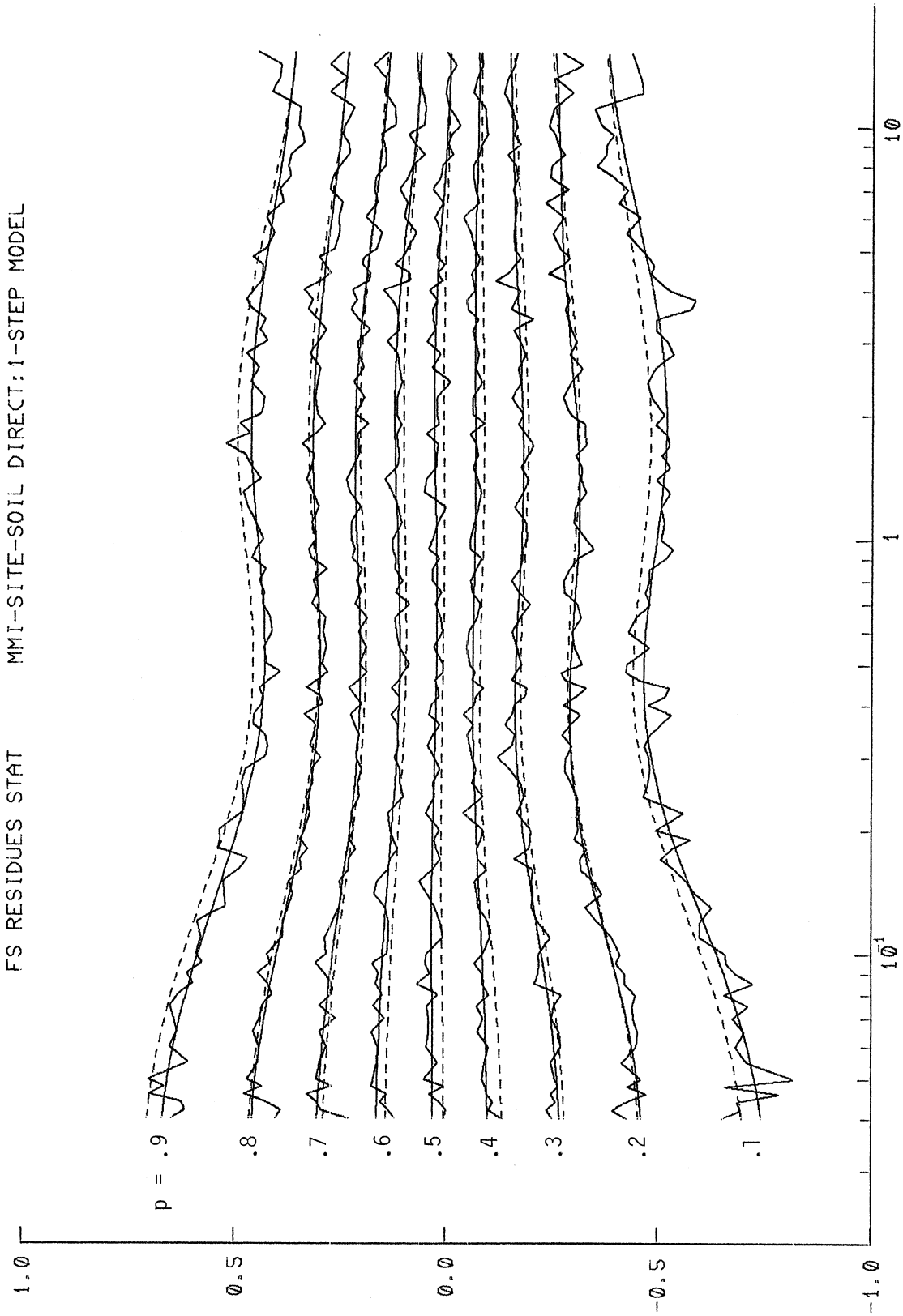
FS RESIDUES STAT
MMI-SITE-SOIL DIRECT: 1-STEP MODEL
p = .9
.8
.7
.6
.5
.4
.3
.2
.1
1.0
0.5
0.0
-0.5
-1.0
10⁻¹
1
10

Figure IV.2.2

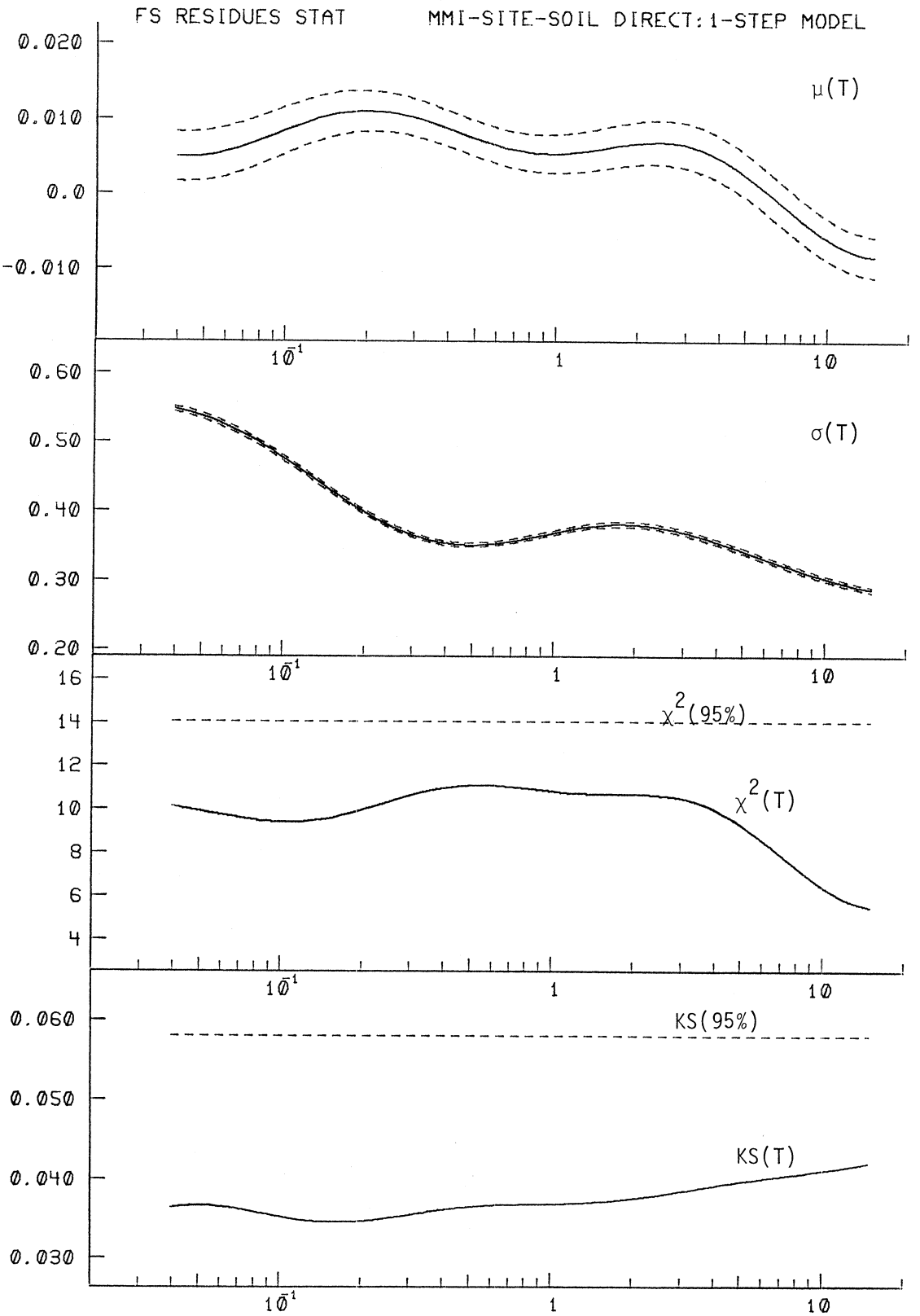
FS RESIDUES STAT
MMI-SITE-SOIL DIRECT: 1-STEP MODEL
μ(T)
σ(T)
χ²(95%)
χ²(T)
KS(95%)
KS(T)
0.020
0.010
0.0
-0.010
0.60
0.50
0.40
0.30
0.20
16
14
12
10
8
6
4
0.060
0.050
0.040
0.030
10⁻¹
1
10

Figure IV.2.3

TABLE IV.2.1

$$\log_{10} FS(T) = b_1(T)\hat{I}_{MM} + b_2^{(1)}(T)S^{(1)} + b_2^{(2)}(T)S^{(2)} + b_3(T)v +$$

$$b_4^{(1)}S^{(1)}v + b_4^{(2)}(T)S^{(2)}v + b_5(T) + b_6^{(1)}(T)S_L^{(1)} + b_6^{(2)}(T)S_L^{(2)}$$

MMI-SITE-SOIL DIRECT:1-STEP MODEL

PERIOD, T(SEC)	.040	.065	.11	.19	.34	.50	.90	1.60	2.80	4.40	7.50	14.0
COEFFICIENTS:												
$b_1(T)$	.378	.356	.333	.312	.295	.292	.305	.330	.336	.306	.215	.046
$b_2^{(1)}(T)$	.048	.055	.064	.059	.018	-.021	-.059	-.035	.033	.085	.122	.134
$b_2^{(2)}(T)$	.239	.195	.105	-.004	-.089	-.111	-.111	-.126	-.182	-.220	-.180	.009
$b_3(T)$	.169	.116	-.027	-.217	-.375	-.416	-.380	-.299	-.240	-.204	-.162	-.135
$b_4^{(1)}(T)$	.015	.019	.021	.027	.059	.104	.177	.180	.076	-.032	-.090	-.016
$b_4^{(2)}(T)$	-.029	-.041	-.027	.022	.098	.146	.203	.258	.300	.269	.080	-.352
$b_5(T)$	-3.110	-2.661	-1.923	-1.263	-.950	-.952	-1.145	-1.379	-1.441	-1.255	-.750	.090
$b_6^{(1)}(T)$	-.352	-.323	-.265	-.185	-.097	-.037	.065	.150	.159	.100	-.000	-.101
$b_6^{(2)}(T)$	-.139	-.159	-.187	-.177	-.124	-.083	-.019	.045	.078	.056	-.032	-.182
RESIDUES:												
p =.1	-.742	-.701	-.624	-.536	-.476	-.468	-.491	-.517	-.510	-.479	-.430	-.384
p =.2	-.462	-.434	-.380	-.323	-.294	-.295	-.311	-.312	-.294	-.278	-.268	-.258
p =.3	-.269	-.253	-.221	-.185	-.165	-.165	-.177	-.182	-.174	-.165	-.157	-.150
p =.4	-.100	-.095	-.086	-.073	-.064	-.063	-.067	-.069	-.067	-.067	-.072	-.076
p =.5	.031	.031	.032	.031	.025	.023	.023	.028	.028	.021	.006	-.007
p =.6	.164	.157	.146	.130	.114	.109	.114	.122	.120	.107	.083	.063
p =.7	.305	.289	.261	.230	.207	.203	.211	.217	.208	.189	.162	.138
p =.8	.459	.435	.391	.341	.306	.299	.307	.316	.308	.289	.262	.236
p =.9	.670	.636	.573	.498	.442	.429	.442	.461	.456	.433	.397	.362
RESIDUE STATISTICS:												
$\mu(T)$	.005	.006	.009	.011	.010	.007	.005	.006	.007	.004	-.003	-.008
$\sigma(T)$	.548	.520	.467	.405	.359	.351	.366	.381	.373	.351	.319	.290
$X^2(T)$	10.121	9.673	9.406	9.899	10.816	11.107	10.901	10.708	10.599	9.763	7.640	5.615
KS(T)	.036	.036	.035	.035	.036	.036	.037	.037	.038	.039	.041	.042

IV.3 The Estimated Fourier Spectra

Figure IV.3.1 presents examples of Fourier amplitude spectra, FS(T), computed from equation (IV.1.2) for $p(\varepsilon,T) = 0.5$, for M.M.I. levels IV, VI, VIII, X and XII and for soil classification $s_L = 1$ (stiff soil). The left figure is for horizontal (v = 0) and the right figure for vertical (v = 1) motion. The solid lines in both graphs correspond to the local geological site condition of s = 2 (rock) while the dashed lines correspond to s = 0 (allivium). The diagonal dashed lines again represent the empirical average Fourier amplitudes of digitization noise. Comparison of this figure with the corresponding Figure III.3.1 of Part III for the MMI-DEPTH-SOIL model again shows detailed resemblance, and hence similar conclusions can be drawn. One difference, however, should be pointed out. At low periods, up to .1 sec., the FS(T) amplitudes at rock sites are slightly higher than those on alluvium. This is due to the fact that at low periods (< .1 sec.), $S_L^{(2)}$ ($s_L = 2$) is slightly positive, though ≈ 0.

Figure IV.3.2 presents another set of estimated FS spectra to illustrate the effect of local soil conditions on the FS(T) amplitudes. The FS(T) have been computed for various M.M.I. levels (IV, VI, VIII, X and XII) and for the local geological site condition s = 0 (alluvium). Again, the left part of this figure is for horizontal (v = 0) and the right one for vertical (v = 1) motions. The solid lines in both figures correspond to the local soil classification $s_L = 0$ (rock) and the dashed lines to $s_L = 2$ (deep soil). As in Figure III.3.2 of the MMI-DEPTH-SOIL model in Part III, the FS(T) amplitudes at rock ($s_L = 0$) are higher than those at deep soil ($s_L = 2$). This trend is observed here up to about 1 sec. period, beyond which the trend is reversed.

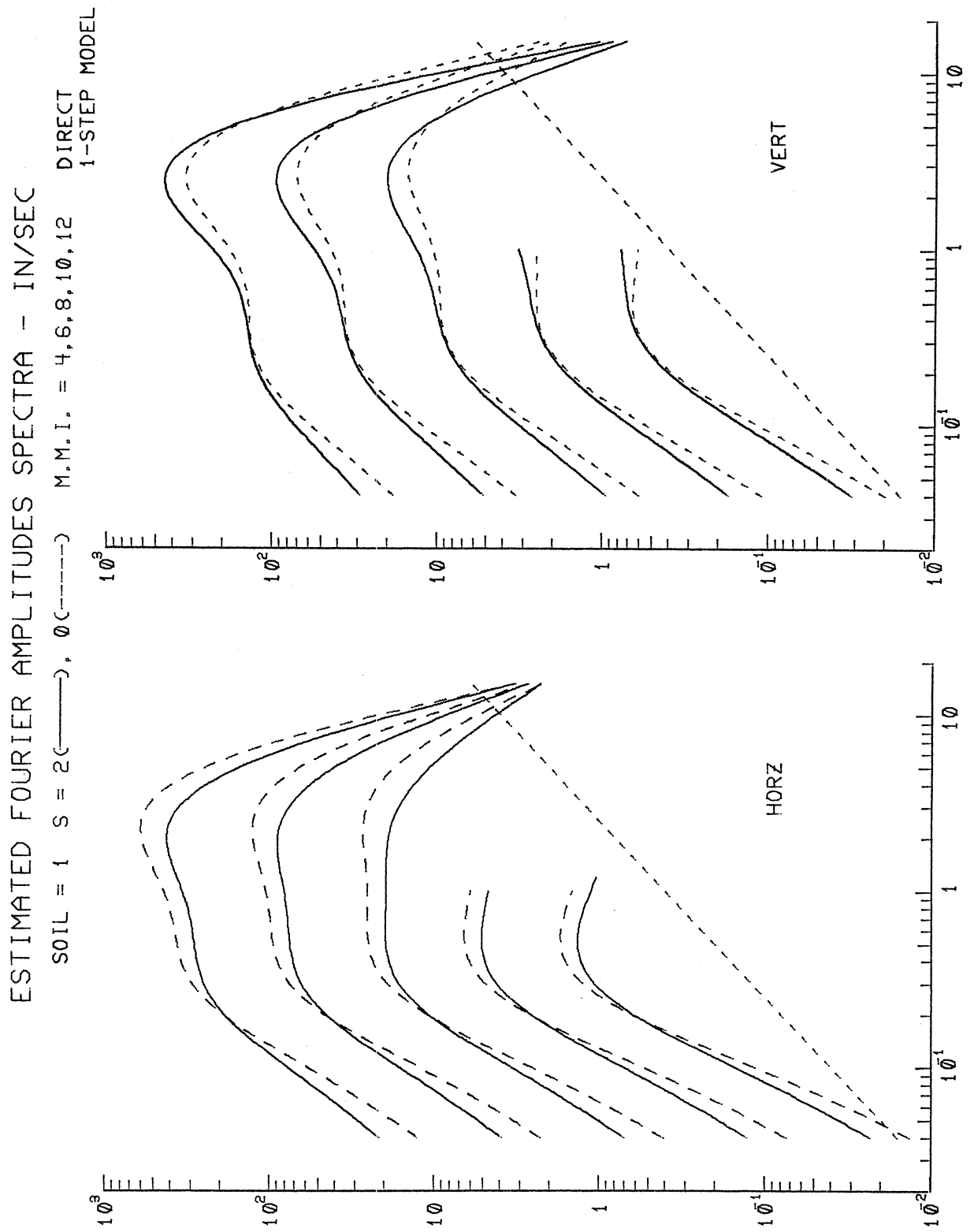
ESTIMATED FOURIER AMPLITUDES SPECTRA - IN/SEC
SOIL = 1 S = 2(———), Ø(– – – –) M.M.I. = 4,6,8,10,12 DIRECT 1-STEP MODEL
HORZ
VERT
PERIOD - SEC

Figure IV.3.1

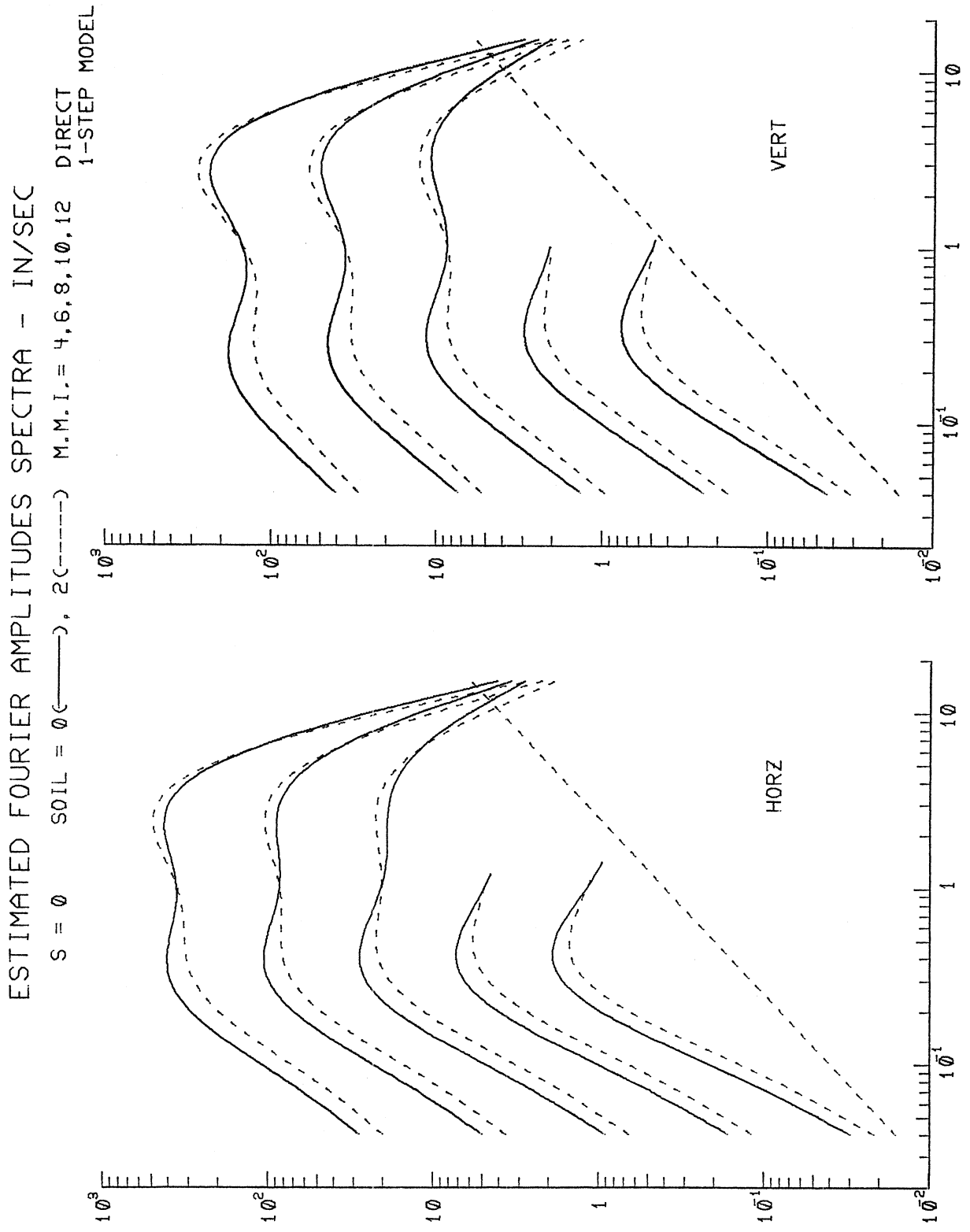
ESTIMATED FOURIER AMPLITUDES SPECTRA - IN/SEC
S = 0 SOIL = 0(———), 2(– – – –) M.M.I.= 4,6,8,10,12 DIRECT 1-STEP MODEL
HORZ
VERT
PERIOD - SEC

Figure IV.3.2

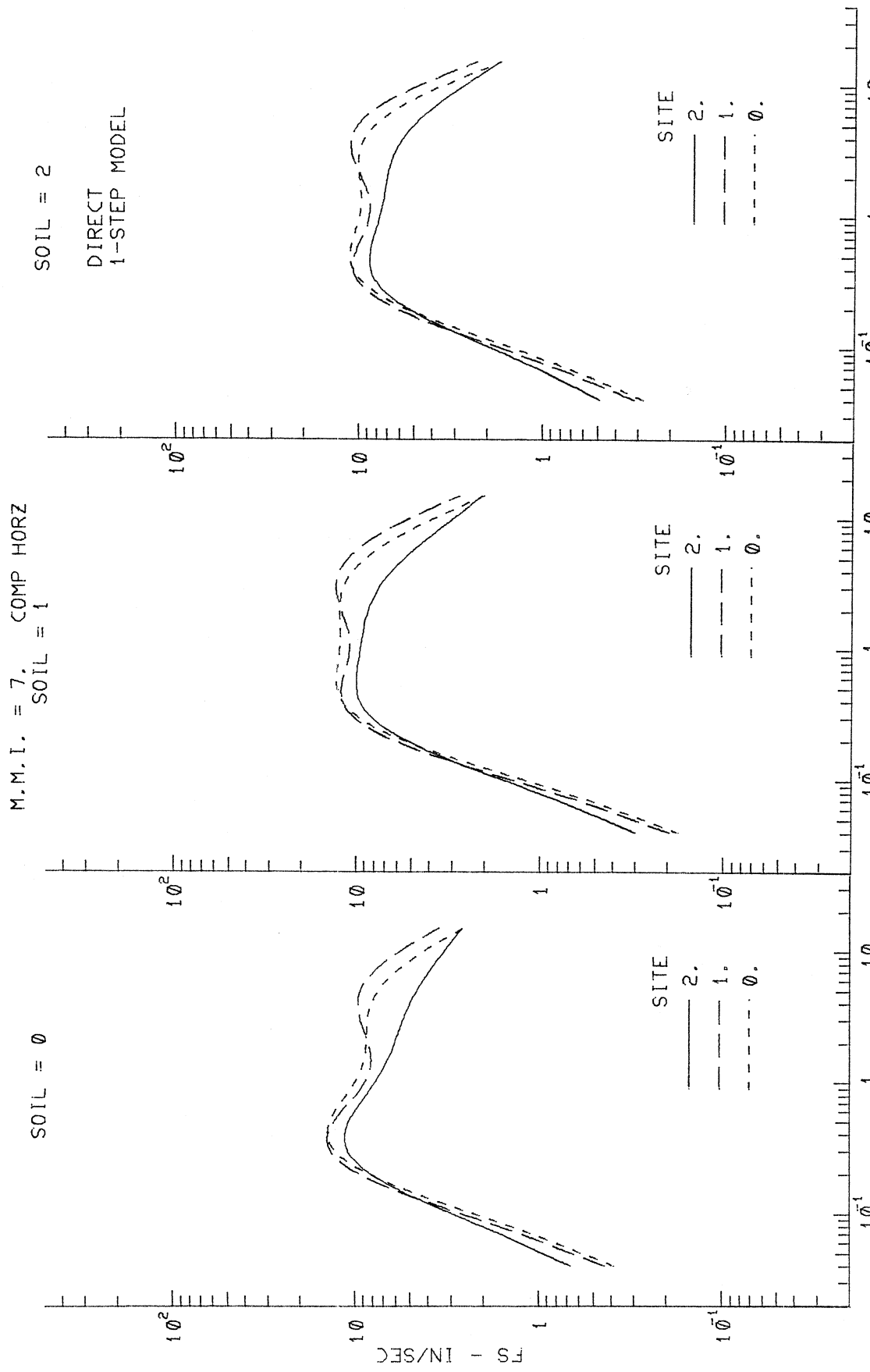
M.M.I. = 7.
COMP HORZ
SOIL = 2
DIRECT
1-STEP MODEL
SOIL = 1
SOIL = 0
SITE
2.
1.
0.
FS - IN/SEC
PERIOD - SEC

Figure IV.3.3

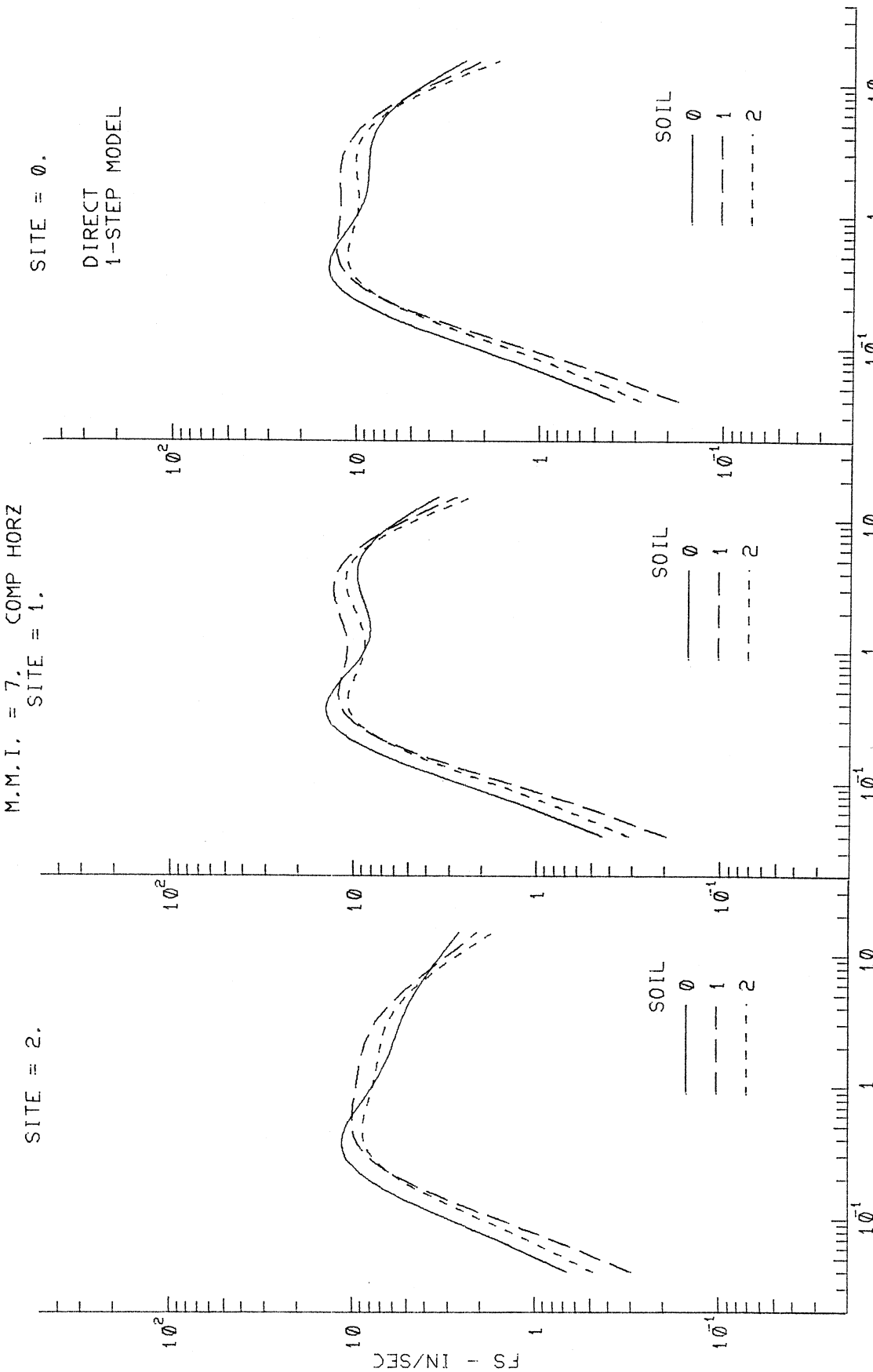
M.M.I. = 7, COMP HORZ
SITE = 2.
SITE = 1.
SITE = 0.
DIRECT
1-STEP MODEL
SOIL
0
1
2
FS - IN/SEC
PERIOD - SEC

Figure IV.3.4

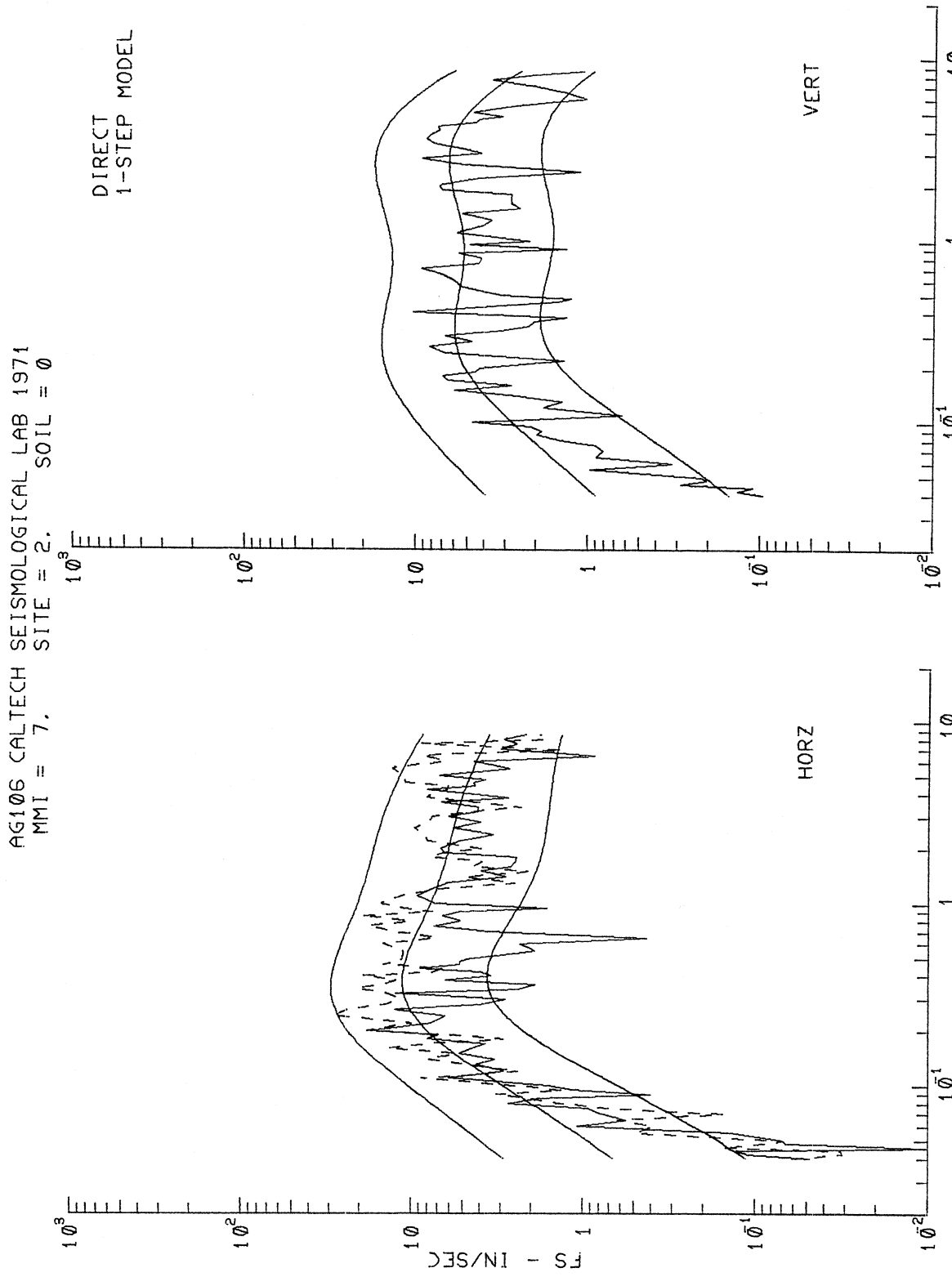
AG106 CALTECH SEISMOLOGICAL LAB 1971
MMI = 7. SITE = 2. SOIL = 0
DIRECT
1-STEP MODEL
VERT
HORZ
FS - IN/SEC
PERIOD - SEC

Figure IV.3.5

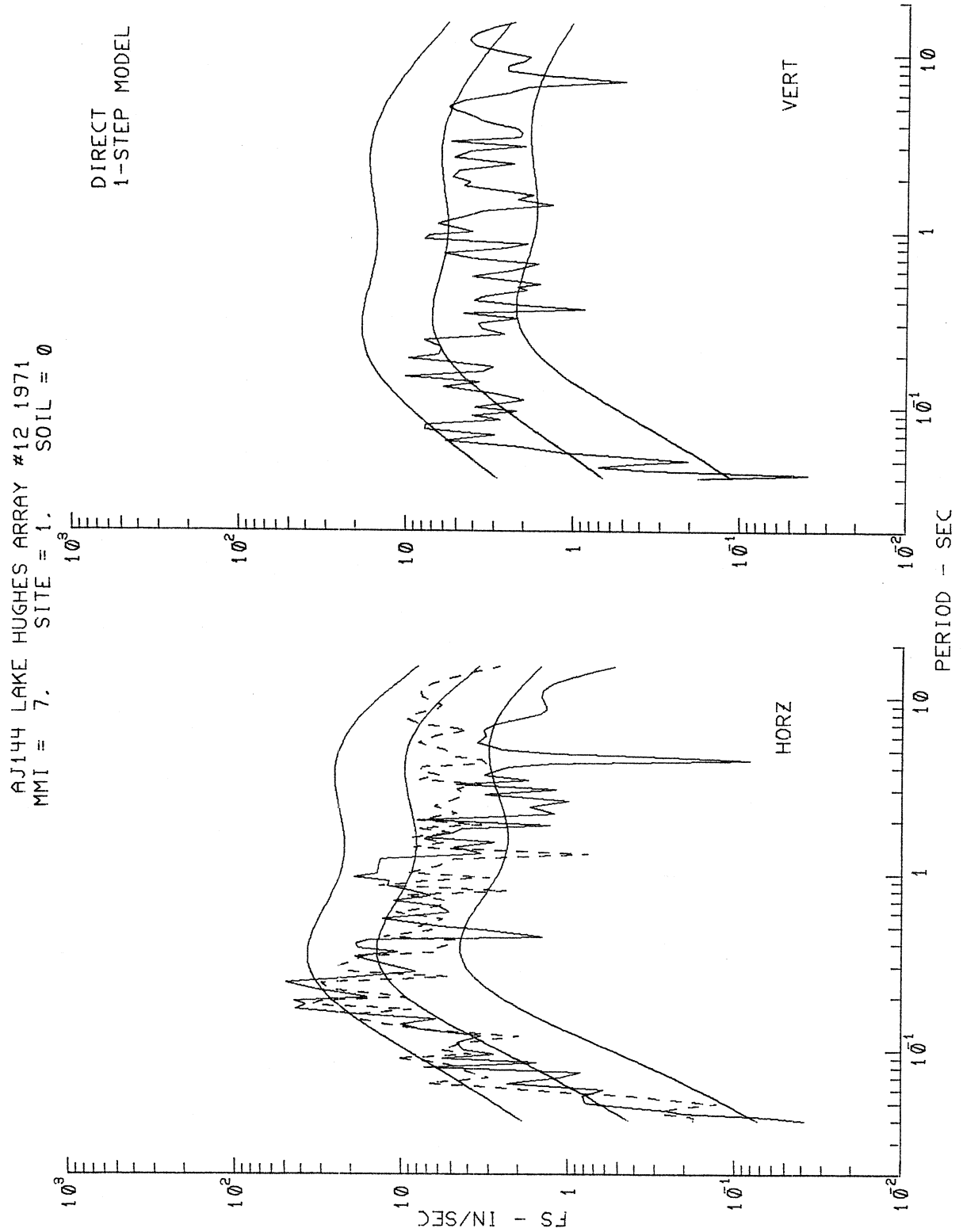
AJ144 LAKE HUGHES ARRAY #12 1971
MMI = 7. SITE = 1. SOIL = 0
DIRECT
1-STEP MODEL
HORZ
VERT
FS - IN/SEC
PERIOD - SEC

Figure IV.3.6

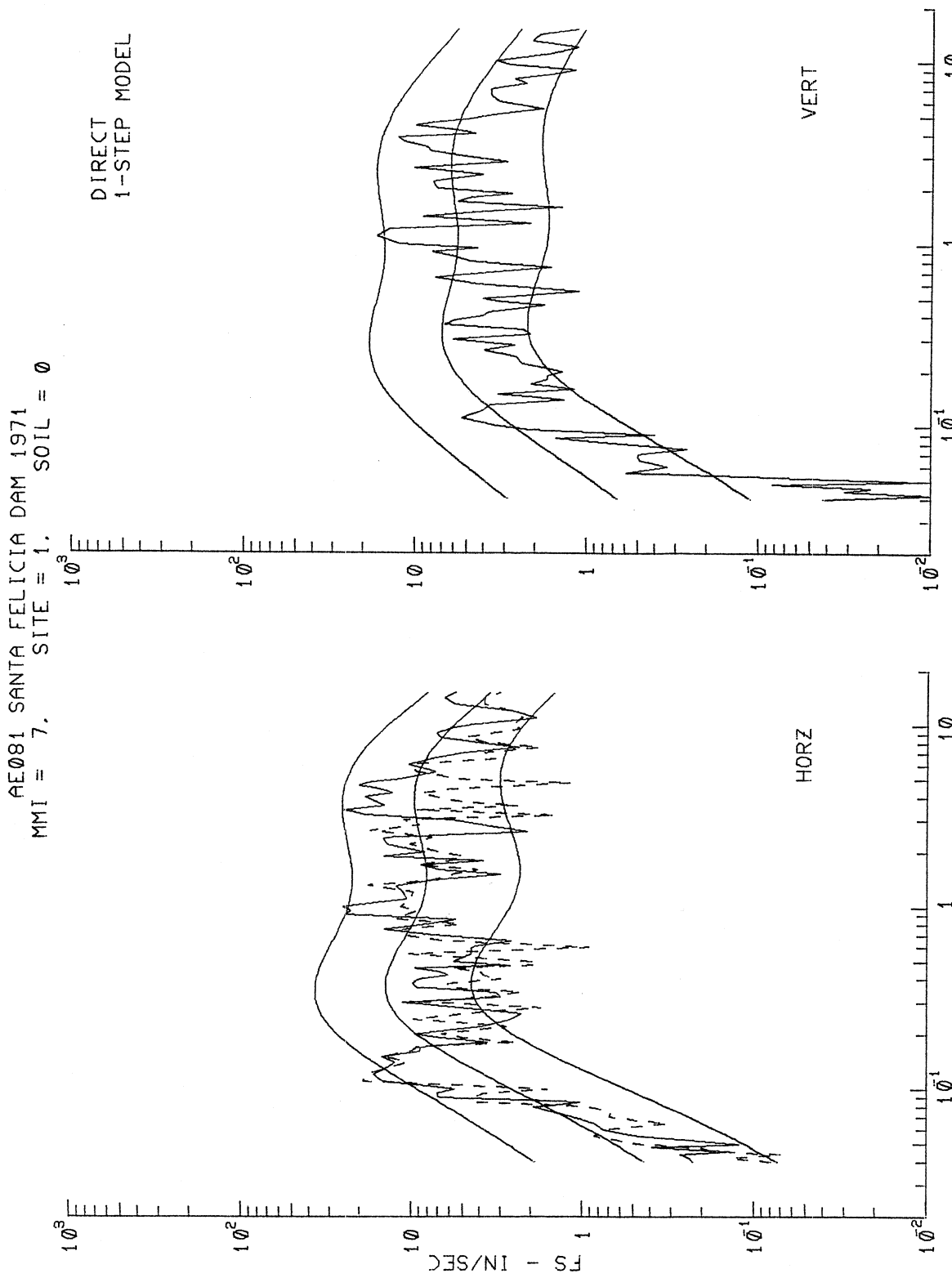
AE081 SANTA FELICIA DAM 1971
MMI = 7. SITE = 1. SOIL = 0
DIRECT
1-STEP MODEL
HORZ
VERT
FS - IN/SEC
PERIOD - SEC

Figure IV.3.7

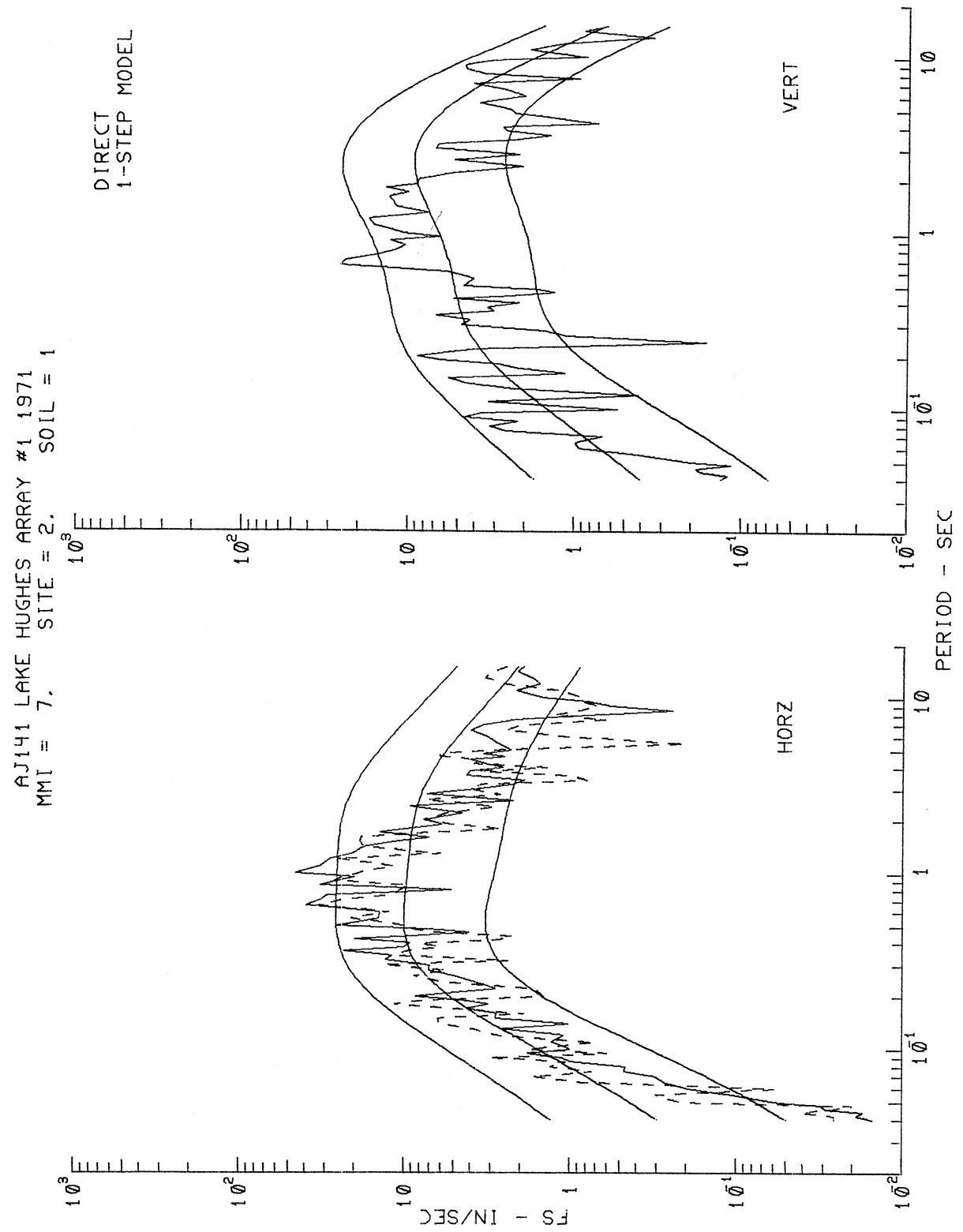
AJ141 LAKE HUGHES ARRAY #1 1971
MMI = 7. SITE = 2. SOIL = 1
DIRECT
1-STEP MODEL
HORZ
VERT
FS - IN/SEC
PERIOD - SEC

Figure IV.3.8

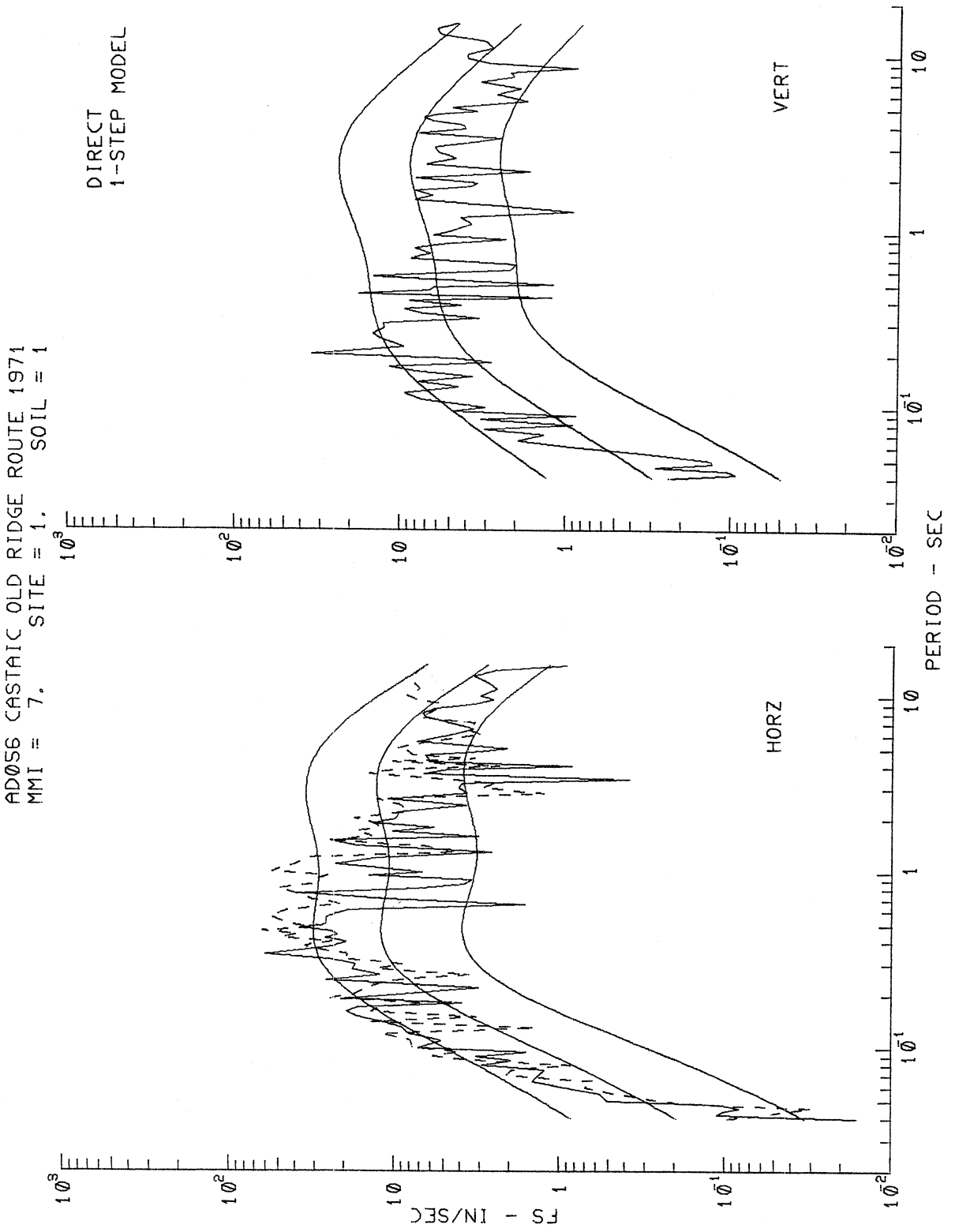
AD056 CASTAIC OLD RIDGE ROUTE 1971
MMI = 7, SITE = 1, SOIL = 1
DIRECT
1-STEP MODEL
VERT
HORZ
FS - IN/SEC
PERIOD - SEC

Figure IV.3.9

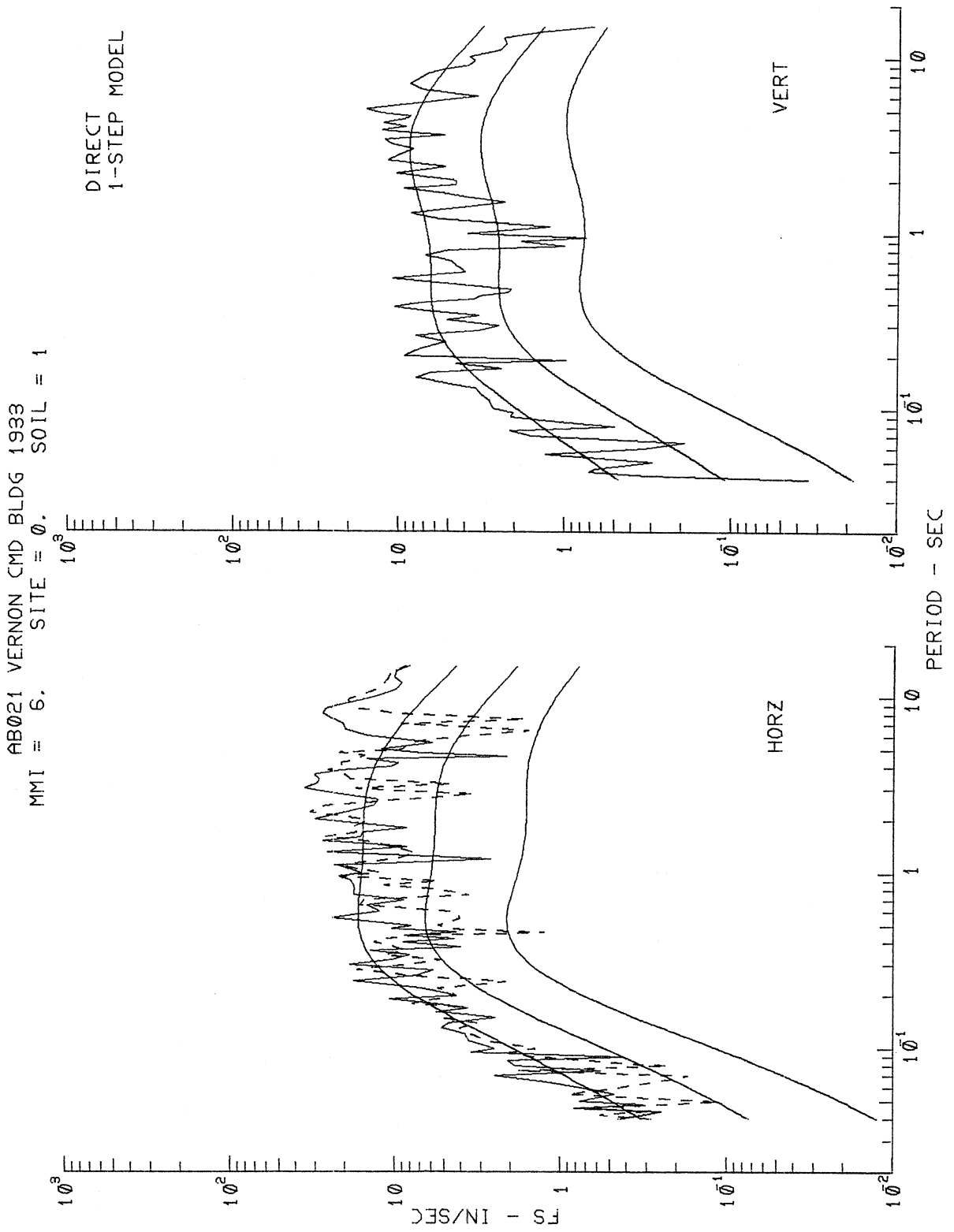

Figure IV.3.10

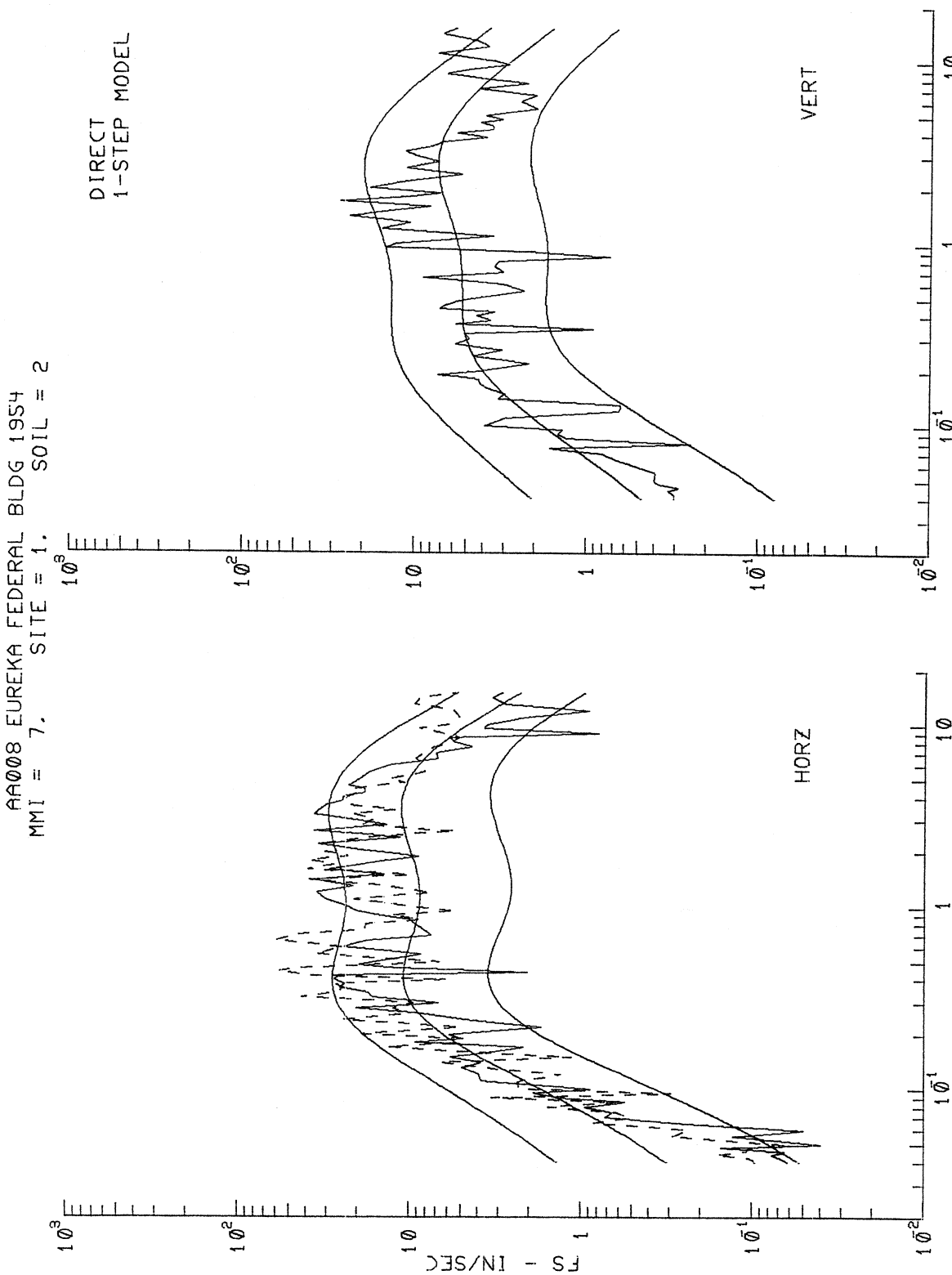

Figure IV.3.11

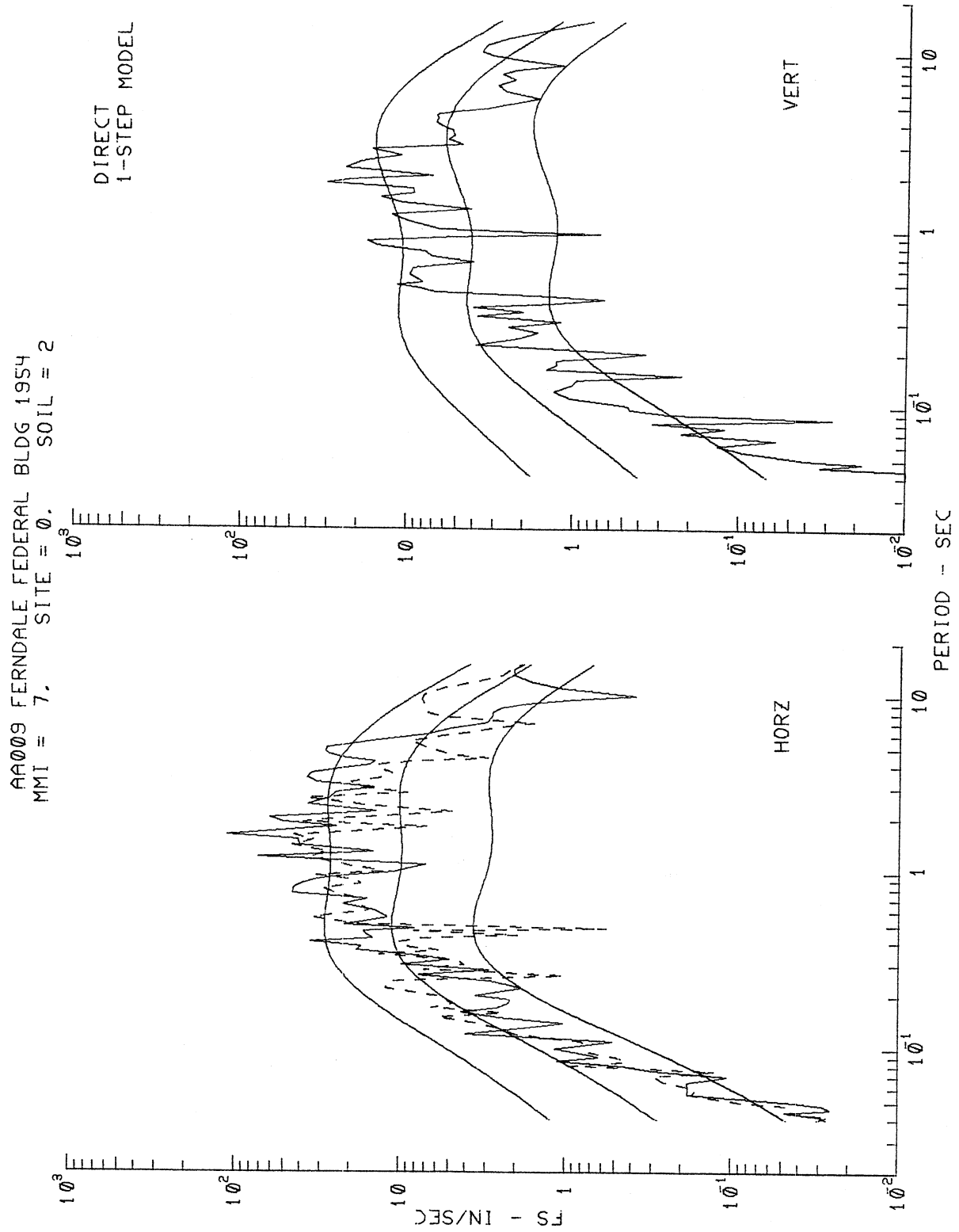

Figure IV.3.12

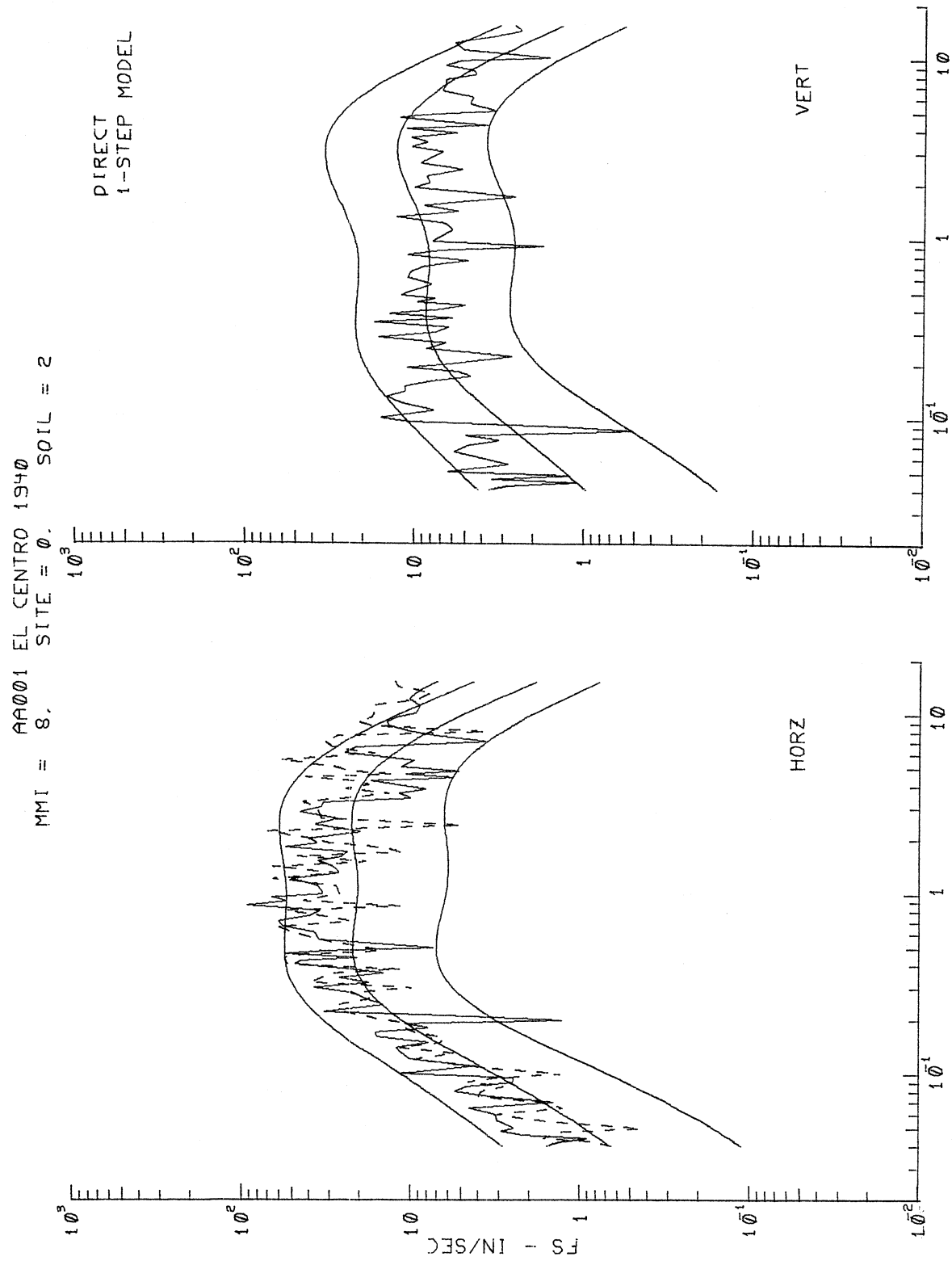

Figure IV.3.13

Figures IV.3.3 and IV.3.4 (as Figure III.3.3 and III.3.4 of Part III) compare the effects of local geologic site conditions (s) and of local soil classifications (s_L) on FS(T). Figure IV.3.3 shows that for all soil site classifications (s_L = 0, 1 or 2), the Fourier amplitudes, FS(T) are higher at alluvium sites (s = 0) than at rock sites (s = 2) for periods longer than about 0.1 sec. Figure IV.3.4 shows that the FS(T) amplitudes at local soil classification s_L = 0 are higher than those at stiff soil (s_L = 1), or deep soil (s_L = 2), for periods up to about 0.5 sec. Between about 0.5 sec. to approximately 8 sec., this trend is reversed.

Figures IV.3.5 through IV.3.13 present the nine examples of how the horizontal and vertical Fourier spectrum amplitudes computed from equation (IV.1.2) compare with the actual Fourier spectra for the corresponding components of recorded strong motion data at various sites (refer to Table II.3.1 of Part II for the description of the local geologic and soil conditions at each site). As in all three previous models of Parts I, II and III, the agreement is good.

IV.4 The Residue Two-Step Model

As in all the previous parts of this work, a residue 2-step procedure for the MMI-SITE-SOIL model will next be presented. The first step of this procedure is to scale Fourier spectra in terms of MMI, local geologic site conditions and component directions, but without considering the soil classification,

$$\log_{10}\hat{FS}(T) = \hat{b}_1(T)I_{MM} + \hat{b}_2^{(1)}(T)S^{(1)} + \hat{b}_2^{(2)}(T)S^{(2)} + \hat{b}_3(T)v + \hat{b}_4^{(1)}(T)S^{(1)}v + \hat{b}_4^{(2)}(T)S^{(2)}v + \hat{b}_5(T) \quad . \tag{IV.4.1}$$

The residues, $\varepsilon(T) = \log_{10}FS(T) - \log_{10}\hat{FS}(T)$, at each site where the local soil classification is available are next fitted by the equation

$$\varepsilon(T) = b_6^{(1)}(T)S_L^{(1)} + b_6^{(2)}(T)S_L^{(2)} + b_7(T) \quad . \tag{IV.4.2}$$

Combining equations (IV.4.1) and (IV.4.2) gives

$$\log_{10}\hat{FS}(T) = \hat{c}_1(T)I_{MM} + \hat{c}_2^{(1)}(T)S^{(1)} + \hat{c}_2^{(2)}(T)S^{(2)} + \hat{c}_3(T)v + \hat{c}_4^{(1)}(T)S^{(1)}v + \hat{c}_4^{(2)}(T)S^{(2)}v + \hat{c}_5(T) + \hat{c}_6^{(1)}(T)S_L^{(1)} + \hat{c}_6^{(2)}(T)S_L^{(2)} \quad , \tag{IV.4.3}$$

where $\hat{c}_i(T) = \hat{b}_i(T)$, except for $\hat{c}_5(T)$, with

$$\hat{c}_5(T) = \hat{b}_5(T) + \hat{b}_7(T) \quad , \tag{IV.4.4}$$

as in Section III.4 of Part III of this work. The regression analyses and the subsequent plots can now be repeated for the present MMI-SITE-SOIL model. Table IV.4.1 shows these and the figure numbers corresponding to the direct 1-step model.

TABLE IV.4.1

FIGURE NUMBERS OF THE MMI-SITE-SOIL MODEL

Figure Description	Direct 1-step Model	Residue 2-step Model
Scaling Functions	IV.2.1	IV.4.1
Residue Levels	IV.2.2	IV.4.2
Residue Statistics	IV.2.3	IV.4.3
Estimated FS	IV.3.1-IV.3.4	IV.4.4-IV.4.7
Estimated versus Actual FS	IV.3.5-IV.3.13	IV.4.8-IV.4.16

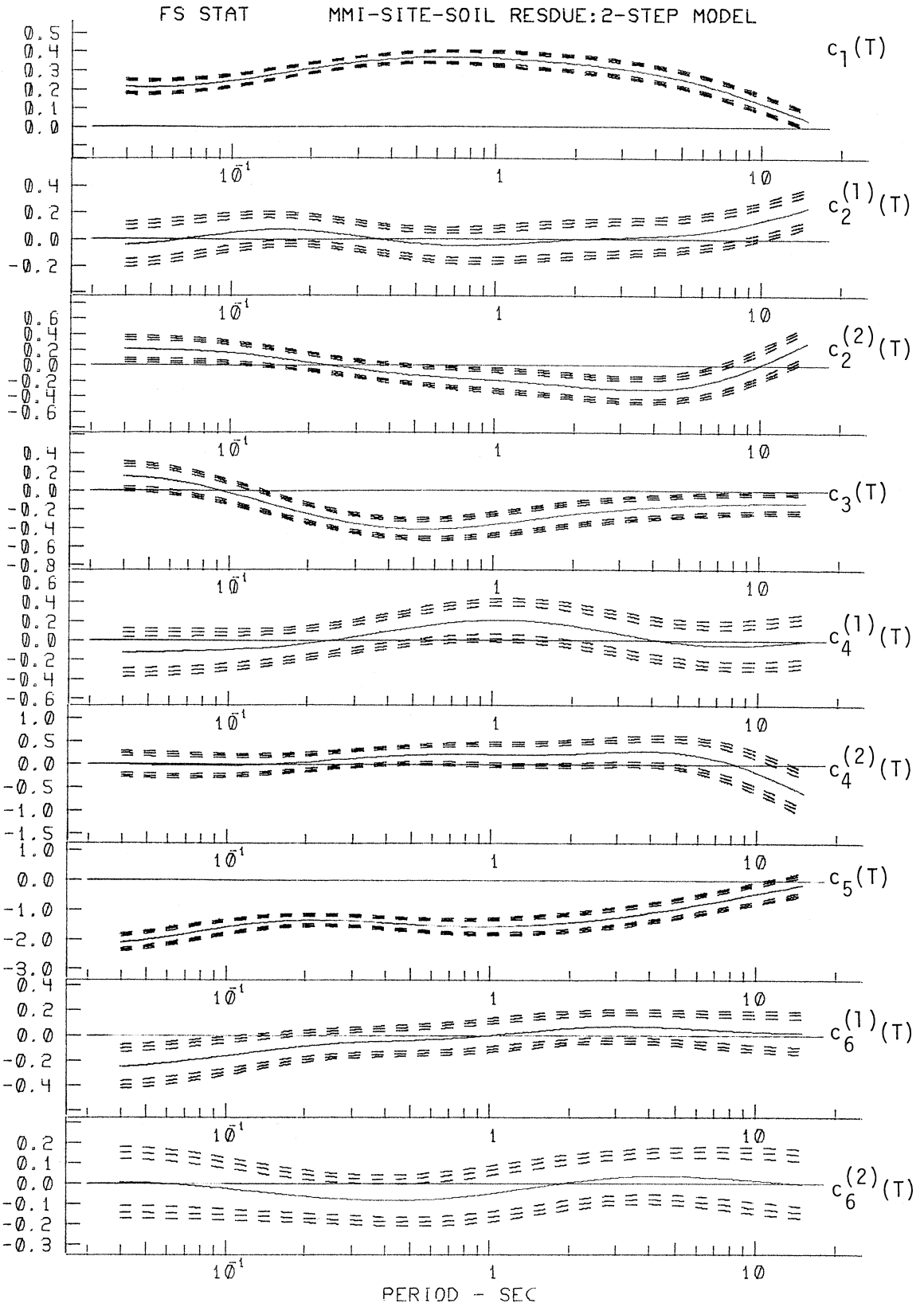
FS STAT
MMI-SITE-SOIL RESDUE:2-STEP MODEL
$c_1(T)$
$c_2^{(1)}(T)$
$c_2^{(2)}(T)$
$c_3(T)$
$c_4^{(1)}(T)$
$c_4^{(2)}(T)$
$c_5(T)$
$c_6^{(1)}(T)$
$c_6^{(2)}(T)$
PERIOD - SEC

Figure IV.4.1

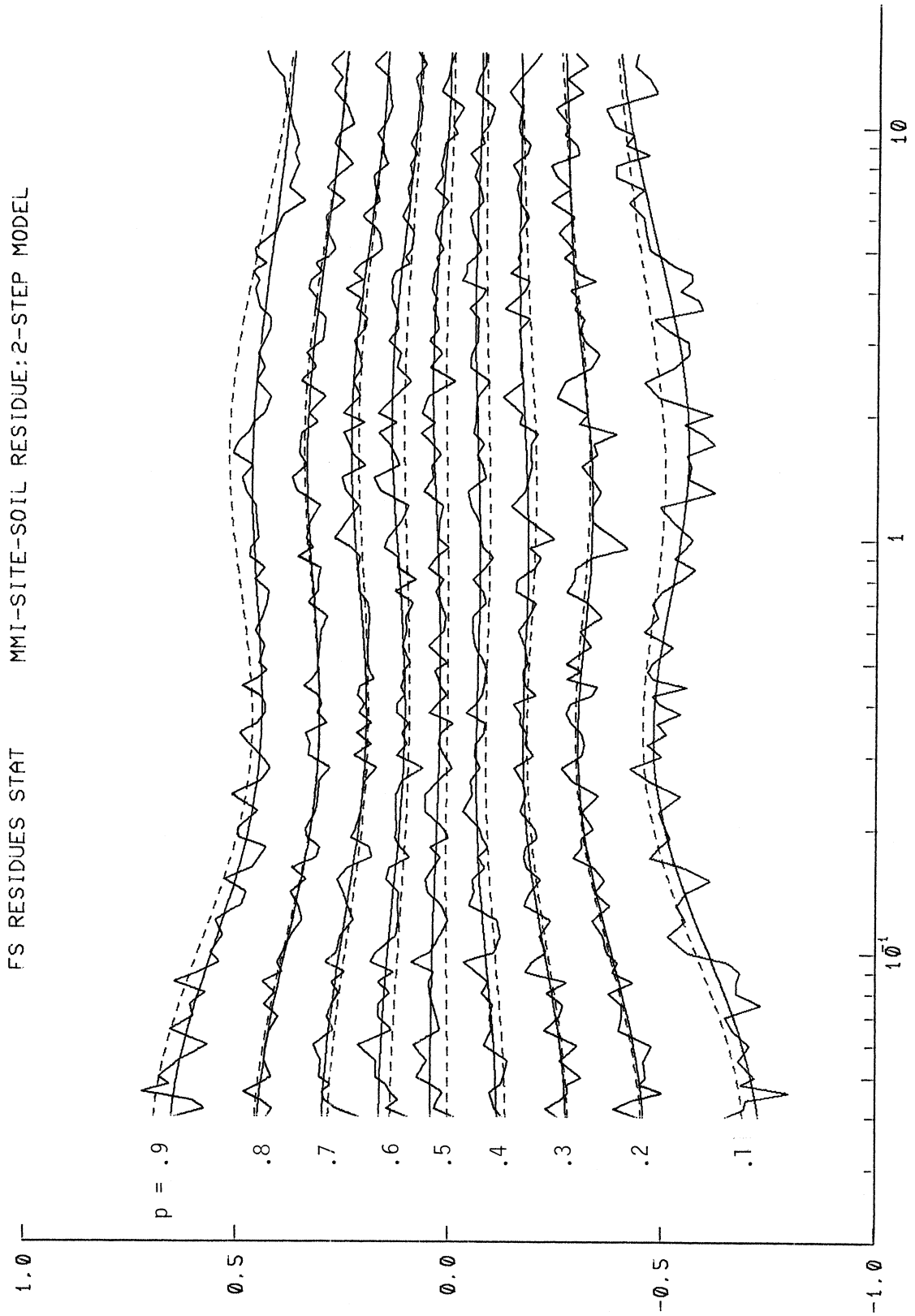
FS RESIDUES STAT
MMI-SITE-SOIL RESIDUE:2-STEP MODEL
p = .9
.8
.7
.6
.5
.4
.3
.2
.1
1.0
0.5
0.0
-0.5
-1.0
10^1
1
10

Figure IV.4.2

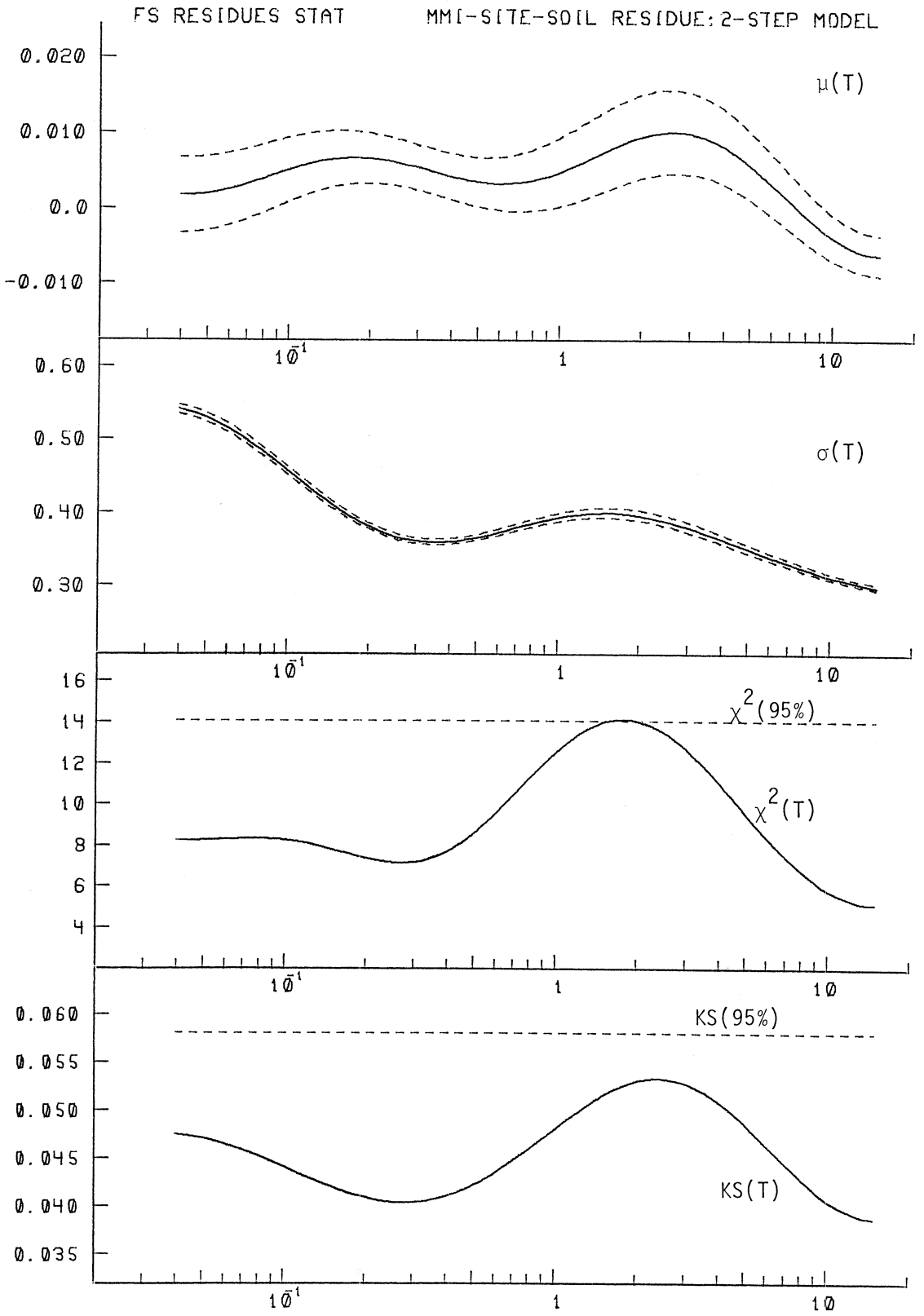
FS RESIDUES STAT
MMI-SITE-SOIL RESIDUE: 2-STEP MODEL
μ(T)
σ(T)
χ²(95%)
χ²(T)
KS(95%)
KS(T)
0.020
0.010
0.0
-0.010
0.60
0.50
0.40
0.30
16
14
12
10
8
6
4
0.060
0.055
0.050
0.045
0.040
0.035
10⁻¹
1
10

Figure IV.4.3

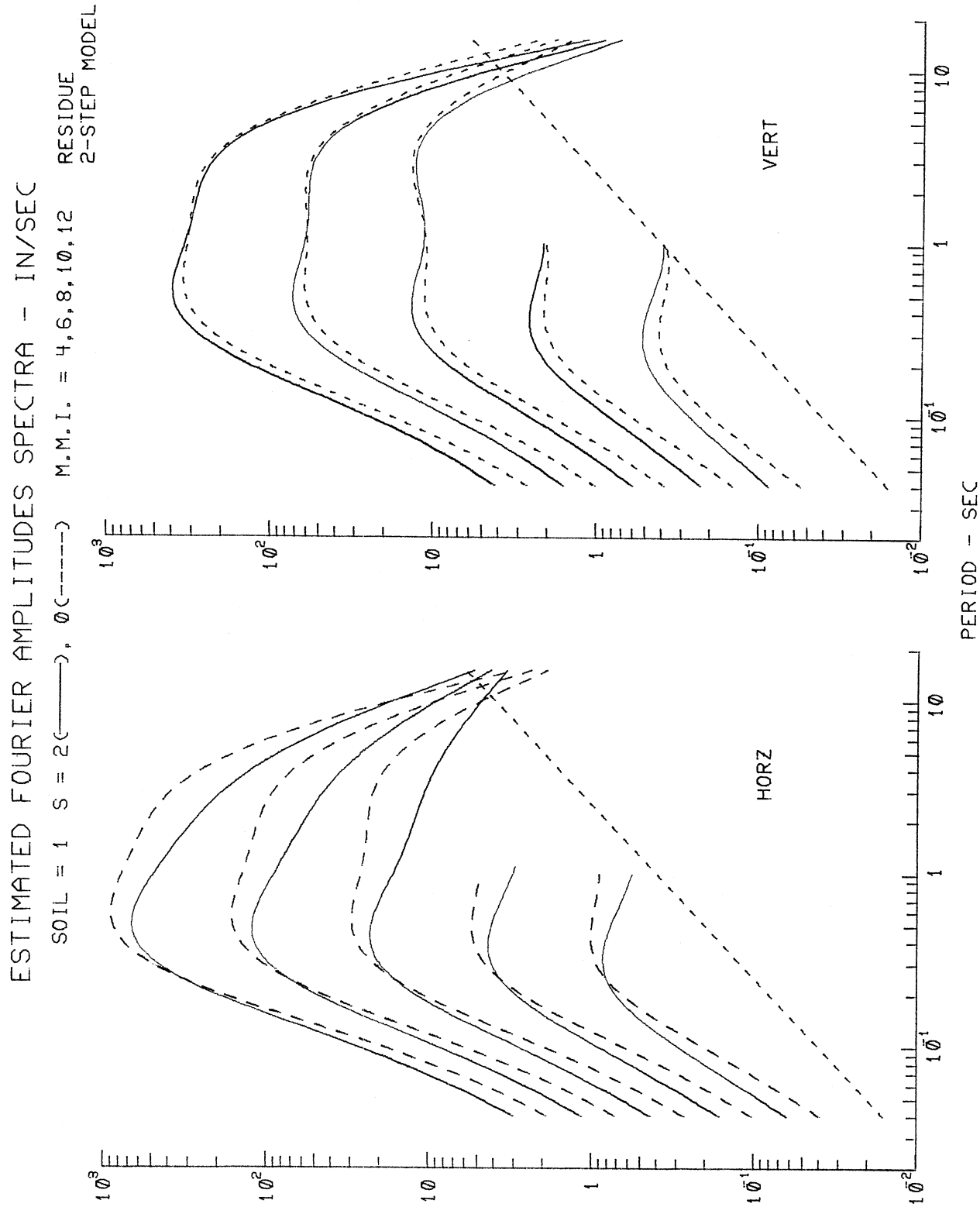
ESTIMATED FOURIER AMPLITUDES SPECTRA - IN/SEC
SOIL = 1 S = 2(———), Ø(- - - - -) M.M.I. = 4,6,8,10,12 RESIDUE
2-STEP MODEL
HORZ
VERT
PERIOD - SEC

Figure IV.4.4

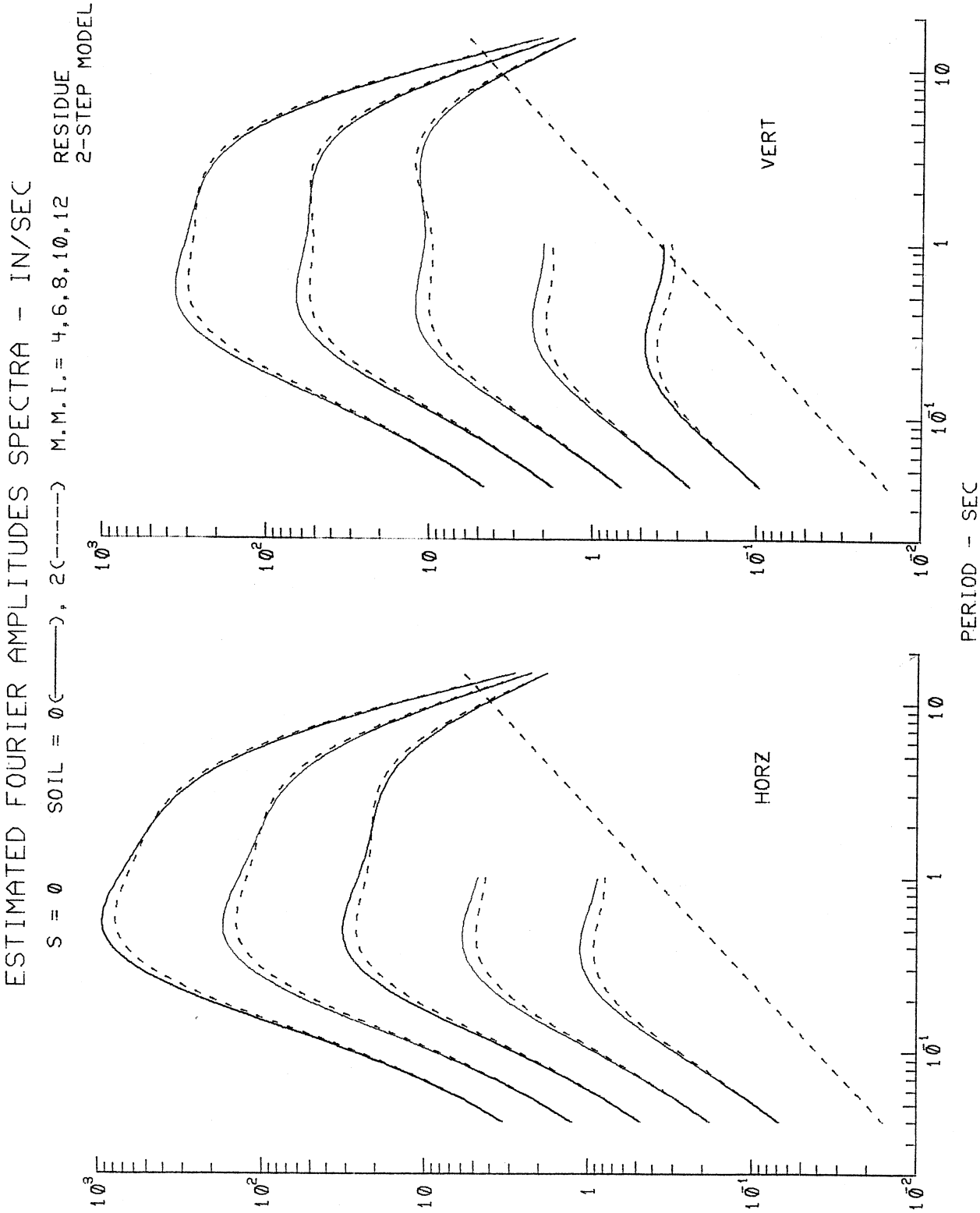
ESTIMATED FOURIER AMPLITUDES SPECTRA - IN/SEC
S = 0 SOIL = 0(———), 2(– – – –) M.M.I.= 4,6,8,10,12 RESIDUE
2-STEP MODEL
HORZ
VERT
PERIOD - SEC

Figure IV.4.5

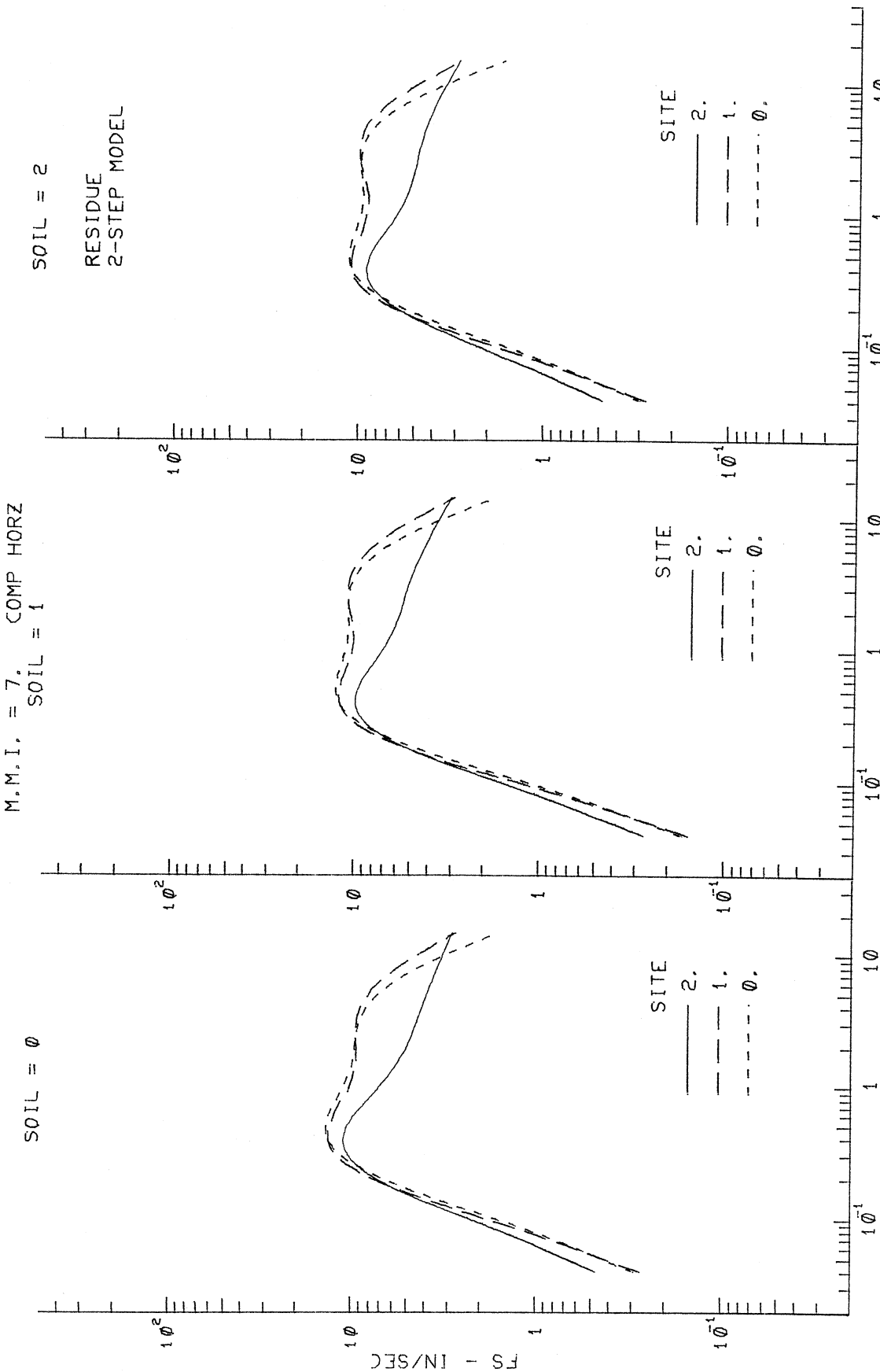
SOIL = 2
RESIDUE
2-STEP MODEL
M.M.I. = 7. COMP HORZ
SOIL = 1
SOIL = 0
SITE
2.
1.
0.
FS - IN/SEC
PERIOD - SEC
1Ø²
1Ø
1
1Ø⁻¹

Figure IV.4.6

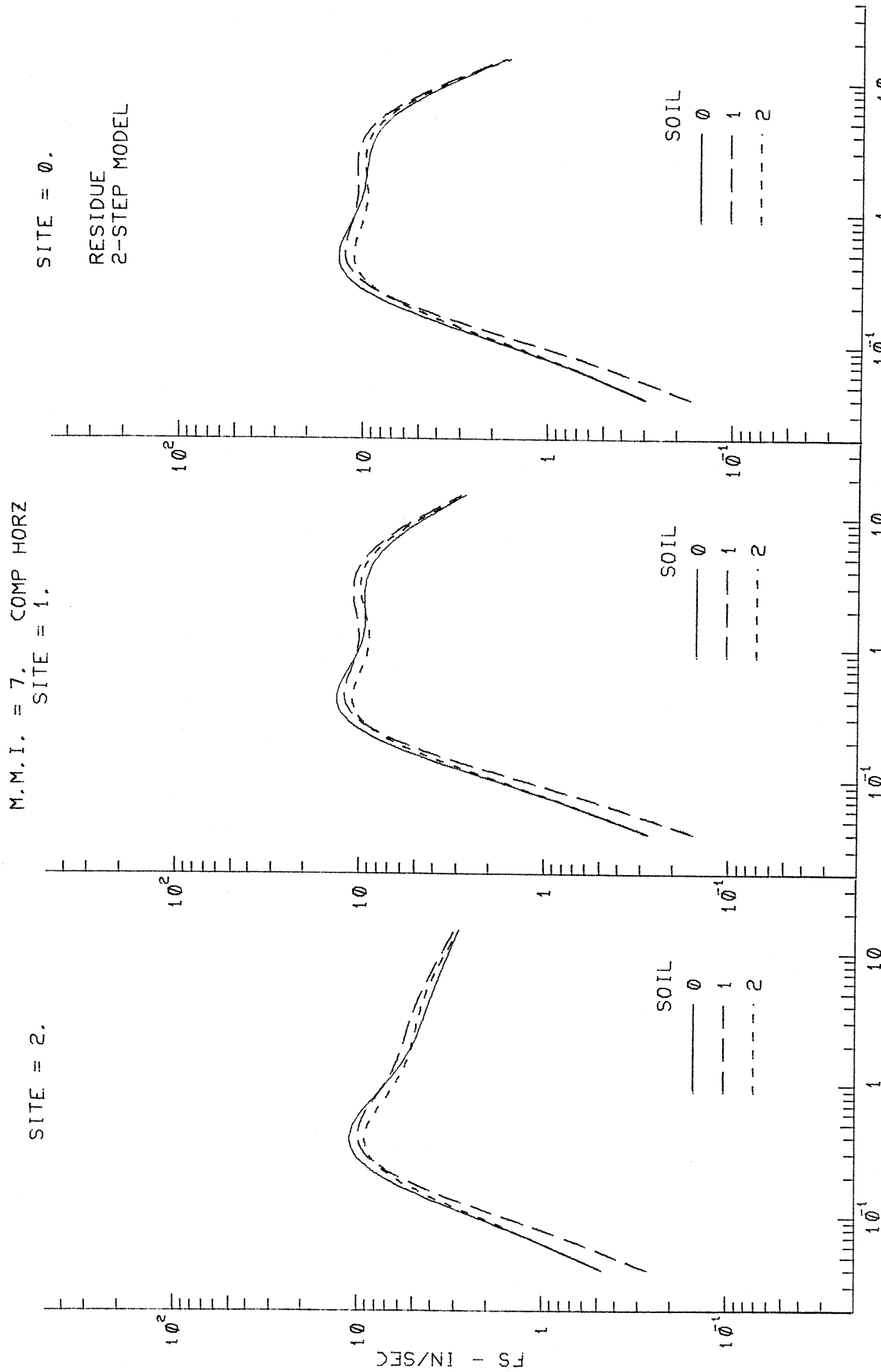
M.M.I. = 7, COMP HORZ
SITE = 2.
SITE = 1.
SITE = 0.
RESIDUE
2-STEP MODEL
SOIL
0
1
2
FS - IN/SEC
PERIOD - SEC

Figure IV.4.7

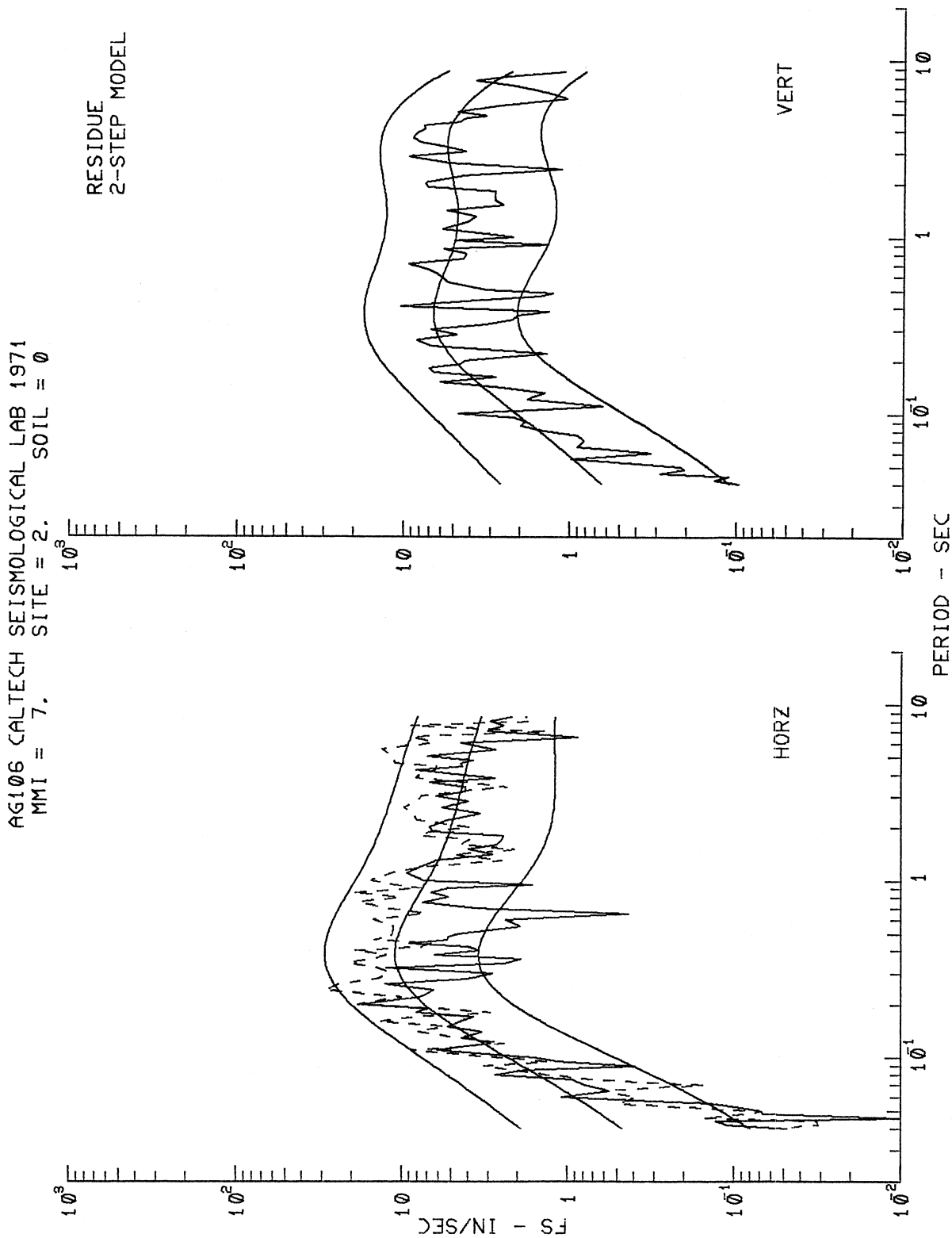
AG106 CALTECH SEISMOLOGICAL LAB 1971
MMI = 7. SITE = 2. SOIL = 0
RESIDUE
2-STEP MODEL
VERT
HORZ
FS - IN/SEC
PERIOD - SEC

Figure IV.4.8

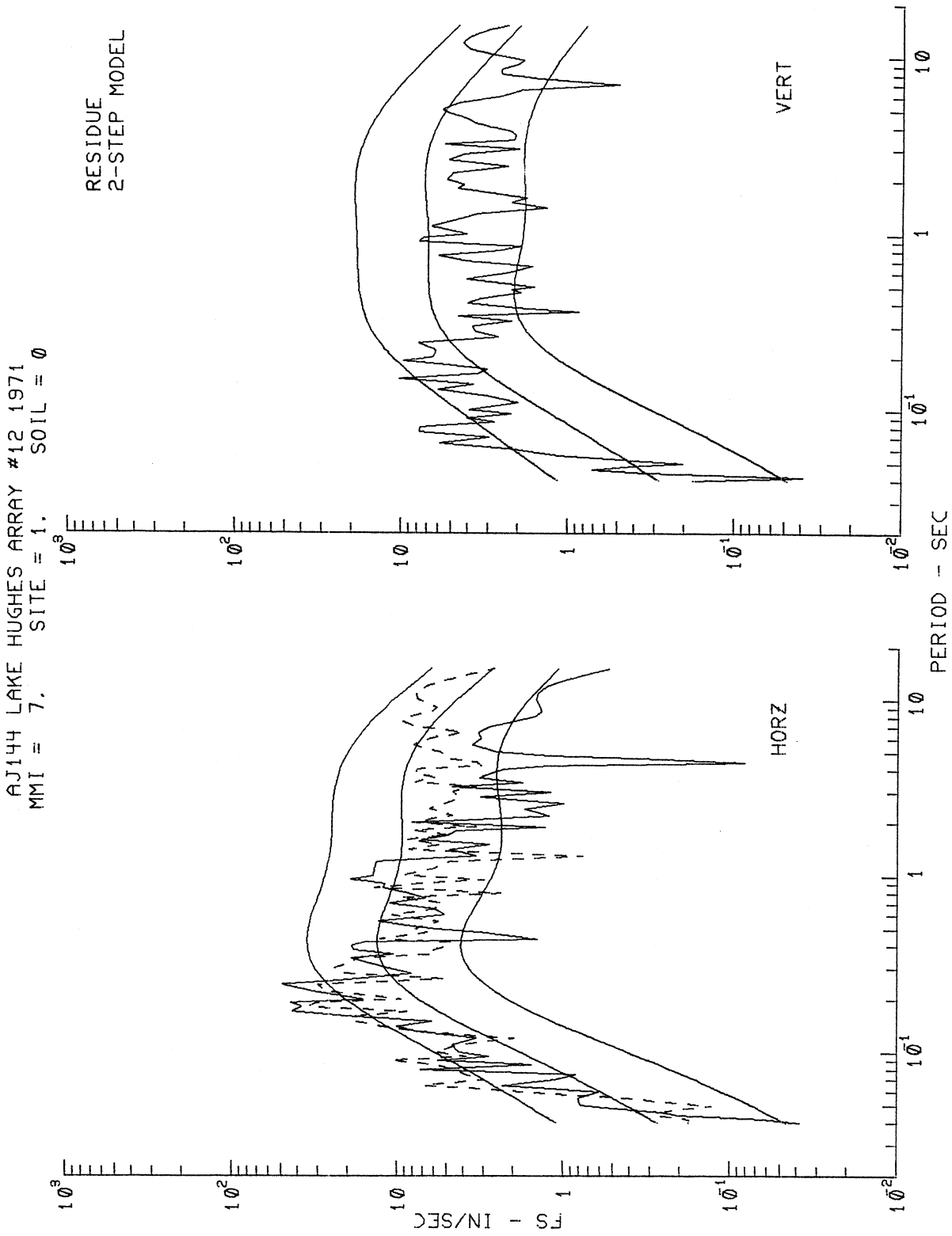
AJ144 LAKE HUGHES ARRAY #12 1971
MMI = 7. SITE = 1. SOIL = 0
RESIDUE
2-STEP MODEL
HORZ
VERT
FS - IN/SEC
PERIOD - SEC

Figure IV.4.9

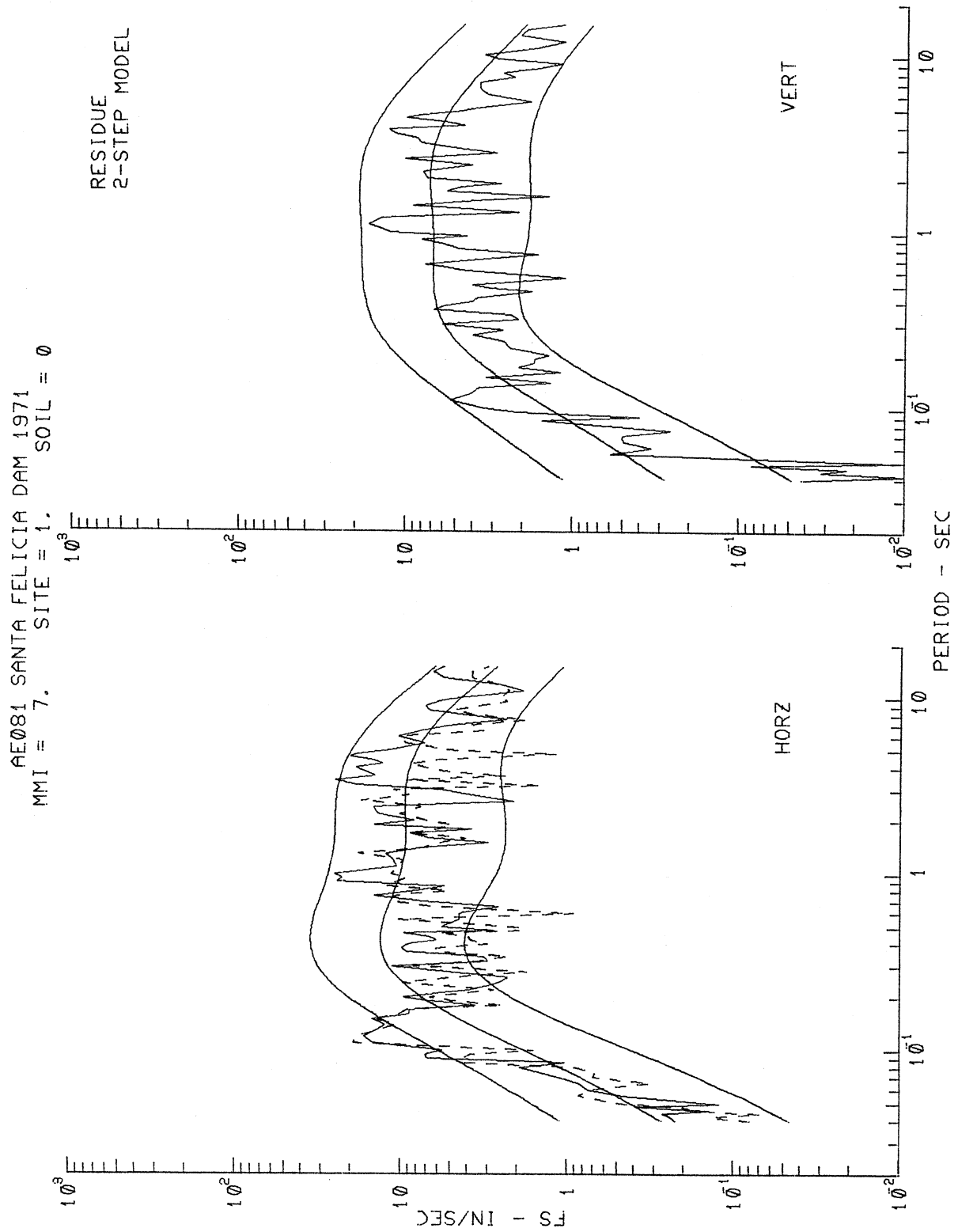

Figure IV.4.10

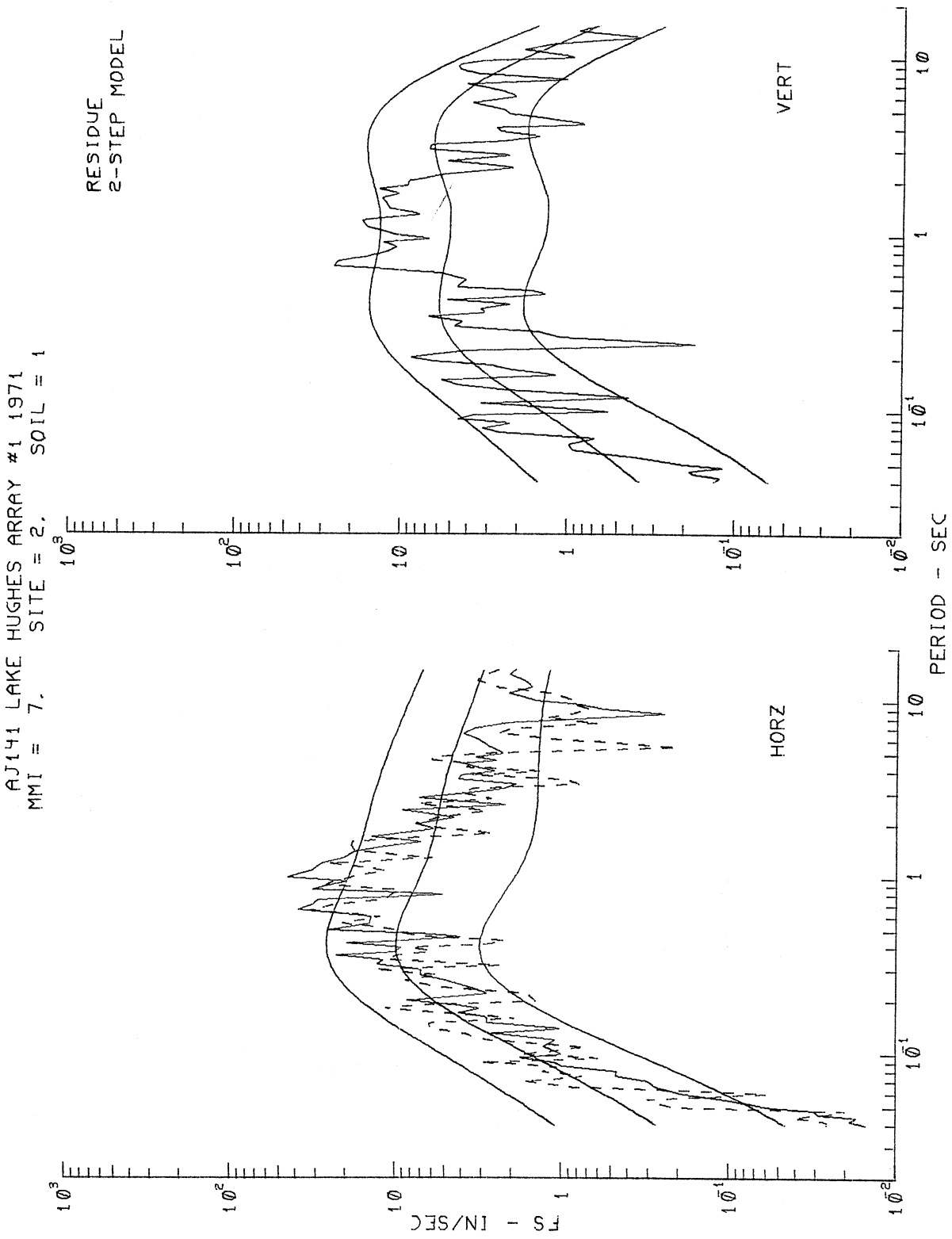

Figure IV.4.11

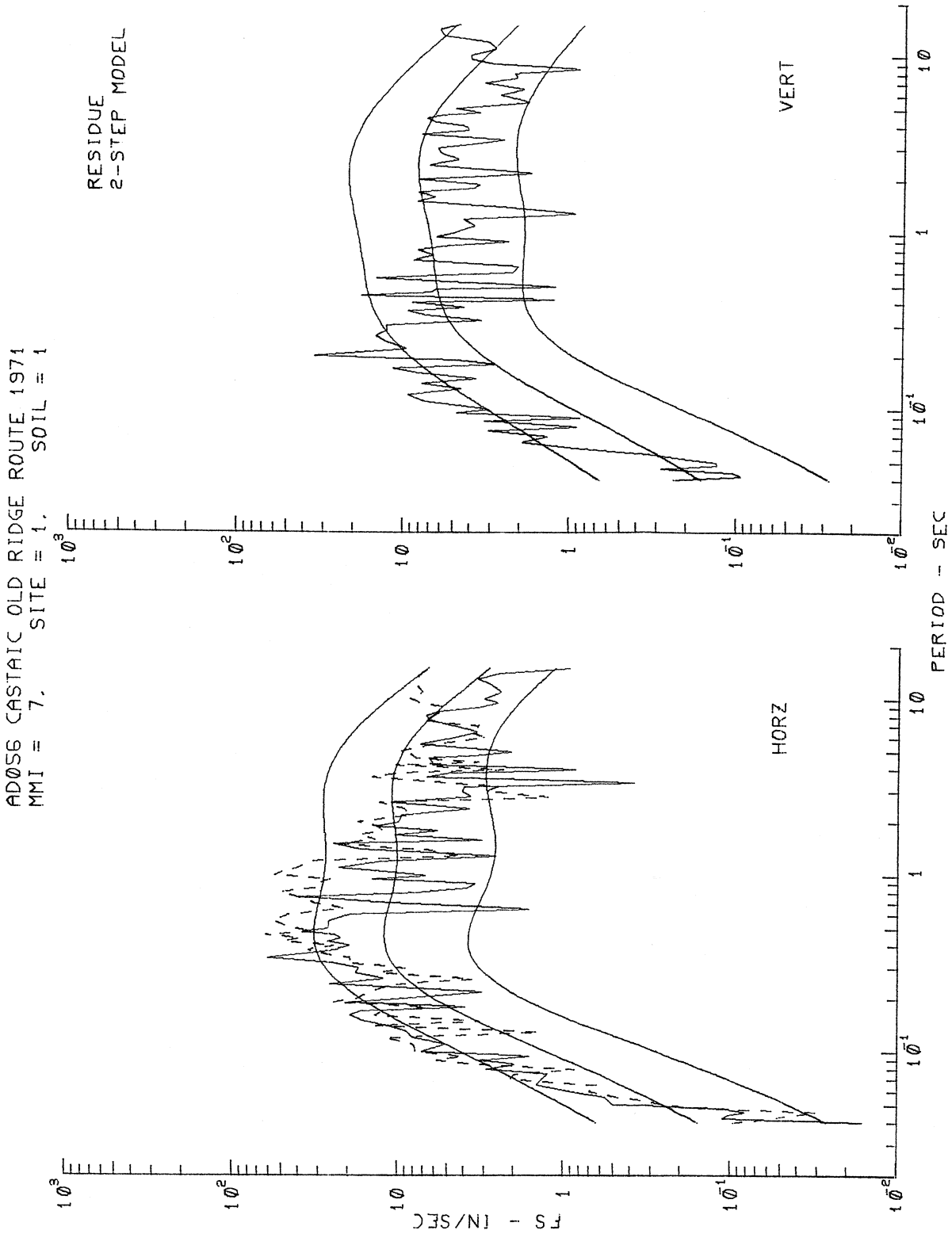

Figure IV.4.12

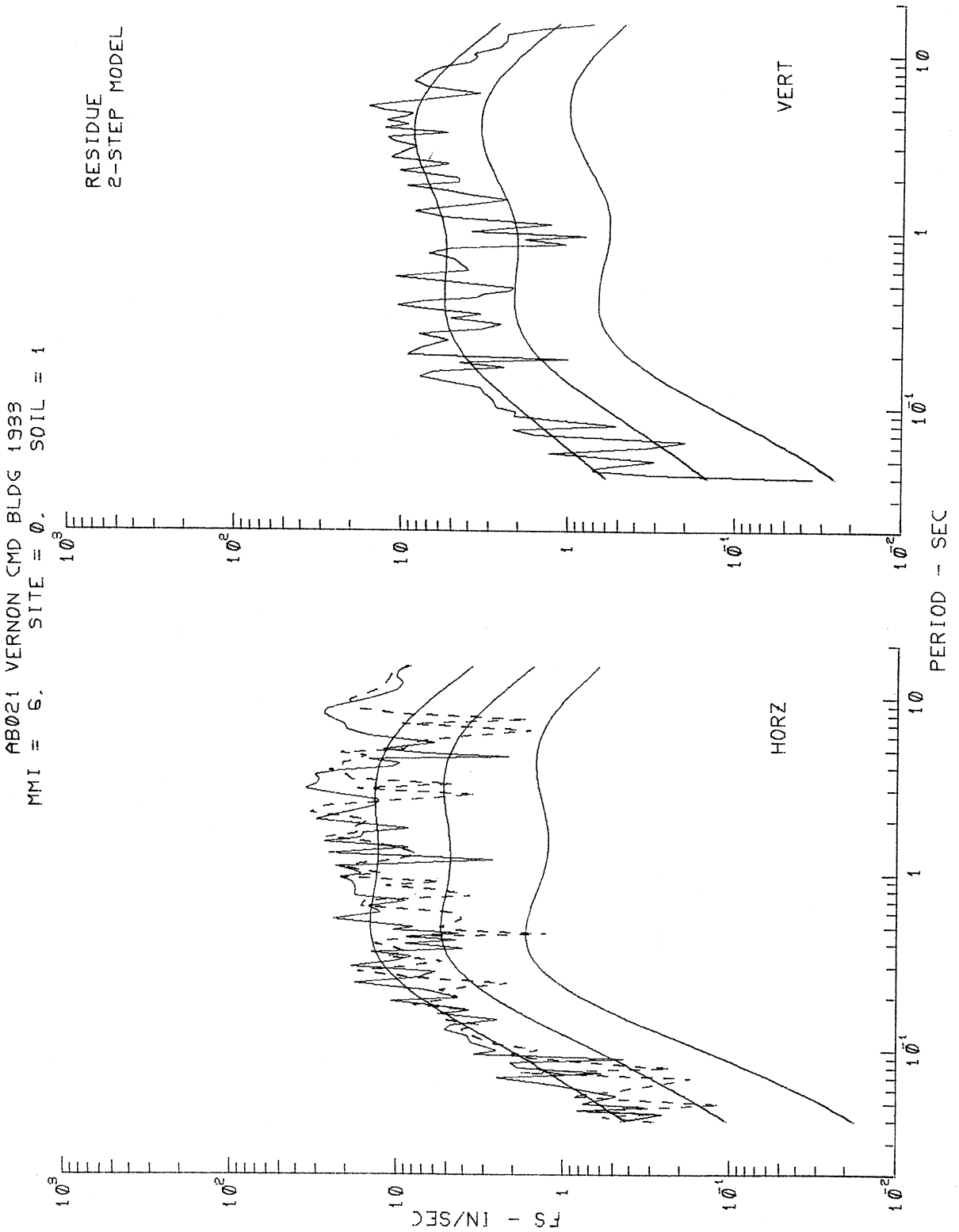

Figure IV.4.13

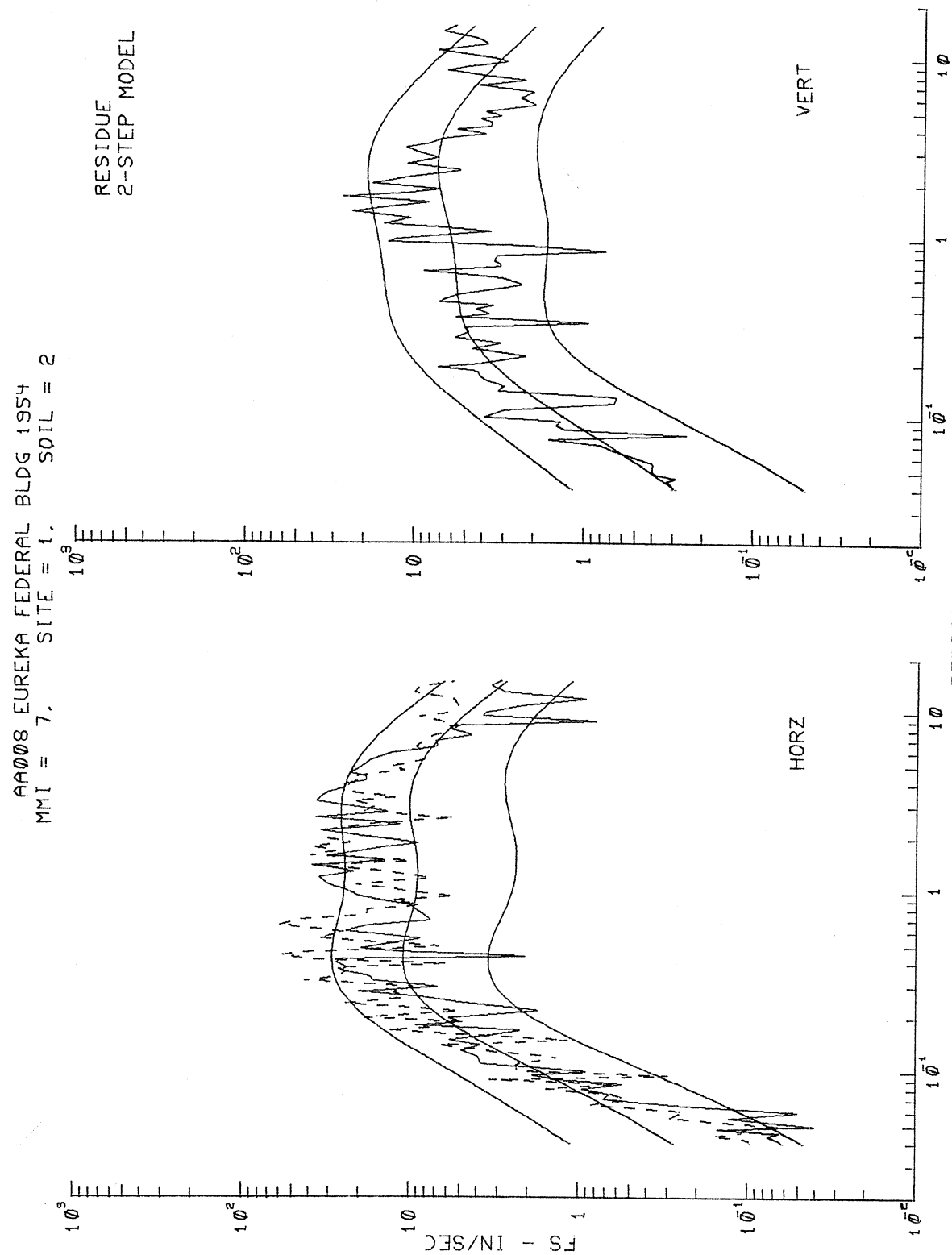

Figure IV.4.14

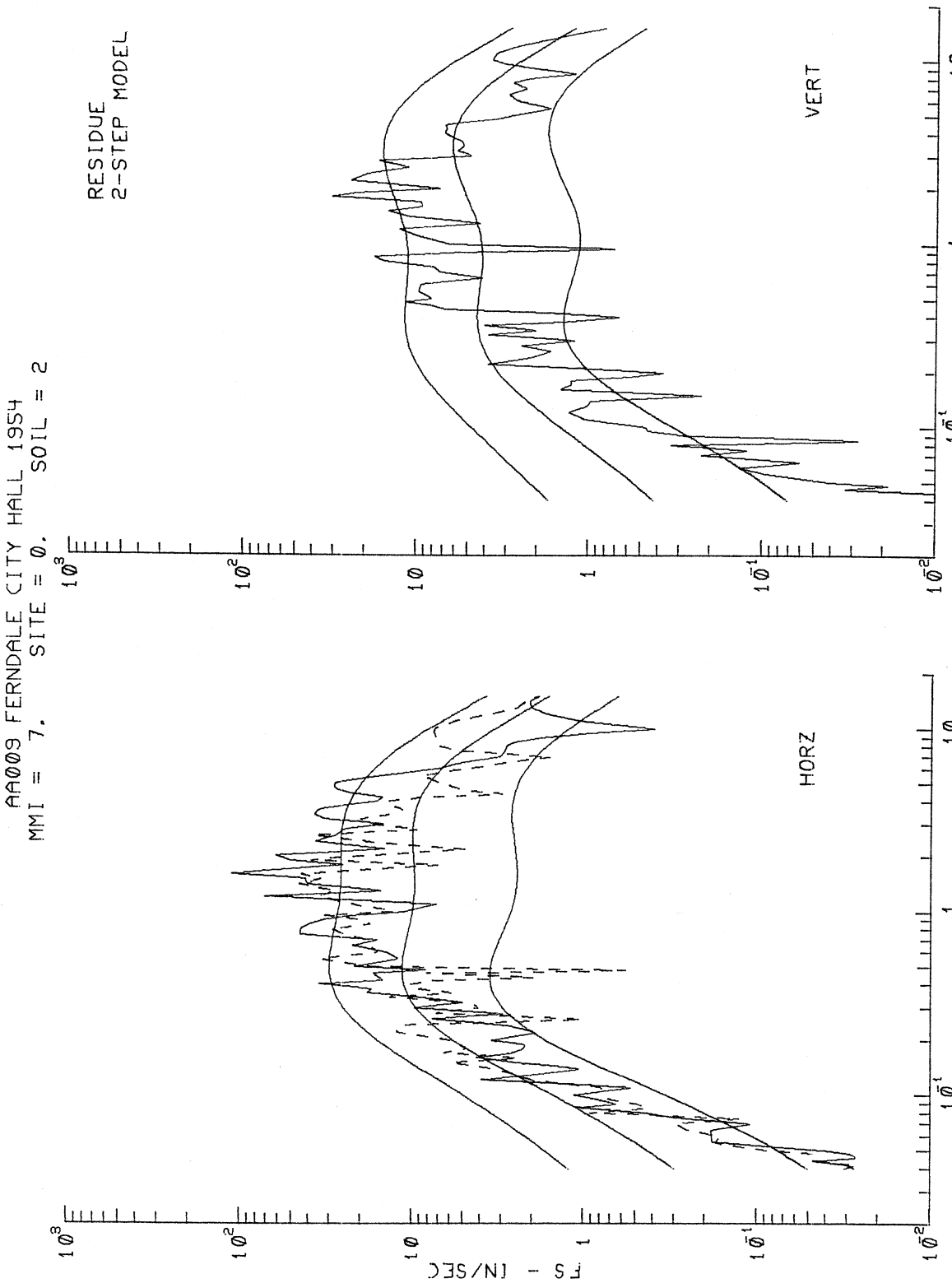

Figure IV.4.15

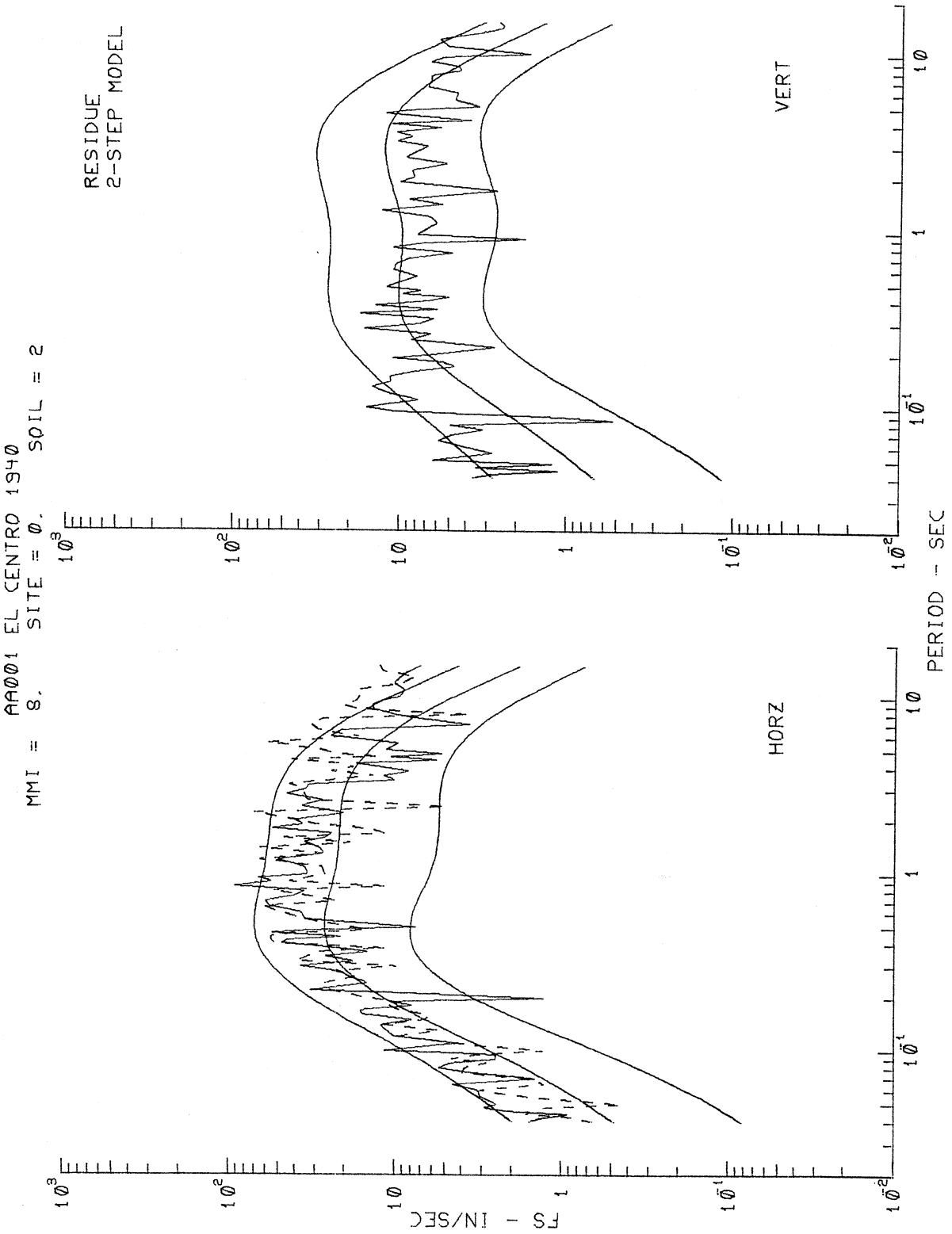

Figure IV.4.16

TABLE IV.4.2

$$\log_{10} FS(T) = c_1(T)\hat{I}_{MM} + c_2^{(1)}(T)S^{(1)} + c_2^{(2)}S^{(2)} + c_3(T)v +$$
$$c_4^{(1)}(T)S^{(1)}v + c_4^{(2)}(T)S^{(2)}v + c_5(T) + c_6^{(1)}(T)S_L^{(1)} + c_6^{(2)}(T)S_L^{(2)}$$

MMI-SITE-SOIL RESIDUES: 2-STEP MODEL

PERIOD, T(SEC)	.040	.065	.11	.19	.34	.50	.90	1.60	2.80	4.40	7.50	14.0
COEFFICIENTS:												
$c_1(T)$	.214	.218	.253	.306	.353	.368	.367	.348	.315	.272	.189	.053
$c_2^{(1)}(T)$	-.040	.001	.062	.071	.009	-.032	-.044	-.013	.012	.030	.086	.221
$c_2^{(2)}(T)$	.203	.194	.149	.053	-.068	-.129	-.186	-.244	-.308	-.304	-.150	.239
$c_3(T)$	.151	.095	-.048	-.229	-.377	-.415	-.380	-.289	-.212	-.170	-.140	-.129
$c_4^{(1)}(T)$	-.132	-.115	-.089	-.034	.062	.132	.204	.185	.085	-.003	-.051	-.011
$c_4^{(2)}(T)$	.003	-.025	-.017	.049	.160	.211	.221	.216	.268	.280	.079	-.521
$c_5(T)$	-2.095	-1.844	-1.512	-1.330	-1.386	-1.479	-1.550	-1.477	-1.273	-1.022	-.650	-.169
$c_6^{(1)}(T)$	-.247	-.211	-.149	-.087	-.050	-.037	-.006	.043	.073	.067	.043	.022
$c_6^{(2)}(T)$	.007	-.003	-.030	-.059	-.079	-.080	-.056	-.012	.027	.038	.027	.002
RESIDUES:												
p =.1	-.725	-.679	-.594	-.512	-.479	-.491	-.534	-.558	-.539	-.499	-.446	-.399
p =.2	-.457	-.428	-.373	-.320	-.302	-.311	-.332	-.330	-.307	-.288	-.276	-.267
p =.3	-.276	-.257	-.219	-.184	-.173	-.177	-.184	-.178	-.166	-.161	-.163	-.163
p =.4	-.114	-.104	-.084	-.067	-.064	-.068	-.072	-.066	-.059	-.059	-.066	-.070
p =.5	.042	.041	.036	.029	.022	.021	.028	.038	.041	.032	.016	.003
p =.6	.164	.156	.139	.119	.105	.107	.123	.137	.134	.118	.092	.074
p =.7	.297	.281	.250	.215	.196	.199	.219	.233	.224	.202	.173	.150
p =.8	.448	.422	.375	.328	.305	.308	.327	.336	.323	.301	.273	.248
p =.9	.652	.613	.542	.475	.442	.443	.459	.465	.449	.427	.398	.371
RESIDUE STATISTICS:												
$\mu(T)$	.002	.003	.006	.007	.005	.003	.004	.008	.010	.007	-.000	-.006
$\sigma(T)$	.540	.507	.445	.385	.359	.365	.389	.399	.383	.358	.327	.300
$X^2(T)$	8.249	8.324	8.205	7.450	7.332	8.588	11.953	14.112	13.065	10.434	7.118	5.188
KS(T)	.047	.046	.044	.041	.041	.042	.047	.052	.053	.050	.044	.039

Table IV.4.2 presents the scaling functions, residue levels and the residue statistics at 12 discrete periods for the 2-step model, similar to Table IV.2.1 for the 1-step model.

This completes the presentation of Part IV of the scaling of FS(T) in terms of M.M.I., s, s_L and v.

PART V: SCALING OF FOURIER SPECTRA IN TERMS OF THE LOCAL SOIL CLASSIFICATION ONLY

V.1 The Scaling Equation: Magnitude, Distance and Soil Classification

The first two parts of this work have presented the scaling of Fourier amplitude spectra in terms of magnitude, source-to-station representative distance, local geological site characterization, local soil site classification and for horizontal and vertical component directions. In the subsequent two parts (Parts III and IV) we replaced the magnitude and the source-to-station distance by the local M.M.I., but kept both the geological characterization and the local soil classification in the scaling. This part of the analysis deals with the following question: What will happen to the scaling of Fourier amplitude spectra if the local site is characterized only by the local soil classification and no geological characterization is to be included? Seed et al. (1976) carried out such a study for the scaling of response spectra, using only the local soil classification. Subsequently, other analyses have been carried out along the similar lines. With a larger database now available, it is interesting to see how different such scaling will be if compared with other results in the previous parts of this work. The scaling equation now becomes:

$$\log_{10} FS(T) = M + \mathcal{A}tt(\Delta, M, T) + b_1(T)M + b_3(T)v + b_5(T) + b_6(T)M^2 + b_7^{(1)}(T)S_L^{(1)} + b_7^{(2)}(T)S_L^{(2)} \quad . \qquad (V.1.1)$$

Here the equation is in the same form as equation (I.3.1) except that the $b_2(T)$ term for h and $b_4(T)$ term for hv are dropped. The scaling functions $b_1(T)$, $b_3(T)$, $b_5(T)$, $b_6(T)$, $b_7^{(1)}(T)$ and $b_7^{(2)}(T)$ are determined through the regression analysis of the same database as in the previous parts of this work. The computed scaling functions at each period T from linear regression will be denoted by $\hat{b}_1(T)$ through $\hat{b}_7^{(2)}(T)$, respectively.

Substituting the fitted coefficients in equation (V.1.1) gives $\hat{FS}(T)$, the estimated spectral amplitudes, where

$$\begin{aligned}\log_{10}\hat{FS}(T) &= M + \mathcal{A}tt(\Delta,M,T) \\ &+ \hat{b}_1(T)M + \hat{b}_3(T)v + \hat{b}_5(T) + \hat{b}_6(T)M^2 \\ &+ \hat{b}_7^{(1)}(T)S_L^{(1)} + \hat{b}_7^{(2)}S_L^{(2)} \quad . \end{aligned} \tag{V.1.2}$$

As in Parts I and II of this work, equation (V.1.2) applies only in the range $M_{min} \leq M \leq M_{max}$, where for each period T:

$$\begin{aligned} M_{min}(T) &= -\hat{b}_1(T)/(2\hat{b}_6(T)) \quad , \text{ and} \\ M_{max}(T) &= -(1+\hat{b}_1(T))/(2\hat{b}_6(T)) \quad , \end{aligned} \tag{V.1.3}$$

and equation (V.1.2) is then modified to:

$$\begin{aligned}\log_{10}\hat{FS}(T) &= M_< + \mathcal{A}tt(\Delta,M,T) \\ &+ \hat{b}_1(T)M_{<>} + \hat{b}_3(T)v + \hat{b}_5(T) + \hat{b}_6(T)M_{<>}^2 \\ &+ \hat{b}_7^{(1)}(T)S_L^{(1)} + \hat{b}_7^{(2)}(T)S_L^{(2)} \quad , \end{aligned} \tag{V.1.4}$$

with

$$M_{<} = \min(M, M_{max})$$

$$M_{<>} = \max(M_{min}, M_{<}) \quad . \qquad \text{(V.1.5)}$$

V.2 The Regression Coefficients

Figure V.2.1 shows the smoothed coefficients $\hat{b}_1(T)$, $\hat{b}_3(T)$, $\hat{b}_5(T)$, $\hat{b}_6(T)$, $\hat{b}_7^{(1)}(T)$ and $\hat{b}_7^{(2)}(T)$ (solid lines) together with the estimates of their 80%, 90% and 95% confidence intervals (dashed lines). It is interesting to compare this figure with the corresponding Figure I.5.1 in Part I for the MAG-DEPTH-SOIL model where the local site geological condition in terms of the local alluvium depth is included in the regression analysis. The comparison shows that the scaling functions $\hat{b}_1(T)$, $\hat{b}_3(T)$, $\hat{b}_5(T)$ and $\hat{b}_6(T)$ corresponding respectively to the parameters M, v, 1 and M^2 are similar both in shape and in amplitudes on both figures. The scaling functions $\hat{b}_7^{(1)}(T)$ and $\hat{b}_7^{(2)}(T)$ for the soil parameter $S_L^{(1)}$ ($s_L = 1$) and $S_L^{(2)}$ ($s_L = 2$) are only similar in shape but exhibit differences in amplitude. The scaling function $\hat{b}_7^{(2)}(T)$ for $S_L^{(2)}$ in Figure I.5.1 of the MAG-DEPTH-SOIL model in Part I has amplitudes around -0.25 for periods less than 0.1 sec. Beyond 0.35 sec., it is positive but is not higher than about 0.15 in the period range 0.35 to 3 sec. On the other hand, the scaling function $\hat{b}_7^{(2)}$ for $S_L^{(2)}$ in the present model (Figure V.2.1) has amplitudes close to -0.1 for periods less than 0.1 sec. Beyond 0.3 sec. it turns positive and has amplitudes as high as 0.3 around period T = 5 sec. Comparison of the scaling functions $\hat{b}_7^{(1)}(T)$ leads to similar observations.

The residues $\varepsilon(T) = \log_{10}FS(T) - \log_{10}\hat{FS}(T)$ describing the distribution of the recorded FS(T) about the estimated $\hat{FS}(T)$ are next calculated. Figure V.2.2 shows the plot of the residue levels corresponding to $p^*(\varepsilon,T) = 0.1$ through 0.9 for $\log_{10}FS(T)$. Refer to the same Figure I.5.2 in Part I for a complete description of each of the nine sets of curves. As in the previous parts, $\varepsilon(T)$ can be described by a normal

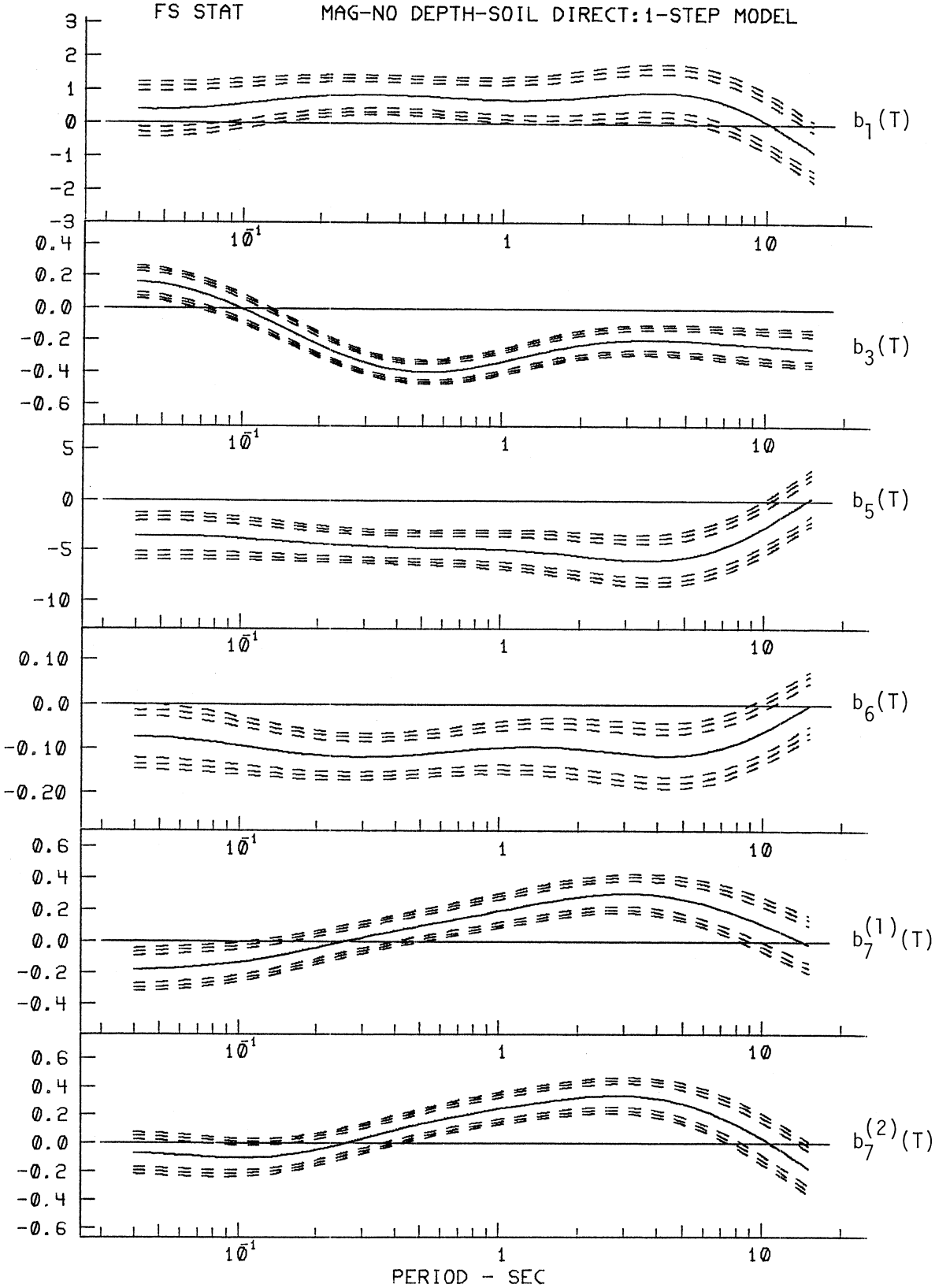
FS STAT
MAG-NO DEPTH-SOIL DIRECT:1-STEP MODEL
b1(T)
b3(T)
b5(T)
b6(T)
b7(1)(T)
b7(2)(T)
PERIOD - SEC

Figure V.2.1

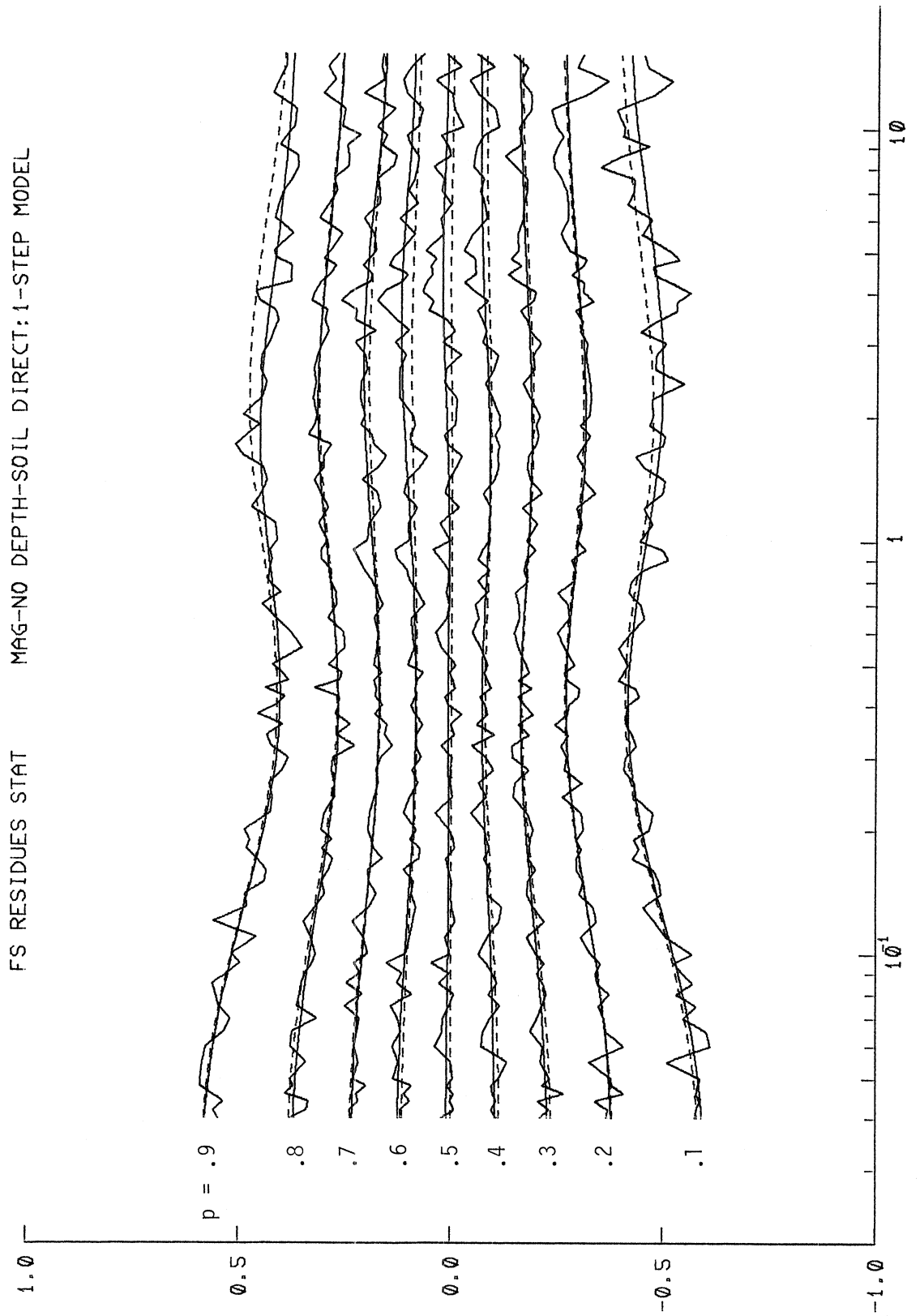
FS RESIDUES STAT
MAG-NO DEPTH-SOIL DIRECT:1-STEP MODEL
1.0
0.5
0.0
-0.5
-1.0
p = .9
.8
.7
.6
.5
.4
.3
.2
.1
10^-1
1
10

Figure V.2.2

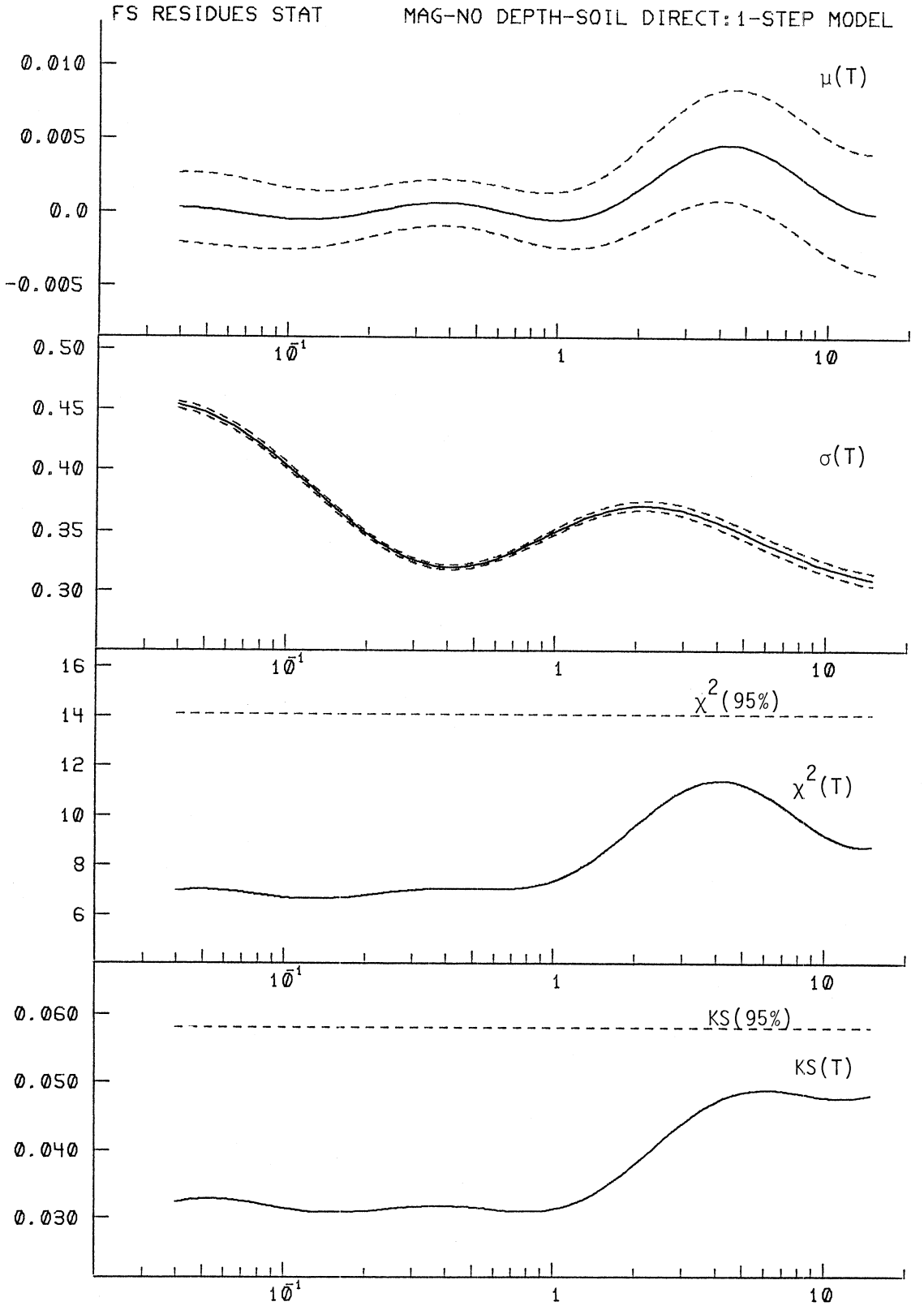
FS RESIDUES STAT
MAG-NO DEPTH-SOIL DIRECT: 1-STEP MODEL
μ(T)
σ(T)
χ²(95%)
χ²(T)
KS(95%)
KS(T)
0.010
0.005
0.0
-0.005
0.50
0.45
0.40
0.35
0.30
16
14
12
10
8
6
0.060
0.050
0.040
0.030
10⁻¹
1
10

Figure V.2.3

TABLE V.2.1

$$\log_{10} FS(T) = M_{<} + \mathcal{A}tt(\Delta,M,T) +$$

$$b_1(T)M_{<>} + b_3(T)v + b_5(T) + b_6(T)M_{<>}^2 +$$

$$b_7^{(1)}(T)S_L^{(1)} + b_7^{(2)}(T)S_L^{(2)}$$

MAG-SOIL CLASSIFICATION ONLY MODEL

PERIOD, T(SEC)	.040	.065	.11	.19	.34	.50	.90	1.60	2.80	4.40	7.50	14.0
COEFFICIENTS:												
$b_1(T)$	.407	.441	.620	.800	.853	.808	.710	.735	.900	.938	.533	-.656
$b_3(T)$	.161	.105	-.034	-.213	-.362	-.397	-.348	-.254	-.200	-.197	-.218	-.244
$b_5(T)$	-3.669	-3.631	-3.902	-4.312	-4.640	-4.750	-4.888	-5.301	-5.905	-5.897	-4.339	-.237
$b_6(T)$	-.075	-.081	-.098	-.114	-.119	-.113	-.100	-.098	-.109	-.117	-.093	-.012
$b_7^{(1)}(T)$	-.182	-.165	-.123	-.048	.043	.098	.178	.256	.302	.285	.189	.004
$b_7^{(2)}(T)$	-.072	-.090	-.103	-.056	.056	.133	.229	.302	.339	.305	.157	-.141
RESIDUES:												
p =.1	-.591	-.567	-.514	-.454	-.418	-.420	-.451	-.486	-.495	-.479	-.448	-.421
p =.2	-.377	-.364	-.333	-.297	-.272	-.273	-.294	-.313	-.310	-.296	-.278	-.266
p =.3	-.228	-.218	-.200	-.178	-.164	-.165	-.179	-.188	-.184	-.174	-.164	-.156
p =.4	-.104	-.100	-.092	-.081	-.072	-.073	-.084	-.090	-.081	-.072	-.066	-.064
p =.5	.010	.009	.006	.005	.007	.007	.006	.010	.019	.024	.020	.013
p =.6	.124	.117	.104	.091	.084	.084	.093	.108	.120	.118	.104	.090
p =.7	.232	.223	.204	.184	.170	.171	.184	.202	.209	.200	.179	.159
p =.8	.370	.355	.325	.289	.267	.269	.291	.313	.313	.299	.277	.259
p =.9	.577	.553	.504	.446	.406	.404	.429	.450	.443	.421	.396	.376
RESIDUE STATISTICS:												
$\mu(T)$	.000	-.000	-.000	-.000	.001	.000	-.000	.001	.003	.005	.003	.000
$\sigma(T)$	.453	.435	.396	.351	.322	.322	.344	.368	.368	.353	.330	.311
$X^2(T)$	6.964	6.948	6.686	6.775	7.051	7.067	7.235	8.711	10.826	11.407	10.167	8.767
KS(T)	.032	.033	.031	.031	.032	.031	.031	.035	.043	.048	.048	.048

distribution function with mean $\mu(T)$ and standard deviation $\sigma(T)$. Figure V.2.3 shows the plot of the statistical parameters in the description of the residues, namely, $\hat{\mu}(T)$, $\hat{\sigma}(T)$, $\chi^2(T)$ and KS(T). The trends shown in both figures are very similar to those (Figures I.5.2 and I.5.3) in Part I of the work.

Finally, Table V.2.1 shows the scaling functions, residue levels, and residue statistics at 12 distinct periods for the "MAG-SOIL classification only" model.

V.3 Examples of Estimated Fourier Spectra

Figure V.3.1 presents four plots of the estimated FS(T) to illustrate the effect of the local soil classification only on the FS(T). The top two plots show examples of FS(T) computed for magnitudes M = 4.5, 5.5, 6.5 and 7.5 at epicentral distance R = 0, focal depth H = 5 km, for $p(\varepsilon,T) = 0.5$, and for the horizontal (v = 0) and vertical (v = 1) motions. The solid lines in both plots correspond to the local soil condition $s_L = 0$ (rock), while the dashed lines correspond to $s_L = 2$ (deep soil). The bottom two plots show examples of FS(T) for magnitude M = 6.5, epicentral distances R = 0, 25, 50 and 100 km, focal depth H = 5 km for $p(\varepsilon,T) = 0.5$, and for the horizontal and vertical motions. The solid lines are again for $s_L = 0$ and the dashed lines for $s_L = 2$.

It is interesting to compare this figure with the corresponding Figure I.6.2 for the MAG-DEPTH-SOIL model, Figure II.3.2 for the MAG-SITE-SOIL model, Figure III.3.2 for the MMI-SITE-SOIL model and Figure IV.3.2 for the MMI-SITE-SOIL model, in the previous four parts of this work. For all previous four models it is observed that at short periods, the Fourier amplitudes FS(T) at rock site ($s_L = 0$) are higher than those at deep soil sites ($s_L = 2$), and this difference is reversed (or is reduced) for the middle and long periods. Figure V.3.1 shows that for short periods, the Fourier amplitudes FS(T) at rock site ($s_L = 0$) also tend to be higher than those at deep soil ($s_L = 2$), but the difference is only slight. In the middle and long period range, this trend is reversed and, the Fourier amplitude FS(T) at rock site ($s_L = 0$) are lower than those at deep soil sites ($s_L = 2$). Thus it is seen that ignoring the local geological characteristics may lead to

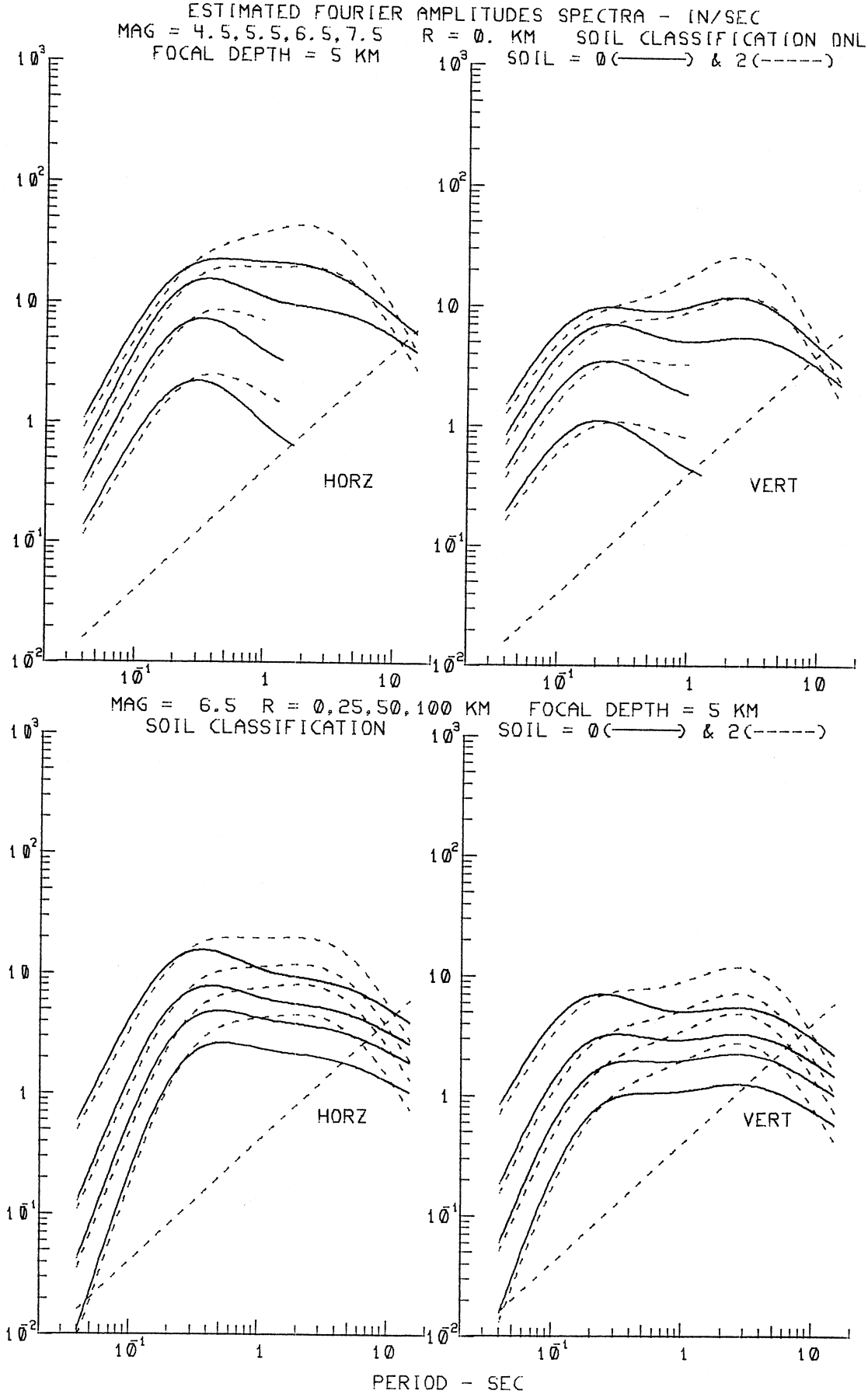
ESTIMATED FOURIER AMPLITUDES SPECTRA - IN/SEC
MAG = 4.5, 5.5, 6.5, 7.5 R = 0. KM SOIL CLASSIFICATION ONLY
FOCAL DEPTH = 5 KM
SOIL = 0(———) & 2(-----)
HORZ
VERT
MAG = 6.5 R = 0, 25, 50, 100 KM FOCAL DEPTH = 5 KM
SOIL CLASSIFICATION
SOIL = 0(———) & 2(-----)
HORZ
VERT
PERIOD - SEC

Figure V.3.1

estimation of the FS(T) for some geologically "average" site (e.g. $h \approx 2$ km) as the above comparisons do suggest. However, as a more detailed analysis of the above mentioned figures will show, using the local soil site classification parameters s_L, will tend to overestimate the actual soil effects for intermediate and long period waves. As long as the stiff or deep soil sites are located on deep sediments, or the "rock" soil sites are over geological basement rock the regression equations which ignore the local geological sites may produce reasonable estimates of FS(T). However, the FS(T) for deep soil sites over the geological basement rock or the "rock" soil sites over the deep sedimentary deposits will be seriously misrepresented by the equations and by the scaling functions presented in this section.

V.4 Scaling in Terms of M.M.I. and Soil Classification Only

Parts III and IV of this work have presented the scaling of Fourier spectra in terms of the Modified Mercalli Intensity (M.M.I.) at the site, local geological characterization, soil classification and the component direction. This part of the analysis deals with the scaling of Fourier spectra in terms of M.M.I., with the local site represented only by the soil classification and with no geological characterization to be included. The scaling equation now becomes

$$\log_{10}FS(T) = b_1(T)\hat{I}_{MM} + b_3(T)v + b_5(T) + b_6^{(1)}(T)S_L^{(1)} + b_6^{(2)}(T)S_L^{(2)} \quad . \qquad (V.4.1)$$

Here, the equation is of the same form as equation (III.2.1) in Part III of this work, except that $b_2(T)$ for depth h and $b_4(T)$ for hv are omitted, since no geological characterization of the site is to be included. The scaling functions $b_1(T)$, $b_3(T)$, $b_5(T)$, $b_6^{(1)}(T)$ and $b_6^{(2)}(T)$ are determined through regression analysis, using the same procedures and the data base as before. The computed scaling functions at each period T will be denoted by $\hat{b}_1(T)$ through $\hat{b}_6^{(2)}(T)$, respectively. Substituting the fitted coefficients in equation (V.4.1) then gives $\hat{FS}(T)$, the estimated spectral amplitudes, where

$$\log_{10}\hat{FS}(T) = \hat{b}_1(T)\hat{I}_{MM} + \hat{b}_3(T)v + \hat{b}_5(T) + \hat{b}_6^{(1)}(T)S_L^{(1)} + \hat{b}_6^{(2)}(T)S_L^{(2)} \quad . \qquad (V.4.2)$$

Figure V.4.1 shows the smoothed coefficients $\hat{b}_1(T)$, $\hat{b}_3(T)$, $\hat{b}_5(T)$, $\hat{b}_6^{(1)}(T)$ and $\hat{b}_6^{(2)}(T)$ (solid lines) together with the estimates of their

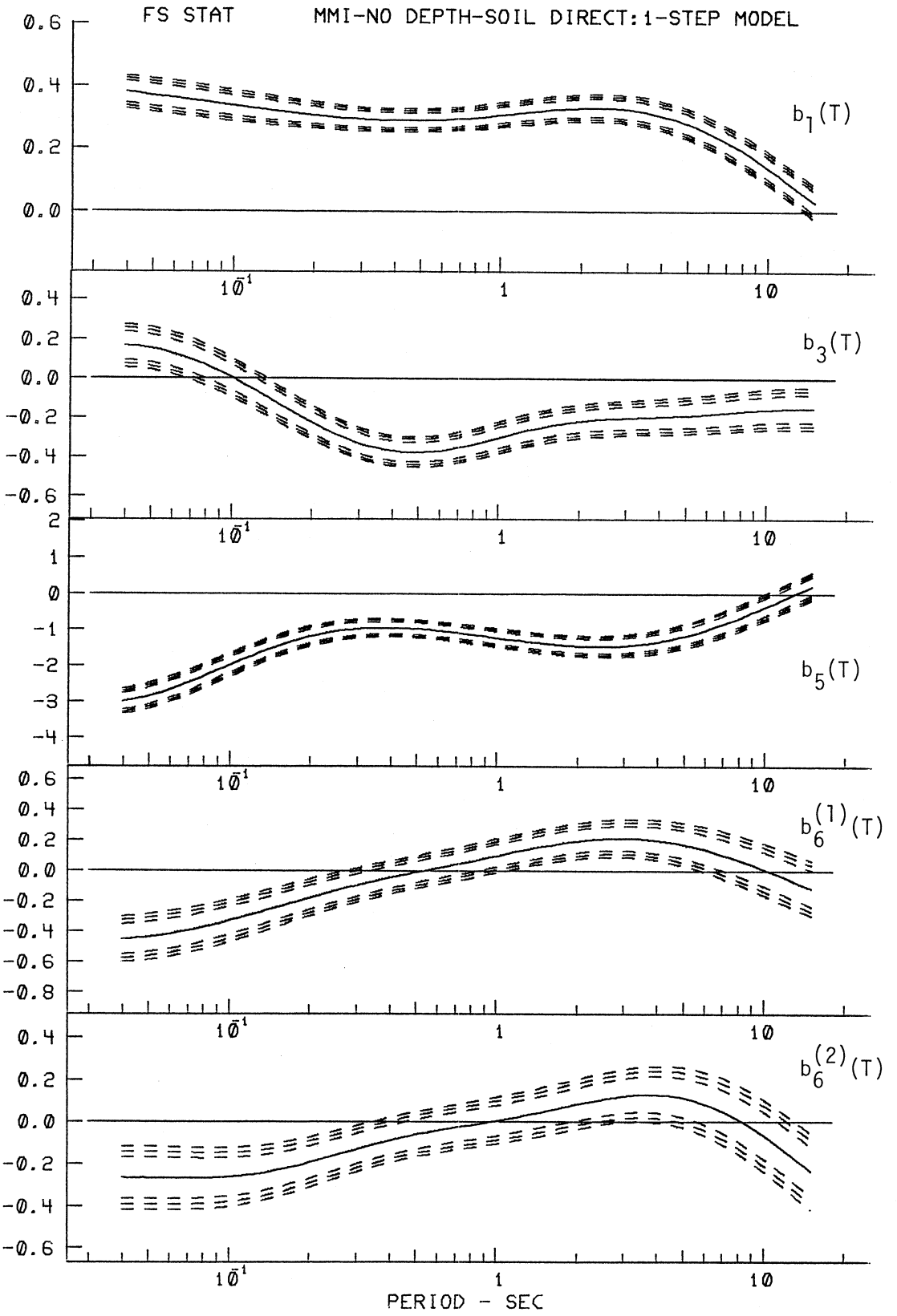
FS STAT
MMI-NO DEPTH-SOIL DIRECT:1-STEP MODEL
$b_1(T)$
$b_3(T)$
$b_5(T)$
$b_6^{(1)}(T)$
$b_6^{(2)}(T)$
PERIOD - SEC

Figure V.4.1

80%, 90% and 95% confidence intervals (dashed lines). It is interesting to compare this figure with the corresponding Figure III.2.1 in Part III for the MMI-DEPTH-SOIL model where the local geological condition in terms of depth, h, is included. The scaling functions $\hat{b}_1(T)$, $\hat{b}_3(T)$, $\hat{b}_5(T)$, $\hat{b}_6^{(1)}(T)$ and $\hat{b}_6^{(2)}(T)$ from both models are very similar. In particular, the scaling functions for the soil indicator variables $S_L^{(1)}$ and $S_L^{(2)}$, respectively $\hat{b}_6^{(1)}(T)$ and $\hat{b}_6^{(2)}(T)$ are similar in both shape and amplitude, more so than in the corresponding comparison of the magnitude models (Section V.3). The scaling functions $b_6^{(1)}(T)$ and $b_6^{(2)}(T)$ are now significantly more negative in the short period range than those of the magnitude-soil only model, and beyond 1 sec. period, they turn positive. This is more consistent with the first four models of Parts I, II, III and IV.

The residues $\varepsilon(T) = \log_{10}FS(T) - \log_{10}\hat{FS}(T)$ describing the distribution of the recorded FS(T) about the estimated $\hat{FS}(T)$ are next calculated. $\varepsilon(T)$ can again be described by a normal distribution function with mean $\mu(T)$ and standard deviation $\sigma(T)$. Figure V.4.2 shows the residue levels for this MMI-SOIL-ONLY model corresponding to $p^*(\varepsilon,T)$ = 0.1 through 0.9. Figure V.4.3 presents the statistical parameters used in the description of the residues and corresponds to Figure V.2.3 for the MAG-SOIL only model.

Figure V.4.4 presents two sets of the estimated FS(T) spectra to illustrate the influence of the local soil conditions on FS(T). Those are computed from equation (V.4.1) for $p(\varepsilon,T)$ = 0.5 and for M.M.I. levels IV, VI, VIII, X and XII. The left part is for the horizontal motion (v = 0) while the right one is for the vertical motion (v = 1). The

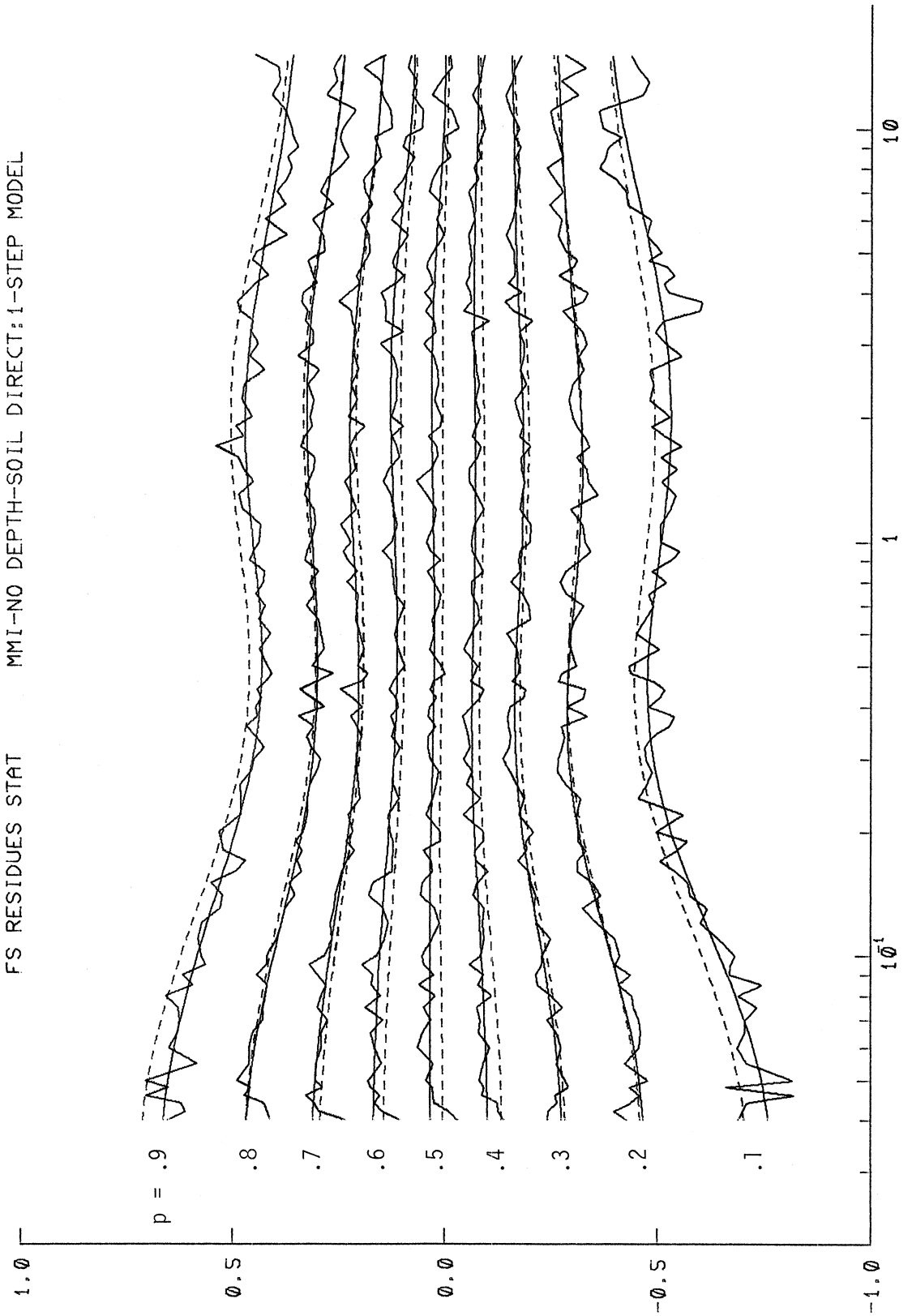
FS RESIDUES STAT
MMI-NO DEPTH-SOIL DIRECT;1-STEP MODEL
p = .9
.8
.7
.6
.5
.4
.3
.2
.1
1.0
0.5
0.0
-0.5
-1.0
10⁻¹
1
10

Figure V.4.2

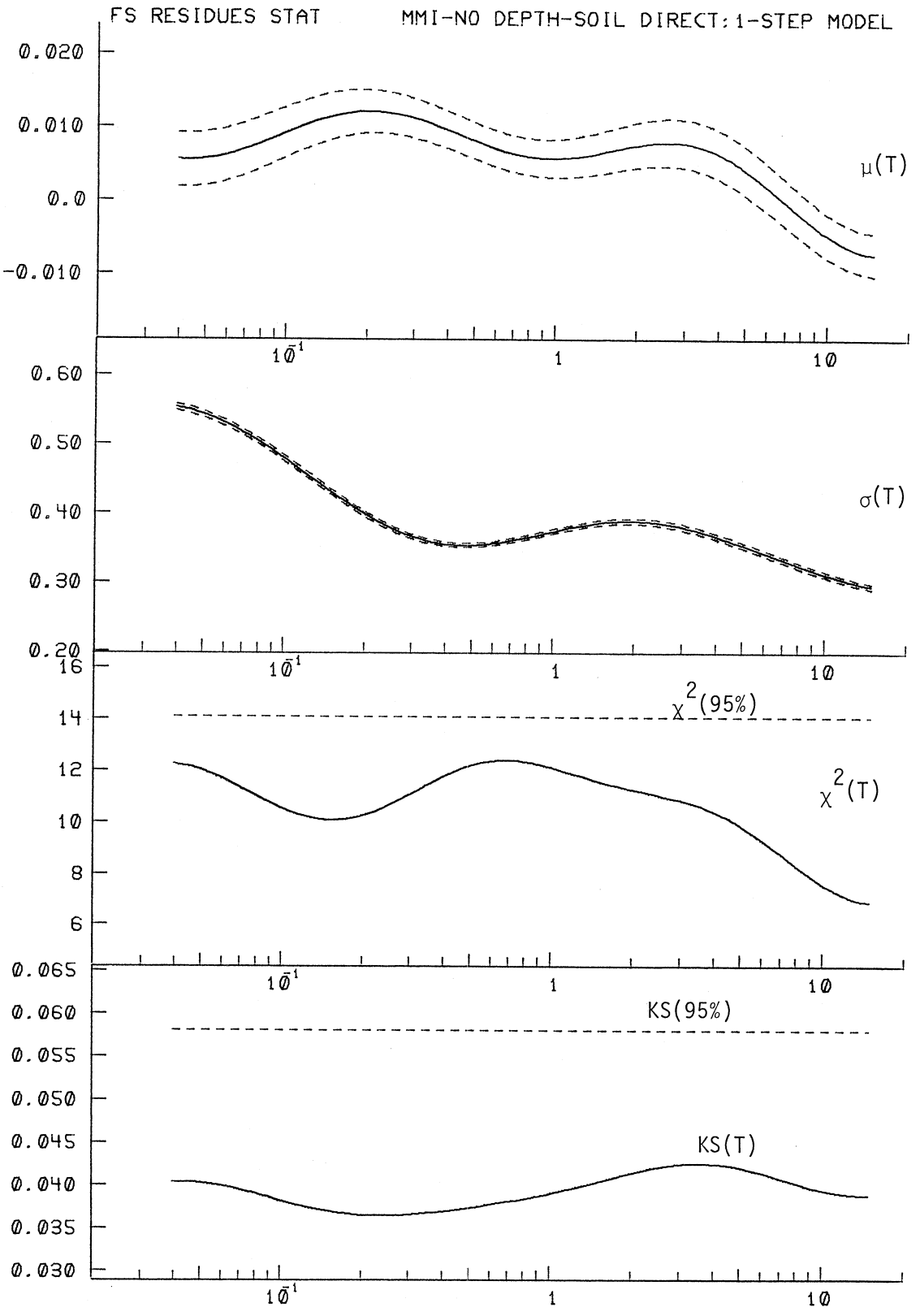
FS RESIDUES STAT
MMI-NO DEPTH-SOIL DIRECT: 1-STEP MODEL
0.020
0.010
0.0
-0.010
μ(T)
10⁻¹
1
10
0.60
0.50
0.40
0.30
0.20
σ(T)
16
14
12
10
8
6
χ²(95%)
χ²(T)
0.065
0.060
0.055
0.050
0.045
0.040
0.035
0.030
KS(95%)
KS(T)

Figure V.4.3

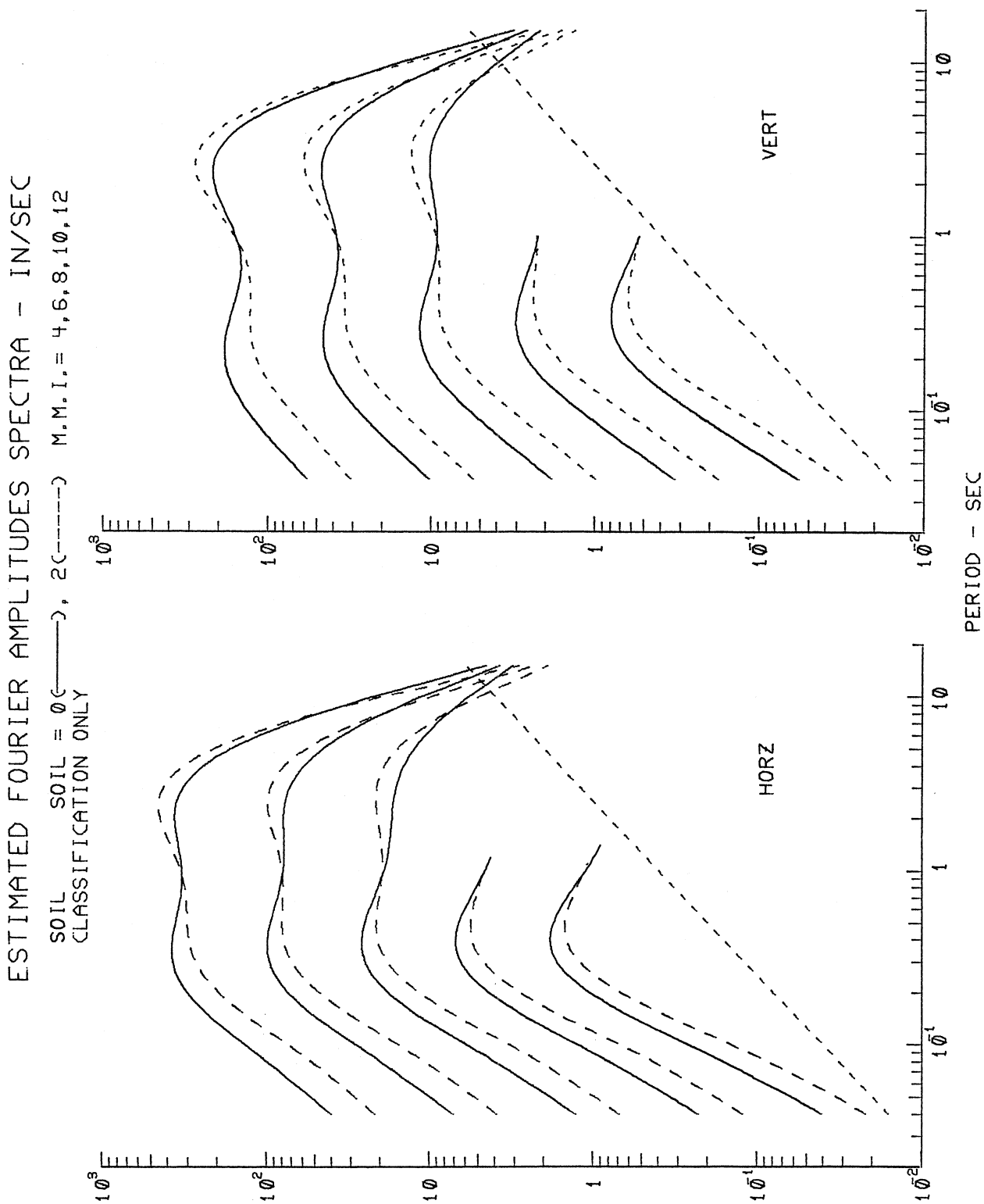
ESTIMATED FOURIER AMPLITUDES SPECTRA - IN/SEC
SOIL CLASSIFICATION ONLY
SOIL = 0(———), 2(- - - - -) M.M.I.= 4,6,8,10,12
HORZ
VERT
PERIOD - SEC

Figure V.4.4

TABLE V.4.1

$$\log_{10} FS(T) = b_1(T)\hat{I}_{MM} + b_3(T)v + b_5(T) + b_6^{(1)}(T)S_L^{(1)} + b_6^{(2)}(T)S_L^{(2)}$$

MMI-SOIL CLASSIFICATION ONLY MODEL

PERIOD, T(SEC)	.040	.065	.11	.19	.34	.50	.90	1.60	2.80	4.40	7.50	14.0
COEFFICIENTS:												
$b_1(T)$	.381	.358	.332	.309	.292	.290	.304	.327	.330	.297	.207	.047
$b_3(T)$	.164	.111	-.029	-.210	-.352	-.376	-.318	-.238	-.202	-.192	-.170	-.152
$b_5(T)$	-2.997	-2.560	-1.843	-1.217	-.949	-.977	-1.181	-1.400	-1.449	-1.264	-.753	.119
$b_6^{(1)}(T)$	-.452	-.405	-.309	-.189	-.073	-.011	.079	.167	.214	.190	.088	-.095
$b_6^{(2)}(T)$	-.268	-.270	-.259	-.202	-.111	-.060	-.005	.056	.117	.125	.031	-.208
RESIDUES:												
p =.1	-.758	-.714	-.630	-.539	-.482	-.476	-.501	-.528	-.523	-.494	-.444	-.396
p =.2	-.465	-.437	-.380	-.320	-.289	-.291	-.313	-.323	-.310	-.294	-.278	-.265
p =.3	-.275	-.258	-.223	-.185	-.165	-.166	-.179	-.185	-.177	-.169	-.163	-.157
p =.4	-.100	-.095	-.084	-.070	-.063	-.064	-.070	-.071	-.067	-.067	-.072	-.077
p =.5	.034	.034	.035	.033	.028	.026	.027	.032	.032	.025	.011	-.000
p =.6	.169	.162	.151	.134	.117	.113	.117	.126	.127	.116	.093	.073
p =.7	.311	.295	.265	.230	.206	.204	.215	.225	.218	.200	.172	.147
p =.8	.468	.441	.393	.341	.307	.301	.310	.324	.322	.305	.272	.240
p =.9	.664	.631	.571	.499	.443	.431	.448	.470	.464	.437	.398	.362
RESIDUE STATISTICS:												
$\mu(T)$	.006	.007	.010	.012	.011	.008	.006	.007	.008	.005	-.001	-.007
$\sigma(T)$	.553	.524	.468	.404	.360	.354	.370	.388	.383	.362	.329	.297
$X^2(T)$	12.240	11.510	10.363	10.181	11.387	12.190	12.248	11.515	10.949	10.210	8.562	6.965
KS(T)	.040	.040	.038	.037	.037	.037	.039	.041	.042	.042	.041	.039

solid lines in both figures correspond to soil classification of $s_L = 0$ (rock) and the dashed lines are for $s_L = 2$ (deep soil). Comparing this with the corresponding Figure III.3.2 of the MMI-DEPTH-SOIL model of Part III shows a lot of similarity, unlike in the case of the MAG-SOIL-ONLY model of Section V.1 and the MAG-DEPTH-SOIL model of Part I of this work.

Finally, Table V.4.1 shows the scaling functions, residue levels, and residue statistics at 12 distinct periods for the MMI-SOIL-CLASSIFICATION-ONLY model.

PART VI: COMPARISON OF THE SCALING FUNCTIONS FOR LOCAL GEOLOGY AND SOIL CLASSIFICATION IN DIFFERENT EMPIRICAL MODELS

The presentation of all the models in this work is now completed. For the direct, 1-step procedures, six models have been considered. Those can be summarized as follows:

1. MAG-DEPTH-SOIL: Part I,
2. MAG-SITE-SOIL: Part II,
3. MMI-DEPTH-SOIL: Part III,
4. MMI-SITE-SOIL: Part IV,
5. MAG-SOIL ONLY: Part V, Sections 1, 2 and 3
6. MMI-SOIL ONLY: Part V, Section 4.

For relative evaluation and to test the mutual consistency of different models, it is interesting to compare the scaling functions for local geology and local soil classifications from different regression analyses. For scaling in terms of the local geology, two different characterizations have been used: one in terms of the overall depth of sediments, h, which was used as a continuous variable in the regression, and the other in terms of the site conditions, s, (= 0,1,2), with s = 0 for alluvium sites and s = 2 for geological basement rock sites. In this work, the local site conditions have been characterized by the indicator variables $S^{(1)}$ and $S^{(2)}$, where $S^{(1)}$ = 1 when s = 1 and 0 otherwise, $S^{(2)}$ = 1 when s = 2 and 0 otherwise, so that both $S^{(1)}$ and $S^{(2)}$ equal 0 when s = 0.

These variables participated in the regressions of different scaling models through the following terms:

1. MAG-DEPTH-SOIL, (Equation (I.3.1)):

$$(b_2(T) + b_4(T)v)h \quad ,$$

2. MAG-SITE-SOIL, (Equation (II.1.2)):

$$(b_2^{(1)}(T) + b_4^{(1)}(T)v)S^{(1)} + (b_2^{(2)}(T) + b_4^{(2)}(T)v)S^{(2)} \quad ,$$

3. MMI-DEPTH-SOIL, (Equation III.1.4):

$$(b_2(T) + b_4(T)v)h \quad ,$$

4. MMI-SITE-SOIL, (Equation IV.1.1):

$$(b_2^{(1)}(T) + b_4^{(1)}(T)v)S^{(1)} + (b_2^{(2)}(T) + b_4^{(2)}(T)v)S^{(2)} \quad ,$$

5. MAG-SOIL ONLY, (Equation V.1.1):

None ,

6. MMI-SOIL ONLY, (Equation V.4.1):

None ,

where v = 0 for horizontal and 1 for vertical components. The last two models above included no scaling in terms of the local geology classification since the local conditions are assumed to depend only on the local soil classification.

To compare the scaling functions in terms of the sedimentary depths (say s = 0 corresponds to h ≈ 3 km), it is necessary to make use of the scaling functions $(b_2^{(\ell)}(T) + b_4^{(\ell)}(T)v)S^{(\ell)}$, $\ell = 1, 2$. Since $S^{(2)} = 1$ is the indicator variable for s = 2 (geological rock site), putting $S^{(2)} = -1$ would "correspond" to the trend in terms of h and average sedimentary sites (say h ≈ 3 km). Thus, for horizontal components (v = 0), the terms $b_2(T)h$ with h ≈ 3 km for models I and III, and $-b_2^{(2)}(T)$ ($S_L^{(2)} = -1$) for models II and IV, will be appropriate to compare. Figure VI.1.1 shows all these scaling functions in the period range from 0.04 sec. to 15 sec. Except for short periods below .3 sec. and for the MMI-SITE-SOIL model, the amplitudes and the shapes of all the scaling functions are fairly consistent. For vertical components, with v = 1, the scaling functions $(b_2(T) + b_4(T))h$, with h = 3 km, for models I and III and $-(b_2^{(2)}(T) + b_4^{(2)}(T))$ ($S_L^{(2)} = -1$) for models II and IV are compared and plotted in Figure VI.1.2. While the scaling function of the MAG-DEPTH-SOIL model (I) agrees well with that of the MMI-DEPTH-SOIL model (III), those of the MAG-SITE-SOIL (II) and MMI-SITE-SOIL (IV) models do not agree with eachother or with the other models at all. The reason for this discrepancy is the fact that the scaling functions $b_4^{(2)}(T)$ for the "site" models (II and IV) (Figures II.2.1 and IV.2.1) are exhibiting statistically insignificant amplitudes in the entire period range, with the zero line practically within the 90% confidence intervals for all periods. Though these coefficients should have been deleted from subsequent scaling, we kept them for the purpose of maintaining similarity of form in all regression models.

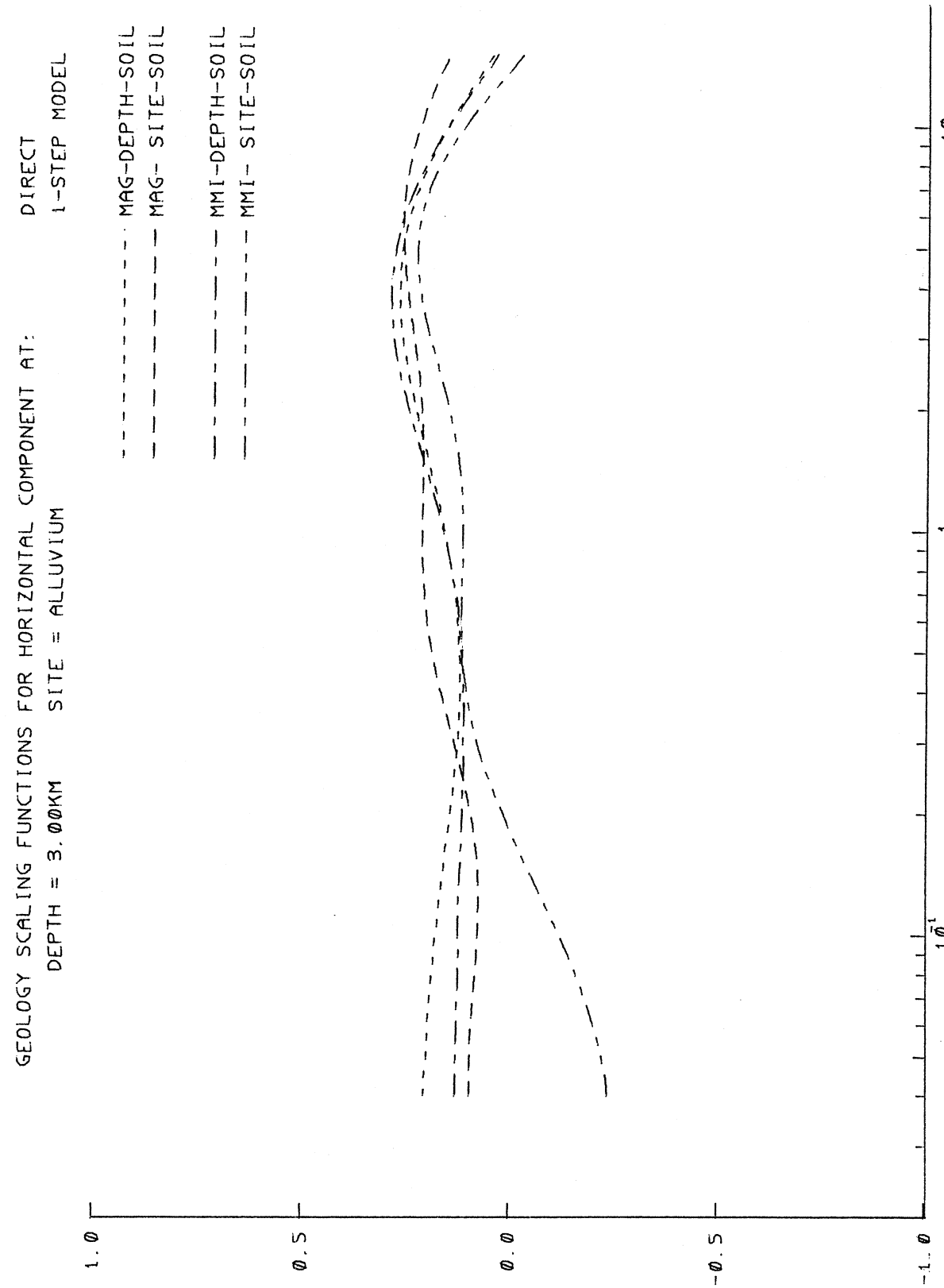
GEOLOGY SCALING FUNCTIONS FOR HORIZONTAL COMPONENT AT:
DEPTH = 3.ØØKM
SITE = ALLUVIUM
DIRECT
1-STEP MODEL
MAG-DEPTH-SOIL
MAG- SITE-SOIL
MMI-DEPTH-SOIL
MMI- SITE-SOIL
1.Ø
Ø.5
Ø.Ø
-Ø.5
-1.Ø
1Ø⁻¹
1Ø
PERIORD - SEC.¹

Figure VI.1.1

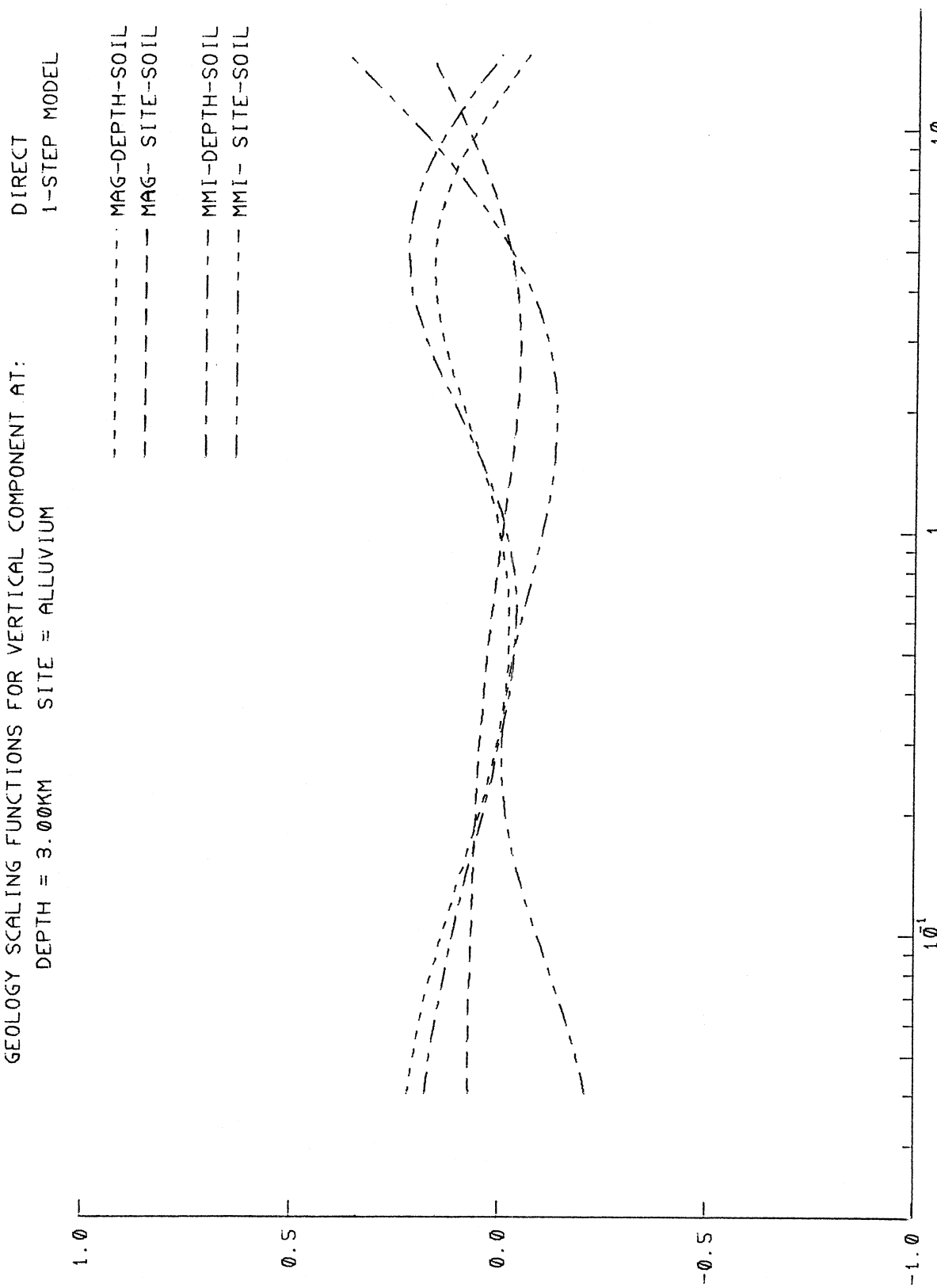
GEOLOGY SCALING FUNCTIONS FOR VERTICAL COMPONENT AT:
DEPTH = 3.00KM SITE = ALLUVIUM
DIRECT
1-STEP MODEL
MAG-DEPTH-SOIL
MAG- SITE-SOIL
MMI-DEPTH-SOIL
MMI- SITE-SOIL
1.0
0.5
0.0
-0.5
-1.0
10^{-1}
1
10
PERIORD - SEC.

Figure V1.1.2

The scaling functions for $S_L^{(1)}$ (stiff soil), $b_7^{(1)}(T)$ of models I, II and V, $b_6^{(1)}(T)$ of models III, IV and V are next compared and plotted in Figure VI.1.3. As can be seen from this figure, the six scaling functions are similar in shape. They all start out negative at the short period and gradually increase and turn positive in the mid period range. Their amplitudes then gradually decrease in the long period range. Similarly, the scaling functions for $S_L^{(2)}$ (deep soil), $b_7^{(2)}(T)$ of models I, II and V, and $b_6^{(2)}(T)$ of models III, IV and V are plotted in Figure VI.1.4. Those are again similar in shape, all start as negative in the low period end, and gradually increase and turn positive in the mid period range. The only exception is $b_6^{(2)}(T)$ of the MMI-DEPTH-SOIL model (IV) which stays negative for all periods.

Similar comparison can next be made for the four residue 2-step models which have been presented in Parts I, II, III and IV of this work. Figure VI.1.5, as Figure VI.1.1 shows the scaling functions for the horizontal components of motion for the depth of sediments equal to 3 km and for s = 0 (alluvium) sites. The agreement of the different functions is very good. Figure VI.1.6 as Figure VI.1.2, shows the scaling functions for the vertical components at the depth of sediments equal to 3 km and for s = 0 (alluvial) sites. As in the cases shown in Figure VI.1.2, the models using alluvium depth (I and III) are mutually consistent. The "discrepancy" of the models (II and IV) which use site classification is due to the insignificance of the $b_4^{(2)}(T)S^{(2)}_V$ term in the regression analysis.

The scaling functions for the models using soil classifications s_L = 1 and 2 is next compared for the residue models. In the first step

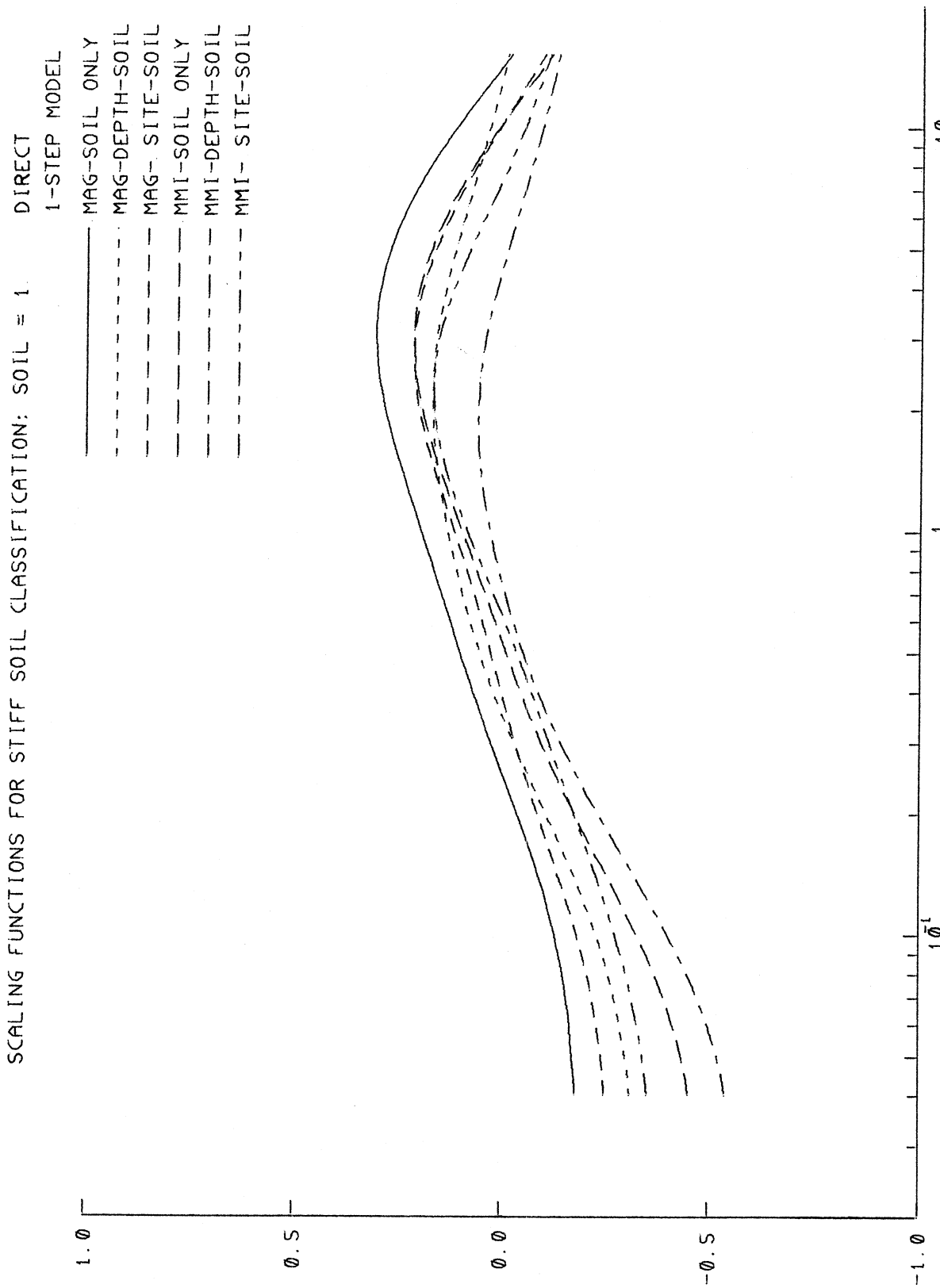
SCALING FUNCTIONS FOR STIFF SOIL CLASSIFICATION: SOIL = 1
DIRECT
1-STEP MODEL
MAG-SOIL ONLY
MAG-DEPTH-SOIL
MAG- SITE-SOIL
MMI-SOIL ONLY
MMI-DEPTH-SOIL
MMI- SITE-SOIL
1.0
0.5
0.0
-0.5
-1.0
10^-1
10
PERIORD - SEC.^1

Figure VI.1.3

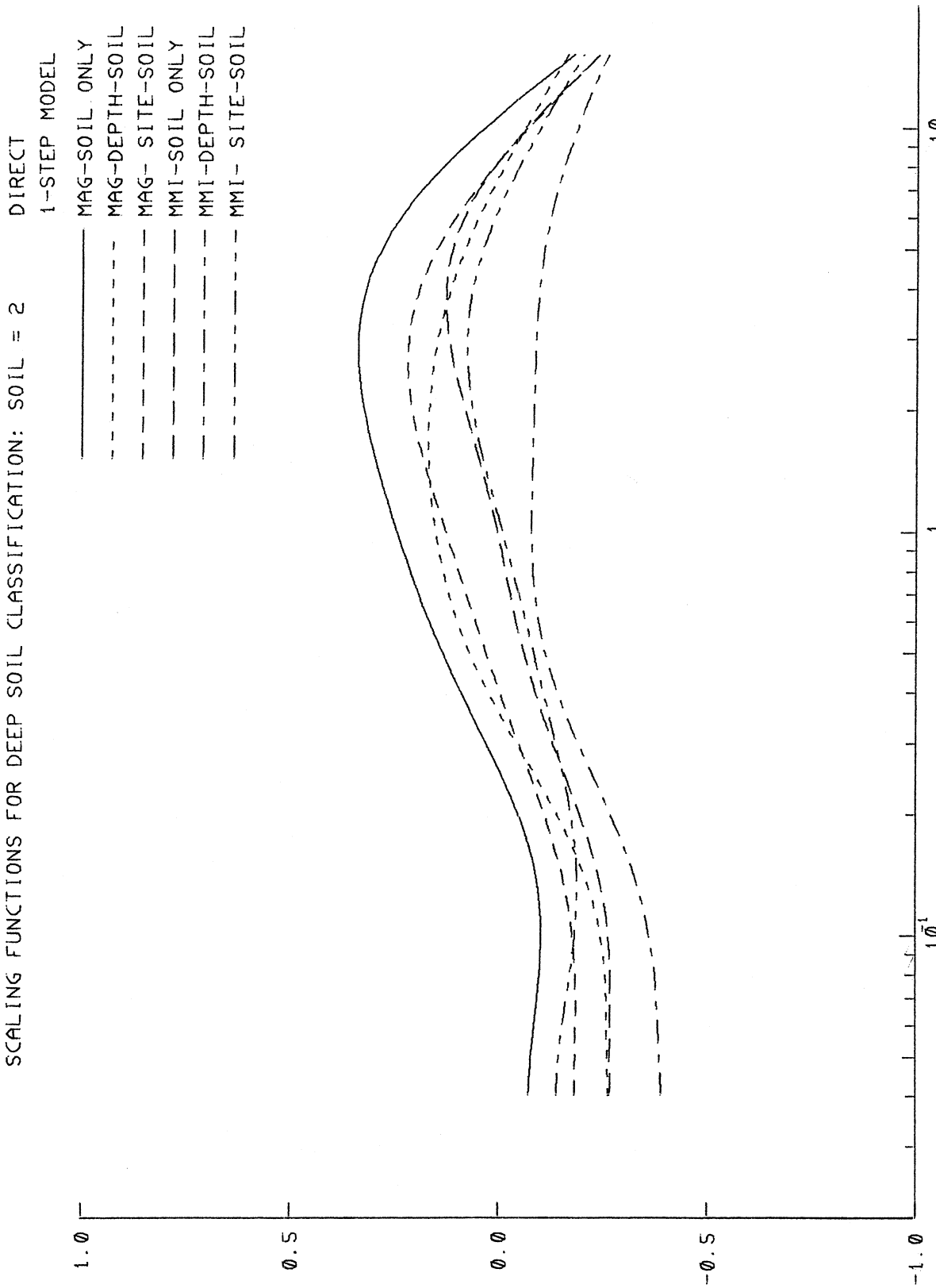
SCALING FUNCTIONS FOR DEEP SOIL CLASSIFICATION: SOIL = 2
DIRECT
1-STEP MODEL
MAG-SOIL ONLY
MAG-DEPTH-SOIL
MAG- SITE-SOIL
MMI-SOIL ONLY
MMI-DEPTH-SOIL
MMI- SITE-SOIL
1.0
0.5
0.0
-0.5
-1.0
10^-1
10
PERIORD - SEC.^1

Figure VI.1.4

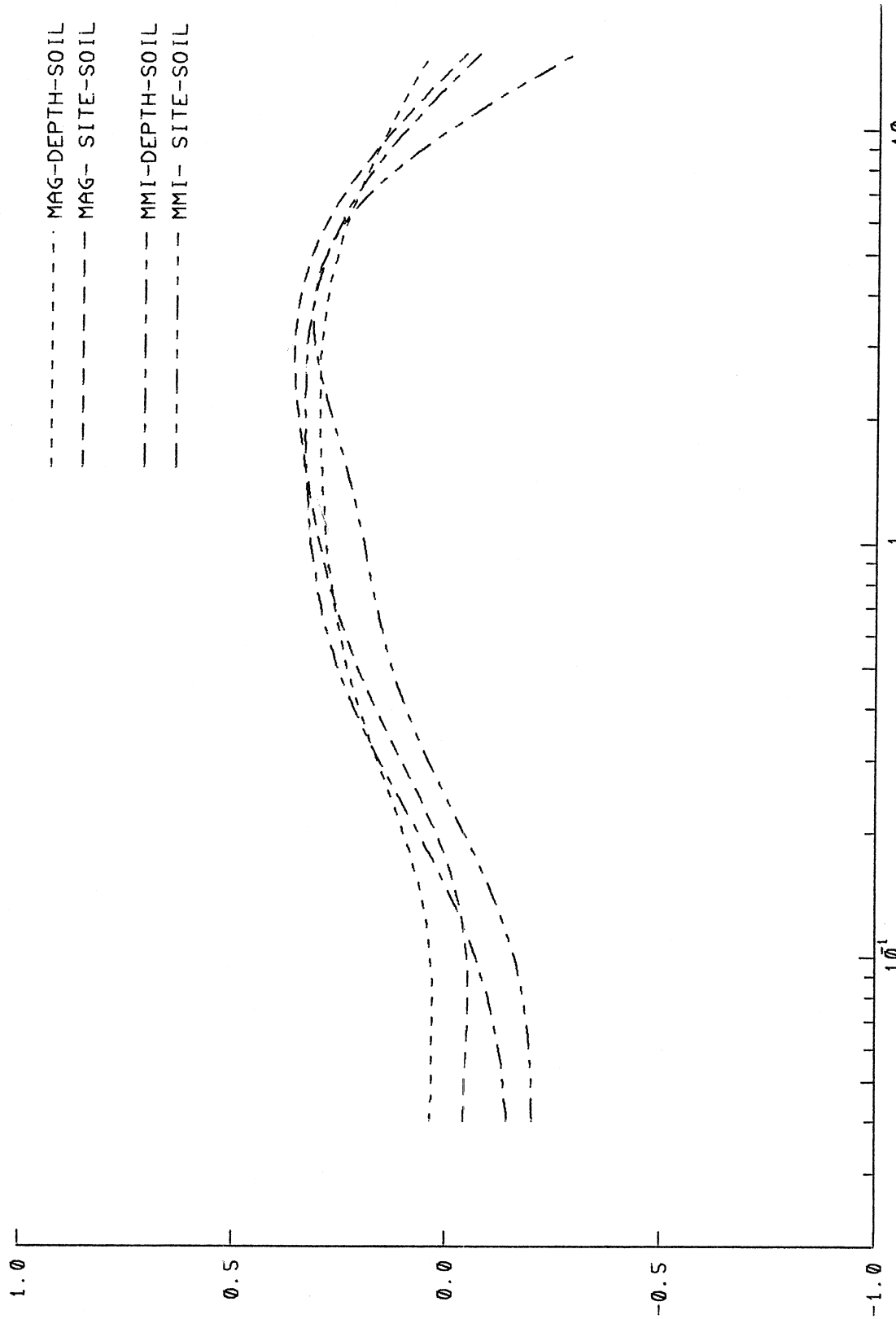
GEOLOGY SCALING FUNCTIONS FOR HORIZONTAL COMPONENT AT:
DEPTH = 3.00KM SITE = ALLUVIUM
RESIDUE
2-STEP MODEL
MAG-DEPTH-SOIL
MAG- SITE-SOIL
MMI-DEPTH-SOIL
MMI- SITE-SOIL
1.0
0.5
0.0
-0.5
-1.0
10^-1
10
PERIORD - SEC.^1

Figure VI.1.5

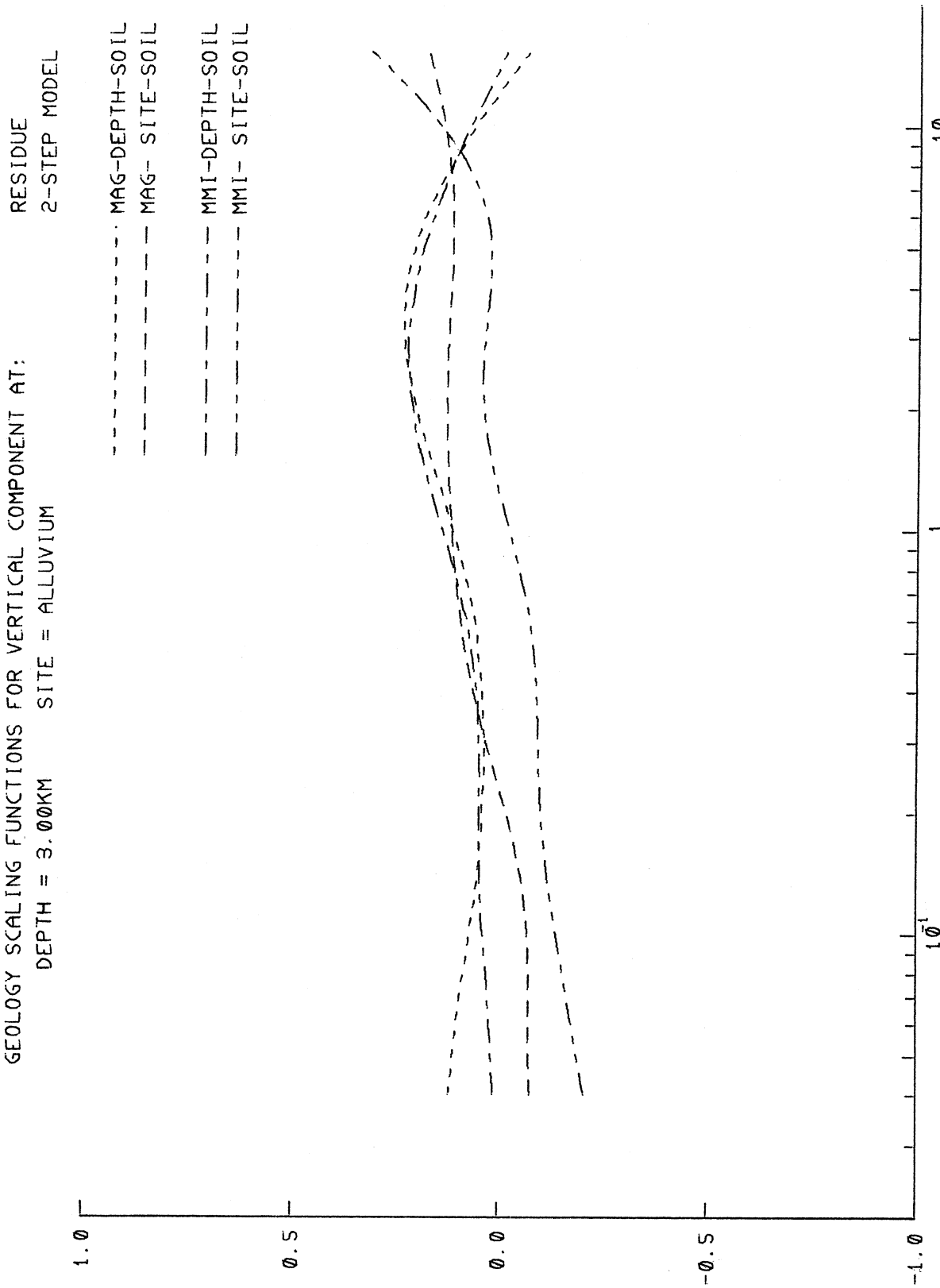
GEOLOGY SCALING FUNCTIONS FOR VERTICAL COMPONENT AT:
DEPTH = 3.00KM SITE = ALLUVIUM
RESIDUE
2-STEP MODEL
MAG-DEPTH-SOIL
MAG- SITE-SOIL
MMI-DEPTH-SOIL
MMI- SITE-SOIL
1.0
0.5
0.0
-0.5
-1.0
10^-1
10
PERIORD - SEC.^1

Figure VI.1.6

for each of the four residue models, the Fourier spectra FS(T) are fitted with all relevant parameters involving magnitude or local intensity (M.M.I.), local geology parameters (depth h or s) and component orientation v (0 or 1), but excluding the soil classification parameters. The residues, $\varepsilon(T)$, at each site where soil classification is available are then fitted in the second step by a linear function of the soil classification parameters, for the magnitude models (I and II) by:

$$\varepsilon(T) = b_7^{(1)}(T)S_L^{(1)} + b_7^{(2)}(T)S_L^{(2)} + b_8(T) \quad , \qquad \text{(VI.1.1)}$$

or, for the intensity models (III,IV) by:

$$\varepsilon(T) = b_6^{(1)}(T)S_L^{(1)} + b_6^{(2)}(T)S_L^{(2)} + b_7(T) \quad . \qquad \text{(VI.1.2)}$$

Subsequently, these terms are added to the equations used in the first step of the regression. From equations (VI.1.1) and (VI.1.2), the case of soil classification with $s_L = 1$ (or $S_L^{(1)} = 1$) thus corresponds to the term $b_7^{(1)}(T) + b_8(T)$ for the models with scaling in terms of magnitude or, $b_6^{(1)}(T) + b_7(T)$ for the models using scaling in terms of local intensity. Similarly, the case of soil classification $s_L = 2$ or ($S_L^{(2)} = 1$) corresponds to the term $b_7^{(2)}(T) + b_8(T)$ for the magnitude model or $b_6^{(2)}(T) + b_7(T)$ for the intensity model.

Figure VI.1.7, as Figure VI.1.3, shows the scaling functions for $S_L^{(1)}$ (stiff soil). As we pointed out in the above, the terms $b_7^{(1)}(T) + b_8(T)$ for the magnitude models (I and II) and $b_6^{(1)}(T) + b_7(T)$ for the intensity models (III and IV) are shown in the plot. All four curves start out negative at the low period end, and increase in amplitudes

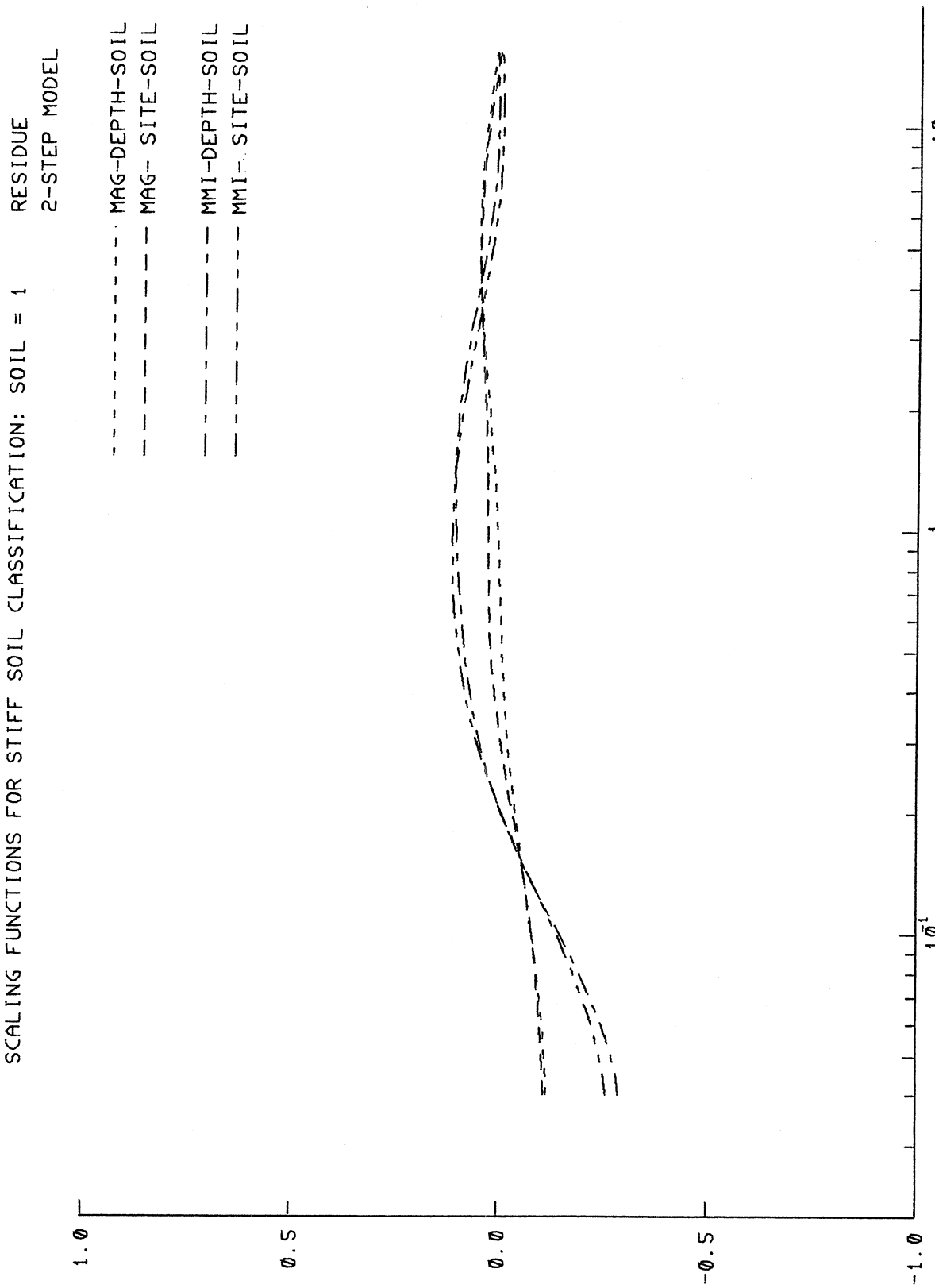
SCALING FUNCTIONS FOR STIFF SOIL CLASSIFICATION: SOIL = 1
RESIDUE
2-STEP MODEL
MAG-DEPTH-SOIL
MAG- SITE-SOIL
MMI-DEPTH-SOIL
MMI- SITE-SOIL
1.0
0.5
0.0
-0.5
-1.0
10^-1
10
PERIORD - SEC.^1

Figure VI.1.7

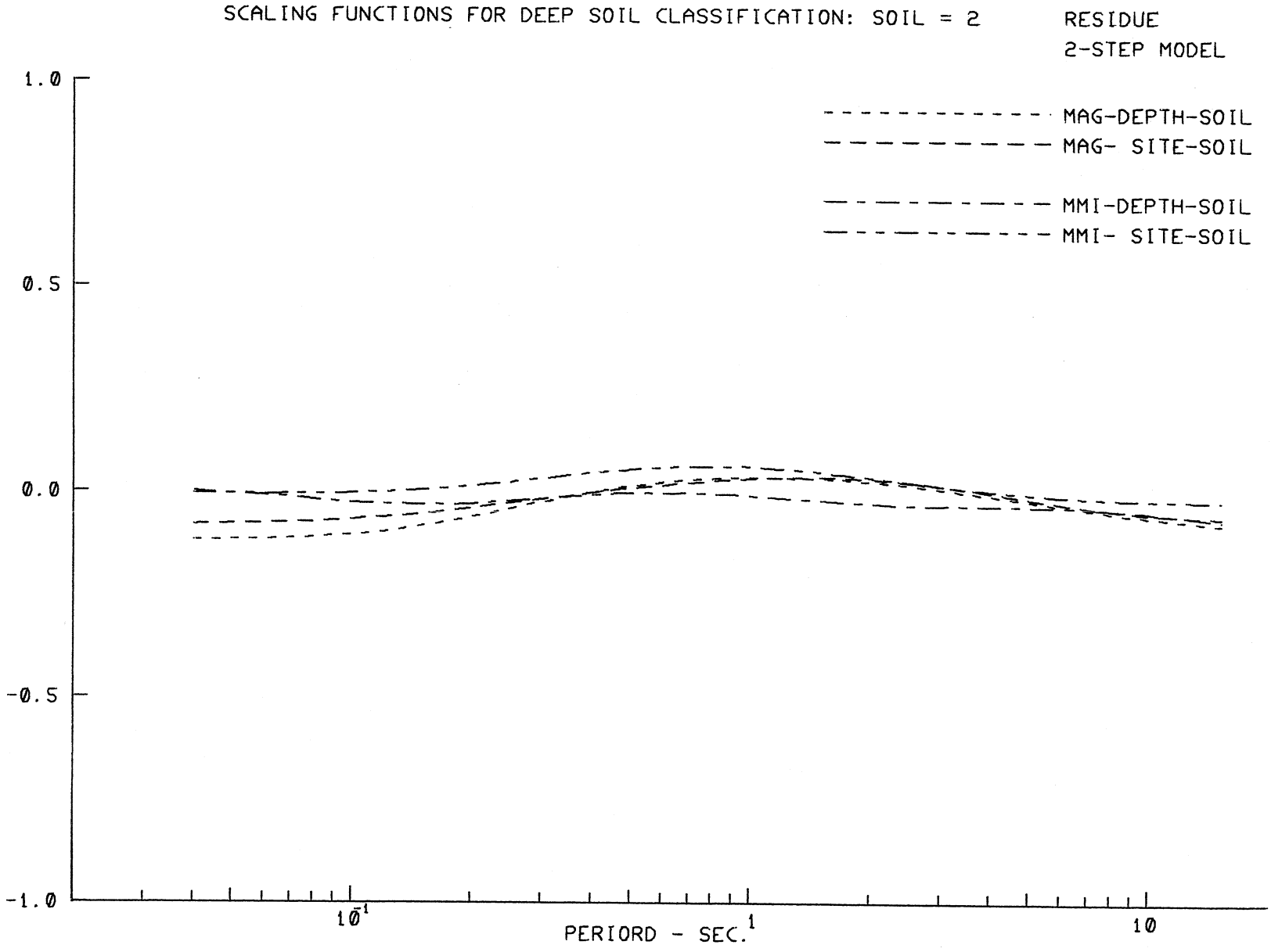
SCALING FUNCTIONS FOR DEEP SOIL CLASSIFICATION: SOIL = 2
RESIDUE
2-STEP MODEL
MAG-DEPTH-SOIL
MAG- SITE-SOIL
MMI-DEPTH-SOIL
MMI- SITE-SOIL
1.0
0.5
0.0
-0.5
-1.0
10^-1
PERIORD - SEC.
1
10

Figure VI.1.8

with increasing periods turning positive in the middle period range. This trend is more noticeable for the intensity models (III and IV) than for the magnitude models (I and II). Similarly, figure IV.1.8, (as the Figure IV.1.4), shows the scaling functions for $S_L^{(2)}$ (deep soil), when the terms $b_7^{(2)}(T) + b_8(T)$ are used for the magnitude models and terms $b_6^{(2)}(T) + b_7(T)$ are used for the intensity models. Those are similar in shape, again starting out negative for short periods and gradually increasing in amplitude and turning positive in the middle period range. The only exception to this is the MMI-DEPTH-SOIL model, for which the amplitudes stay netative but are close to zero for all periods.

CONCLUSIONS

The aim of this report has been to determine which type of scaling equations and what detail in the parametric representation of the Fourier spectral amplitudes may describe best the observed strong earthquake ground motions. The functional forms of the empirical equations we used are not new, but have evolved, with minor refinements, from our previous work (Trifunac 1976, 1979; Trifunac and Lee, 1987b,c). The idea, which has been introduced here for the first time, was to use the local soil and the local geologic characteristics of the site simultaneously in the development of the regression models. Also, the term hv (or sv), reflecting the directional dependence of the amplification has not been employed in our previous analyses.

We found that essentially all four models fit the data quite well and that in general there is much consistency among different regression models. The best fit and the highest degree of mutual compatability among different models has been achieved by MAG-DEPTH-SOIL 1-STEP and MMI-DEPTH-SOIL 2-STEP models.

Characterization of the local geological site conditions in terms of the local depth of sediments, h, is better than the site classification in terms of s = 0, 1 or 2 (s = 0 for sediments and s = 2 for basement rock). In terms of the observed amplitudes of the residuals the spectral amplitudes scaled by the magnitude parameter, M, fit the data better than the spectra scaled in terms of the MMI at the site. No significant differences in the overall residual amplitudes have been observed between 1-step and 2-step regression models. Relative to our previous studies, the amplitudes of the residuals we found in this investigation are smaller.

To enable qualitative comparison of our results with some earlier investigations, which employed the local site characterization in terms of the local soil classification only, we carried out such analyses as well, by ignoring the local geologic features of the sites. Since the functional form of the dependence of the spectral amplitudes on the depth of sediments is similar to its dependence on the local soil conditions, we found that ignoring the local geologic conditions may lead to exagerated amplitude factors "representing" the local soil conditions. We conclude that both the local soil and the local geologic site conditions must be used together in the selection of the site specific Fourier amplitude spectra.

REFERENCES

Duke, M. (1958). Effects of Ground on Descructiveness of Large Earthquakes, Proc. ASCE, 84, No. SM3.

Gusev, A. A. (1983). Descriptive Statistical Model of Earthquake Source Radiation and Its Application to an Estimation of Short Period Strong Motion, Geoph. J. R. Astr. Soc. 74, 787-808.

Gutenberg, B. (1957). Effects of Ground on Earthquake Motion, Bull. Seism. Soc. Amer., 47, 221-520.

Haskell, N. (1960). Crustal Reflection of Plane SH Waves, J. Geoph. Res., 65, 4147-4150.

Kanai, K. (1949,1951). Relation Between the Earthquake Damage of Non-Wooden Buildings and the Nature of the Ground, Bull. Earthquake Res. Inst., Vol. 27, p. 97 (1979); Vol. 29, p. 209 (1951).

Lee, V. W. and M. D. Trifunac (1985). Attenuation of Modified Mercalli Intensity for Small Epicentral Distance in California, Dept. of Civil Eng. Report No. CE 85-01, Univ. Soutnern Calif. Los Angeles, California.

Lee, V. W. and M. D. Trifunac (1987). Strong Earthquake Ground Motion Data in EQINFOS: Part 1, Dept. of Civil Eng. Report No. CE 87-01, Univ. of Southern Calif., Los Angeles, California.

Medvedev, S. V. (1955). Ocenka Seizmicheskoi balnoski u zavisimosti ot gruntovih uslovi, Tr. Geofiz. Inst. AN SSSR No. 4 (141).

Montgomery and Peck (1982). Introduction to Linear Regression Analysis, J. Wiley and Sons, 1982.

Richter, C. F. (1958). Elementary Seismology, Freeman and Co., San Francisco.

Seed, H. B., C. Ugas and J. Lysmer (1974). Site Dependent Spectra for Earthquake Resistant Design, E.E.R.C. 74-12, U.C. Berkeley.

Seed, H. B., C. Ugas and J. Lysmer (1976). Site Dependent Spectra for Earthquake Resistant Design, Bull. Seism Soc. Amer., 66, 221-243.

Trifunac, M. D. (1971). Surface Motion of Semi-Cylindrical Alluvial Valley for Incident Plane SH Waves, Bull. Seism. Soc. Amer., 61, 1755-1770.

Trifunac, M. D. (1976). Preliminary Empirical Model for Scaling Fourier Amplitude Spectra of Strong Ground Acceleration in Terms of Earthquake Magnitude, Source to Station Distance and Recording Site Conditions, Bull. Seism. Soc. Amer., 66, 1343-1373.

Trifunac, M. D. (1979). Preliminary Empirical Model for Scaling Fourier Amplitude Spectra of Strong Motion Acceleration in Terms of Modified Mercalli Intensity and Geologic Site Conditions, Int. J. Earthquake Eng. and Structural Dynamics, 7, 63-74.

Trifunac, M. D. and V. W. Lee (1985a). Preliminary Empirical Model for Scaling Fourier Amplitude Spectra of Strong Ground Acceleration in Terms of Earthquake Magnitude, Source to Station Distance, Site Intensity and Recording Site Conditions, Dept. of Civil Eng. Report No. CE 85-03, Univ. Southern Calif., Los Angeles, California.

Trifunac, M. D. and V. W. Lee (1985b). Preliminary Empirical Model for Scaling Pseudo Relative Velocity Spectra of Strong Earthquake Accelerations in Terms of Magnitude, Distance, Site Intensity and Recording Site Conditions, Dept. of Civil Eng. Report No. CE 85-04, Univ. Southern Calif., Los Angeles, California.

Trifunac, M. D. and V. W. Lee (1987a). Frequency Dependent Attenuation of Strong Earthquake Ground Motion, Int. J. Soil Dynamics and Earthquake Eng. (in press).

Trifunac, M. D. and V. W. Lee (1987b). Empirical Models for Scaling Fourier Amplitude Spectra of Strong Ground Acceleration in Terms of Earthquake Magnitude, Source to Station Distance, Site Intensity and Recording Site Conditions, Inc. J. Soil Dynamics and Earthquake Eng. (in press).

Trifunac, M. D. and V. W. Lee (1987c). Empirical Models for Scaling Pseudo Relative Velocity Spectra of Strong Earthquake Accelerations in Terms of Magnitude, Distance, Site Intensity and Recording Site Conditions, Inc. J. of Soil Dynamics and Earthquake Eng. (in press).

Tsai, N. C. (1969). Influence of Local Geology on Earthquake Ground Motion, EERL, Calif. Inst. of Tech., Pasadena.